THE JOURNAL OF

PHYSICAL CHEMISTRY

Volume 74, Number 24 November 26, 1970

NOTES

COMMUNICATIONS TO THE EDITOR

AUTHOR INDEX

THE JOURNAL OF
PHYSICAL CHEMISTRY
Registered in U. S. Patent Office

VOLUME 74, NUMBER 24 NOVEMBER 26, 1970

Heterogeneous Collisional Deactivation in Chemical Activation Systems[1a]

by Kenneth M. Maloney[1b]

Chemistry Research Department, Pacific Northwest Laboratories, Battelle Memorial Institute, Richland, Washington 99352
(Received December 2, 1969)

The contribution of simple heterogeneity to the observed rate for chemical activation systems has been investigated. The diffusion equation was solved with the appropriate boundary conditions and application made to the collisional deactivation of chemically activated ethane. The functional dependence of the concentration of the activated ethane molecules, $C_E^*(r)$, on the radial distance, r, is illustrated for a cylindrical reactor. A heterogeneity function for chemical activation systems, $H(E)$, is defined, and its variation with pressure is illustrated.

Introduction

In view of the fact that in a closed system the physical extent of the reaction vessel is finite, the occurrence of heterogeneous effects at low pressure, in kinetic reaction systems, is generally unavoidable. Therefore, it is desirable that one is able to assess quantitatively the contribution of heterogeneity to the observed rate of reaction in order to explore effectively all pressure regions in which a given reaction is studied. The problem of heterogeneity in a thermal unimolecular reaction system[2a] (on a collisional activation–deactivation basis) and the problem of the deexcitation probability of an externally excited molecule by the wall of a reaction vessel[2b] (on a collisional deexcitation basis) have been treated previously.

In the present paper, we are concerned with collisional deactivation of chemically activated molecules by the wall in the absence of catalytic effects. The system is one in which the chemically activated molecule is produced in a static cylindrical reactor and the wall of the reactor is an inert energy acceptor.

Theory

We consider a reactive system in which (a) there is a steady state of A* (the vibrationally excited molecule) and (b) the concentration of the parent species, M, from which A* derives, is essentially unperturbed as a result of the formation of A*. Such a system is described by the diffusion equation[3] as

$$D\nabla^2 C_E^*(r) + R - k_{VE} C_E^*(r) = 0 \qquad (1)$$

where the boundary conditions are

$$C_E^*(r) = \text{finite} \qquad (r = 0) \qquad (2)$$

and

$$-D\frac{dC_E^*(r)}{dr} = k_w C_E^*(r_0) \qquad (r = r_0) \qquad (3)$$

$C_E^*(r)$ is the concentration of A*, D is the diffusion coefficient, r_0 is the radius of the reaction vessel, k_w is the velocity constant for wall reaction, $k_{VE} = k_V C_M + k_E$ where k_V is the specific rate constant for gas phase collisions, and k_E is the specific reaction rate constant. R is the rate of production of vibrationally excited molecules.

(1) (a) This paper is based on work performed under U. S. Atomic Energy Commission Contract AT(45-1)-1830; (b) correspondence should be addressed to: Lighting Research Laboratory, General Electric Co., Nela Park, Cleveland, Ohio 44112.

(2) (a) K. M. Maloney and B. S. Rabinovitch, *J. Phys. Chem.*, **72**, 4483 (1968); (b) K. M. Maloney, *ibid.*, **73**, 3158 (1969).

(3) J. L. Hudson and J. Heicklen, *ibid.*, **71**, 4180 (1967).

In cylindrical coordinates, eq 1 is

$$\frac{d^2C_E^*(r)}{dr^2} + \frac{1}{r}\frac{dC_E^*(r)}{dr} + \frac{R}{D} - \frac{k_{VE}C_E^*(r)}{D} = 0 \quad (4)$$

The general solution of eq 4 is

$$C_E^*(r) = B_1J_0(ik_{VE}^{1/2}r/D) + B_2Y_0(ik_{VE}^{1/2}r/D) + \frac{R}{Dk_{VE}} \quad (5)$$

However, B_2 must be zero in order that boundary condition 2 is satisfied (Neumann's bessel function of the second kind of order zero, Y_0, is infinite at $r = 0$). Thus

$$C_E^*(r) = B_1J_0(ik_{VE}^{1/2}r/D) + \frac{R}{Dk_{VE}} \quad (6)$$

Since the modified bessel function

$$I_0(k_{VE}^{1/2}r/D) \equiv J_0(ik_{VE}^{1/2}r/D)$$

one obtains[3] with use of boundary condition 2

$$\frac{DC_E^*(r)}{Rr_0^2} = \frac{1}{K_{VE}} - \frac{(K_w/K_{VE})I_0(K_{VE}^{1/2}r/r_0)}{K_{VE}^{1/2}I_1(K_{VE}^{1/2}) + K_wI_0(K_{VE}^{1/2})} \quad (7)$$

where $K_{VE} = k_{VE}r_0^2/D$ and $K_w = k_wr_0/D$ (see Appendix).

The total rate of *chemical* reaction for molecules in unit range at E is

$$R_{TE} = 2\pi Lk_E\int_0^{r_0} C_E^*(r)rdr = \frac{K_ERV_c}{K_{VE}}\left[1 - \frac{(K_w/K_{VE}^{1/2})I_1(K_{VE}^{1/2})}{K_{VE}^{1/2}I_1(K_{VE}^{1/2}) + K_wI_0(K_{VE}^{1/2})}\right] \quad (8)$$

$K_E = k_Er_0^2/D$, L is the length of cylindrical reactor, and V_c is the volume.

The net contribution of heterogeneous collisional deactivation to the reaction, R_{wE}, is therefore

$$R_{wE} = R_{VE} - R_{wE} = \frac{R_{VE}(K_w/K_{VE}^{1/2})I_1(K_{VE}^{1/2})}{K_{VE}^{1/2}I_1(K_{VE}^{1/2}) + K_wI_0(K_{VE}^{1/2})} \quad (9)$$

R_{VE} is the total homogeneous rate in the absence of any wall effects and is defined as

$$R_{VE} = 2\pi Lk_E\int_0^{r_0} C_E^*(ss)rdr = k_EC_E^*(ss)V_c \quad (10)$$

where $C_E^*(ss) = [k_VC_M/(k_VC_M + k_E)]F(E)C_M$, the steady-state concentration that would exist in the absence of heterogeneity, and $F(E)$ is the appropriate distribution function expression.

In the low-pressure limit, the total rate of reaction becomes

$$R_{TE} = 2\pi Lk_E\int_0^{r_0} C_E^*(r)rdr = RV_c \quad (11)$$

which is the total rate of activation.

The Heterogeneity Function

As was done in the case of a thermal unimolecular reaction system,[1] we define heterogeneity for a chemical activation system, as it refers to collisional deactivation at the wall, in a general manner applicable to any pressure region. For a chemical activation system, the contribution of heterogeneity to the rate of reaction is a negative one. Thus, under equivalent conditions, the total observed rate, in a given size reactor, is less than the corresponding rate that would prevail in the same volume of a reactor of infinite extent. The heterogeneity function, $H(E)'$, is defined as

$$H(E)' = C_E^*(ss) - \langle C_E^*(r)\rangle$$

or

$$H(E) = 1 - \frac{\langle C_E^*(r)\rangle}{C_E^*(ss)} = \frac{(K_w/K_{VE}^{1/2})I_1(K_{VE}^{1/2})}{K_{VE}^{1/2}I_1(K_{VE}^{1/2}) + K_wI_0(K_{VE}^{1/2})} \quad (12)$$

$\langle C_E^*(r)\rangle$ is the average concentration of activated molecules

$$\langle C_E^*(r)\rangle = \int_0^{r_0} C_E^*(r)rdr \Big/ \int_0^{r_0} rdr$$

$H(E)$ is defined such that the limits are zero (no heterogeneity) and unity (complete heterogeneity).

Since $I_1(K_{VE}^{1/2})/I_0(K_{VE}^{1/2}) \rightarrow$ unity as $P \rightarrow \infty$, the high-pressure limit can be simplified to give

$$H(E) \approx K_{VE}^{-1/2}\left[\frac{K_{VE}^{1/2}}{K_w} + 1\right]^{-1} \quad (P \rightarrow \infty)$$

Although $I_1(K_{VE}^{1/2})/I_0(K_{VE}^{1/2})$ decreases below unity as $P \rightarrow 0$, it should be noted that the k_E's that apply to most chemical activation systems are in the range 10^5–10^9 sec^{-1}, in which case $I_1(K_{VE}^{1/2})/I_0(K_{VE}^{1/2})$ is not very different from unity. When one has the case $k_E > 10^5$ sec^{-1} as $P \rightarrow 0$, then $K_{VE}^{1/2}/K_w > 1$ and $H(E)$ can be approximated by $H(E) = K_w/K_{VE}$.

Results and Discussion

Heterogeneous Collisional Deactivation of Chemically Activated Ethane. As a practical example, we shall consider the heterogeneous collisional deactivation of vibrationally excited ethane produced as a result of acetone and azomethane photolysis.[4]

Shaw, Menczel, and Toby (SMT)[4] investigated the kinetics of vibrationally excited ethane produced in the photolysis of gaseous acetone (at 121, 216, and 298°

(4) H. Shaw, J. H. Menczel, and S. Toby, *J. Phys. Chem.*, **71**, 4180 (1967).

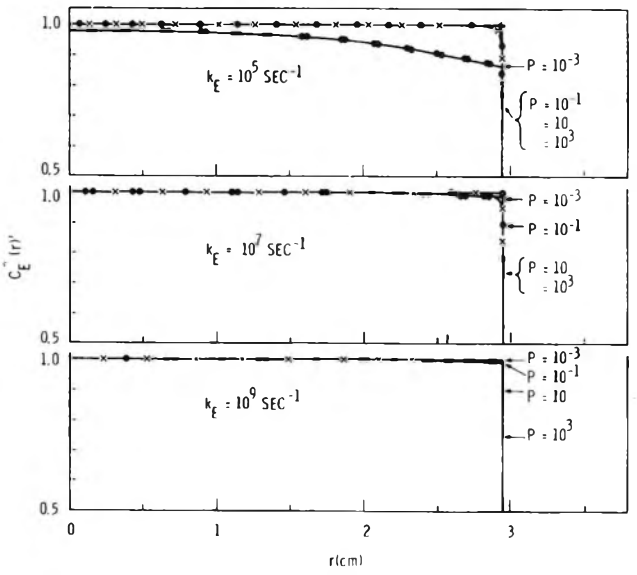

Figure 1. Concentration profiles $C_E^*(r)$ *vs.* r at 10^{-3}, 10^{-1}, 10, and 10^3 mm pressure for k_E's of 10^5, 10^7, and 10^9 sec^{-1} are shown. $C_E^*(r)$ *vs.* r profiles are represented by the following: -·-·-, 10^{-3} mm; -×-, 10^{-1} mm; ·-·-, 10 mm, and ——, 10^3 mm. SMT's value of $\sigma = 5.3$ Å was used for the complex of acetone with vibrationally excited ethane. Representative k_E's for the acetone system are 10^7–10^9 sec^{-1}.

over a 2000-fold pressure range) and gaseous azomethane (at 100, 135, 150, and 180° over a 1000-fold pressure range). The acetone photolysis was examined down to $\sim 10^{-1}$ mm and the azomethane photolysis down to 5×10^{-1} mm. In both cases, essentially negligible heterogeneous effects were observed. SMT passed the light beam through the center of the cell in the azomethane photolysis where the light beam diameter was ~42% of the cell diameter, and no significant heterogeneous component was introduced as a result of methyl radicals diffusing to the cell wall.

To illustrate the dependence of $C_E^*(r)$ on r, k_E, and pressure (P), concentration profiles[5a] at 10^3, 10, 10^{-1}, and 10^{-3} mm are shown in Figure 1 for the vibrationally excited ethane produced in the acetone photolysis. The low value of k_E ($= 10^5$ sec^{-1}), while not applicable to the vibrationally excited ethane produced in either the acetone or azomethane photolysis, is included to further illustrate the behavior of $C_E^*(r)$.

Specifically, the reduced concentration, $C_E(r)'$ ($= C_E^*(r)/C_E^*(\text{ss})$) is plotted *vs.* r in Figure 1. The only significant deviation of $C_E^*(r)$ away from $C_E^*(\text{ss})$ is at $P = 10^{-3}$ mm for $k_E = 10^{-5}$ sec^{-1}. This deviation decreases markedly as k_E increases even for $p = 10^{-3}$ mm. In other words, for large k_E's (or high energy), there is no appreciable wall deactivation of excited molecules (except immediately at the wall), due to the fact that an excited molecule with a high specific reaction probability will not diffuse very far from its point of origin before reaction takes place. However, in the case of small k_E's (or low energy), significant diffusion of the excited molecule away from its point of origin can indeed occur. Thus, even at very low pressure on a collisional deactivation basis (in the absence of catalytic effects), one should not observe any appreciable amount of heterogeneity for reactions with high specific reaction rates (*i.e.*, high average energy of the activated molecule).

An examination of $H(E)$ for representative k_E's confirms the experimental results of SMT (Table I). On a collisional deactivation basis (the strong collision assumption is implicit), for representative k_E's, the contribution of heterogeneity to the observed rate is indeed negligible even down to 10^{-3} mm as shown in Table I.

Table I illustrates that $H(E)$ is a strong function of E and, therefore, only approaches the simple collision theory result for very small values of k_E at zero pressure.[5b] Therefore, one cannot simply assess the heterogeneous component on a collisional deactivation basis by the comparison of the relative number of collisions with the wall to the number of collisions in the gas phase. It appears that systems[6,7] in which a large amount of heterogeneity is observed has to be explained in another manner. Particularly in the case of acetone photolysis at low pressure, Konstantatos and Quinn (KQ)[8] have shown that the following wall reaction between

$$CH_3 + [CH_3COCH_3]\ \text{wall} \longrightarrow CH_4 + [CH_3COCH_2\cdot]\ \text{wall}$$

methyl radicals and adsorbed acetone contributes significantly to the yield of methane below 7.5 mm pressure. In view of KQ results, the apparent increase in stabilized ethane could be explained by the reactions

$$CH_3\cdot + \cdot CH_2COCH_3 \longrightarrow C_2H_5COCH_3$$

$$C_2H_5COCH_3 + h\nu \longrightarrow C_2H_5\cdot + CH_3CO\cdot$$

$$C_2H_5\cdot + CH_3COCH_3 \longrightarrow C_2H_6 + CH_3COCH_2\cdot$$

$$C_2H_5\cdot + [CH_3COCH_3]\ \text{wall} \longrightarrow C_2H_6 + CH_3COCH_2\cdot$$

Since KQ have shown that φ ($= k(CH_4)/k(C_2H_6)^{1/2}$, where $k(CH_4)$ and $k(C_2H_6)$ are the observed rates of formation of methane and ethane, respectively) is inde-

(5) (a) The concentration profiles are given in Figure 1 for the acetone system at one temperature (121°), insofar as only one temperature is necessary to illustrate the salient aspects of the behavior of $C_E^*(r)$. k_w is taken as $\bar{c}/4$ where $\bar{c}$ is the mean speed. (b) The heterogeneity function averaged over the distribution function for the reacting molecule, $H(E)$, is

$$\langle H(E)\rangle = \int_{E_{min}}^{\infty} H(E)\left(\frac{k_E}{\omega + k_E}\right)F(E) \times dE \Big/ \int_{E_{min}}^{\infty}\left(\frac{k_E}{\omega + k_E}\right)F(E)dE$$

However, $H(E) \approx \langle H(E)\rangle$ for a representative k_E.

(6) A. D. Kennedy and H. O. Pritchard, *J. Phys. Chem.*, **67**, 161 (1963).

(7) S. W. Benson and G. N. Spokes, *J. Amer. Chem. Soc.*, **89**, 2525 (1967).

(8) J. Konstantatos and C. P. Quinn, *Trans. Faraday Soc.*, **65**, 2693 (1969).

Table I: The Variation of $H(E)$ As a Function of k_E and Pressure[a]

P, mm	F_w[b]	$H(E)$ $k_E = 10^6$ sec^{-1}	$H(E)$ $k_E = 10^7$ sec^{-1}	$H(E)$ $k_E = 10^9$ sec^{-1}
		$T = 121°$		
10^3	0.5543×10^{-6}	0.1669×10^{-6}	0.1425×10^{-6}	0.1356×10^{-6}
10^2	0.5543×10^{-5}	0.2003×10^{-5}	0.1980×10^{-5}	0.1311×10^{-5}
10	0.5543×10^{-4}	0.2042×10^{-4}	0.1939×10^{-4}	0.3384×10^{-5}
1	0.5540×10^{-3}	0.2036×10^{-3}	0.1383×10^{-3}	0.4188×10^{-5}
10^{-1}	0.5513×10^{-2}	0.1941×10^{-2}	0.3401×10^{-3}	0.4373×10^{-6}
10^{-2}	0.5252×10^{-1}	0.1330×10^{-1}	0.4211×10^{-3}	0.4411×10^{-5}
10^{-3}	0.3566	0.3328×10^{-1}	0.4399×10^{-3}	0.4433×10^{-5}
		$T = 216°$		
10^3	0.6880×10^{-6}	0.2308×10^{-6}	0.2266×10^{-6}	0.2156×10^{-6}
10^2	0.6880×10^{-5}	0.2500×10^{-5}	0.2478×10^{-5}	0.1571×10^{-5}
10	0.6879×10^{-4}	0.2536×10^{-4}	0.2343×10^{-4}	0.3844×10^{-5}
1	0.6875×10^{-3}	0.2525×10^{-3}	0.1599×10^{-3}	0.4675×10^{-5}
10^{-1}	0.6833×10^{-2}	0.2395×10^{-2}	0.3863×10^{-3}	0.4873×10^{-5}
10^{-2}	0.6437×10^{-1}	0.1586×10^{-1}	0.4709×10^{-3}	0.4921×10^{-5}
10^{-3}	0.4076	0.3765×10^{-1}	0.4906×10^{-3}	0.4927×10^{-5}
		$T = 298°$		
10^3	0.8033×10^{-6}	0.2329×10^{-6}	0.2362×10^{-6}	0.2307×10^{-6}
10^2	0.8033×10^{-5}	0.2936×10^{-5}	0.2894×10^{-5}	0.1779×10^{-5}
10	0.8032×10^{-4}	0.2961×10^{-4}	0.2780×10^{-4}	0.4205×10^{-5}
1	0.8026×10^{-3}	0.2946×10^{-3}	0.1814×10^{-3}	0.5074×10^{-5}
10^{-1}	0.7969×10^{-2}	0.2783×10^{-2}	0.4230×10^{-3}	0.5284×10^{-5}
10^{-2}	0.6437×10^{-1}	0.1730×10^{-1}	0.5090×10^{-2}	0.5329×10^{-5}
10^{-3}	0.4455	0.4106×10^{-1}	0.5304×10^{-3}	0.5336×10^{-5}

[a] The $H(E)$ values are given here for the acetone system. The k_E's for the azomethane system span essentially the same range as that for the acetone system; therefore, it would serve no real purpose to present the $H(E)$ values for both systems. [b] F_w is the fraction of the number of collisions with the wall of the reaction vessel as compared to the number of collisions in the gas phase (based on simple collision theory).

pendent of the incident light intensity when the surface process is important, it appears and is pointed out by KQ that direct photolysis of adsorbed acetone is not a significant process.[4]

Of course, in a thermal system where one has wall activation in addition to deactivation, $C_E^*(r)$ and $H(E)$ have the opposite dependence on E.

Since the average level populated by each mode of a large molecule is lower than that for a smaller molecule with the same critical energy, eq 12 (Figure 1, Table I) supports a very important experimental observation, namely, collisional deactivation processes increase in importance as the complexity of the reacting molecule increases (or as the number of degrees of vibrational freedom increase).[9-13]

Conclusions

Heterogeneous collisional deactivation, $[H(E)]$, is a strong function of energy and its contribution to the observed rate of reaction cannot be determined on the simple collision theory basis, except in the limit of unrealistically small k_E's. The large amount of heterogeneous effects, observed in some systems at low pressure, cannot be explained on a simple collision theory basis. It is therefore suggested that either a different reaction mechanism is operative in these systems and/or that catalytic effects may be the case.

Appendix

If $x \geq 10$ in $I_0(x)$ or $I_1(x)$, then $C_E^*(r)$ can be determined rather easily by means of a desk calculator with the use of the following approximations[14] for the modified bessel functions

$$I_0(K_{VE}^{1/2}r/r_0) \simeq \frac{0.3989 \exp(K_{VE}^{1/2}r/r_0)}{(K_{VE}^{1/2}r/r_0)} \times \left(1 + \frac{r_0}{8K_{VE}^{1/2}r} + \frac{9r_0}{128K_{VE}r^2} + \frac{75r_0^3}{1024K_{VE}^{3/2}r^3}\right)$$

(9) J. R. Dacey, W. C. Kent, and G. O. Pritchard, *Can. J. Chem.*, **44**, 969 (1966).

(10) H. Cerfontain and K. O. Kutschke, *ibid.*, **36**, 344 (1958).

(11) R. H. Riem and K. O. Kutschke, *ibid.*, **38**, 2332 (1960).

(12) J. L. Weininger and O. K. Rice, *J. Amer. Chem. Soc.*, **74**, 6216 (1952).

(13) R. W. Durham and E. W. R. Steacie, *Can. J. Chem.*, **31**, 377 (1953).

(14) N. W. McLachlan, "Bessel Function for Engineers," The Clarendon, Press, Oxford, 1955.

and

$$I_1(K_{VE}^{1/2}) \simeq \frac{0.3989 \exp(K_{VE}^{1/2})}{K_{VE}^{1/4}} \times \left(1 - \frac{3}{8K_{VE}^{1/2}} - \frac{15}{128K_{VE}} - \frac{105}{1024K_{VE}^{3/2}}\right)$$

Rearrangement of eq 7 gives

$$\frac{DK_{VE}C_E^*(r)}{Rr_0^2} = 1 - \left\{\frac{I_0(K_{VE}^{1/2}r/r_0)}{I_0(K_{VE}^{1/2})} \Big/ \times \left[\frac{K_{VE}^{1/2}}{K_w}\frac{I_1(K_{VE}^{1/2})}{I_0(K_{VE}^{1/2})} + 1\right]\right\}$$

where

$$\frac{I_0(K_{VE}^{1/2}r/r_0)}{I_0(K_{VE}^{1/2})} = \left(\frac{r_0}{r}\right)^{1/2} \exp\left[-K_{VE}^{1/2}\left(1 - \frac{r}{r_0}\right)\right] \times \left(\frac{1 + \frac{r_0}{8K_{VE}^{1/2}r} + \frac{9r_0^2}{128K_{VE}r^2} + \frac{75r_0^3}{1024K_{VE}^{3/2}r^3}}{1 + \frac{1}{8K_{VE}^{1/2}} + \frac{9}{128K_{VE}} + \frac{75}{1024K_{VE}^{3/2}}}\right)$$

and

$$\frac{I_1(K_{VE}^{1/2})}{I_0(K_{VE}^{1/2})} = \frac{1 - \frac{1}{8K_{VE}^{1/2}} - \frac{15}{128K_{VE}} - \frac{105}{1024K_{VE}^{3/2}}}{1 + \frac{1}{8K_{VE}^{1/2}} + \frac{9}{128K_{VE}} + \frac{75}{1024K_{VE}^{3/2}}}$$

Gas-Phase Recombination of Bromine Atoms[1]

by B. A. DeGraff* and K. J. Lang

Department of Chemistry, University of Virginia, Charlottesville, Virginia 22901 *(Received May 12, 1970)*

The gas-phase recombination of bromine atoms in the presence of various chaperons was studied by kinetic spectroscopy. Where comparison values for the recombination rate constant, k_M, are available, the results of this study are in good agreement with the most recent literature values. Room temperature values for k_M were determined to be $k_{CO} = (4.2 \pm 0.4) \times 10^9\ M^{-2}\ sec^{-1}$, $k_{CF_3Br} = (8.4 \pm 0.8) \times 10^9\ M^{-2}\ sec^{-1}$, $k_{SF_6} = (8.1 \pm 0.8) \times 10^9\ M^{-2}\ sec^{-1}$, $k_{CCl_4} = (20.9 \pm 2) \times 10^9\ M^{-2}\ sec^{-1}$, and $k_{C_6F_6} = (25.8 \pm 3) \times 10^9\ M^{-2}\ sec^{-1}$. The temperature dependence of k_M for three chaperons of rather different efficiencies was studied from room temperature to 100°. Apparent "activation energies" for Ne, SF_6, and CCl_4 are −0.98, −1.83, and −2.44 kcal/mol, respectively. The relative importance of the "energy transfer" and "radical–molecule complex" mechanisms is discussed. The results for bromine recombination are compared with those available for iodine and chlorine.

Introduction

The homogeneous recombination of atoms following dissociation of the parent diatomic molecule by shock-wave, microwave discharge, or flash photolysis has been studied intensively. Of the various systems studied, the recombination of iodine atoms has been examined over a wider range of conditions and chaperons than any other. The recombination of bromine atoms has received somewhat less attention, due in part to experimental difficulties which can be traced either to bromine's weaker visible absorption spectrum or to the high reactivity of the atoms. The latter consideration has tended to limit the chaperons used in bromine recombination studies to the rare gases and a few diatomic molecules.

One of the most interesting results of the iodine studies is the very high efficiency shown by certain chaperons in promoting recombination (*e.g.*, alkyl iodides, aromatic hydrocarbons, and iodine).[2a] To account for this, a charget-transfer type of atom–chaperon interaction has been suggested.[2b] Because of bromine's higher electron affinity, it is of interest to see if it spanned a similar range of recombination rates with different chaperons and further to see if charge-transfer or other specific interactions are needed to correlate the observed rate constants on the basis of the simpler termolecular recombination models. To this end we have determined, by kinetic spectroscopy, the termolecular recombination rate constants and "activation energies" for bromine atoms in the presence of various chaperons of differing molecular complexity. Since we also wished to check the flash apparatus recently constructed

* To whom correspondence should be addressed.

(1) Presented in part at the 21st Southeast Regional American Chemical Society Meeting, Richmond, Va., Nov 1969.

(2) (a) K. E. Russell and J. Simons, *Proc. Roy. Soc. Ser. A*, **217**, 271 (1953); (b) G. Porter and J. A. Smith, *ibid.*, **261**, 28 (1961).

in our laboratory, we also determined recombination rate constants using several chaperons for which comparison values were available. While this paper was in preparation, a study of the bromine recombination over a wide temperature range was reported.[3] In the following we compare, where possible, our results with those presently in the literature and present some new results with polyatomic chaperons and discuss their implication.

Experimental Section

The flash photolysis system was of generally conventional design. Four 5-μF, low-inductance capacitors were discharged through two 25-cm flash tubes filled with a xenon–hydrogen mixture. The 20-cm photolysis cell was mounted coaxially to the lamps and both lamps and cell were mounted in an aluminum chamber which served as a reflector and oven. The analysis light was a 200-W mercury–xenon arc powered by two 12-V truck batteries. A Beckman quartz monochromator with a 300μ-slit served to isolate the monitoring wavelength, 440 nm. A 1P28 photomultiplier biased at 375–425 V was used as the detector. Following the suggestion of Davidson,[4] the final dynode was biased with its own battery supply.

Lamp intensity, extinction coefficients, and photometric concentration determinations were done with the same optical arrangement but with the photomultiplier output dc coupled and displayed on a 0–10 mV recorder whose exact span had been accurately determined. Both the dc and ac coupled systems were checked for linear response by neutral density filters over the optical density range $0 \rightarrow 2$. The ac response of the detection circuit was checked with a 1 MHz square wave generator and was found adequate and linear over the range of signals encountered in this work.

The chaperon materials used in this study were of reagent grade and used without further purification. The bromine was dried over P_2O_5 and twice distilled. All stopcocks were greased with Kel-F or were of the Teflon plug, O-ring type.

The photolysis cell was filled using a conventional glass vacuum line. A Teflon plug, Viton O-ring stopcock served to seal the cell and it was found that mixtures could be kept for several weeks with no appreciable change. To load the cell, bromine was distilled into a calibrated volume to a pressure of 10–20 Torr as measured by a glass spoon gauge–oil manometer combination. The vapor was then expanded into another volume so that the final cell pressure was between 2.2 and 3.2 Torr. The cell was then placed in the optical train and its transmission noted. Next the chaperon or mixture of chaperons was added to the cell and this mixture flashed about ten times to mix the gases. After this flashing procedure the optical density of the sample was again determined to detect any permanent chemical change. When the chaperon absorbed light at $\lambda > 200$ nm a sleeve of No. 7740 glass was placed around the cell. With this precaution no permanent chemical changes in the sample were observed. The manometric and photometric values of the bromine pressure agreed to within 5%, the limit of the manometric measurement. The photometric value was always used in calculations (ϵ = 140 l./mol-cm at 440 nm, in good agreement with Seery and Britton[5]).

Because of small fluctuations in the arc, it was necessary to determine the base line for each kinetic trace. This was accomplished by initiating the flash sequence from the oscilloscope. The scope sweep was triggered manually and after 150 μsec a 15-V pulse from the scope triggered the gate on a monostable multivibrator which in turn fired the 35-kV trigger to discharge the flash lamps. The oscilloscope traces were recorded on Polaroid film.

The cell temperature was varied by wrapping the aluminum housing (*vide supra*) with heating tape and adjusting the current until the desired temperature was obtained. Three calibrated copper–constantin thermocouples were used to monitor the temperature along the reaction cell. The greatest temperature differential observed between any two thermocouples was 0.4° in the room to temperature 100° range used for this work.

Thermal Effects. The observation that a radially nonuniform distribution of sample gas can result from the thermal gradient generated by the heat released from the recombination has been made by several workers.[4,6,7] The severity of the effect is a function of, among other things, the percentage of dissociation, the energy of the "average" absorbed quantum, the cell volume sampled by the analysis beam, and the time span over which the observations are made. Several approaches have been put forth to correct for this effect[8–10] but it appears that at best these corrections require additional experiments and still leave some uncertainty in the correction factor. However, through choice of experimental conditions, thermal effects can be minimized[9,10] even for experiments in which large temperature changes are expected.[11]

For this work the flash energies centered around 850 J which produced a 12–15% initial decomposition of the bromine which should generate a 10 to 20° temperature rise in the sample gas at the completion of the

(3) J. K. K. Ip and George Burns, *J. Chem. Phys.*, **51**, 3414 (1969).
(4) D. L. Bunker and N. Davidson, *J. Amer. Chem. Soc.*, **80**, 5085 (1958).
(5) D. J. Seery and D. Britton, *J. Phys. Chem.*, **68**, 2263 (1964).
(6) M. I. Christie, A. J. Harrison, R. G. W. Norrish, and G. Porter, *Proc. Roy. Soc. Ser. A*, **231**, 446 (1955).
(7) G. Burns and D. F. Hornig, *Can. J. Chem.*, **38**, 1702 (1960).
(8) W. G. Givens and J. E. Willard, *J. Amer. Chem. Soc.*, **81**, 4773 (1959).
(9) M. R. Basila and R. L. Strong, *J. Phys. Chem.*, **67**, 521 (1963).
(10) G. Burns, *Can. J. Chem.*, **46**, 3229 (1968).
(11) G. Burns, *ibid.*, **45**, 2369 (1967).

recombination. For a few special experiments a temperature rise of up to 40° was expected. The analysis beam sampled between $^1/_2$ and $^2/_3$ of the cell volume. Experiments were done holding the flash energy and bromine concentration constant, but the $[Br_2]/[M]$ ratio was varied from 2.5 to 30 $\times$ 10^{-3} for three inert gases (He, Ne, and Ar). Data taken at 100-μsec intervals starting at 120 μsec and completed by 1 msec after the flash gave consistent values of k_{obsd} over the whole range of $[Br_2]/[M]$ ratios and individual plots of $1/[Br]$ *vs.* time showed no discernible curvature. However, when the observation period extended to 2 msec, the values of k_{obsd} for $[Br_2]/[M] \geq 15 \times 10^{-3}$ were systematically lower than expected and the plots of $[Br]^{-1}$ *vs.* time showed some curvature at longer observation times. These deviations were most severe in the case of helium. Thus, as observed by others, thermal effects can be minimized by taking the data in the earlier stages of the recombination. Since the experiments just described were calculated to have a temperature increase greater than or equal to the most severe conditions in this study, no corrections for thermal effects were made inasmuch as the observation period never extended beyond 1 msec.

Kinetic Effects. As a consequence of taking the data at short time intervals after the flash, the concentration of Br_2 during the observation period is significantly lower than for the unflashed mixture and is changing rapidly during this period. Since the observed rate constant contains a contribution from Br_2 as a chaperon, the value of k_{obsd} should increase as the recombination progresses. This effect is significant when the percentage of dissociation is high and the halogen is an efficient third body.[12] For this study, the change in the percentage dissociation from the first point to last was typically between 5 and 7%. While the $[Br_2]/[M]$ ratio used for plots to determine k_M (*vide infra*) were corrected to the average Br_2 concentration during the observation period, no attempt was made to correct each datum for the dissociated bromine. The justification for this lies in the fact that bromine is an average chaperon and because of the relative concentrations of chaperon and bromine, the recombination with bromine as chaperon was usually less than 10% of the total rate. Hence the small correction due to changes in the bromine contribution would be much less than experimental error.

Results

As with previous studies, the data could be adequately treated by

$$\frac{-d[Br]}{dt} = 2k_{obsd}(M,T)[Br]^2[M] \qquad (I)$$

where $k_{obsd} = k_M + [Br_2]/[M]\, k_{Br_2}$. The contribution from atomic bromine as a chaperon was neglected.

The voltage–time data were read from photographs of the oscilloscope trace. This was converted to concentration–time units and least-squares fitted to the integrated form of (I) by a B5500 computer. This was done for each experiment or trace, and at least eight experiments at a given $[Br_2]/[M]$ ratio were used to determine the value of k_{obsd}. When appropriate, computer plots were made to check for systematic curvature or other abnormalities. Using at least six values of $[Br_2]/[M]$ spanning a tenfold range in the ratio, plots of k_{obsd} *vs.* $[Br_2]/[M]$ were constructed to assign values to k_M and k_{Br_2}. However, for the more efficient chaperons (*e.g.*, $k_M > 1 \times 10^{10}$ l.^{2}/mol^2-sec) the slope of such plots is somewhat arbitrary due to comparable magnitudes of the bromine term and the absolute value of the experimental error. The standard deviation of k_{obsd} ranged from $\pm 5\%$ for the inert gases to $\pm 9\%$ for hexafluorobenzene and carbon tetrachloride. The higher deviation arises from the fact that for efficient third bodies the scope deflection becomes rather small toward the end of the observation period as recombination is nearly complete and hence the signal/noise ratio is lower *vis-à-vis* a less effective third body.

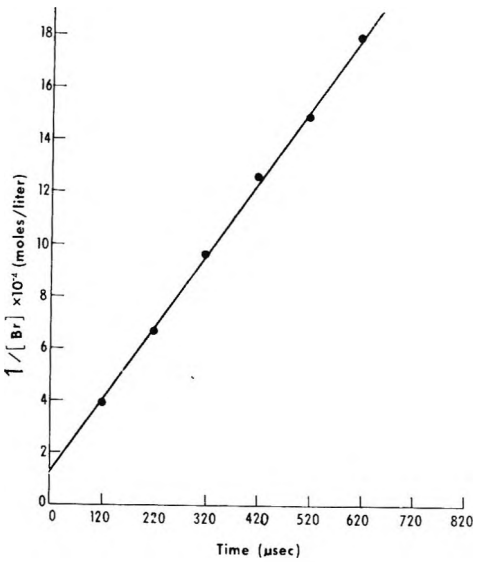

Figure 1. Second-order plot of bromine atom recombination following flash photolysis of a bromine–sulfur hexafluoride mixture. $[Br_2]/[SF_6] = 3.2 \times 10^{-2}$.

Figures 1 and 2 show representative plots for determining k_{obsd} and k_M, respectively, for sulfur hexafluoride as a chaperon. The best values for k_{Br_2} were felt to be those obtained with helium, neon, or argon as chaperons. Table I presents the room temperature values of k_M for bromine recombination determined in this study along with some other data to be discussed in the next section. Table II presents a comparison of room temperature rate constants available in the literature with the results of this study.

(12) R. Engleman, Jr., and N. R. Davidson, *J. Amer. Chem. Soc.*, **82**, 4770 (1960).

Table I: Observed and Calculated Room Temperature Rate Constants for Halogen Atom Recombination

	Br recombination				
Chaperon	k_M calculated from "energy transfer mechanism" only; $k_M \times 10^{-9}$ M^{-2} sec^{-1}	k_M calculated from "radical–molecule complex mechanism" only; $k_M \times 10^{-9}$ M^{-2} sec^{-1}	k_M calculated from combined mechanism; $k_M \times 10^{-9}$ M^{-2} sec^{-1}	k_M (experimental values) $k_M \times 10^{-9}$ M^{-2} sec^{-1}	I recombination $k_M \times 10^{-9}$ M^{-2} sec^{-1} (experimental values)
He	0.052			1.2 ± 0.1	1.5[a]
Ne	0.104	0.674	0.778	1.5 ± 0.1	1.9[b]
Ar	0.114	2.91	3.02	2.2 ± 0.2	2.9[a]
N_2	0.133	2.59	2.72	3.3 ± 0.3	4.5[c]
CO	0.136	2.82	2.96	4.2 ± 0.4	6.3[d]
CF_3Br	0.119	11.2	11.3	8.4 ± 0.8	15.7 (CF_3I)[e]
SF_6	0.113	10.5	10.6	8.1 ± 0.8	
CCl_4	0.146	24.0	24.1	20.9 ± 2	50.4[c]
C_6F_6	0.132	22.3[g]	22.4	25.8 ± 3	50[f]
X_2	0.113	35.0	35.1	44.2 ± 10	1368[a]

[a] Data from reference 2. [b] Data from reference 22. [c] Data from reference 1. [d] Calculated from data in reference 12. [e] Estimated from data in G. S. Laurence, *Trans. Faraday Soc.*, **63**, 1155 (1967). [f] Unpublished data, this laboratory. [g] Lennard-Jones parameters for benzene were used for this calculation.

Table II: Room Temperature Recombination Rate Constants of Br Atoms in Selected Third Bodies, *M*

M	$k_M \times 10^{-9}$ M^{-2} sec^{-1}	Reference
He	1.4 ± 0.2	a
	1.3 ± 0.1	b
	1.1 ± 0.2	c
	1.2 ± 0.1	d
Ar	2.4 ± 0.5	a
	2.8 → 3.6	e
	2.7	f
	3.0	b
	2.4	g
	2.4 ± 0.2	c
	2.2 ± 0.2	d
N_2	4.5 ± 0.7	a
	3.43 ± 0.33	e
	3.3 ± 0.2	c
	3.3 ± 0.3	d
Ne	1.5 ± 0.1	c
	1.5 ± 0.1	d
Br_2	43 ± 13	h
	260	i
	48	j
	49	f
	44 ± 10	d

[a] E. Rabinowitch and W. C. Wood, *Trans. Faraday Soc.*, **32**, 907 (1936). [b] See ref 7. [c] See ref 3. [d] This work. [e] R. L. Strong, J. C. W. Chien, P. E. Graf, and J. E. Willard, *J. Chem. Phys.*, **26**, 1287 (1957). [f] See ref 9. [g] P. Cadman, Ph.D. Thesis, University of Birmingham, England, 1965. [h] See ref 10. [i] See ref 8. [j] M. I. Christie, R. S. Roy, and B. A. Thrush, *Trans. Faraday Soc.*, **55**, 1139 (1959).

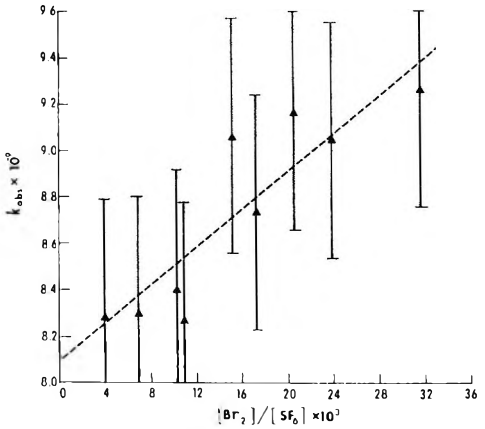

Figure 2. Plot of the observed rate constant as a function of the bromine/chaperon ratio for SF_6 as chaperon.

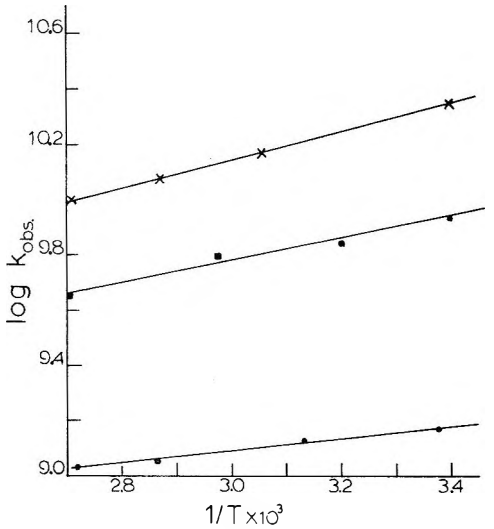

Figure 3. Arrhenius plot of the observed rate constants for bromine recombination with neon, ●; sulfur hexafluoride, ■; and carbon tetrachloride, ×; as chaperons.

Apparent activation energies were determined for three of the chaperons with widely varying efficiency. An Arrhenius plot for these chaperons is shown in Figure 3. The $[Br_2]/[M]$ ratio for the temperature depen-

dence studies was such that the contribution to k_{obsd} by the k_{Br_2} term was less than 6% at room temperature. Since the reported value of the "activation energy" for bromine as a chaperon is not greatly different than the values found for the three chaperons studied,[8] the error in interpreting the temperature dependence of the observed rate constant in our studies as arising solely from the k_M term is well within experimental error.

Discussion

From a comparison of the spectral distribution of the flash light and the absorption spectrum of bromine, it was evident that some of the dissociation could produce $Br(^2P_{1/2})$ atoms. The question arises as to whether the observed recombination rates contained any contribution from mechanisms in which one or both of the atoms were excited. Recent studies by Donovan and Husain[13] indicate that relaxation of $Br(^2P_{1/2})$ atoms by Br_2 is fairly efficient. Using their rate constants, we calculate that with our experimental conditions the relaxation reaction would have passed through 10 half-lives in less than 10 μsec after the flash. Further, the thermal equilibrium population of $Br(^2P_{1/2})$ atoms is negligible around room temperature. Thus we conclude that our observed rates represent the recombination of ground state atoms.

As shown in Table II, the agreement between our room temperature rate constants and those available from the literature is reasonably good. The correspondence is particularly good for the recent work of Ip and Burns. Our value for bromine as a chaperon is a simple average taken from the slopes of k_{obsd} *vs.* $[Br_2]/[M]$ plots for He, Ne, and Ar as the majority chaperon.

The close agreement between our values and those of Ip and Burns provides some insight into the need for "thermal effect" corrections. Thus Ip and Burns used a smaller percentage dissociation and lower bromine concentration coupled with a longer absorption path than used previously to reduce the expected temperature rise so that no effect was expected. In our work a relatively high atom concentration was generated. However, a short observation period was used to avoid the problems due to density gradients resulting from the cooling of the reaction mixture at the cell walls.[6] Burns and Hornig[7] have suggested that "thermal effects" can also arise from a radially nonuniform distribution of radicals resulting from the flash. In experimental terms this effect should be most pronounced when a single tube without reflector is used to flash an optically dense sample. For our apparatus, using two tubes and a circular reflector, crude calculations indicate that this effect should not be troublesome as long as the linear approximation to Beer's Law using the "average extinction coefficient" is valid for the sample across the cell diameter. On one occasion a mixture of hexafluorobenzene and bromine was flashed with the Pyrex sleeve accidentally omitted and strong pressure oscillations were observed in the scope trace.

The temperature coefficients of selected rate constants are reported in terms of "apparent activation energies." Our results for Ne cast in the form used by Ip and Burns yield $\log k_{Ne} = (9.18 \pm 0.02) - (1.58 \pm 0.08) \log (T/300)$ in reasonable agreement with their value. Comparison values are not available for SF_6 and CCl_4.

The mechanism of recombination can be described by the following sequence.

$$X + X \underset{k_{-1}}{\overset{k_1}{\rightleftharpoons}} X_2^* \quad (1)$$

$$X_2^* + M \xrightarrow{k_2} X_2 + M \quad (2)$$

$$X + M \underset{k_{-3}}{\overset{k_3}{\rightleftharpoons}} XM \quad (3)$$

$$XM + X \xrightarrow{k_4} X_2 + M \quad (4)$$

These steps could be further subdivided, but this outline will suffice for the following discussion. Reactions 1 and 2 have been called the "energy transfer mechanism," while the sequence 3 and 4 has been termed the "radical-molecule complex mechanism." From even simple calculations it is evident that both mechanisms contribute under experimental conditions such as those in this study and the relative contribution is naturally dependent on the model one uses for calculation.

Numerous approaches of varying sophistication have been suggested for calculating the overall observed rate constants.[14-19] From the standpoint of a physical picture it is useful to consider some of the simpler models since these yield results comparable to the more sophisticated calculations and focus attention on the major physical effects which govern the recombination process.

Following Rabinowitch,[17] we have calculated the contribution of reactions 1 and 2 to the recombination rate constant. That is

$$k_M = p_1 z_1 p_2 z_2 \tau N^2 \times 10^{-6} \text{ (l.}^2\text{/mol}^2 \text{ sec)}$$

where $p_1 z_1$ and $p_2 z_2$ are the steric factor and collision rate per molecule for Br + Br → and Br^*_2 + M →, respectively, and τ is the vibrational period of Br^*_2. The steric factor for Br + Br → was taken as $^1/_{16}$ while that for Br^*_2 + M → was taken as $^1/_2$ since a collision may involve excitation or deexcitation by about kT. The

(13) R. J. Donovan and D. Husain, *Trans. Faraday Soc.*, **62**, 2643 (1966).

(14) E. Wigner, *J. Chem Phys.*, **5**, 720 (1938).

(15) J. E. Keck, *ibid.*, **29**, 410 (1958); **32**, 1035 (1960).

(16) J. C. Light, *ibid.*, **36**, 1016 (1962).

(17) E. Rabinowitch, *Trans. Faraday Soc.*, **33**, 283 (1937).

(18) D. L. Bunker and N. Davidson, *J. Amer. Chem. Soc.*, **80**, 5090 (1958).

(19) S. Y. Kim, *J. Chem. Phys.*, **46**, 123 (1967).

collision rates were corrected crudely for angular momentum effects and nonhead-on collisions through the use of a Lennard-Jones attractive term. The value of τ was taken to be 10^{-13} sec. The rate constants calculated with these assumptions are shown in column two of Table I.

Assuming that our calculations are good to an order of magnitude, the "energy transfer" contribution to the rate at room temperature is expected to be small and does not account for the widely differing chaperon efficiencies. The two major uncertainties in the estimates are the steric factor for and the duration of the Br·Br collision. From considerations of electronic degeneracy a factor of $^1/_{16}$ is predicted. Bunker[20] has argued that for iodine it should not be greater than $^1/_8$ and is probably closer to $^1/_{16}$. For bromine, with weaker spin-orbit coupling, a factor of $^1/_{16}$ seems most reasonable. If we take as an upper limit to τ the time for a thermalized bromine atom to traverse the distance from which the Lennard-Jones attractive term is 5% of its maximum to σ and back, τ has a value of 2×10^{-12} sec. This is a very generous upper limit, but does indicate that the true value lies in the range 10^{-13} to 10^{-12} sec.

Other methods for calculating the "energy transfer" mechanism's contribution which allow for additional degrees of freedom to participate in the energy exchange have been used.[21] However, like the method discussed above, it does not reproduce well the temperature dependence near room temperature and cannot accommodate the observed variation in chaperon efficiency without unrealistic assumptions regarding the number of contributing degrees of freedom.

The reaction sequence (3)–(4) has been treated theoretically by several investigators using the basic assumption that step (3) is in equilibrium and that the classical expression for K_3 is valid. Using the approach of Bunker and Davidson,[18] we calculated the expected contribution of the radical–molecule complex mechanism when only bound states are considered in calculating K_3. The calculation was done with (ϵ/k) for the Br atom equal to the value for Kr and also using the value for Br_2. The latter choice is felt to allow, albeit somewhat crudely, for the rather different electronegativity properties expected of a bromine atom *vis-á-vis* an inert gas atom. The collision diameter of the Br atom was taken to be the L-J σ value for Kr. The Br–M potential was cast as a central force model, namely the Lennard-Jones potential. The chaperons used in this study were all of high symmetry specifically to improve this approximation. The value of k_4 was calculated from the simple collision model but corrected by a Lennard-Jones attractive potential term (*vide supra*).

The values of k_M obtained using the (ϵ/k) value for Br_2 and a best average fit steric-degeneracy product term of 0.10 (except for k_{Br_2} for which a value of 0.2 was used) are shown in the third column of Table I. A similar set of values was obtained when (ϵ/k) for Kr was used as the Br atom potential term. In this case the best steric-degeneracy product term was 0.23. Both sets of values calculated by this method do follow the observed trend of chaperon efficiency and are absolutely correct to within a factor of two. However, if, as suggested by Kim[19] and others, the value of the electronic degeneracy term should be between $^1/_{16}$ and $^1/_8$ and the steric factor for reaction 4 is 0.5 except for Br_2 as a chaperon, then both sets of calculations demand steric-degeneracy terms which are too large. Also, the temperature dependence of the rate constants calculated using the B and D model do not reproduce the experimental values very closely. As an example, when log k_M *vs.* T^{-1} is plotted for CCl_4 using rate constants calculated by the B and D method using the (ϵ/k) value for Br_2 for Br atoms, an "apparent activation energy" of -1.0_5 kcal/mol is obtained as compared to the observed value of -2.4_4 kcal/mol. It would appear that the difficulties with the steric-degeneracy term and the temperature dependence are, in part, due to a poor choice of potential values. The $(\epsilon/k)_{BrM}$ values obtained from the mixture rule using the (ϵ/k) values of Br_2 for the Br atom are too low by a factor of about four as compared with the experimental values (*vide infra*). This discrepancy has been noted previously for the case of iodine.[19]

In order to obtain a better fit with the observed temperature dependence of the various k_M's, Porter and Smith,[2b] and later Kim[19] suggested models based on reactions 3 and 4, but which used the experimental data to define the interaction potential. Using the model of Porter and Smith[2b] we calculated the expected room temperature rate constants for Ne, SF_6, and CCl_4 as chaperons. The results, shown in Table III, were obtained using an L-J attractive term to "correct" the collision rate of reaction 4 and the steric-degeneracy term was taken to be $^1/_{32}$. The agreement is reasonably good.

Table III: Calculated and Observed Rate Constants and Arrhenius Parameters for Bromine Atom Recombination

	Observed			Calculated[a]
Chaperon	E_a, kcal/mol	$A \times 10^{-8}$, M^{-2} sec^{-1}	k_M (25°), M^{-2} sec^{-1}	k_M (25°), M^{-2} sec^{-1}
Ne	−0.98	2.8	1.5×10^9	0.97×10^9
SF_6	−1.83	3.7	8.1×10^9	6.9×10^9
CCl_4	−2.44	3.4	20.9×10^9	25.1×10^9

[a] Computed as per reference 2.

As Kim[19] has pointed out, rather different sets of σ

(20) D. L. Bunker, *J. Chem. Phys.*, **32**, 1001 (1960).
(21) H. B. Palmer and D. Hornig, *ibid.*, **26**, 98 (1957).

and (ϵ/k) values can yield nearly equivalent results. Hence, it seems unprofitable to "interpret" such calculations as those done here. Both of the latter calculations, however, emphasize the importance of the chemical nature of the chaperon, a view which is borne out by experiment. Still somewhat vague is the answer to the question of when the atom–chaperon interaction is best described by a potential derived from dispersive forces such as the Lennard-Jones and when more specific interactions such as the charge transfer type need to be included. Because of the uncertainty in other parameters, specifically the correct collision diameters and steric factors, used in computing the rate constant, a comparison of calculated and experimental values on absolute terms may be misleading. As with iodine recombination the efficiency of a molecule as a chaperon can be crudely correlated with one of several parameters such as boiling point, critical temperature, ionization potential, and others.[2,6] However, the crudeness of fit in all cases would seem to preclude a detailed interpretation.

For iodine recombination with the chaperons such as I_2 and NO,[22] the formation of a semistable intermediate seems almost certain. For bromine recombination with Br_2 as the chaperon, the rate constant is much less than for iodine, but quite similar to that found for the recombination of chlorine atoms with Cl_2 as the chaperon ($k_{Cl_2} \simeq 27 \times 10^9$ l.^{2}/mol^2-sec).[23] Interestingly, the rate constant for argon as a chaperon is nearly the same for the recombination of I, Br, and Cl atoms.[24]

A comparison of values for k_M found in this work with those for the same chaperon for I atom recombination (see Table I) shows the values are quite similar for the inert gases and diatomics except the halogen itself. In all cases the iodine value is greater. For CCl_4 and C_6F_6 the value of k_M is a factor of two greater for I than for Br recombination. Since both of these chaperons are expected to have some charge-transfer interaction, factors other than the electron affinity of the acceptor must be the dominant influence. If we interpret the temperature dependence in terms of bond strengths, it appears that bromine forms complexes with bond energies comparable to that of iodine and that the rate constants differ in the A factor. Due to uncertainties in the quantities used in calculating the A factor, no one term can be singled out as being responsible. As predicted by Porter and Smith's model, for the same halogen the majority of the variation in k_M's results from changes of the X–M bond strength, as reflected by the observed differences in the temperature dependence of the k_M's.

Acknowledgments. This research was supported in part by the Petroleum Research Fund, the Cottrell Fund of the Research Corporation, and the National Science Foundation.

(22) G. Porter, Z. G. Szabo, and M. G. Townsend, *Proc. Roy. Soc., Ser. A*, **270**, 493 (1962).

(23) L. W. Bader and E. A. Ogryzlo, *Nature*, **201**, 491 (1964).

(24) E. Hutton and M. Wright, *Trans. Faraday Soc.*, **61**, 78 (1956).

The Reaction of Ozone with Carbon Disulfide

by Kenneth J. Olszyna[1] and Julian Heicklen*

Department of Chemistry and Center for Air Environment Studies, The Pennsylvania State University, University Park, Pennsylvania 16802 *(Received June 8, 1970)*

The reaction of O_3 with CS_2 was found to be rapid at room temperature (~30°). Ozone disappearance was monitored by absorption spectroscopy and followed the rate law, $-d[O_3]/dt = k'[O_3]^2/[O_3]_0$, where $[O_3]_0$ is the initial value of $[O_3]$ in any experiment. This rate law held for at least 80% decomposition. The rate constant k' is 1.13 min^{-1} for most conditions but does rise to a maximum value of about 3.0 min^{-1} for $[CS_2]/[O_3]_0 \sim 3$. The reaction has been studied for CS_2 pressures from 0.9 to 80 Torr, initial ozone pressures of 0.15–4.0 Torr, and $[CS_2]/[O_3]_0$ ratios from 1.0 to 530, in an unpacked cell and one packed with glass beads, and in the presence of foreign gases. The results are the same in the packed and unpacked cell if the cells are conditioned. Otherwise, the results are not reproducible. The products of the reaction are O_2, SO_2, OCS, CO, and CO_2 in the relative amounts, normalized to $[O_3]_0$, of 0.85, 0.36, 0.16, 0.10, and 0.03. Also produced is a polymer and probably SO_3. The products do not influence the reaction when added in amounts comparable to those produced. However, NO_2 or an excess of SO_2 inhibits the reaction and the rate law becomes third order in $[O_3]$. The results are interpreted by a chain mechanism involving O atoms, CS, SO, and excited molecules as carriers, with the carbon-containing products coming from the reaction of ozone with CS. The initiating step is almost surely the slow heterogeneous decay of ozone.

Introduction

Carbon disulfide is used as a solvent in industrial processing, notably in rubber and viscose rayon manufacture. It may also be present in small amounts in petroleum. Consequently it may be emitted into the atmosphere and undergo oxidation.

During the oxidation of CS_2, the intermediates CS and SO have been observed in the cold flame,[2a,b] in the explosion,[3] and in photochemical oxidation.[4,5] An examination of the oxidation of these species will aid our understanding, not only of CS_2 oxidation, but also of the oxidation of other compounds which can produce these intermediates. For example, CS has been reported in the photolysis of thiophene[6] and should be produced in the photolysis of thioketones and thioaldehydes. We have evidence in our laboratory[7] that SO can be produced in the photolysis of SO_2 at 3130 Å in the presence of CO or C_2F_4.

We have initiated a comprehensive program for studying the oxidation of CS and SO. In this paper we present our results on the room temperature studies of the reaction of O_3 with CS_2. Apparently this reaction has not been studied previously.

Experimental Section

Most of the gases used were from the Matheson Co. These included extra dry grade O_2, CP grade CO, and Technical grade NO (98.5%), all of which were used without further purification. Anhydrous grade SO_2 showed no impurities and was used after degassing at −196°. Commercial grade CO_2 showed one unidentified impurity (~3%), but was used without purification except for degassing at −196°. The introduction of CO_2 into the O_3–CS_2 reaction had no noticeable effect, so the impurity is of no consequence. The OCS contained about 3% CO_2 and much smaller amounts of H_2S. Since CO_2 does not influence the reaction and the amount of H_2S is too small to be of any significance, the OCS was not purified. It was used after degassing at −196°. Both Fisher Scientific Co. spectral grade and Matheson Coleman and Bell reagent grade CS_2 were used after degassing at −196°. No impurities were present.

Ozone was prepared from a tesla coil discharge through O_2. In the initial experiments the O_3 was collected at −196° and the residual O_2 removed. For later experiments the ozone was triply distilled at −186° and collected at −196° with continuous degassing. The undistilled ozone was used for the results reported in Tables I–III and Figures 1–4, 9 and 10, whereas the triply distilled ozone was used for the results reported in Tables IV and V and Figures 5–8.

Gas pressures were measured by an H_2SO_4 manometer. The O_3 pressure was checked by optical absorption at 2537 Å. The gases were introduced into the cell and the reaction monitored continually by ultraviolet absorption spectroscopy utilizing low intensities so that photochemical reaction was not induced by the moni-

* To whom correspondence should be addressed.

(1) U. S. Public Health Service Air Pollution Trainee.

(2) (a) V. N. Kondratiev, *Zh. Fiz. Khim.*, **13**, 1260 (1939); as reported in *Chem. Abstr.*, **35**, 3544 (1941); (b) V. N. Kondratiev, *Zh. Fiz. Khim.*, **14**, 287 (1940); as reported in *Chem. Abstr.*, **36**, 4011[6] (1942).

(3) A. L. Myerson, F. R. Taylor, and P. L. Hanst, *J. Chem. Phys.*, **26**, 1309 (1957).

(4) V. N. Kondratiev and A. Yakovleva, *J. Exp. Theor. Phys.*, **10**, 1038 (1940).

(5) F. J. Wright, *J. Phys. Chem.*, **64**, 1648 (1960).

(6) H. A. Wiebe and J. Heicklen, *Can. J. Chem.*, **47**, 2965 (1969).

(7) E. Cehelnik and C. Spicer, unpublished results, Pennsylvania State University, 1969.

Table I: Reaction of CS_2 with Undistilled O_3

$[O_3]_0$, Torr	$[CS_2]$, Torr	Temp, °C	k, Torr^{-1} min^{-1}	$[O_2]/[O_3]_0$	$[CO]/[O_3]_0$	$[CO_2]/[O_3]_0$	$[OCS]/[O_3]_0$	$[SO_2]/[O_3]_0$	[P]/$[O_3]_0$, absorbance/ Torr	$\frac{[OCS]+2[CO]+2[CO_2]}{[SO_2]}$	$\frac{\Sigma[O]}{3[O_3]_0}$
0.147	80	26	9.5	0.64	0.068	0.053	0.225	0.419	0.054	1.12	0.96
0.202	6.9	27.4	7.6	0.76	0.086	0.064	0.204	0.394	0.030	1.14	0.87
0.200	76	26	7.7								
0.460	18.5	33.7	3.77	0.612		0.063	0.154	0.359	0.0065		
0.480	26	32.8	4.65[a]	0.761	0.098	0.046	0.179	0.396	0.0083	1.19	0.89
0.666	23	28.8	2.45	0.806	0.114		0.189	0.410	0.015		
0.772	51.7	34.1	2.95				0.165	0.456	0.0026		
1.05	48	24.2	1.96	0.894	0.100	0.043	0.203	0.331	0.0057	1.46	0.87
1.06	23	30.6	2.16	0.895	0.118	0.038	0.178	0.440	0.021	1.10	0.985
1.08	60.4	36.6	1.97	0.794	0.106	0.034	0.160	0.343	0.013	1.28	0.865
1.12	56	24.7	2.24	0.728	0.080	0.045	0.223		0.0045		
1.52	26.2	30.8	1.20	0.829	0.114		0.156	0.408	0.018		
1.55	77.7	29.1	0.79	0.749	0.093	0.019	0.165	0.370	0.013	1.05	0.845
1.59	4.8	28.0	2.78	0.835	0.096	0.033	0.164	0.390	0.011	1.08	0.925
1.76	31	29.3	0.72	0.920	0.105	0.026	0.170	0.392	0.011	1.11	0.985
1.85	63	28.2	0.43	0.682	0.081	0.031	0.195	0.459	0.011	0.92	0.74
1.93	33	31.8	0.73	0.748	0.079			0.453	0.0093		
1.97	7.8	26.5	0.93	0.910	0.085	0.043	0.169	0.434	0.0076	0.98	0.98
3.94	13.8	~26	1.04			0.024	0.167	0.371	0.0066		
3.97	83		0.48	0.808	0.092	0.033	0.182	0.447	0.0073	0.965	0.945
				0.787 ± 0.072	0.095 ± 0.012	0.040 ± 0.011	0.180 ± 0.017	0.404 ± 0.031		1.139	0.912

[a] Monitoring light off until reaction ~70% complete.

Table II: Incomplete Reaction of CS_2 with Undistilled O_3

$[O_3]_0$, Torr	$[CS_2]$, Torr	Temp, °C	k, Torr^{-1} min^{-1}	Time of run, min	% O_3 dec	$[O_2]/[O_3]_0$	$[CO]/[O_3]_0$	$[CO_2]/[O_3]_0$	$\frac{[OCS]}{[O_3]_0}$	$\frac{[SO_2]}{[O_3]_0}$	[P]/$[O_3]_0$, absorbance/ Torr
1.69	13	31.1	1.62	0.7	70						0.0021
1.66	27	27.1	0.86	2.1	73			0.014		0.306	0.0036
1.80	16	28.0	1.12	2.9	85	0.784	0.089	0.031	0.165	0.382	0.0055
1.52	29	31.5	1.41	2.9	85	0.771	0.090	0.040	0.178	0.390	0.0046
1.55	11	25.3	1.07	4.7	90	0.814	0.084	0.023	0.153	0.373	0.0064

toring lamp. The monitoring light source was a Philips 93109E low-pressure mercury resonance lamp. The radiation passed through a Corning 7-54 filter to remove radiation below 2200 Å and a cell filled with chlorine to remove radiation above 2800 Å before passing through the reaction vessel to a RCA 9-35 phototube.

The reaction vessel was a quartz cell 5 cm long and 5 cm in diameter. If a fresh cell was used the experimental results were not reproducible. However after a number of experiments were done, the cell became coated with a thin layer of polymer and reproducible results could be obtained. The results reported here are for a cell conditioned in this way, unless specifically stated to the contrary. To test the effect of surface area, runs were done in the vessel unpacked, as well as packed with 1000 solid spherical glass beads (Kimax, 3 ± 0.5 mm diameter). The addition of the beads increased the surface area from 139 to 412 cm^2 and reduced the volume from 102.3 to 88.1 cm^3.

In each experiment, after the reaction was terminated, the products were collected and analyzed by gas chromatography. Aliquot portions of the noncondensable gases were analyzed on an 8 ft long 5 A molecular sieve column at roomt emperature with an He flow rate of 100–122 cc/min. The condensable gases were passed through a Porapak T column 8.5 ft long operated at 81–84° and an He flow rate of 217 cc/min. For both fractions a Gow Mac Model 40-05D voltage regulator with a thermistor detector was used in conjunction with a 1-mV recorder.

An attempt was also made to analyze for SO_3 by passing the products condensable at −160° through either oxalic acid or an oxalate salt immediately after the reaction. It has been reported[8] that oxalic acid quan-

Table III: Reaction of CS_2 with Undistilled O_3 in the Presence of Other Gases

$[O_3]_0$, Torr	$[CS_2]$, Torr	$[X]_0$, Torr	Temp, °C	k, Torr^{-1} min^{-1}	$k[O_3]_0$, min^{-1}	$[O_2]/[O_3]_0$	$[CO]/[O_3]_0$	$[CO_2]/[O_3]_0$	$[OCS]/[O_3]_0$	$[SO_2]/[O_3]_0$	$[P]/[O_3]_0$, absorbance/Torr
				X = O_2							
1.11	70	10	37.8	2.9[a]	3.22		0.131	0.049	0.212	0.471	0.017
0.89	15	13	35.9	1.67	1.49			0.047	0.201	0.534	0.0135
1.01	56	27	31.3	0.655	0.66			0.065	0.272	0.465	0.002
0.524	41.8	52	31.0	1.29	0.68		0.229	0.029		0.668	~0
1.26	30	~60	~30	0.55[a]	0.69			0.054	0.276	0.465	0.0032
				X = CO							
1.46	35	1.2	26.4	1.10	1.61	0.904		0.027	0.171	0.416	0.015
				X = CO_2							
0.830	28.3	1.3	32.3	3.51	2.91	0.720	0.090		0.180	0.392	0.023
1.07	54.0	13	31.8	2.48	2.67	0.731	0.092		0.177	0.437	0.014
1.75	60.6	13	29.4	1.09	1.91	0.778	0.107		0.177	0.432	0.014
0.680	57.2	27	32.3	3.32	2.25	0.602	0.084		0.169	0.426	0.009
1.12	38	180	32.4	1.99[a]	2.41	0.965	0.113			0.425	0.0035
				X = OCS							
1.39	34.8	~0.40	27.1	1.19	1.66	0.827	0.109			0.424	0.0165
1.31	28	2.1	27.4	1.33	1.74	0.908	0.103	0.029		0.390	0.014
1.35	28.5	4.0	26.1	1.52	2.05	0.845	0.097	0.040		0.338	0.024
1.45	28	6.2	28.8	1.02	1.48	0.855	0.107	0.026		0.358	0.011
				X = SO_2							
0.785	23	1.2	33.0	3.02	2.38	0.856	0.099	0.051	0.213		0.0038
1.42	25	4.3	33.8	0.74[a]	1.05	0.676	0.060	0.056	0.170		0.0049
0.93	75	6.4	26.1	1.45[a]	1.35	0.821	0.092	0.033	0.202		
0.90	6.9	8.1	27.8	~0.2[a]	0.2	0.864	0.058	0.064	0.132		
0.680	23	8.4	27.2	0.37[a]	0.25			0.100	0.188		0.021

[a] From initial slope of reciprocal absorbance *vs.* time. The third-order rate constants, k'', are 1.01, 1.31, 0.17, and 0.66 Torr^{-2} min^{-1}, respectively, for the four runs with added SO_2.

titatively reacts with SO_3 to produce CO_2. We have verified this result for samples of SO_3 corresponding to about 50 μ or more SO_3 in our reaction vessel. In none of our experiments did we find evidence of SO_3 formation using this technique. However, SO_3 may have been produced, but in an insufficient quantity to be detected.

Results

When CS_2 was added to the reaction cell containing O_3, the O_3 rapidly disappeared. The rate of disappearance was at least 100 times as fast as that due to the slow heterogeneous decay of pure O_3. A typical plot of the reciprocal O_3 absorbance at 2537 Å *vs.* reaction time is shown in Figure 1. The monitoring light source was weak and separate experiments were done with the lamp off for the first few minutes of the reaction or with intermittent light. The results were the same in all cases, thus eliminating the possibility of a photoinduced decomposition.

The results in Figure 1 clearly demonstrate that the decay is second order in $[O_3]$, at least to 83% decomposition. Every experiment gave a second-order plot over the whole measurable range (at least 80% O_3 decomposition). The second-order rate constants, k, are listed in Table I for experiments with O_3 pressures between 0.147 and 4.0 Torr and CS_2 pressures between 4.8 and 83 Torr. The CS_2 was always in excess, the $[CS_2]/[O_3]_0$ ratio varying between 3.0 and 530 where $[O_3]_0$ is the initial O_3 pressure. Since the CS_2 is always in excess, its pressure may be considered constant throughout the experiment. The values obtained for k in the various experiments varied between 0.44 and 9.6 Torr^{-1} min^{-1}. They are plotted *vs.* $[O_3]_0$ in Figure 2. Except for three points, the data are well fitted by a line of negative unit slope. We have no explanation for the one low point. However, the two points that lie well above the line correspond to the experiments with the lowest $[CS_2]/[O_3]_0$ and are apparently real. The other points correspond to $[CS_2]/[O_3]_0$ in excess of 4.0 and lead to the surprising result that k is independent of $[CS_2]$ in this regime. The rate law which describes the results is

$$-d[O_3]/dt = k'[O_3]^2/[O_3]_0 \quad (I)$$

(8) R. Bent, W. R. Ladner, and W. J. Mullin, *Chem. Ind. (London)*, 461 (1967).

Table IV: Reaction of CS_2 with Distilled O_3 in the Unpacked Cell

$\frac{[CS_2]}{[O_3]_0}$	$[O_3]_0$, Torr	$[CS_2]$, Torr	Temp, °C	Ozone dec[a]	k, Torr^{-1} min^{-1}	$\frac{[O_2]}{[O_3]_0}$	$\frac{[SO_2]}{[O_3]_0}$	$\frac{[OCS]}{[O_3]_0}$	$\frac{[CO]}{[O_3]_0}$	$\frac{[CO_2]}{[O_3]_0}$	$\frac{[OCS] + 2[CO] + 2[CO_2]}{[SO_2]}$	$\frac{\Sigma[O]}{3[O_3]_0}$
0.90	0.99	0.90	28.8	2.6	1.18	0.948	0.220	0.065	0.052	0.052	1.24	0.855
0.96	1.35	1.3	29.8	3.4	1.39	0.918	0.284	0.082	0.062	0.055	1.11	0.886
1.57	1.40	2.2	25.2	3.5	2.24	0.907	0.325	0.114	0.080	0.046	1.13	0.903
2.90	1.38	4.0	24.6	0.7	1.83	0.903	0.335	0.148	0.084	0.029	1.12	0.921
2.90	1.45	4.2	26.5		2.00	0.884	0.361	0.146	0.087	0.043	1.26	0.936
3.25	0.62	2.0	29.7	3.6	4.98	0.861	0.340	0.126	0.075	0.054	1.12	0.903
3.53	1.19	4.2	25.5	1.2	2.66	0.865	0.332	0.150	0.089	0.024	1.13	0.900
4.31	1.46	6.3	28.0	1.6	1.78	0.795	0.353	0.151	0.085	0.044	1.15	0.874
6.00	1.35	8.1	28.6	3.6	2.86	0.889	0.356	0.154	0.098	0.034	1.17	0.970
6.15	1.35	8.3	27.6	3.4	1.72	0.881	0.337	0.157	0.098	0.038	1.27	0.924
6.88	1.61	11	27.6	2.5	1.70	0.839	0.340	0.150	0.089	0.019	1.08	0.879
11.7	1.54	18	24.8		0.70	0.835	0.346	0.161	0.092	0.019	1.11	0.885
12.0	1.42	17.1	27.1	2.6	1.08	0.863	0.364	0.151	0.095	0.025	1.10	0.971
13.7	1.42	19.4	24.0	1.6	0.79	0.923	0.352	0.166	0.102	0.023	1.18	0.989
14.1	2.06	29		1.7	0.45	0.855	0.353	0.151	0.091	0.017	1.04	0.901
20	1.39	28	24.8	1.8	0.72	0.915	0.350	0.160	0.083	0.022	1.05	0.940
20.2	1.41	28.5	25.9	2.4	1.38	0.872	0.366	0.164	0.097	0.022	1.10	0.930
20.6	1.36	28	25.9	1.2	0.68	0.830	0.340	0.159	0.091	0.021	1.19	0.878
22	1.38	31	24.5	2.4	0.64	0.859	0.333	0.153	0.094	0.020	1.14	0.892
27.6	0.34	9.3	25.1	2.4	2.86	0.765	0.308	0.163	0.080	0.036	1.12	0.820
28[b]	0.98	28	28.1		0.76[c]	1.18	0.328	0.151	0.083	0.025	1.12	1.10
34	0.53	18	23.1		1.69	0.773	0.316	0.152	0.075	0.019	1.08	0.818
						0.850[d]	0.344[d]	0.157[d]	0.091[d]	0.025[d]	1.12[d]	0.905[d]

[a] Per cent ozone decomposed in 20–30 min before addition of CS_2. [b] 88 μ NO added. [c] From initial decay rate. [d] Average value for runs with $[CS_2]/[O_3]_0 > 4$, but omitting run with added NO.

Table V: Reaction of CS_2 with Distilled O_3 in the Packed Cell

$\frac{[CS_2]}{[O_3]_0}$	$[O_3]_0$, Torr	$[CS_2]$, Torr	Temp, °C	Ozone dec[a]	k, Torr^{-1} min^{-1}	$\frac{[O_2]}{[O_3]_0}$	$\frac{[SO_2]}{[O_3]_0}$	$\frac{[OCS]}{[O_3]_0}$	$\frac{[CO]}{[O_3]_0}$	$\frac{[CO_2]}{[O_3]_0}$	$\frac{[OCS] + 2[CO] + 2[CO_2]}{[SO_2]}$	$\frac{\Sigma[O]}{3[O_3]_0}$
1.03	1.16	1.20	26.1	2.0	1.64	0.896	0.319	0.094	0.084	0.054	1.16	0.905
1.03	1.70	1.76	26.0	1.6	1.24	0.960	0.336	0.099	0.090	0.044	1.09	0.956
1.20	0.38	0.45	27.4	3.1	0.76	0.868	0.265	0.061	0.061	0.069	1.21	0.848
1.23	0.80	0.98	26.7	(20.3)	(3.04)	0.887	0.290	0.082	0.103	0.099	1.66	0.940
2.32	1.35	3.14	27.0	1.0	2.23	0.916	0.375	0.131	0.097	0.032	1.03	0.958
5.08	1.42	7.2	27.0	(9.3)	(6.0)	0.824	0.329	0.123	0.103	0.040	1.24	0.874
8.02	2.77	22.2	25.5		(1.41)	0.870	0.358	0.138	0.113	0.026	1.16	0.919
12.5	1.37	17	28.5	(>13)	(2.18)							
17.0	2.24	38	28.7	0.8	0.422	0.853	0.406	0.159	0.098	0.019	0.97	0.938
19.0	1.51	30	27.2		0.58	0.888	0.411	0.159	0.107	0.023	1.02	0.969
21.0	1.41	29.7	25.9	(8.3)	(2.22)	0.837	0.389	0.155	0.106	0.032	1.11	0.927
21.2	0.88	18.5	25.2	1.0	1.55	0.832	0.358	0.152	0.105	0.025	1.15	0.973
25.6	1.75	45	27.6	0.4	0.88	0.849	0.406	0.144	0.097	0.020	0.93	0.931
32.6	0.55	18	26.9	1.9	2.14							
101	0.39	43	29.7		3.38	0.803	0.419	0.175	0.092	0.036	1.02	0.925
						0.844[b]	0.384[b]	0.152[b]	0.103[b]	0.028[b]	1.08[b]	0.932[b]

[a] Per cent ozone decomposed in 20–30 min before addition of CS_2. [b] Average value for $[CS_2]/[O_3]_0 > 4.0$.

where k' is a constant independent of $[CS_2]$, $[O_3]_0$, or $[O_3]$. The intercept of the log–log plot gives $k' = 1.83\ \text{min}^{-1}$.

After the O_3 was consumed the products of the reaction were measured. The absorption never returned to zero and a polymer was deposited on the cell wall. The polymer was measured from the residual absorption after the gases were removed. The gaseous products of the reaction were O_2, CO, CO_2, OCS, and SO_2. We looked for, but did not find, S_2O or significant amounts

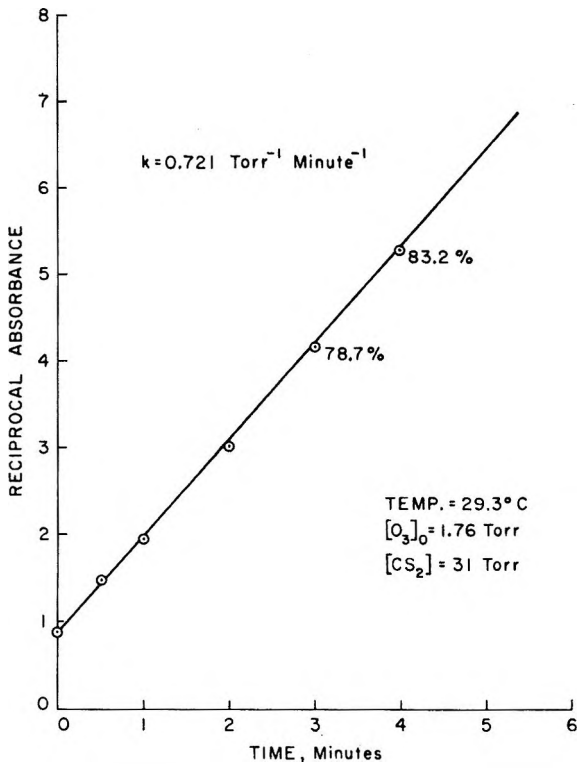

Figure 1. Plot of reciprocal absorbance of O_3 at 2537 Å *vs.* reaction time for an initial mixture of 1.76 Torr O_3 and 31 Torr CS_2 at 29.3°. The numbers next to the data points indicate per cent O_3 decomposed.

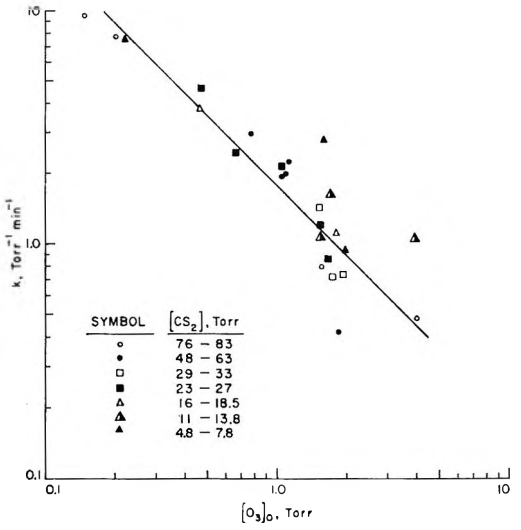

Figure 2. Plot of the second-order rate constant, k, *vs.* the initial O_3 pressure in the reaction of undistilled O_3 with CS_2 at room temperature.

of SO_3. Several careful attempts were made to find SO_3, but to no avail. Certainly neither S_2O nor SO_3 is a major product, but minor amounts of either one might have been produced. The results of the analyses, normalized to $[O_3]_0$, are reported for the various experiments in Table I. The order of importance of the products is O_2, SO_2, OCS, CO, and CO_2. Within the experimental uncertainty, the relative amounts of the gaseous products remained the same for all the experiments, and their average value and mean deviations are listed in the table. The experimental uncertainty in the polymer analysis is so large that it is difficult to make a judgment.

In order to see if any of the products resulted from secondary reactions, some experiments were done in which the reaction mixture was removed from the reaction vessel before the O_3 was exhausted. The results are shown in Table II. There is some indication that the polymer may be a secondary product. However in view of the experimental uncertainties the evidence is not convincing. The ratios of the gaseous products are similar to those in Table I, and there is no evidence from these results to suggest that any of the gaseous products are secondary.

As a further check of the influence of the products of the reaction, O_3 was mixed with each gaseous product, one at a time. With O_2, CO_2, and SO_2, the decay of O_3 was no faster than in their absence. With $[CO]/[O_3]$ less than 5 there was also no enhancement of the decay, though at larger ratios O_3 removal can be very rapid indeed.[9] This reaction is currently being studied in our laboratory. With OCS added, O_3 removal appears to be slightly enhanced, but it is still very much slower than in the presence of CS_2.

Finally mixtures of CS_2, O_3, and each of the gaseous products were studied. The results are shown in Table III. For none of the experiments was there any evidence that the ratio of product pressures was altered. This confirms that the products do not enter into the chemical reaction to any significant extent. Furthermore at low initial pressure of each product gas, the constant $k' = k[O_3]_0$ was unaffected, even though more product gas was initially present than produced in the reaction.

If larger pressures of O_2 were initially present, the rate constant k' could be lowered, but the second-order relationship remained. An example of such a result is shown in Figure 3. Even though 27 Torr of O_2 was present, the plot is second order in $[O_3]$ for at least 82% decomposition; yet k' is reduced from 1.83 to 0.66 min^{-1}.

At even higher pressures of added gas (60 Torr O_2, 180 Torr CO_2, or 4–8 Torr SO_2), the second-order plots deviate from linearity indicating a further inhibition as the reaction progresses. An example of such a plot with 4.3 Torr SO_2 is shown in Figure 4. Furthermore, with SO_2 present, k' seems to depend on $[CS_2]$, its value diminishing as $[SO_2]_0/[CS_2]$ increases.

The above results can be summarized as follows: (1) for CS_2–O_3 mixtures with $[CS_2]/[O_3]_0 \geq 4$, the O_3 decays *via* eq I; (2) none of the gaseous products enter the reac-

(9) C. Goldman, unpublished results, Pennsylvania State University, 1969.

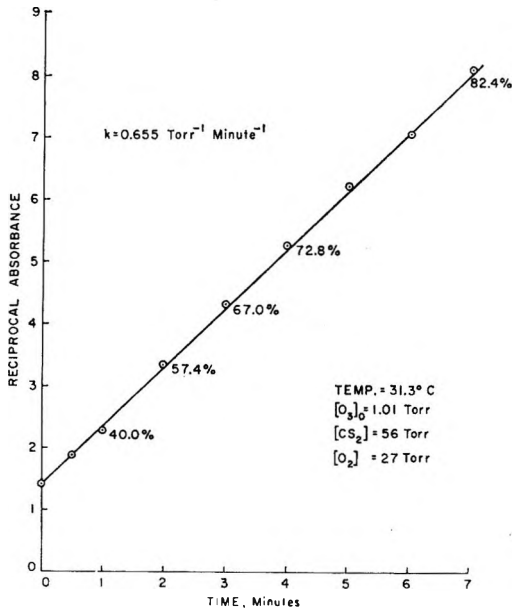

Figure 3. Plot of reciprocal absorbance of O_3 at 2537 Å *vs.* reaction time for an initial mixture of 1.01 Torr O_3, 56 Torr CS_2, and 27 Torr O_2 at 31.3°. The numbers next to the data points indicate per cent O_3 decomposed.

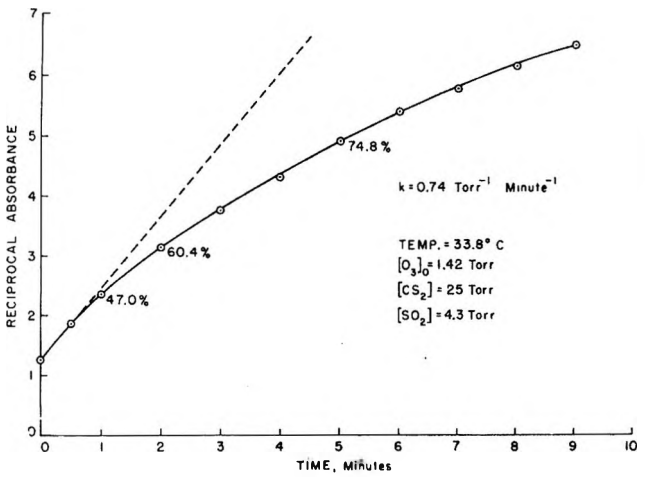

Figure 4. Plot of reciprocal absorbance of O_3 at 2537 Å *vs.* reaction time for an initial mixture of 1.42 Torr O_3, 25 Torr CS_2, and 4.3 Torr SO_2 at 33.8°. The numbers next to the data points indicate per cent O_3 decomposed.

tion nor alter the rate law or rate constant, unless added in large excess initially.

The rate law as given by eq I is unusual in that there is a dependence on $[O_3]_0$. This suggests that some impurity may have been present in the ozone which terminates the reaction without being consumed. Therefore we repeated some of the earlier experiments with ozone which has been subjected to more thorough purification procedures. In the previous experiments the ozone was prepared from a tesla coil discharge through oxygen. The O_3 was collected at −196° and the residual O_2 removed. Since the oxygen contains some N_2

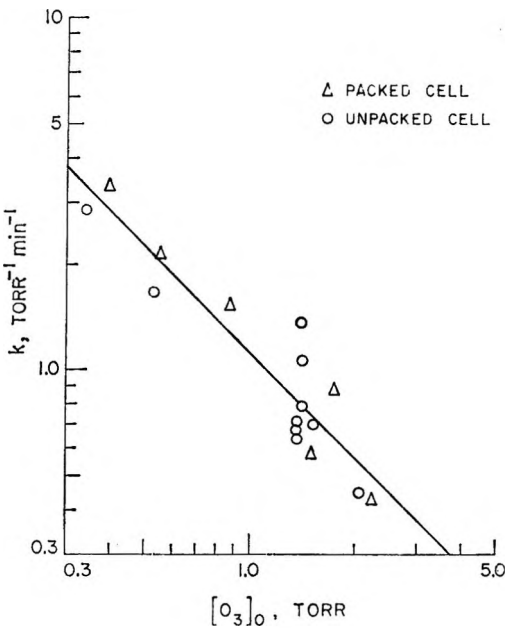

Figure 5. Plot of the second-order rate constant, k, *vs.* the initial O_3 pressure in the reaction of distilled O_3 with CS_2 for $[CS_2]/[O_3]_0 > 10$ at room temperature.

as an impurity, oxides of nitrogen could be formed in the discharge and retained in the ozone. For all the subsequent experiments the ozone was triply distilled at −186° and collected at −196° with continuous degassing. Any NO_2 or heavier oxides of nitrogen should be retained at −186°, whereas NO would be removed at −196°.

The results in the unpacked cell with the distilled O_3 are listed in Table IV; those in the packed cell, in Table V. For each run the ozone was introduced first and its decay monitored for 20–30 min before CS_2 was added. The per cent decompositions for pure ozone are listed in the tables. For most of the runs the percent decomposition in this time period was between 1 and 4% and there is no discernible difference at different ozone pressures or between the packed and unpacked cell. The average first-order rate constant would be about 10^{-3} min^{-1}. However, the decomposition is not first order but is markedly inhibited with time. Actually most of the decomposition occurs in the first few minutes and the initial first-order decay constant is about 10 to 100 times as large. Some runs were done in the packed cell before it was conditioned. In those cases (shown in parenthesis in Table V) the ozone decomposition is significantly larger, indicating that the ozone decomposition is heterogeneous.

When CS_2 was added to the ozone, the rate of ozone disappearance was markedly enhanced and followed a rate law second-order in ozone concentration for at least 80% decomposition. There was no evidence for deviation from this rate law even for further decomposition, but absorption due to the polymer and SO_2 products increased the uncertainty of the measurements.

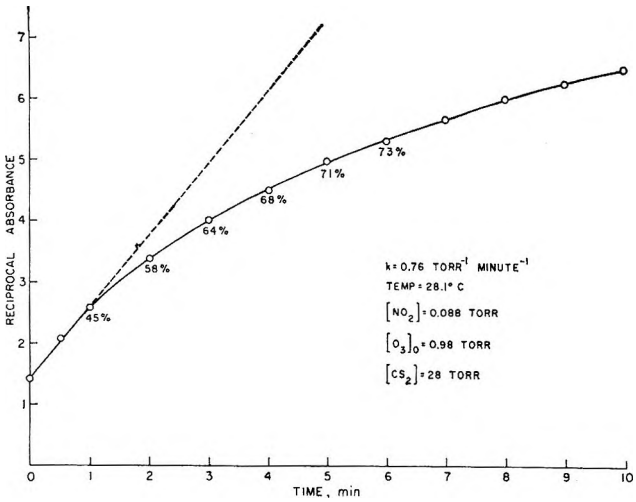

Figure 6. Plot of the reciprocal ozone absorbance at 2537 Å *vs.* reaction time for a mixture of 0.088 Torr NO_2, 0.98 Torr $[O_3]_0$, and 28 Torr CS_2 at 28.1°. The NO_2 was prepared by mixing 0.088 Torr NO with 1.07 Torr ozone before adding CS_2.

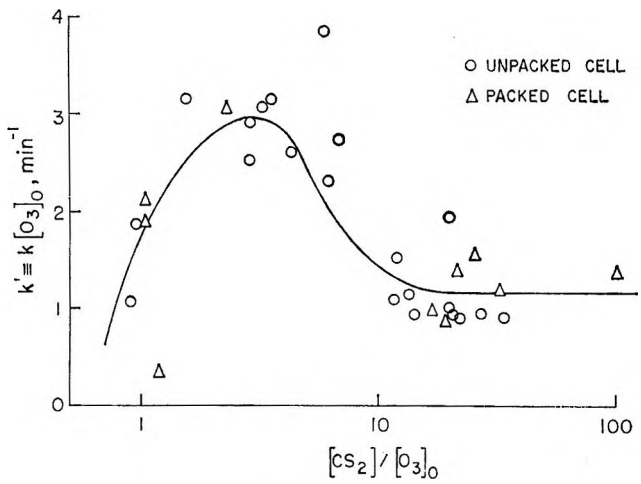

Figure 7. Semilog plot of $k' \equiv k[O_3]_0$ *vs.* $[CS_2]/[O_3]_0$ in the reaction of distilled O_3 with CS_2 at room temperature.

The second-order rate constants, k, are listed in Tables IV and V. For $[CS_2]/[O_3]_0$ in excess of 10, these rate constants are plotted *vs.* $[O_3]_0$ in Figure 5. The log–log plot is nicely fitted by a line with slope of -1 indicating an inverse relationship between k and $[O_3]_0$. The results are independent of $[CS_2]$ and are the same in the packed and unpacked cell. This is the same result as found with the undistilled O_3, and the rate law is given by eq I with $k' = 1.13$ min^{-1}. In the previous work $k' = 1.83$ min^{-1}, but these two values are probably within the experimental uncertainty of the measurements. The dispersion among the data points is less and the ozone was purified more thoroughly for the results in Figure 5. Therefore the lower value is preferred. Those rate constants obtained in the unconditioned packed cell where the pure ozone decomposition was

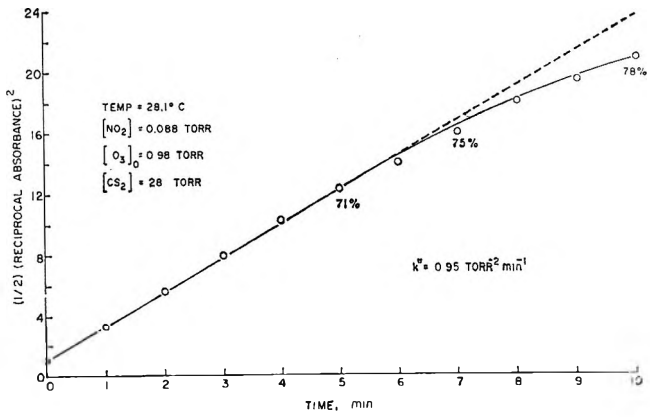

Figure 8. Plot of one-half the square of the reciprocal ozone absorbance at 2537 Å *vs.* reaction time for an initial mixture of 0.088 Torr NO_2, 0.98 Torr O_3, and 28 Torr CS_2 at 28.1°. The NO_2 was prepared by mixing 0.088 Torr NO with 1.07 Torr ozone before adding CS_2. The numbers next to the points represent per cent ozone removed.

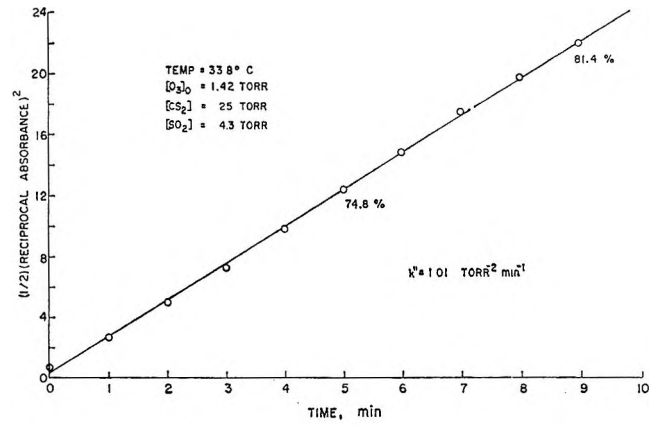

Figure 9. Plot of one-half the square of the reciprocal ozone absorbance at 2537 Å *vs.* reaction time for an initial mixture of 1.42 Torr O_3, 4.3 Torr SO_2, and 25 Torr CS_2 at 33.8°. The numbers next to the points represent per cent ozone removed.

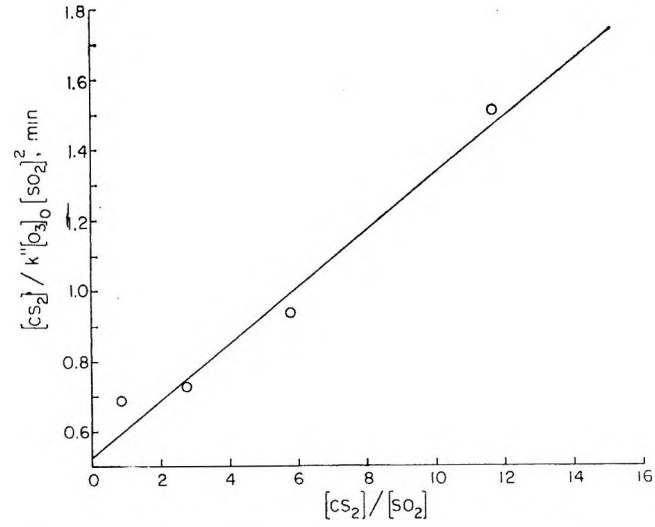

Figure 10. Plot of $[CS_2]/k''[O_3]_0[SO_2]^2$ *vs.* $[CS_2]/[SO_2]$ in the reaction O_3–CS_2–SO_2 mixtures at room temperature.

Table VI: Product Ratios in the Reaction of O_3 with CS_2 for $[CS_2]/[O_3]_0 > 4$

	From Table I	From Table IV	From Table V	Predicted from mechanism	
$[O_2]/[O_3]_0$	0.787 ± 0.072	0.850 ± 0.037	0.844 ± 0.020	0.860[a]	0.871[b]
$[SO_2]/[O_3]_0$	0.404 ± 0.031	0.344 ± 0.013	0.384 ± 0.027	0.468[a]	0.347[b]
$[OCS]/[O_3]_0$	0.180 ± 0.017	0.157 ± 0.005	0.152 ± 0.012	0.180[a]	0.165[b]
$[CO]/[O_3]_0$	0.095 ± 0.012	0.091 ± 0.006	0.103 ± 0.005	0.113[a]	0.104[b]
$[CO_2]/[O_3]_0$	0.040 ± 0.011	0.025 ± 0.007	0.028 ± 0.006	0.031[a]	0.029[b]
$\frac{([OCS] + 2[CO] + 2[CO_2])}{[SO_2]}$	1.14	1.12	1.08		
$\Sigma[O]/3[O_3]_0$	0.91	0.91	0.93		

[a] Assuming no SO_3 produced. [b] Assuming $[SO_3]/[O_3]_0 = 0.082$.

abnormally large were not plotted in Figure 5. They lie above the line. In fact even with $[CS_2]/[O_3]_0$ below 10, the O_3–CS_2 reaction was much more rapid if the pure ozone decomposition was excessive.

These results confirm that the rate law has the peculiar feature of depending on the initial concentration of one of the reactants. Perhaps some impurity is still present in the ozone in spite of the extensive purification procedure. The most likely impurity is NO_2 which might remove oxygen atoms to produce NO and O_2 and then be regenerated by the O_3–NO reaction. To test this hypothesis 1.07 Torr of ozone was mixed in the reaction vessel with 0.088 Torr of NO. Some of the ozone is consumed and converts the NO to NO_2. Then 28 Torr of CS_2 was added and the reaction monitored. A second-order plot is shown in Figure 6. The reaction is inhibited as the ozone is consumed, but the initial slope gives an initial second-order rate constant of about 0.76 $Torr^{-1}$ min^{-1} which is only slightly reduced from that in the absence of NO_2. Consequently the rate law cannot be attributed to NO_2 as an impurity.

After the ozone was completely consumed in each run, the gaseous products were collected and measured by gas chromatography. The relative yields are listed in Tables IV and V. Polymer was also produced, but it was not measured. For $[CS_2]/[O_3]_0 > 4$, the product yields, based on $[O_3]_0$, were invariant to $[CS_2]$ or $[O_3]_0$. The average values and their mean deviations are tabulated in Table VI. The results are the same in the packed and unpacked cell and the same as with undistilled O_3. With distilled O_3 the deviations were reduced, and the relative yields are 0.85, 0.36, 0.155, 0.097, and 0.027, respectively, for O_2, SO_2, OCS, CO, and CO_2. For $[CS_2]/[O_3]_0 < 4$ the results are somewhat altered. As this ratio is reduced, relatively more O_2 and CO_2 are produced, whereas the SO_2, OCS, and CO are diminished.

If the five gaseous products were the sole products, then mass balance requirements for carbon–sulfur and oxygen would lead to the respective expressions

$$[SO_2] = [OCS] + 2[CO] + 2[CO_2] \quad \text{(II)}$$

$$3[O_3]_0 = \Sigma[O] \equiv 2[O_2] + [CO] + 2[CO_2] + [OCS] + 2[SO_2] \quad \text{(III)}$$

The ratios of the right-hand side to the left-hand side of the equations are tabulated in Tables I, IV, and V. For $[CS_2]/[O_3]_0 > 4$ these results are independent of $[CS_2]$ or $[O_3]$ and the average values are compared in Table VI. In all cases there is both a sulfur and oxygen deficiency in the gas-phase products. Part of this deficiency may be accounted for by the polymer. However, it seems likely that some SO_3 may bep resent ($[SO_3]/[O_3]_0 \leq 0.08$).

At $[CS_2]/[O_3]_0$ less than about 10, the rate constant $k' \equiv k[O_3]_0$ obtained from each experiment is larger than the value of 1.13 min^{-1} predicted by Figure 5. The results are shown in Figure 7 where k' is seen to rise to a maximum value of about 3.0 min^{-1} at $[CS_2]/[O_3]_0 = 3$. The semilogarithmic plot tends to overemphasize the importance of the deviation which is less than a factor of 3 even though the abscissa varies by a factor in excess of 100 (in excess of 500 including the undistilled O_3 results where values of $[CS_2]/[O_3]_0$ up to 530 were used). Furthermore, the data points are scattered. Nevertheless, the deviation exceeds the scatter in the data and the increase in k' at low $[CS_2]/[O_3]_0$ appears to be real.

Discussion

There are three important observations that must be considered in formulating a mechanism. First is the fact that the decay rates are the same in the unpacked and conditioned packed cell for either pure ozone or O_3–CS_2 mixtures, but that both rates were enhanced in the unconditioned packed cell. This strongly suggests that the pure ozone decomposition initiates the O_3–CS_2 reaction. Second, our results have shown unambiguously that the gas-phase products are initial reaction products and do not interfere with the reaction unless added in large excess of that produced in the reaction. The carbon-containing products almost certainly arise from parallel reactions of ozone with CS. Finally, the rate of ozone disappearance is much greater in the presence of CS_2 than in its absence, suggesting a chain reaction in the former case. This conclusion is substantiated by the fact that NO_2 or excess SO_2 can inhibit the O_3–CS_2 reaction.

The initial ozone decay must be heterogeneous. The

marked inhibition as the reaction proceeds probably means that active centers in the surface are destroyed in the reaction. However, for a conditioned cell, the per cent ozone decomposed is about the same for any ozone pressure in any time interval. This is consistent with a first-order decay law. Thus we propose that the rate law for the initiating step by ozone decay has the following form

$$-\mathrm{d}[O_3]/\mathrm{d}t = k_0[O_3]^2/[O_3]_0 \qquad \text{(IV)}$$

The rate constant, k_0, depends on the nature of the surface, though it is apparently not much affected by the addition of the Pyrex beads once they are conditioned by repeated experiments. In the absence of CS_2, the constant drops as the reaction proceeds and the surface is deactivated. However, with CS_2 present, polymer is continuously deposited so that fresh surface is always available; the reaction is no longer self-inhibiting, and the constant is about 10^{-1} to 10^{-2} min^{-1}.

The reaction steps which we envision are the following

$$2O_3 \xrightarrow{\text{wall}} 2O_2 + O_2^* \qquad (1)$$

$$O_2^* + O_3 \longrightarrow 2O_2 + O \qquad (2)$$

$$O + O_3 \longrightarrow 2O_2 \qquad (3)$$

where O_2^* is an excited oxygen molecule, possibly in a singlet state. Reaction 1 occurs on the wall and is highly exothermic. It is not unreasonable to expect that some of the oxygen produced is energized. The excited O_2 produced could easily have enough energy to dissociate another ozone molecule. In fact if singlet O_2 is produced, reaction 2 is well established.[10] The ozone removal rate would be 4 times the rate of reaction 1. The rate law would be predicted if reaction 1 were second-order in $[O_3]$, but for some reason the number of active surface centers was inversely proportional to $[O_3]_0$.

In the presence of CS_2 the carbon-containing products are presumed to come from the reaction of CS with O_3 in parallel paths

$$CS + O_3 \longrightarrow \begin{cases} \longrightarrow CS + O_3 \\ \longrightarrow O_2 + OCS \\ \longrightarrow O_2 + CSO \longrightarrow OCS \\ \longrightarrow CO + SOO \longrightarrow SO_2 \\ \longrightarrow SO + COO \longrightarrow CO_2 \end{cases}$$

(C—S, O, O, O)

The five paths correspond to the five different ways of splitting the intermediate into a diatomic and a triatomic fragment. The first path just returns the intermediate to reactants. The second and third paths ultimately give the same products. The experimental results for $[CS_2]/[O_3]_0 > 4$ indicate that the relative importance of the paths giving OCS, CO, and CO_2 is 55.5, 34.8, and 9.7%, respectively. Each of the product-producing paths is highly exothermic. Particularly the OCS, SO_2, and CO_2 products formed in the last three paths, respectively, must contain rearrangement energy and are therefore highly excited when formed. Furthermore the spin conservation rules require that the O_2 produced in the second path be singlet. Consequently at least one of the products in each path should be highly excited. Rather than consider each path separately we shall compress the mechanism by combining the product-producing paths as follows

$$CS + O_3 \longrightarrow X^* \qquad (4)$$

where X^* is an excited product molecule. For simplicity we shall assume that all the X^* react similarly as follows

$$X^* + O_3 \longrightarrow X + O_2 + O \qquad (5a)$$

$$\longrightarrow X + O_3 \qquad (5b)$$

Of course reactions 5a and 5b now represent some average reactions for all the excited molecules. In fact a satisfactory fit of the data results if the excited molecules from the OCS and CO producing paths always react *via* reaction 5a, whereas the excited CO_2 from the last path always reacts *via* reaction 5b. In that case $k_{5b}/k_5 = 0.097$ where $k_5 \equiv k_{5a} + k_{5b}$. As will be shown, the value needed for k_{5b}/k_5 to fit the data lies between 0.03 and 0.1.

Independent evidence that CS is a chain carrier comes from results of O_3 decay in the absence of CS_2 but in the presence of OCS. We have found that the addition of OCS to pure O_3 does not significantly alter the O_3 removal rate even though CO and SO_2 are produced. The only difference that can be envisioned between the O_3–CS_2 and O_3–OCS systems is that the CS produced in the CS_2–O_3 system is replaced by CO in the OCS–O_3 system. Thus CS must be a chain carrier, whereas CO is not.

The only additional reactions needed to complete the mechanism are the well known ones[11]

$$O + CS_2 \longrightarrow CS + SO \qquad (6)$$

$$SO + O_3 \longrightarrow SO_2 + O_2 \qquad (7)$$

However to anticipate the results with added gases we include the possible terminating reactions

$$O_2^* + M \longrightarrow \text{termination} \qquad (8)$$

$$X^* + M \longrightarrow \text{termination} \qquad (9)$$

$$O + M \longrightarrow \text{termination} \qquad (10)$$

where M may be any gas except O_3 or CS_2.

For long chains the mechanism predicts that the relative product ratios be 0.860, 0.468, 0.180, 0.113, and 0.031, respectively, for O_2, SO_2, OCS, CO, and CO_2.

(10) E. C. Zipf, *Can. J. Chem.*, **47**, 1863 (1969).

(11) N. Cohen and J. Heicklen, "Comprehensive Chemical Kinetics," Vol. 6, Elsevier, in press.

These values are listed in Table VI and except for SO_2 they compare favorably with those obtained experimentally. Mass balance considerations have shown that SO_3 may have been produced to about 8% of the initial ozone concentration. If we consider that some of the excited SO_2 produced might have reacted with O_3 *via*

$$SO_2^* + O_3 \longrightarrow SO_3 + O_2 \qquad (11)$$

then the predicted product ratios are shown in the last column of Table VI assuming $[SO_3]/[O_3]_0 = 0.082$. These values exactly fit those observed experimentally.

The mechanism predicts the following rate law

$$-d[O_3]/dt = 2R\{1\} + \frac{R\{1\}k_2[O_3]}{(k_2[O_3] + k_8[M])} \times \left\{1 + \frac{(k_3[O_3] + \alpha k_6[CS_2])}{(\beta k_6[CS_2] + k_3[O_3] + k_{10}[M])}\right\} \qquad (V)$$

where $R\{1\}$ is the rate of reaction 1 and is given by eq IV, α is $2.10 + k_5[O_3]/(k_3[O_3] + k_9[M])$ if reaction 11 is omitted, but $2.38 + k_5[O_3]/(k_5[O_3] + k_9[M])$ if reaction 11 is included, and β is defined as

$$\beta \equiv (k_{5b}[O_3] + k_9[M])/(k_5[O_3] + k_9[M]) \qquad (VI)$$

where $k_5 \equiv k_{5a} + k_{5b}$. The generalized rate law is complex, but a number of simplifications can be made. First the quantity α is not markedly dependent on the ratio of $[O_3]$ to $[M]$ and can be considered to have a constant value of about three. Second, the rate constants k_3 and k_6 are well known. The former constant is $6 \times 10^7\ M^{-1}\ sec^{-1}$ at room temperature,[12] whereas the latter is $2 \times 10^9\ M^{-1}\ sec^{-1}$ at room temperature.[11] Since in this study $[CS_2]/[O_3] \geq 1$, then $k_3[O_3] \ll \alpha k_6[CS_2]$. Finally, the chain length of the reaction is long (about 10–100) so that the first term on the right-hand side of eq V, as well as the 1 in brackets, can be neglected. The rate law is reduced to

$$-d[O_3]/dt = \frac{k_0k_2[O_3]^3\alpha k_6[CS_2]/[O_3]_0}{(k_2[O_3] + k_8[M])(\beta k_6[CS_2] + k_3[O_3] + k_{10}[M])} \qquad (VII)$$

The observed rate law is always second order in $[O_3]$ in the absence of added foreign gases. This can be only if $k_3[O_3]$ is always negligible in the denominator of eq VII. Furthermore the independence of the rate law on $[CS_2]$ at high $[CS_2]/[O_3]_0$ ratios also requires that $k_3[O_3]$ be negligible. Since the smallest value of $k_6[CS_2]/k_3[O_3]$ employed was about 30, this requires that $\beta > 0.03$. An upper limit to β comes from the restriction that the chain length be long (*i.e.*, $10 \leq 1/\beta < 100$). Thus β must be between about 0.03 and about 0.1 in all our experiments.

Let us first consider the case with no added gases so that $k_8[M]$, $k_9[M]$, and $k_{10}[M]$ as well as $k_3[O_3]$ can be dropped from eq VII. Then the rate law even further simplifies to the observed rate law at high $[CS_2]/[O_3]_0$

$$-d[O_3]/dt = \alpha k_5k_0[O_3]^2/k_{5b}[O_3]_0 = k'[O_3]^2/[O_3]_0 \qquad (VIII)$$

Let us now consider the case when an excess of foreign gas is added. Assume that sufficient gas is added so that $k_8[M] > k_2[O_3]$, but that this gas is not effective in reaction 9. Then, with the $k_3[O_3]$ term also neglected, eq VII reduces to

$$-d[O_3]/dt = \frac{\alpha k_0k_2k_6[O_3]^3[CS_2]}{k_8[M][O_3]_0(k_{10}[M] + k_{5b}k_6[CS_2]/k_5)} \qquad (IX)$$

Equation IX predicts an inhibition as the ozone is removed. A third-order plot is shown for the run with NO_2 present in Figure 8. The data fit a good straight line for about 75% ozone removal and give a third-order rate constant of 0.95 $Torr^{-2}\ min^{-1}$. In Table III several runs were done with SO_2 added and an inhibition was observed. The results of those runs fit a rate law third order in $[O_3]$ extremely well. One such plot is shown in Figure 9. No deviation from linearity is seen even for 81.4% ozone removal. The third-order rate constants, k'', are listed in the footnote of Table III. These constants increase as the CS_2 pressure is increased or the SO_2 pressure is decreased. If eq IX applies then the following relationship should hold

$$[CS_2]/k''[O_3]_0[SO_2]^2 = k_8(k_{10} + k_{5b}k_6[CS_2]/k_5[SO_2])/\alpha k_0k_2k_6 \qquad (X)$$

Figure 10 is a plot of the left-hand side of eq X *vs.* $[CS_2]/[SO_2]$. The data points are reasonably well fitted by a straight line of intercept 0.53 min and slope 0.083 min. The ratio of slope to intercept gives $k_{5b}k_6/k_5k_{10} = 0.156$. Since k_{5b}/k_5 lies between 0.03 and 0.1 and $k_6 = 2 \times 10^9\ M^{-1}\ sec^{-1}$, then k_{10} should be between 4.0×10^8 and $1.3 \times 10^9\ M^{-1}\ sec^{-1}$. These are not unreasonable values if reaction 10 is really second order. However, most investigators[11] agree that reaction 10 is third order with a rate constant of about $10^{10}\ M^{-2}\ sec^{-1}$ with SO_2 as a chaperone. These conclusions are based on results in flow tubes where the total pressures were lower than used here. Perhaps at our pressures reaction 10 is approaching second-order behavior. A study at high pressures was made by Jaffe and Klein.[13] With SO_2 as a chaperone they found the transition region between second and third-order behavior to be about one atmosphere with a second-order rate constant $1.1 \times 10^9\ M^{-1}\ sec^{-1}$. Our findings are in excellent agreement with this value, but our results do require that CS_2 be about 100 times as efficient as SO_2 as a chaperone in reaction 10. It is not clear why this should be.

The product of k', as found in the absence of foreign

(12) DASA Reaction Rate Handbook, 1967.

(13) S. Jaffe and F. S. Klein, *Trans. Faraday Soc.*, **62**, 2150 (1966).

gases, and the slope of Figure 10 gives $k_8/k_2 = 0.094$. If O_2^* is the $^1\Delta_g$ state of O_2, then $k_2 \simeq 10^6\ M^{-1}\ sec^{-1}$ [10] and k_8 is about one-tenth as large.

Finally, we consider the results in the absence of foreign gases at low $[CS_2]$ to $[O_3]_0$ ratios. The second-order rate constants are enhanced and the product ratios shifted. Under these conditions OCS and CO are apparently undergoing some secondary ozonation to produce CO_2 and O_2. The details of these secondary processes are not clear, but we do know that CO does react rapidly with O_3 under some conditions.[9]

Acknowledgment. The authors wish to thank Dr. H. A. Wiebe for his many useful contributions.

The Gas-Phase Photolysis of 2-Picoline

by W. Roebke[1]

Department of Chemistry, The University of Texas at Austin, Austin, Texas 78712 *(Received May 22, 1970)*

The gas-phase photolysis of 2-picoline in the $\pi-\pi^*$ region yields 3- and 4-picoline. The isomerization quantum yields increase with increase in frequency of the incident light as well as with increase in intensity but do not exceed 0.002. Vibrational relaxation also decreases the yields. Oxygen and *cis*-2-butene both cause yields to decrease, and this effect may possibly be associated with destruction of the triplet state. The triplet-state yield (determined by the biacetyl method) is about 0.21 for irradiation at the 0–0 band of the $n-\pi^*$ transition (280 nm) but decreases at short wavelengths and is not more than 0.03 at 248 nm.

Introduction

Radiationless transitions, namely internal conversion and intersystem crossing, are important in photochemistry. Theoretical treatments of radiationless transitions have appeared over the past few years.[2,3] The theory predicts that internal conversion depends largely on three factors: (1) the electronic energy differences between the two states; (2) the number of fundamental vibrational modes in each electronic state; and (3) the energies of the fundamental vibrational modes.

Thermodynamically unstable isomers of the absorbing molecules may be formed by radiationless transitions. If an unstable isomer reverts to the ground state of the absorbing molecule by a thermal reaction, a pathway is provided for relaxation of electronic energy.[4] Simple aromatic molecules such as benzene irradiated at 253.7 nm may yield fulvene,[5] prismane, and benzvalene.[6] Recently, it has been shown that benzene-*1,3,5-d*$_3$ rearranges to the *1,2,4* isomer at 253.7 nm in the vapor phase.[7] In the presence of additives which facilitate vibrational relaxation, a steady-state mole fraction of benzvalene greater than 0.01 can be attained.[8] A careful study of the photochemical and photophysical effects of the xylenes has been carried out. The photochemical transformation of one xylene to another must proceed through intermediates such as dimethyl benzvalene and dimethyl prismane.[9-12] Similar results were obtained for pyrazine and its methyl derivatives.[13,14]

In pyridine and in the picolines neither fluorescence nor phosphorescence has been observed, indicating that the energy is dissipated by radiationless transitions. No products could be identified upon irridation of pyridine vapor. Only a small triplet yield[15] was observed by the Cundall method.[16]

(1) The author is greatly indebted to Professor W. Albert Noyes, Jr., for his help and encouragement throughout the course of this work. He wishes to express his appreciation to the Robert A. Welch Foundation for support of this work through a grant to Dr. W. Albert Noyes, Jr., of the University of Texas at Austin. Dr. K. Nakamura was very helpful in obtaining the absorption spectra and in searching for fluorescent emission.

(2) J. Jortner, S. A. Rice, and R. M. Hochstrasser, *Advan. Photochem.*, **7**, 149 (1969), and references therein.

(3) J. Jortner, "Transitions Non Radiatives dans les Molécules," 20th Meeting of the Société de Chimie Physique, Paris, 1969, p 9.

(4) D. Phillips, J. Lemaire, D. S. Burton, and W. A. Noyes, Jr., *Advan. Photochem.*, **5**, 329 (1968).

(5) J. M. Blair and D. Bryce-Smith, *Proc. Chem. Soc.*, 287 (1957).

(6) K. E. Wilzbach, J. S. Ritcher, and L. Kaplan, *J. Amer. Chem. Soc.*, **89**, 1031 (1967).

(7) K. E. Wilzbach, A. L. Harkness, and L. Kaplan, *ibid.*, **89**, 1031 (1967).

(8) L. Kaplan and K. E. Wilzbach, *ibid.*, **90**, 3291 (1968).

(9) W. A. Noyes, Jr., and D. A. Harter, *ibid.*, **91**, 7585 (1969).

(10) D. Anderson, *J. Phys. Chem.*, **74**, 1686 (1970).

(11) L. Kaplan, K. E. Wilzbach, W. G. Brown, and S. S. Yang, *J. Amer. Chem. Soc.*, **87**, 675 (1965).

(12) I. E. Den Besten, L. Kaplan, and K. E. Wilzbach, *ibid.*, **90**, 5868 (1968).

(13) F. Lahmani and N. Ivanoff, *Tetrahedron Lett.*, 3913 (1967).

(14) F. Lahmani, H. Ivanoff, and M. Magat, *Compt. Rend.*, **263**, 1005 (1966).

The study of 2-picoline might prove interesting since ring positions are fixed by the nitrogen atom and by the methyl group, respectively. Hence the formation of 3- and 4-picoline might indicate benzvalene or prismane-type intermediates.

2-Picoline has two low excited singlet states, the $n-\pi^*$ with the 0–0 band at 277.6 nm and the $\pi-\pi^*$ with the 0–0 band at 265.7 nm.[17]

Experimental Section

Materials. 2-Picoline (Eastman) was purified by bulb-to-bulb distillation. About 20% was taken as the middle fraction. This was further purified by repeated preparative vapor phase chromatography (vpc) until no impurities could be detected by gas chromatography.

The benzene was Matheson Coleman and Bell chromatographic grade. It was purified by preparative vpc.

Biacetyl was supplied by Matheson Coleman and Bell. After two bulb-to-bulb distillations and further purification in the preparative vapor phase chromatograph, no impurity could be observed by capillary vpc.

Neopentane, isobutane, and *cis*-2-butene were Phillips research grade. Oxygen was taken from a lecture bottle (Matheson Coleman and Bell). These gases were used without further purification.

A conventional high-vacuum grease-free line was employed. Most experiments were carried out in a 2.5-ml cell which had a diameter of 1.8 cm and a length of 1 cm. For comparison a bigger cell (diameter 5 cm, length 8 cm) was employed. The emission spectra and emission quantum yields were obtained in a cross-shaped cell with 4-cm path length for the exciting light. The distance from the center of the emission zone to the exit windows of the side arm was 2.5 cm. The main light source was a Hanovia 929 B-9-U 2500-W mercury–xenon high pressure arc. Other light sources were a Hanovia S100 medium pressure arc, an Osram HBO 500-W high pressure mercury arc, and a Hanovia 977 B-1 1000-W mercury–xenon high-pressure arc. The latter was used for study of emission and sensitized emission. The total light intensity was varied by placing screens between the exit slit of the monochromator and the lens (f = 9 cm). The distance between lens and screen was 1 cm. The cell was located 8 cm behind the lens. A simple calculation shows that the reduction of light intensity in the cell is uniform across the light beam.

For photochemical experiments a grating monochromator (Baush and Lomb, Model 33-86-45) with a reciprocal linear dispersion of 1.6 nm/mm was employed. Since 2-mm entrance and exit slits were used, the maximum wavelength range for a given setting was about 6 nm, but over 80% was within a 3-nm range. For absorption and emission spectra a Jarrel-Ash, Czerny-Turner scanning spectrometer was used. The reciprocal linear dispersion was 0.8 nm/mm. The absorption spectrum was measured with a slit of 0.05 mm. The slit width for the emission data was 2 mm.

The light transmitted by the cell was measured with an RCA 935 phototube connected to a Keithley micromicroammeter Model 410. The emission intensity was measured by an Emi 6255 B photomultiplier. The phototube was calibrated by the use of the ferrioxalate actinometer.[18]

The products were analyzed on a Wilkins Hi-Fi aerograph chromatograph. Two different columns were used: (1) 1,2,3-tris(2-cyanethoxy)propane on Chromosorb W,[19] and (2) the column described by W. W. Hannemann and coworkers.[20] A slightly modified procedure led to the best results. Untreated Chromosorb W was washed in 10% KOH and thereafter with water until no alkaline reaction was observed. A 30-g sample of a eutectic mixture, composed of sodium, potassium, and lithium nitrates (18.2:54.4:27.3 wt %) was prepared and dissolved in water. Chromosorb W (100 g), 60–80 mesh, was added. The resulting mixture was evaporated to dryness and dried very carefully at 120° in a vacuum oven for 36 hr. A stainless steel tube 610 × 0.32 cm was used. Thereafter the column was kept for 25 hr in an oven at 200° and subsequently baked for 12 hr at 350°. The column was conditioned by repeated injection of 10^{-3} ml of 2-picoline.

Results

Absorption Spectrum of 2-Picoline. The spectrum of 2-picoline in the gas phase is shown in Figure 1. It shows absorption bands in the $\pi-\pi^*$ region which were analyzed by Rush and Sponer.[17] The oscillator strength for the $\pi-\pi^*$ band is f = 0.048, which agrees very well with the value reported by Stephenson[21] for the liquid phase. From this the mean radiative lifetime can be calculated to be τ_0 = 19 nsec.

Emission of 2-Picoline. Emission of 2-picoline, either fluorescence or phosphorescence, could not be observed. Attempts to excite emission by wavelengths 240–300 nm in the gas phase failed. No emission could be observed with the Jarrell-Ash spectrometer. In a glassy matrix no emission could be observed with the Amico-Bowman spectrofluorimeter.

Photochemistry of 2-Picoline. Long irradiation of 2-picoline in the liquid phase with an integrated absorption of 10^{20} quanta ml^{-1} in either the $\pi-\pi^*$ (248 nm) or

(15) J. Lemaire, *J. Phys. Chem.*, 71, 612 (1967).

(16) R. B. Cundall, F. J. Fletcher, and D. G. Milne, *Trans. Faraday Soc.*, 60, 1146 (1964).

(17) J. H. Rush and H. Sponer, *J. Chem. Phys.*, 20, 1847 (1952).

(18) J. H. Baxendale and N. K. Bridge, *J. Phys. Chem.*, 59, 783 (1955).

(19) L. D. Turkova, A. G. Vitenberg, and B. G. Belen'kii, *Neftekhimiya*, 7, 458 (1967).

(20) W. W. Hannemann, C. F. Spencer, and J. F. Johnson, *Anal. Chem.*, 32, 1386 (1960).

(21) H. P. Stephenson, *J. Chem. Phys.*, 22, 1077 (1954).

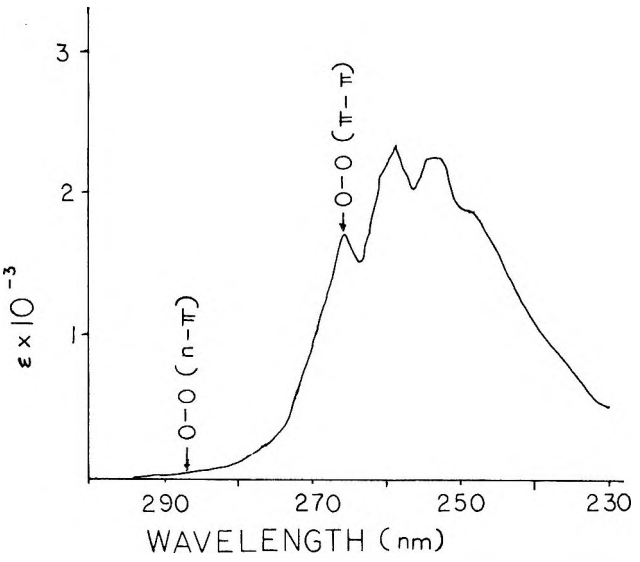

Figure 1. Absorption spectrum of 2-picoline in the gas phase: $P_{2\text{-picoline}}$ = 1 Torr, room temperature.

the n–π^* (265 nm) region did not produce products which could be detected by gas chromatgraphy.

The gas-phase photolysis of 2-picoline yields both 3- and 4-picoline. These compounds were identified by comparing retention times and peak forms of the pure isomers with the irradiated material on both columns described above. Table I shows the quantum yields

Table I: Isomerization of 2-Picoline to 3-Picoline and 4-Picoline

Wavelength, nm	Pressure of 2-picoline, Torr	Light absorbed, quanta/(ml sec)	$\Phi_{3\text{-picoline}} \times 10^4$	$\Phi_{4\text{-picoline}} \times 10^5$
238	1.5	2.2×10^{13}	5.1	4
248	1.0	2.6×10^{13}	3.4	3
266	1.5	3.0×10^{13}	0.9	0
280	6.0	2.2×10^{13}	0.0	0
293	7.0	1.7×10^{13}	0.0	0

of conversion into 3-picoline and to 4-picoline at various levels. The amount of light absorbed per second was in the range from 1.7 to 3.0×10^{13} quanta (ml sec)$^{-1}$. By varying the pressure of 2-picoline this range could be achieved over the whole spectrum. This was necessary to minimize the variation of intensity. The intensity effect will be discussed later.

Table I shows that on irradiation in the n–π^* transition no conversion of 2-picoline could be observed. In the π–π^* transition the quantum yields increase from 9×10^{-5} at the 0–0 band (266 nm) to 5.1×10^{-4} at 238 nm. At 238 and at 248 nm, 4-picoline could be observed. The ratio 3-picoline:4-picoline was at both wavelengths 10:1.

Figure 2 shows the increase of the quantum yield of conversion increases strongly with intensity up to about

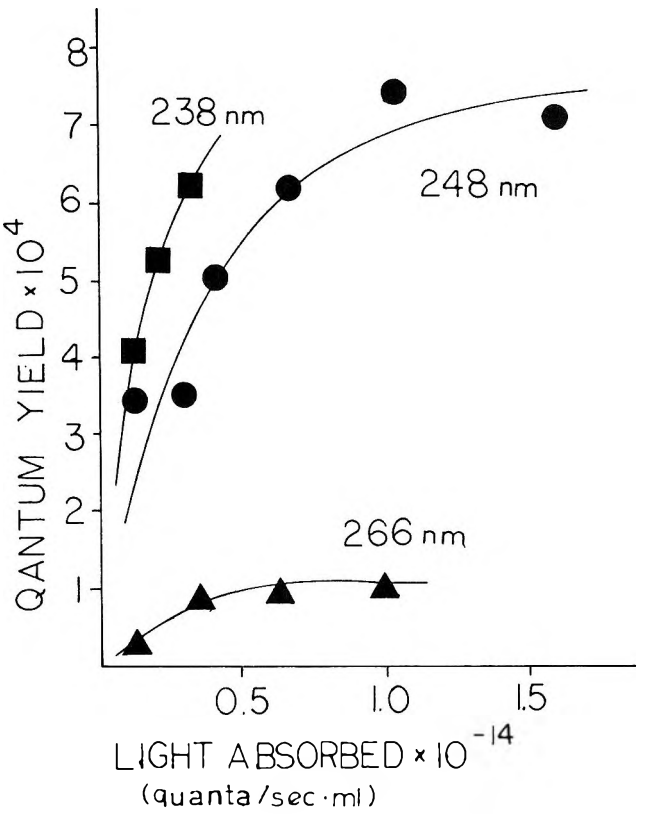

Figure 2. The quantum yield of the 3-picoline formation as a function of the light absorbed: room temperature.

5×10^{13} photons (ml sec)$^{-1}$. At high intensities the quantum yields do not change. The effect of intensity was much greater at short wavelengths. The value of Φ_I also increases at short wavelengths at high intensities. At 238 nm a constant value could not be obtained because the intensity of the lamp was not sufficient.

Cell size and surface coating have strong influences on conversion yields. In the bigger cell (diameter 5 cm, length 8 cm) the light beam covered an area of 4 cm^2. At 1 Torr pressure of 2-picoline and a total absorbed intensity of 3.2×10^{14} photons sec^{-1} a quantum yield of 1.4×10^{-3} was reached. The ratio of starting material to 3-picoline was very high because of the large volume of the cell. This made a good chromatographic separation very difficult, especially after only short irradiation times. After long times of irradiation the depolymerization of the product polymer might make the results meaningless. The latter effect will be discussed later.

Table II indicates that the coating of the surface of the cell has a strong influence. The highest yield of conversion was obtained with a conditioned surface. The cell was conditioned by irradiating 2-picoline vapor in the cell. However, if the cell was conditioned by irradiation of a mixture of 2-picoline and *cis*-2-butene, the quantum yield was much lower.

Neopentane (Figure 3, IV) and isobutane (III) at relatively high pressure quenched the formation of 3-

Table II: Wall Effects on the Photolysis of 2-Picoline λ 248 nm; Pressure of 2-Picoline 1 Torr

Cell surface/volume, cm^{-1}	Condition of the cell	Light absorbed, quanta/sec	$\Phi_{3\text{-picoline}} \times 10^{3}$	$\Phi_{4\text{-picoline}} \times 10^{1}$	$\Phi_{polymer}$, arbitrary units
4.2	Acid washed	4.3×10^{14}	1.4	1	2.5
4.2	Freshly flamed	4.4×10^{14}	0.6	0	0.9
4.2	Conditioned with polymer formed by irradiation of pure 2-picoline	4.0×10^{14}	7.0	6	1.5
1.1	Conditioned with polymer formed by irradiation of pure 2-picoline	3.2×10^{14}	14.0	8	1.3
4.2	Conditioned with polymer formed by irradiation of 2-picoline + *cis*-2-butene	5.1×10^{14}	3.7	...	...

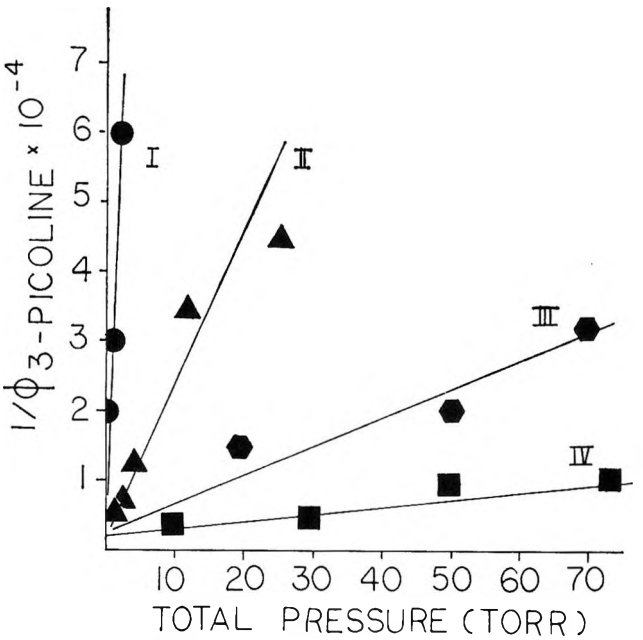

Figure 3. The quenching of 3-picoline formation: I, oxygen; II, *cis*-2-butene, III, isobutane; IV, neopentane, room temp, exciting wavelength = 248 nm.

picoline. From these experiments it can be concluded that vibrationally excited molecules play a significant role in the isomerization of 2-picoline. *cis*-2-Butene (II) is a very effective quencher for the isomerization. It is improbable that *cis*-2-butene is ten times more effective for vibrational relaxation than is isobutane. Therefore a reaction between a singlet or a triplet and *cis*-2-butene probably occurs. Oxygen is a very effective quencher for the isomerization of 2-picoline. A pressure as low as 1 Torr reduced the quantum yield of 3-picoline to about 2×10^{-5}, the limit of sensitivity of the analysis.

Sensitized Isomerization of 2-Picoline. The photochemistry of benzene is fairly well known. Attempts were made to sensitize the isomerization with benzene (Table III). The cell surface was conditioned by irradiating a mixture of benzene and 2-picoline. The addition of 56 Torr of benzene decreased the quantum yield

Table III: Benzene-Sensitized Isomerization of 2-Picoline at 248 nm; Cell Surface/Volume = 1:1

Pressure of 2-picoline, Torr	Pressure of benzene, Torr	$\Phi_{3\text{-picoline}} \times 10^{3}$
6.0	0.0	1.6
6.0	56.0	1.3
3.0	58.0	0.8
0.5	61.0	0.3

by only a small amount. If the total pressure is kept constant the quantum yield of isomer formation decreases with decreasing 2-picoline pressure.

Polymer Formation. For the formation of polymer, no reproducible results could be obtained. Some qualitative results follow. The amount of polymer increases with decreasing wavelength. A dependence of polymer formation on light intensity could not be found. Much more polymer is formed in the presence of oxygen as measured by light absorption by the windows. If the polymer is irradiated at 248 or 238 nm, depolymerization occurs. The following quantum yields of depolymerization are only accurate to an order of magnitude. 2-Picoline ($\Phi_{max} = 2 \times 10^{-3}$) and 3-picoline ($\Phi_{max} = 1 \times 10^{-3}$) could be observed. Small amounts of a lower boiling product could not be identified. These quantum yields represent maximum values obtained in a cell of the ratio surface/volume of 4.2 cm^{-1} with a fresh polymer coating. Aged polymer and polymer which was exposed to oxygen yielded only traces of depolymerization products. A far more detailed study of the polymerization and depolymerization processes is needed before conclusions concerning their nature can be reached.

Exposure of 2-picoline in the gas phase in either the $n-\pi^*$ or the $\pi-\pi^*$ region does not lead to emission. The radiative lifetime for the upper $n-\pi^*$ singlet is estimated to be 590 nsec by use of the value for the oscillator strength given by Stephenson.[21] The lifetime was calculated using the equation $\tau = 1.50/\bar{\nu}f$. $\bar{\nu}$ denotes the wave number of the maximum absorption, and f sym-

Properties of the θ-Pinch Flash Lamp[1a]

by Eric E. Daby, Joe S. Hitt, and Gilbert J. Mains[1b]

Departments of Chemistry and Electrical Engineering, University of Detroit, Detroit, Michigan 48221
(Received June 25, 1970)

The θ-pinch plasma device has been investigated as a light source for flash photochemical applications. The electrodeless flash lamp emits a many line spectrum superimposed upon an underlying continuum. The intensity and duration of the optical emission was studied as a function of circuit inductance, capacitance, drive coil geometry, gas composition, gas pressure, and lamp geometry. Flash intensities greater than 10^{22} quanta cm^{-2} sec^{-1} have been attained at flash lifetimes less than 10 μsec. The θ-pinch flash lamp is shown to be a reliable and inexpensive high-intensity light source suitable for photochemical studies from the vacuum ultraviolet through the visible regions of the spectrum. The vacuum ultraviolet flash photolysis of acetaldehyde and the kinetic spectroscopic study of naphthalene are briefly described applications of the θ-pinch flash lamp.

Introduction

The fast magnetic compression of plasmas has been the subject of intensive research for the past two decades.[2] These "pinch devices" are usually classified according to the motion of the plasma current as "z-pinch" (axial current) or "θ-pinch" (circular current). The prime interest in these devices stems from early observations of neutron emission from the plasma formed from deuterium gas and the potential applications of these neutrons in controlled thermonuclear reactions. Recent studies of ion heating,[3] energy losses from short θ-pinch devices,[4] and long pinches[5] have all been undertaken from this viewpoint. The studies of radiation emission, of direct interest in the present investigation, have been performed using only low-pressure deuterium gas plasmas.[6] However, optically dense plasmas are desirable in studies in which the light emission is of prime concern.

Dense θ-pinch discharges, while not the subject of intensive research, have attracted the attention of Feldman, Hitt, and coworkers[7-9] mainly as an optical pump for lasers. Some circuit characteristics have been reported by Silberg,[10] and Buser, *et al.*,[11] have reported on the effects of preionization of the lamp gas. However, except for a publication dealing with the z-pinch[12] and a preliminary report of the present research,[13] the application of pinch devices as high-intensity light sources in photochemistry has received little attention. In this paper we describe the dense θ-pinch flash lamp, examine the effect of circuit parameters on the optical characteristics of the discharge, and demonstrate the utility of the θ-pinch for flash photolysis and kinetic spectroscopy.

Experimental Section

Figure 1 depicts the relative simplicity of the θ-pinch device. A low inductance capacitor (or bank of capacitors) is discharged through a high-capacity switch (often a spark gap) to produce a current (of the order of megaamperes) in the drive coil. The lamp, which is electrodeless, is located within the drive coil and may be of the annular geometry of Figure 1 or of other configurations. In the experiments reported here the lamp was constructed of Pyrex or fused quartz although any nonconductive material may be used. The lamps were evacuated overnight prior to filling. The lamp gas, Xe, Ar, Kr, or their mixtures, was then expanded from a storage bulb into the lamp to a pressure of approximately 10 Torr. The antenna from a Raytheon Model PGM-10 microwave generator was located close to the lamp and used to excite a microwave discharge within the lamp. The discharge, initially the characteristic color of the filling gas, gradually became white as the water vapor was driven from the lamp walls. The gas was then pumped from the lamp through a liquid nitrogen trap, and the lamp was refilled with fresh filling gas. This procedure was repeated until the

(1) (a) Taken in part from a thesis submitted by E. E. Daby to the Graduate School, University of Detroit, in partial fulfillment of the requirements for the Ph.D. degree. (b) To whom correspondence should be addressed.

(2) W. E. Quinn in "Plasma Physics and Thermonuclear Research," Vol. 2, C. L. Longmire, *et al.*, Ed., Macmillan, New York, N. Y., 1963.

(3) R. Wilhelm, *Z. Phys.*, 222, 208 (1969).

(4) W. B. Jones, L. M. Goldman, R. W. Kilb, and R. L. Bingham, *Phys. Fluids*, 13, 800 (1970).

(5) A. D. Beach, H. A. B. Bodin, C. A. Bunting, D. J. Dancy, G. C. H. Heywood, M. R. Kenward, J. McCartan, A. A. Newton, I. K. Pasco, R. Peacock, and J. L. Watson, *Nucl. Fusion*, 9, 215 (1969).

(6) T. S. Green, D. L. Fisher, A. H. Gabriel, F. J. Morgan, and A. A. Newton, *Phys. Fluids*, 10, 1663 (1967).

(7) R. Brandewie, J. S. Hitt, and J. Feldman, *J. Appl. Phys.*, 34, 3415 (1963).

(8) J. S. Hitt, "Investigation of High Luminosity Theta-pinch Discharges with Application to Laser Pumping," Ph.D. Thesis, Carnegie Institute of Technology, Pittsburgh, Pa., 1964.

(9) J. Feldman, *J. Appl. Phys.*, 37, 674 (1966).

(10) P. Silberg, *ibid.*, 37, 2155 (1966).

(11) R. G. Buser and A. Papayoanou, *IEEE J. Quantum Electron.*, QE-3, 227 (1967).

(12) E. G. Niemann and M. Klenert, *J. Appl. Optics*, 7, 295 (1968).

(13) E. E. Daby and G. J. Mains, 153rd National Meeting of the American Chemical Society, Miami Beach, Fla., April 1967.

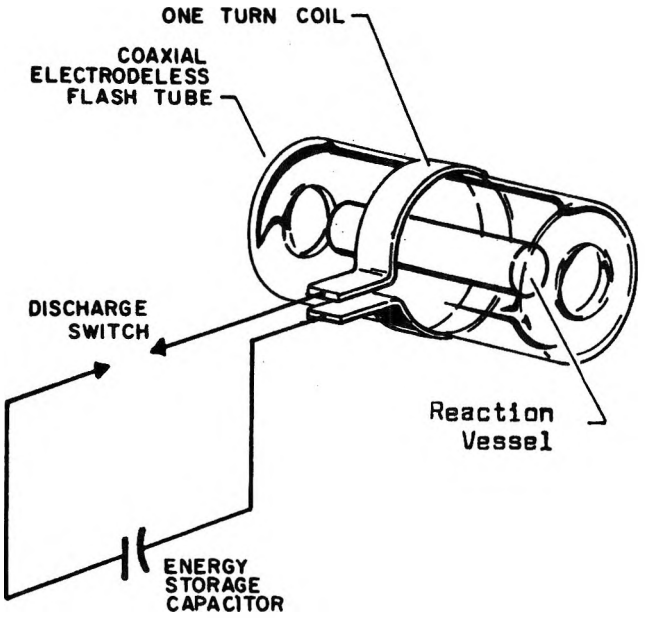

Figure 1. Schematic diagram of the dense θ-pinch flash lamp system.

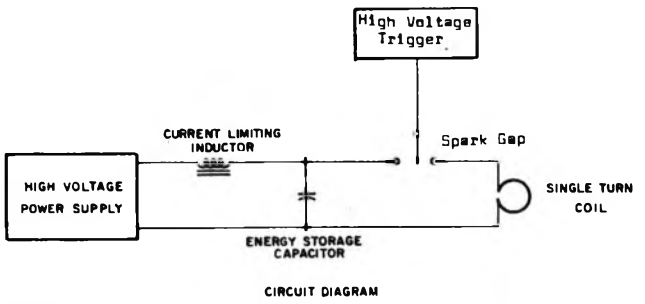

Figure 2.

discharge retained the characteristic color of the filling gas for at least 20 min. The lamp was then sealed by collapsing a constriction on the filling line. Lamps filled in this manner have been used for 3 years with little change in their emission characteristics. The sealed lamp was then located within the drive coil and ready for use.

The drive coil was one or more turns of 0.25-in. copper tubing or large diameter copper wire. Most efficient coupling was obtained when the coil diameter was slightly larger than the lamp diameter. If the drive coil fit too snugly, the lamp would shatter, presumably a result of magnetostriction of the drive coil during the discharge.

The circuit diagram is given in Figure 2. The high voltage dc power supply was continuously variable from zero to 60 kV. The energy storage capacitors were one or more General Electric heavy-duty storage capacitors (14F734G) rated at 1.0 μF at 50 kV with an internal inductance of 0.01 μH. Construction details for the triggered spark gap and high-voltage trigger circuit have been published.[1]

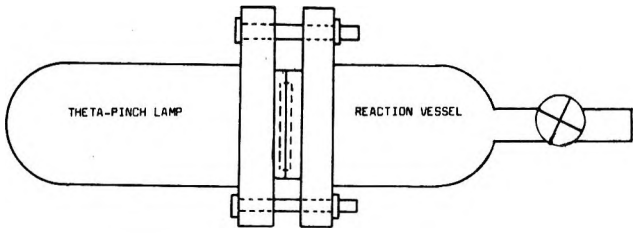

Figure 3. Schematic diagram of the lamp and reaction vessel used in vacuum uv photolysis experiments.

The temporal profile of the θ-pinch emission was followed using a 929 photodiode which was coupled to a 515A or 533 Tektronix oscilloscope through a cathode follower circuit. The lifetime was defined as the time interval for the light flux to rise and fall from half its maximum value.

Light intensities were calculated from chemical actinometry data combined with lifetime measurements. In the visible–near-uv region, 2500–5770-Å region, the potassium ferrioxalate actinometer of Hatchard and Parker[14,15] was employed. An optically dense potassium ferrioxalate solution was placed in a quartz reaction vessel, 3.30 cc in volume, and located in the annular section of the lamp in Figure 1. The yield of ferrous ion was found to be linearly dependent on the number of flashes. Later, it was established that the maximum signal from the 929 photodiode was proportional to the light intensity as determined by chemical actinometry provided the optical geometry was not altered. The phototube signal provided a measure of the light intensity in some later experiments.

In the vacuum ultraviolet region of the spectrum carbon dioxide actinometry was employed. For these experiments an end-on geometry was employed as shown in Figure 3. The lamp and the reaction vessel were constructed from Pyrex O-ring joints, 40 mm i.d., by substituting a two-piece Teflon gasket for the 50-mm O-ring. The Teflon gasket was machined to provide a compression seal against the Pyrex and a 50-mm diameter, 2 mm thick LiF window which separated the θ-pinch flash from the reaction zone. The quantum yield of carbon monoxide was taken as unity.[16]

Results and Discussion

Circuit Parameters. The light emission was studied as a function of capacitance, discharge voltage, and drive coil geometry (inductance). The choice of these parameters stems from the temporal profile of the θ-pinch emission (Figure 4 is a typical observation) which is similar to the light emission from a typical gas-filled flash lamp in an underdamped RCL circuit.

(14) C. A. Parker and C. G. Hatchard, *Proc. Roy. Soc., Ser. A*, **235**, 518 (1956).

(15) C. A. Parker, *ibid.*, **220**, 104 (1953).

(16) A. Ung and H. I. Schiff, *Can. J. Chem.*, **44**, 1981 (1966).

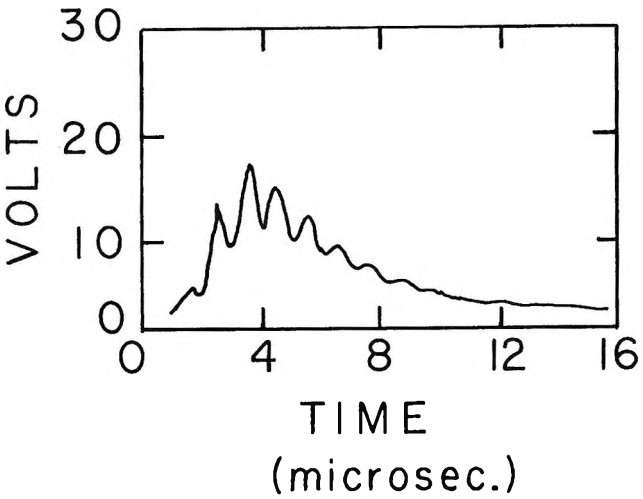

Figure 4. Signal response of 929 photodiode to typical θ-pinch discharge.

Unfortunately, neither the light emission nor the discharge current is readily amenable to such a simple mathematical analysis because the effective resistance of the plasma changes during the discharge.[10] Nonetheless, from a practical viewpoint a knowledge of the qualitative effects of these parameters is necessary for the intelligent design of a θ-pinch lamp system for photochemical studies. For this reason we report the effects of varying the capacitance, discharge voltage, and circuit inductance and direct the interested reader to Silberg's excellent paper[10] for insight into the mathematical analysis. The lamp parameters, to be discussed later, were fixed for the following sequence of experiments. The lamp geometry was identical with that shown in Figure 1. The lamp diameter was 24 mm; the annulus diameter was 10 mm; the lamp was constructed of fused quartz and filled with a gas mixture [100 ppm Xe in Ar] to a pressure of 10 Torr.

Capacitance. Three capacitors were employed to provide a range of 0.33 to 3.0 μF by wiring in series and in parallel. The drive coil was a single turn of copper wire and the discharge voltage maintained at 35 kV. The results are given in Table I. Instead of the expected linear dependence of energy dissipated per flash upon capacitance ($E = CV^2/2$), a much more complicated situation was encountered. Because of the low inductance in the electrical circuit any rewiring of the capacitors also produced a significant change in the circuit inductance which, in turn, affected the lifetime of the discharge and the efficiency with which energy was dissipated in the plasma. It is readily seen from Table I that additional wiring for the 0.33 μF (series hook-up) and 3.0 μF (parallel hook-up) both caused significant increases in the discharge lifetime. In fact, the simplest circuit (one capacitor, 1.0 μF) was the most efficient in our experiments. Therefore, the only efficient way to increase energy storage *via* increasing capacitance is to utilize larger single capacitors. The use of a large bank of capacitors, common in the usual flash lamp systems, is simply not practical for the θ-pinch lamp.

Table I: Plasma Emission Dependence on Capacitance

Capacitance, μF	Lifetime, μsec	Photoconversion, quanta cc^{-1} flash^{-1} $\times$ 10^{-17}
0.33	12	0.8
0.50	8	1.4
1.0	7	2.3
2.0	15	2.6
3.0	24	2.8

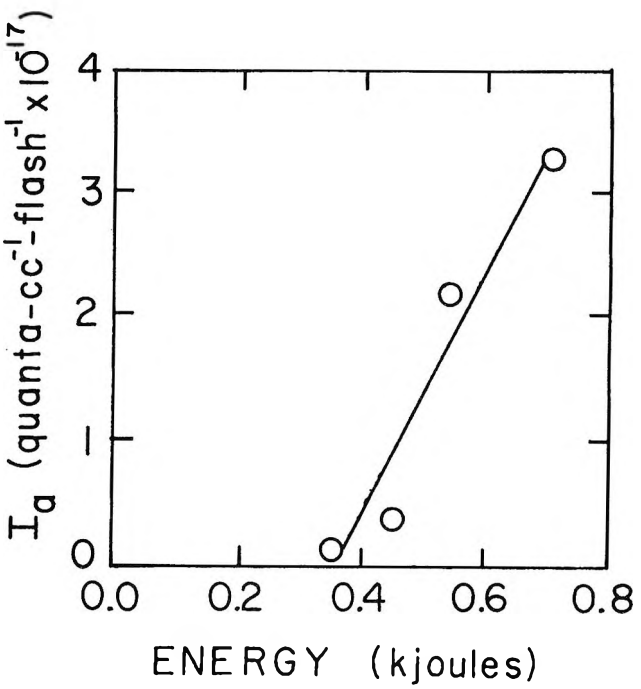

Figure 5. Light output as a function of stored energy: C = 1.0 μF; one-turn drive coil; 6-μsec lifetime.

Discharge Voltage. Provided the inductance and the capacitance of the circuit were fixed, the light output was a linear function of the stored energy, $CV^2/2$. This is illustrated by the results, presented in Figures 5 and 6, of experiments in which the discharge voltage was varied from 20 to about 40 kV. In Figure 5, the light output as measured by chemical actinometry is presented as a function of the stored energy of a single 1-μF capacitor. Each point represents the average of three actinometric determinations. The reproducibility of the θ-pinch lamp emission is demonstrated by the results presented in Figure 6. In this experiment the phototube signal was used to monitor the light output. Each point represents a single measurement of the emission from the lamp driven by a capacitor bank of three parallel 1-μF capacitors. The flash lifetime was essentially constant over this voltage range at 6

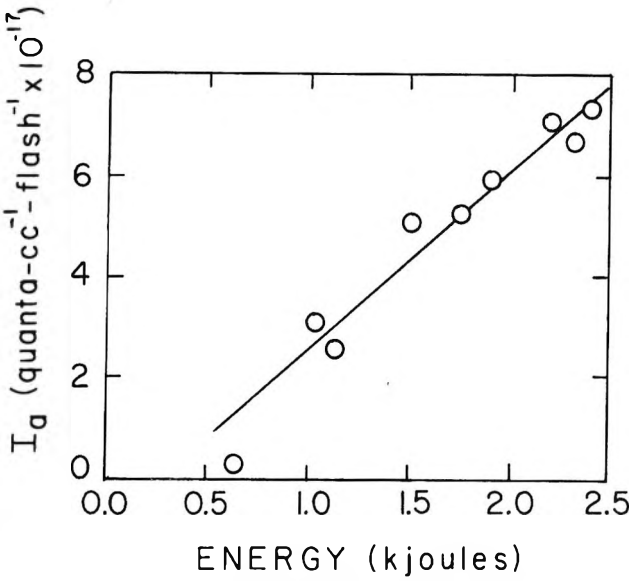

Figure 6. Light output as a function of stored energy: C = 3.0 μF; one-turn drive coil; 22-μsec lifetime.

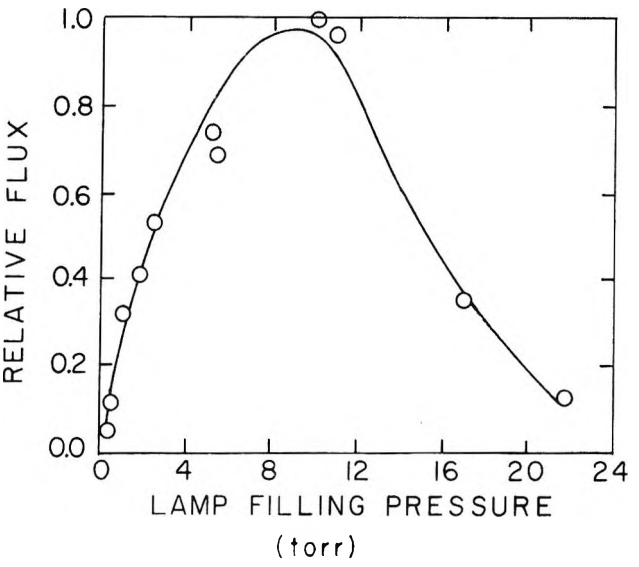

Figure 7. Light output as a function of lamp-filling pressure (see text for details).

and 22 μsec for the 1 and 3-μF capacitors, respectively. Above the threshold energy for plasma generation, light output was linearly dependent on the energy stored in the capacitor. It should be noted here that the threshold energy was markedly dependent on the geometry of the spark gap switch. Spark gap designs which lowered the switch inductance decreased the threshold energy.

Coil Inductance and Geometry. The problems arising from the low impedance requirements of the θ-pinch circuitry became most evident when attempts were made to examine the effect of the drive coil in the emission process. Coil sizes ranged from a single turn, 1-in. diameter coil to a seven-turn, 2-in. diameter coil. Qualitatively, as the coil inductance was increased by either increasing the coil diameter or the number of turns, the emissive output was increased. Furthermore, the lifetime of the discharge was not measurably changed during this variation in coil geometry suggesting that the drive coil inductance was a small part of the circuit inductance. These qualitative observations are in agreement with Silberg's study[10] which employed a 1.125-in. diameter lamp filled with 5 Torr of Ar. It is also pertinent to note that Silberg found that 59% of the stored energy (measured calorimetrically) could be dissipated in such a lamp using an eight-turn drive coil! Such efficiencies are indeed comparable to those obtained using conventional flash lamps.

Lamp Parameters. The parameters considered in this study were the nature of the lamp gas, the pressure of the gas, and the lamp geometry. For these experiments the most efficient circuit parameters were employed, *i.e.*, one capacitor (1.0 μF), discharge voltage fixed at 28 kV, and a single-turn, 1-in. diameter drive coil. The most critical lamp parameter was found to be gas pressure. Figure 7 shows the dependence of light emission on filling pressure for the gas mixture, 100 ppm of Xe in Ar. Below 1 and above 20 Torr the plasma could not be formed without altering the circuit parameters. The light flux at the maximum corresponded to 3×10^{22} quanta cm^{-2} sec^{-1} in the annulus. Argon, krypton, and xenon were also investigated in this study and exhibited pressure dependencies similar to that of Figure 7. The pure gases exhibited maxima in the same pressure range but lower maximum light flux than the mixture. That is, the observed order of light flux emission was as follows: 100 ppm of Xe in Ar > pure Xe > pure Kr > pure Ar. However, there was less than a factor of ten variation between the gases and discussion of the reasons for these observations is not necessary here. The final parameter, lamp geometry, had very little effect on the light output except for the interdependence of lamp diameter and drive coil diameter noted earlier. It should be noted, however, that very short lamps tended to confine the plasma and reduce the light output. While we do not report the spectral distributions of the lamps employed in this research, it is pertinent to note that they are similar to those reported by Feldman.[9] Lines in the emission from a krypton discharge have been assigned to Kr(IV) transitions and to Si (arising from quartz walls). Some of the transitions have not been assigned and may be the result of dielectronic excitation in the plasma. These characteristic lines are broadened and superimposed upon continuum to which a black-body temperature in excess of 10,000°K has been assigned. Thus, the light emission from a dense θ-pinch lamp may be thought of in terms of a continuum of almost uniform intensity throughout the visible–uv region with characteristic lines from the filling gas and wall material superimposed.

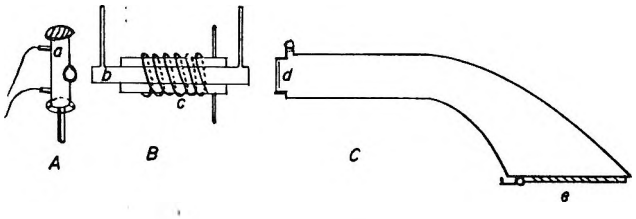

Figure 8. Kinetic θ-pinch photolysis apparatus: A, xenon flash lamp; a, lamp housing; B, θ-pinch lamp; b, reaction vessel; c, discharge coil; C, spectrograph; d, slit; e, photographic plate holder.

Applications to Kinetic Spectroscopy. One of the earliest applications of conventional flash lamps was in the area of kinetic spectroscopy. The techniques, involving conventional flash lamps, have been adequately reviewed by Norrish[17] and Porter.[18] To determine the suitability of the θ-pinch flash lamp for such studies the apparatus, diagrammed in Figure 8, was constructed. The annular design θ-pinch lamp is shown in section B of Figure 8. The reaction vessel, designated as "b," is a fused quartz cylinder, 25 mm diameter, 300 mm in length, closed at either end with optical quality fused quartz windows. The θ-pinch lamp, surrounding the reaction vessel, is 55 mm in diameter and 200 mm in length and was filled with 10 Torr of Xe. The drive coil was seven turns of 0.25-in. copper tubing which loosely fitted the θ-pinch lamp. The other circuit parameters for the θ-pinch lamp were as follows: capacitance, 1.0 μF; discharge voltage, 25 kV. The lifetime of the θ-pinch flash was 18 μsec. The spectrographic flash lamp, designated as section A of Figure 8, was a special design, U-shaped, xenon flash lamp constructed by E.G.G. Co. A 0.5-μF capacitor, charged to 10 kV, was discharged through the spectrographic flash within 25 μsec. Conventional circuitry[19] was used to delay the spectrographic flash for 0–1000 μsec after the θ-pinch flash. The absorption spectrum of the sample in the reaction vessel was recorded on Kodak spectrographic plates, Type 103-F, using the Hilger medium quartz spectrograph, Model E-498, designated as section C on Figure 8. For the experiments reported here the reaction vessel was filled with a 0.031 *M* solution of naphthalene in ethanol and thoroughly outgassed using conventional high vacuum techniques. Spectra, recorded at various time intervals following the θ-pinch flash, are presented in Figure 9. Two transient absorptions were observed. The shorter lived transient near 3900 Å and the longer lived absorption near 4100 Å have been observed previously by Porter[20] and have been assigned to $T_0 \rightarrow T_2$ and $T_0 \rightarrow T_1$ transitions of the triplet state of naphthalene.

The relative ease with which the θ-pinch flash lamp was adapted to kinetic spectroscopic experiments suggests that further refinements (*i.e.*, increasing the light output of the θ-pinch and decreasing the lifetime of the two flashes) will be forthcoming in the near future.

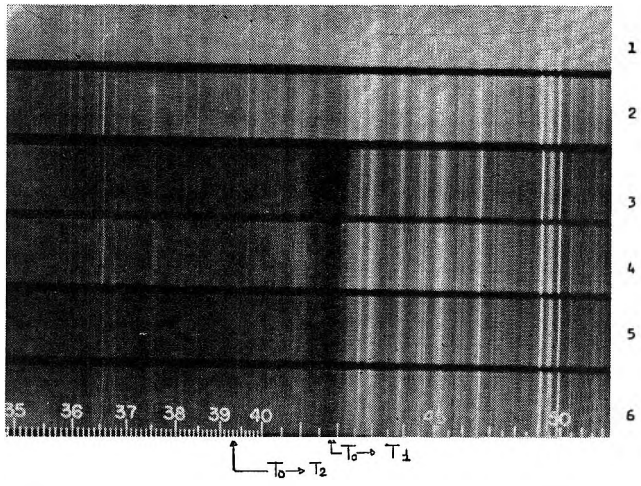

Figure 9. Plasma pinch kinetic flash spectroscopy of 0.031 *M* naphthalene in ethanol. Spectrographic flash without the plasma pinch flash (1), fired 0.00 μsec after plasma pinch flash (2), fired 25 μsec after flash (3), fired 50 μsec after flash (4), fired 75 μsec after flash (5), fired 90 μsec after flash (6).

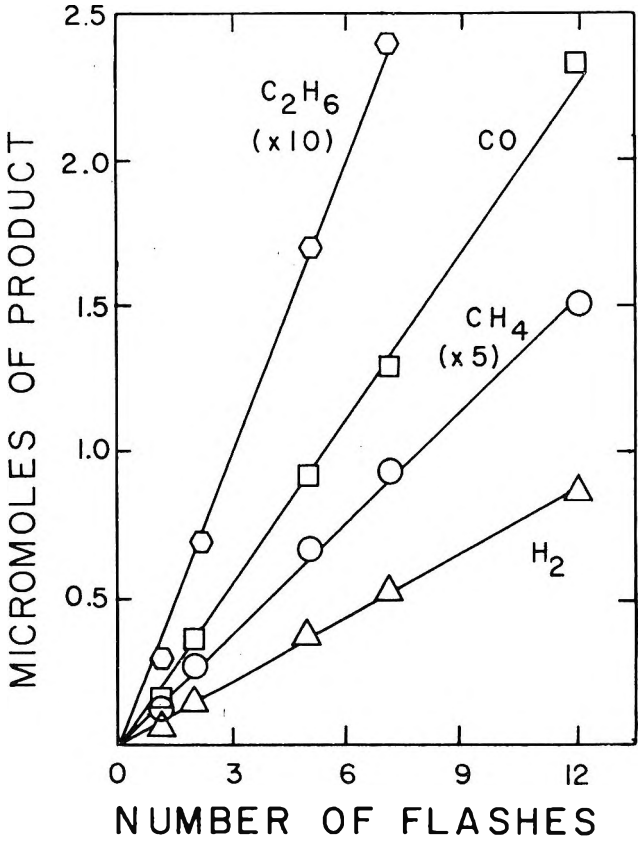

Figure 10. Product yields from acetaldehyde as a function of the number of θ-pinch flashes (see text for details).

(17) R. G. W. Norrish, "Nobel Symposium 5 Fast Reactions and Primary Processes in Chemical Kinetics," Stig Claesson, Ed., 1967, p 33.

(18) G. Porter, ref 17, p 141.

(19) G. Porter, "Technique of Organic Chemistry," A. Weissberger, Ed., Interscience, New York, N. Y., 1963, p 1055.

(20) M. Windsor and G. Porter, *Discussions Faraday Soc.*, 17, 178 (1954).

Although it must be admitted that the θ-pinch kinetic spectroscopy system will never become competitive with the recently developed Q-spoiled laser systems[21,22] for kinetic spectroscopy because of the nanosecond resolution times of the latter, it must also be pointed out that the θ-pinch kinetic spectroscopy system is currently considerably less expensive, requires less technical skill to build and maintain, and is not limited to a single wavelength as is the laser system.

θ-Pinch Vacuum Uv Flash Photolysis. In view of the high-temperature black-body continuum which underlies the emission from the dense θ-pinch flash it is not surprising that considerable radiation must be emitted at wavelengths shorter than 2000 Å as limited by fused quartz. This is simply demonstrated by using a θ-pinch lamp of the end-on design, illustrated in Figure 3, with polished LiF windows which transmit to 1150 Å. Carbon dioxide, which absorbs light below 1650 Å at the pressures employed here and decomposes into carbon monoxide, was employed as an actinometer. Based on the yield of carbon monoxide per flash, we estimate a light emission of 2×10^{16} quanta cm^{-2} $flash^{-1}$ in the region 1650–1150 Å. In view of the fact that the light emission in the region 2000–5770 Å was only 2.3×10^{17} quanta cm^{-2} $flash^{-1}$ (see Table I) it must be concluded that the θ-pinch is indeed a very intense flash lamp in the vacuum ultraviolet.

To demonstrate the utility of the θ-pinch flash lamp in the vacuum uv region some preliminary results from the flash photolysis of acetaldehyde[23] are presented in Figure 10. The initial pressure of acetaldehyde was 5 Torr at 25° and 0.5% was decomposed per flash. The products were analyzed using a C.E.C. 21-103C (modified) mass spectrometer. The linearity of the product yields suggests that secondary reactions can be ignored up to 5% conversion in the vacuum uv photolysis, simplifying the interpretation of the data. A more complete report, utilizing mixtures of acetaldehyde and perdeuterioacetaldehyde, will be published[23] and the mechanistic implications of Figure 10 will be discussed in more detail then. These data are presented here solely to illustrate the versatility of the θ-pinch flash lamp.

Conclusions

The θ-pinch flash lamp is a convenient and inexpensive flash lamp system for simple flash photolysis experiments or kinetic spectroscopy experiments. Because of the electrodeless nature of the θ-pinch lamp, construction and maintenance are simple and inexpensive. Although the light flux is of the same order of magnitude as conventional flash lamps, the microsecond lifetime region is more easily accessible. Also, because of the higher black-body temperature of θ-pinch lamps they are efficient sources in the vacuum ultraviolet. However, the low-inductance circuitry of the θ-pinch devices is not readily "scaled up" as has been done in the case of conventional flash lamp systems. Also, because a microsecond or so is usually required to build up the plasma and pinch it, the θ-pinch flash will not be extended into the nanosecond lifetime region. In spite of these limitations the authors believe that the θ-pinch flash lamp is a useful addition to the light sources available for photochemical studies.

Acknowledgments. The U. S. Air Force Office of Scientific Research has patiently supported this new research effort at the University of Detroit and must be thanked by the authors. Mr. Randolph Mateer constructed the kinetic spectroscopy system and Mr. Cesar Castillo obtained the data recorded in Figure 9; their contributions are gratefully acknowledged.

(21) J. R. Novak and M. Windsor, *J. Chem. Phys.*, **47**, 3075 (1967).
(22) M. R. Topp and G. Porter, *Proc. Roy. Soc., Ser. A*, **315**, 163 (1970).
(23) E. E. Daby and G. J. Mains, to be published.

Radiolysis of 1 *M* Aqueous Ethanol Solutions of Potassium Nitrate

by Ch. Baquey, J. C. Roux,* and J. Sutton[1]

Centre d'Etudes Nucléaires de Bordeaux-Gradignan, Le Haut-Vigneau 33, Gradignan, France (*Received May 19, 1970*)

Deaerated solutions containing 1 *M* ethanol and different concentrations of nitrate ion have been irradiated with cobalt-60 γ radiation and the following products analyzed: hydrogen, nitrite ion, acetaldehyde, 2,3-butanediol, hydrogen peroxide, methane, ethane, and ethylene. The formation of an apparently "molecular" yield of acetaldehyde with $G = 1.3 \pm 0.15$ has been demonstrated and its origin explained in terms of the capture of radical pairs close to their site of production. The nitrite yields in the range $[NO_3^-] = 10^{-3}$ to 5×10^{-3} *M* lead to a value for the free ion solvated electron yield $G_{e_s^-(f.i.)} = 2.55 \pm 0.10$ and the data at high nitrate concentrations indicate that in 1 *M* aqueous ethanol G(total ionization) ≥ 4.15 and $G(-H_2O) = 4.6 \pm 0.4$.

In the search to unravel the mechanism of the radiolytic decomposition of liquid water and to establish accurate values of the initial yields of the known radical and molecular products, numerous authors have employed low concentrations of alcohols[2-13] to scavenge hydrogen atoms and hydroxyl radicals usually in the presence of a second solute such as O_2, N_2O, etc. to capture solvated electrons. From the measured yields of the stable products such as hydrogen, aldehydes, glycols, etc., and information on the mechanisms involved in their formation, values of the primary yields of the various aqueous species designated, respectively, $G_{e_s^-}$, G_H, G_{OH}, G_{H_2}, and $G_{H_2O_2}$, have been derived. The yield of H_3O^+ has been almost entirely neglected.[14,15]

Current diffusion theories of liquid radiolysis[16,17] suppose that in water a large fraction of the yields of H, H_2, and H_2O_2 are formed by radical recombination processes in the regions of high ionization density, the spurs, where high initial concentrations and strong coulombic interactions may play an important role. Some evidence for the existence of such inhomogeneous distributions of primary species is to be found in recent esr relaxation time studies.[18,19]

Certain of the intraspur reactions will lead to the reformation of water; consequently, it is impossible to determine the overall decomposition of water, $G(-H_2O)$, or the total ionization yield, $G_{e_T^-}$, from results such as those mentioned above obtained with low solute concentrations. On the other hand, the use of high concentrations of scavenging solutes introduces problems due to the direct absorption of energy by these solutes with the resultant formation of products indistinguishable from those formed by the indirect effect. The difficulties of interpretation thus introduced have tended to discourage work in this direction. Moreover in the few studies[20,21] that exist, product analyses, and hence the conclusions, have only been partial.

The present paper describes the results obtained in the radiolysis of concentrated aqueous solutions of ethanol containing potassium nitrate. The ethanol concentration was kept constant at 1 mol $l.^{-1}$ while the nitrate ion concentration was varied between 10^{-5} and 3 mol $l.^{-1}$. All significant products were analyzed.

Experimental Section

Triply distilled water, radiolyzed and then photolyzed to destroy H_2O_2, was used, after degassing, to make up the solutions. Ethanol (Merck absolute) was refluxed in the presence of 2,4-dinitrophenylhydrazine for 12 hr and then distilled in a stream of oxygen-free nitrogen. Its purity was checked by gas chromatography and by measuring its radiolytic hydrogen yield which gave a value, $G(H_2) \geq 4.85$. Nitrate solutions were prepared from the potassium salt (Hopkin and Williams

*To whom correspondence should be addressed.

(1) Service de Chimie Physique, C.E.N. de Saclay.

(2) G. G. Jayson, G. Scholes, and J. Weiss, *J. Chem. Soc.*, 1358 (1957).

(3) J. T. Allan and C. M. Beck, *J. Amer. Chem. Soc.*, **86**, 1483 (1963).

(4) J. T. Allan, *J. Phys. Chem.*, **68**, 2697 (1964).

(5) W. A. Seddon and A. O. Allen, *ibid.*, **71**, 1914 (1967).

(6) B. H. J. Bielski and A. O. Allen, *Int. J. Radiat. Phys. Chem.*, **1**, 153 (1969).

(7) T. A. Woodward and H. C. Sutton, *Trans. Faraday Soc.*, **62**, 70 (1966).

(8) J. T. Allan and G. Scholes, *Nature*, **187**, 218 (1960).

(9) A. Appleby, G. Scholes, and M. Simic, *J. Amer. Chem. Soc.*, **85**, 3891 (1963).

(10) M. Anbar and D. Meyerstein, *Proc. Chem. Soc.*, 23 (1964).

(11) P. Kelley and M. Smith, *J. Chem. Soc.*, 1487 (1961).

(12) J. Rabani and G. Stein, *J. Chem. Phys.*, **37**, 1865 (1962).

(13) G. Scholes and M. Simic, *J. Phys. Chem.*, **68**, 1738 (1964).

(14) B. Cercek and M. Kongshaug, *ibid.*, **73**, 2056 (1969).

(15) K. H. Schmidt and S. M. Ander, *ibid.*, **73**, 2846 (1969).

(16) A. Kupperman, *Actions Chim. Biol. Radiat.*, **5**, 85 (1961).

(17) A. Kupperman, "Radiation Research," Ed. Silini, North-Holland Publishing Co., Amsterdam, 1967, p 212.

(18) J. Kimbrick and L. Kevan, *J. Chem. Phys.*, **47**, 2367 (1967).

(19) B. G. Ershov, G. P. Tchernova, O. Ya. Grinberg, and Ya S. Lebedov, *Izv. Akad. Nauk S.S.S.R., Ser. Khim.*, 2439 (1968).

(20) H. A. Mahlman, *J. Phys. Chem.*, **70**, 3983 (1966).

(21) J. C. Russell and G. R. Freeman, *J. Chem Phys..*, **48**, 90 (1968).

Analar). All other products used for analyses were of standard analytical reagent grade.

The methods of preparing, degassing, and irradiating the solutions have been previously described.[22] Irradiations were carried out using a cobalt-60 source (Gammacell) which furnished a dose rate of about 2×10^{19} eV g^{-1} hr^{-1} as measured with the Fricke dosimeter. All absorbed doses were corrected for the electron density of the solution.

After irradiation the contents of the ampoules were analyzed for hydrogen, nitrite ions, acetaldehyde, butane-2,3-diol, methane, ethane, ethylene, acetylene, and hydrogen peroxide.

Gaseous products were extracted in a modified Van Slyke apparatus and injected directly into a gas chromatograph (Jobin-Yvon "Bretagne" for hydrogen, Aerograph "Hi-Fi" for the hydrocarbons). Hydrogen was separated at room temperature on a 4-m column of molecular sieve 5A protected by a 30-cm precolumn of silical gel and measured with a catharometer; the carrier gas was argon. The hydrocarbons were separated on a 2-m column packed with activated alumina and maintained at 40°. Nitrogen was the carrier gas and a flame ionization detector was employed. Both apparatus were calibrated by injecting known quantities of the gases to be analyzed. The estimated error in these determinations was ±6%.

Glycol was also determined by gas chromatography (F & M 700 equipped with a flame ionization detector). The column, 2 m long, was packed with 2% Carbowax 20 M plus 10% polyphenyl ether on a fluoropak support and maintained at 110°. Samples of 4 μl of the irradiated solutions were injected, the injector temperature being 275°. The error in these determinations was ±10%.

Nitrite was determined colorimetrically by the modified Shinn method.[23] The extinction coefficient of the product dye was determined to be ϵ 53,200 ± 1600 cm^2 mol^{-1} at 540 nm. The precision of the results was ±4%.

Acetaldehyde was determined by the method of Johnson & Scholes.[24] The extinction coefficient of the phenylhydrazone was found to be ϵ 18,700 ± 500 cm^2 mol^{-1} at 428.5 nm. The presence of nitrite interfered with this determination so calibration measurements were carried out on synthetic mixtures containing known nitrite and acetaldehyde concentrations in the ethanolic solvent. From the results thus obtained correction factors were calculated. The estimated precision of the corrected results from the irradiated solutions is ±7%.

Hydrogen peroxide was determined by Ghormley's[25] method using ϵ 2336 at 400 nm. Where necessary, corrections were applied for the nitrite concentration as indicated by Schwartz and Salzmann.[26] The error in the final result was ±5%.

In view of the large difference between the radiolytic yields of the major and minor products and also the varied sensitivities of the analytical methods employed in their measurement, it was necessary to use quite different dose ranges for their determinations. These ranges expressed in eV g^{-1} were as follows: hydrogen, 10^{17}–2×10^{18}; hydrocarbons, 10^{17}–2×10^{18}; glycol, 5×10^{18}–4×10^{19}; nitrite, 10^{16}–2×10^{17}; acetaldehyde, 10^{17}–2×10^{18}; hydrogen peroxide, 10^{17}–2×10^{18}.

The concentration dose plots for all products were linear within the estimated limits of error over these dose ranges.

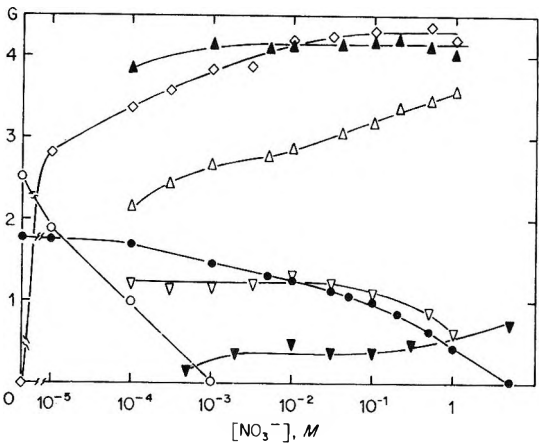

Figure 1. Yields of products as a function of nitrate concentration: ●, $G(H_2)$; △, $G(NO_2^-)$; ▼, $G(H_2O_2)$; ◊, $G(CH_3CHO)$; ○, G(glycol); ▲, $[G(NO_2^-) + G(H_2)]$; ▽, $[G(CH_3CHO) - G(NO_2^-)]$.

Results

Figure 1 shows the experimental yields of hydrogen $G(H_2)$, hydrogen peroxide $G(H_2O_2)$, acetaldehyde $G(CH_3CHO)$, glycol G(glycol), and nitrite $G(NO_2^-)$ as functions of the initial nitrate ion concentration. Curves of $[G(NO_2^-)+G(H_2)]$ and $[G(CH_3CHO) - G(NO_2^-)]$ also appear in the figure.

The yields of the hydrocarbon gases remained unchanged, within the limits of error of their measurement, in the presence of nitrate ions. The values found were $G(CH_4) = 0.40$, $G(C_2H_6) = 0.004$, and $G(C_2H_4) = 0.057$.

It is of interest to compare the present results with those of previous studies in which an alcohol was used to scavenge H and OH radicals, and nitrate or nitrous oxide to capture solvated electrons. Thus the $G(NO_2^-)$ curve of Figure 1 is practically identical with that found by Allan,[4] who studied 10^{-2} M and 10^{-1} M methanol

(22) C. Baquey, Thèse 3ème Cycle, Bordeaux, July 12, 1968.

(23) (a) M. B. Shinn, *Ind. Eng. Chem., Anal. Ed.*, **13**, 33 (1941); (b) Rider and M. G. Mellon, *ibid.*, **18**, 96 (1946).

(24) G. R. A. Johnson and G. Scholes, *Analyst (London)*, **79**, 217 (1954).

(25) A. O. Allen, C. J. Hochanadel, J. A. Ghormley, and T. W. Davis, *J. Phys. Chem.*, **56**, 575 (1952).

(26) H. A. Schwartz and J. A. Salzmann, *Radiat. Res.*, **9**, 502 (1958).

the solution, *i.e.*, to the free ion yield $G_{e_s^-(f.i.)}$. The disappearance of the glycol yield at $[NO_3^-] \geq 10^{-3}\ M$ and the simultaneous appearance of a constant yield of hydrogen peroxide, indicating that this product is no longer competing with nitrate ions for solvated electrons, lend further support to this assumption. The value thus obtained, $G_{e_s^-(f.i.)} = 2.70 \pm 0.10$ at $[NO_3^-] = 2 \times 10^{-3}\ M$ will be slightly high due to a small degree of intraspur capture of electrons but may be corrected using the method of Fielden and Hart[39] based on the calculations of Flanders and Fricke[40] for a one radical model. Taking the values of the nondimensional parameters E and B as 2.5 and $1.3[NO_3^-]$, respectively, one obtains $G_{e_s^-(f.i.)} = 2.55 \pm 0.10$ for $[NO_3^-] = 10^{-3}\ M$.

On the basis of the above considerations, it should be possible to describe the overall mechanism in terms of the reactions 7, 10, 16 through 19 with lesser contributions from (2) and (3). Neglecting any other possible sources of H_2O_2 the inclusion of reaction 3 indicates that in 1 M ethanol solutions the intraspur scavenging of OH radicals is still incomplete and hence that reactions 4, 5, and 6 may also be occurring to some extent.

The "Molecular" Aldehyde Yield. One of the most interesting features of the present study is the observation of an apparently "molecular" yield of acetaldehyde. Whereas the mechanism proposed above implies the formation of one nitrite ion and one molecule of acetaldehyde for each solvated electron captured, the total acetaldehyde yield is much greater than that of nitrite. The plot of $[G(CH_3CHO) - G(NO_2^-)]$ *vs.* the nitrate ion concentration (see Figure 1) shows a constant value of 1.25 ± 0.1 for $10^{-4}\ M < NO_3^- < 5 \times 10^{-2}\ M$. This excess aldehyde yield must have some other origin than reaction 19 and the fact that it only begins to decrease when the nitrate ion concentration becomes greater than $5 \times 10^{-2}\ M$ indicates that it is formed in an intraspur reaction. Moreover, since the nitrate ion is a specific scavenger of electrons, this latter species would seem to be involved in its formation. Such a conclusion, however, appears incompatible with the known inertness of both ethanol and the hydroxyethyl radical toward the solvated electron.

This difficulty is removed in the following explanation which is based on the classical spur diffusion model and may be particularly relevant to single ion pairs. An electron which normally remains in the coulombic field of its parent ion has approximately equal probability of being recaptured by the H_3O^+ ion or by the OH radical formed close together in the extremely rapid reaction

$$[H_2O^+ + H_2O \longrightarrow H_3O^+ + OH] \qquad (20)$$

Recapture by H_3O^+, reaction 4, leads to the formation of a hydrogen atom which may either recombine with the OH to reform water or diffuse into the bulk of the solution giving the hydrogen atom yield G_H. Recapture by the OH radical, reaction 5, can only lead to water formation. If, in 1 M ethanol, the OH radical has been transformed into $CH_3\dot{C}HOH$ *via* reaction 7 then, since this radical is unreactive toward the returning electron, reaction 4 will be promoted. The hydrogen atom thus formed, finding itself close to an ethanol radical, will react with it to give hydrogen and acetaldehyde

$$H + CH_3\dot{C}HOH \longrightarrow H_2 + CH_3CHO \qquad (21)$$

Thus measurable products appear where otherwise water would have been re-formed.

An alternative interpretation based on Hamill's[41] recent model would involve the capture of a pair of radicals from the group (OH, OH, H, H) (Hamill's entity I) by an adjacent ethanol molecule.

In their study of 1.8 M ethanol, Russell and Freeman[21] proposed that their high hydrogen yields resulted from the process

$$H_2O \rightsquigarrow H_2O^* \longrightarrow H + OH \qquad (22)$$

occurring with a net yield of 1.3. The high ethanol concentration would lead to the capture of the radical pairs near their point of origin thus increasing the hydrogen yield and reducing the yield of geminate recombination. These authors did not measure the aldehyde yields.

Thus, all three models provide convenient explanations for the formation of the high hydrogen yields found in molar alcohol solutions and for the apparent "molecular" nature of part of the acetaldehyde yield.

Turning now to the mass balance for the system where $[NO_3^-] = 2 \times 10^{-3}\ M$, the concentration at which G(glycol) has just become zero and $G(H_2O_2)$ has reached a plateau, one may write

$$G(NO_2^-) = G_{e_s^-} = G_{OH} + G_H = 2.70 \pm 0.10 \qquad (23)$$

$$G(\text{ald}) = (G_{OH} + G_H + G_{e^-})/2 + \Delta G_{H_2O_2} + \Delta G_{H_2} + G(6) = 3.90 \pm 0.30 \qquad (24)$$

$$G(H_2) = G_{H_2} + \Delta G_{H_2} + G_H + G(6) = 1.40 \pm 0.07 \qquad (25)$$

$$G(H_2O_2) = G_{H_2O_2} - \Delta G_{H_2O_2} = 0.35 \pm 0.02 \qquad (26)$$

where ΔG_{H_2} and $\Delta G_{H_2O_2}$ represent, respectively, the contributions to the aldehyde yield made by the capture of pairs of H atoms and of OH radicals, $G(6)$ is the measure of the inhibition of water recombination, and the other symbols have their usual signification. From these equations and the expressions for the net yields of oxidizing and reducing radicals, G_{ox} and G_{red}

$$G_{red} = G_H + 2G_{H_2} + G_{e_s^-} + G(6) = G - H_2O \qquad (27)$$

$$G_{ox} = G_{OH} + 2G_{H_2O_2} + G(6) = G - H_2O \qquad (28)$$

one obtains

$$G_{ox} - G_{red} = 0.3$$

(39) E. M. Fielden and E. J. Hart, *Radiat. Res.*, **33**, 426 (1968).
(40) D. A. Flanders and H. Fricke, *J. Chem. Phys.*, **28**, 1126 (1958).
(41) W. H. Hamill, *J. Phys. Chem.*, **73**, 1341 (1969).

which, in view of the experimental errors, indicates good material balance.

For the total yield of water decomposition, the above values lead to the result

$$G(-H_2O) = 4.25 + G_{H_2} - \Delta G_{H_2}$$

Assuming that the molecular hydrogen yield stems mainly from reaction 2 its value will be little influenced by the ethanol concentration and this assumption also implies that ΔG_{H_2} will be small, probably not greater than 0.1. Hence

$$G(-H_2O) = 4.25 + 0.45 - 0.1 = 4.60 \pm 0.40$$

One may derive for the yield of inhibition of reaction 6

$$G(6) = 0.85 - \Delta G_{H_2} = 0.75$$

which leads also to

$$G_H = 0.20$$

This low value for G_H, the yield of hydrogen atoms captured in the bulk of the solution, coupled with the value obtained for G (6) suggests that, in the presence of 1 M ethanol, most of the normal bulk hydrogen atom yield $G_H \approx 0.55$, is captured together with its geminate OH partner near the site of their production and that the major part of the "molecular" aldehyde yield also originates in this process. The net inhibition of water formation is thus only about 0.4 G unit, a surprisingly low value which, however, is consistent with the value $G(-H_2O) = 4.60$.

Any one of the three models described can account satisfactorily for these quantitative results.

B. High Nitrate Ion Concentration Region: $[NO_3^-] \geq 5 \times 10^{-2}$ M. In this region, the nitrite yield again increases, while the hydrogen yield decreases in a more or less symmetrical fashion, approaching a value of zero at $[NO_3^-] = 5.0$ M. The curve of $[G(NO_2^-) + G(H_2)]$ against $[NO_3^-]$ is almost flat above 10^{-2} M nitrate, the plateau value being 4.15. Within the limits of error of the measurements, this value is equal to the aldehyde yield over the same range. Above 10^{-1} M nitrate, the decrease in $G(H_2)$ becomes sharper and, simultaneously, $G(H_2O_2)$ increases while G("molecular" aldehyde) decreases.

These results indicate that at concentrations above 5×10^{-3} M the nitrate ion interferes increasingly with the intraspur reactions and that different mechanisms intervene above and below 10^{-1} M nitrate.

On the basis of the classical spur model, the increasing concentration of nitrate ions will capture more and more electrons which would normally disappear by reactions 2, 4, and 5. Thus both the molecular and the atomic hydrogen yields should decrease, a result which has previously been demonstrated.[42] Since $k_{H+NO_3^-} \approx 4 \times 10^6$ l. mol^{-1} sec^{-1} and $k_{10} = 1.7 \times 10^7$ l. mol^{-1} sec^{-1} then, assuming homogeneous competition for the hydrogen atom yield, one concludes that (a) the half-life of hydrogen atoms in the medium will be about 2×10^{-8} sec, and (b) about one-half of those H atoms should react with ethanol to give H_2. The present result thus indicates that very few H atoms are formed in times shorter than 10^{-8} sec. Hence, the explanation of the high hydrogen atom yield supplied by Russell and Freeman[21] can only be retained (a) if the excited water molecule has a long half-life,[43] or (b) if it reacts very rapidly with the nitrate ion, without forming hydrogen.

For each electron scavenged from reactions 2 or 4, one nitrite ion will replace one hydrogen molecule and the constancy of the sum $[G(NO_2^-) + G(H_2)]$ is thus explained.

Since the presence of 1 M ethanol essentially reduces the effective radius of the spurs in which reaction 5 takes place, interference with this reaction will only occur at relatively high nitrate concentrations. The capture of electrons in this case will liberate OH radicals able to recombine to form H_2O_2 and this may be the explanation of the increase in $G_{H_2O_2}$ above 10^{-1} M nitrate. Some of these OH radicals may diffuse away and react with ethanol thus increasing the total aldehyde yield. As the oxidation reduction balance at $[NO_3^-] = 1$ M shows there appears to be little inhibition of water reformation over and above that already observed for $[NO_3^-] = 2 \times 10^{-3}$ M.

On the basis of Hamill's[41] model, the nitrate ion will successively scavenge the "dry" electrons and the H_2O^+ ions. In the first case, entity I will be transformed into (H_3O^+, OH, NO_2, 2 OH^-), or, if the OH radical has already reacted with an ethanol molecule, into (H_3O^+, $CH_3\dot{C}HOH$, NO_2, 2 OH^-) which will ultimately give CH_3CHO, NO_2^-, and 2 H_2O. In the presence of ethanol alone, entity I gives (H_2, CH_3CHO, $2H_2O$), so the replacement of H_2 by NO_2^- with $(G(NO_2^-) + G(H_2))$ and G(total aldehyde) remaining constant appears to be satisfactorily explained.

At higher nitrate concentrations, above 10^{-1} M in the present case, the NO_3^- may react with H_2O^+ as first suggested by Kevan.[34] Hamill showed how such a process could transform entity I into (NO_2, H_2O_2, e_m^-) thus reducing both the hydrogen and the "molecular" aldehyde yields while increasing the yield of hydrogen peroxide. This appears to be a plausible explanation of the trends observed at $[NO_3^-] > 10^{-1}$ M.

It is clear that the intraspur scavenging of H_2O^+ by the nitrate ion may also be considered in the framework of the classical spur diffusion model where it would lead to similar conclusions.

The oxidation reduction balance is less satisfactory at high nitrate concentrations than at 2×10^{-3} M. Taking the experimental values from Figure 1 one

(42) M. Chouraqui and J. Sutton, *Trans. Faraday Soc.*, 62, 2111 (1966).

(43) E. Hayon, *ibid.*, 60, 1059 (1964).

obtains, respectively, for 10^{-1} and 1.0 M nitrate the values $G_{ox} = 4.74$ and 4.80 while $G_{red} = 4.15$ in both cases. Inclusion of the hydrocarbon yields makes only a negligible improvement and this difference remains unexplained. On the basis of these values, it appears that the total ionization yield is ≥ 4.1.[5]

In conclusion, it may be stated that the ensemble of the present results obtained in 1 M ethanol solution which show two distinct regions of radical scavenging by the nitrate ion may be satisfactorily explained by either a classical spur model or by the model of Hamill in which a major role is attributed to single ionization events. Further study is necessary to decide whether one or the other can be specifically eliminated. The intervention of excited water molecules as the source of atomic hydrogen requires that their lifetimes be of the order of 10^{-7} sec. The existence of an apparent "molecular" yield of acetaldehyde has been explained in terms of the capture by individual ethanol molecules of pairs of geminate radicals close to their point of origin. The quantitative data indicate that in this system there is a negligible increase in the inhibition of water reformation with increasing nitrate concentration and that the overall water decomposition yield, $G(-H_2O)$, is 4.6 ± 0.4, a value not much larger than that found in dilute solutions of both radical scavengers.

Application of Microwave Spectroscopy to the Self-Exchange of Deuterium in Propylene-3-d_1 Catalyzed by Group VIII Metals

by Tomiko Ueda[1] and Kozo Hirota

The Institute of Physical and Chemical Research, Yamato-machi, Saitama Prefecture, Japan *(Received June 15, 1970)*

The self-exchange of deuterium in propylene-3-d_1 was investigated on nickel, nickel–alumina, palladium, platinum, and rhodium catalysts in the absence of water, and on nickel in the presence of water. The reaction products, the isotopic isomers of mono- and dideuterated propylene, were determined quantitatively by the microwave spectroscopy. At the initial stage transfer of deuterium from the methyl to the methine position was much slower than that to the methylene position in all the catalysts, and both absolute rates decreased in the presence of water-on-nickel catalyst. From these results, it was concluded that the self-exchange occurs through the three adsorbed intermediates, π-allyl, n-propyl, and isopropyl adsorbed species. Isopropyl intermediate is more important than n-propyl intermediate in the self-exchange mechanism.

Introduction

Up to the present, not enough attention has been given to the dissociative states of chemisorbed olefinic hydrocarbons in the study of their catalytic hydrogenations, even if they are often recognized as intermediates. This tendency may be a reason why the mechanism of the hydrogenation has not reached the final conclusion. With regard to the chemisorbed alkylbenzenes, the present authors found the catalytic "self-exchange" of deuterium in monodeuterated toluene,[2] *i.e.*, transfer of deuterium in monodeuterated toluene between different positions. This finding was easily explained by assuming the dissociative adsorption of toluene on metal catalysts. From this study, it is estimable that the self-exchange of deuterium in monodeuterated olefins may also take place. Since various chemisorbed olefinic species play an important role in the mechanism of cis–trans isomerization and double bond migration of olefinic hydrocarbons, the self-exchange of deuterium in propylene-3-d_1 is investigated on nickel, nickel–alumina, palladium, platinum, and rhodium catalysts. In addition, this reaction is carried out in the presence of water (H_2O) on nickel catalyst with relation to the exchange of propylene with deuterium oxide, which was reported by one of the authors.[3] The microwave spectroscopy[4] is applied to the analyses of propylene and its isotopic species so as to determine the relative abundance of the isotopic isomers quantitatively, since neither infrared nor nuclear magnetic resonance spec-

(1) To whom correspondence should be addressed.

(2) K. Hirota and T. Ueda, *Tetrahedron Lett.*, 2351 (1965); *J. Phys. Chem.*, 72, 1976 (1968).

(3) K. Hirota, Y. Hironaka, and E. Hirota, *Tetrahedron Lett.*, 1645 (1964).

(4) Y. Morino and E. Hirota, *Nippon Kagaku Zasshi*, 85, 535 (1964).

troscopy can distinguish *cis*- and *trans*-propylene-1-d_1 easily.

Experimental Section

Materials. Propylene-3-d_1 $CH_2D \cdot CH:CH_2$ was prepared by treating allyl chloride with D_2O in the presence of zinc dust and excess acetic anhydride.[5] By the microwave spectroscopy it was indicated that the isotopic purity of the propylene-3-d_1 was 86% with propylene-d_0 as a main impurity (14%). This analytical value agrees well with that obtained by mass spectrometric measurement. The amount of other impurities was found to be less than 1% from gas chromatography and infrared spectroscopy.

Nickel catalyst was prepared by decomposing nickel formate at 270°. The decomposition product was degassed at the same temperature. The preparation of nickel supported on γ-alumina[6] was done in a similar way starting from a 1:1 mixture of Ni–Al_2O_3 by weight. Platinum black[7] was obtained from chloroplatinic acid by the Willstätter method and degassed at 150°. Palladium black[8] was made similarly to platinum black. Rhodium catalyst was prepared by reducing rhodium hydroxide with hydrogen at 120° for 10 hr and degassing at the same temperature. The preparation of rhodium hydroxide was as follows. To a solution of 2 g of rhodium trichloride in 100 ml of water is added an aqueous solution of 10% sodium hydroxide and the mixture is heated at 95°. After 30 min, the solution is allowed to cool and the precipitate is isolated by filtration, washed, and dried in desiccator.

Procedure. The catalyst was placed on the bottom of a cylindrical glass reaction vessel of volume 50 ml. The vessel was connected to a conventional vacuum apparatus which was maintained at 10^{-4} Torr or lower by means of a mercury diffusion pump backed by an oil rotary pump. A required amount of $CH_2D \cdot CH:CH_2$ (sometimes with H_2O) was admitted to the reaction vessel from the corresponding storage vessel. During the reaction the ampoule was kept at 30 or 40°. At the required reaction time, a small amount of the sample was repeatedly extracted by expanding into an evacuated vessel and transferred to the analysis system.

Analysis. Composition of the deuterated propylenes was determined quantitatively by measuring the intensities of the rotational 1_{01}–0_{00} transition for various species;[4,5,9–11] their frequencies are listed in Table I. The rotational spectrum of propylene was measured with a conventional 100-kHz sinusoidal Stark modulation microwave spectrometer by the method of Morino and Hirota.[4] The measurements were made at Dry Ice temperature by using a 3-m absorption cell. The absorption lines were recorded under the condition of Stark dc voltage gradient of about 250 V/cm with sinusoidal modulation amplitude of 150 V/cm. On the basis of the ratio[12] $f_v(CH_3)/f_v(CH_2D) = 1.0740$ it was calculated that the correction coefficients of intensities of absorption lines used to estimate the relative abundance of deuterated propylene from the appearance intensities of absorption lines were $D_2/D_4 = 1.0488$, $D_1/D_3 = 1.0576$ and $D_6/D_3 = 1.0990$.

Table I: Microwave Spectra of the 1_{01}–0_{00} Transition for the Normal and Monodeuterated Species of Propylene

Species	Notation	Frequency, MHz
$CH_3 \cdot CH:CH_2$	D_0	17439.49
cis-$CH_3 \cdot CH:CHD$	D_1	16769.75
trans-$CH_3 \cdot CH:CHD$	D_2	16090.18
sym-$CH_2D \cdot CH:CH_2$	D_3	16832.97
asym-$CH_2D \cdot CH:CH_2$	$D_{4 \text{ or } 5}$	16377.13
$CH_3 \cdot CD:CH_2$	D_6	17138.99

Although the reaction products were analyzed by infrared spectroscopy and gas chromatography in order to gain information on the occurrence of side reactions other than isotopic exchange, *e.g.*, self-hydrogenation, the amount of hydrocarbons other than propylene before and after reaction in all the catalysts was observed to be less than 1%.

Results

Propylene-3-d_1 Self-Exchange in the Absence of Water. Table II (a) lists the experimental conditions, and Table II (b)[13] shows the degrees of isotopic exchange of the four monodeuterated propylenes observed on platinum and nickel catalysts. Fraction ϕ/Z to be called the degree of isotopic exchange is defined by the ratio of percentage composition (ϕ) of a monodeuterated propylene to the number of equivalent hydrogen atoms (Z) attached to the carbon position just considered. Variations of ϕ/Z *vs.* reaction time on palladium, rhodium, and nickel–alumina catalysts are shown in Figures 1–3. These results indicate that the transfer rates of deute-

(5) D. R. Herschbach and L. C. Krisker, *J. Chem. Phys.*, **28**, 728 (1958).

(6) K. Hirota and T. Ueda, *Bull. Chem. Soc. Jap.*, **35**, 228 (1962).

(7) R. Willstätter and E. Waldschmidt-Leitz, *Ber.*, **54**, 121 (192[illegible]).

(8) R. Willstätter and E. Waldschmidt-Leitz, *ibid.*, **54**, 123 (192[illegible]).

(9) D. R. Lide, Jr., and D. E. Mann, *J. Chem. Phys.*, **27**, 868 (1957); D. R. Lide, Jr., *ibid.*, **35**, 1374 (1961).

(10) E. Hirota and Y. Morino, *ibid.*, **45**, 2327 (1966); E. Hirota, *ibid.*, **45**, 1984 (1966).

(11) The notation D_i adopted for the sake of convenience designates a deuterated species, in which the ith hydrogen atom has been replaced by a deuterium atom. Numbering of the atoms is the same as that used in ref 9.

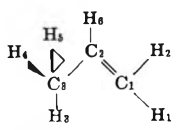

(12) C. H. Townes and A. L. Schawlow, "Microwave Spectroscopy," McGraw-Hill, New York, N. Y., 1955, p 102.

(13) Measurement of experiment number 2 was carried out by Professor E. Hirota of the University of Tokyo.

Table II: Propylene-3-d_1 Self-Exchange in the Absence of Water on Pt and Ni Catalysts

(a) Experimental Conditions

Expt no.	Catalyst, g	Propylene-3-d_1, mol	Reaction Temp, °C	Reaction Time, hr
1	Pt 0.5	2.0×10^{-3}	30	25
2	Pt 0.5	2.0×10^{-3}	30	50
3	Pt 0.5	2.0×10^{-3}	30	40
4	Pt 0.5	2.0×10^{-3}	30	80
5	Pt 0.5	2.0×10^{-3}	30	200
6	Pt 0.5	2.0×10^{-3}	Room temp	2200
7	Ni 1.0	2.0×10^{-3}	30	80
8	Ni 1.0	2.0×10^{-3}	30	200
9	Ni 1.0	1.0×10^{-3}	40	40
10	Ni 1.0	1.0×10^{-3}	40	80

(b) Degrees of Isotopic Exchange of Monodeuterated Propylenes

Expt no.	Degrees of isotopic exchange (ϕ/Z): $CH_2D \cdot CH:CH_2$ ($Z = 3$)	t-$CH_3 \cdot$ $CH:CHD$ ($Z = 1$)	c-$CH_3 \cdot$ $CH:CHD$ ($Z = 1$)	$CH_3 \cdot CD:CH_2$ ($Z = 1$)
1	30.6 ± 0.2	4.6 ± 0.4	3.6 ± 0.3	
2	26.6 ± 0.5	9.6 ± 0.9	9.5 ± 0.9	1.1 ± 0.2
3	28.2 ± 0.2	7.1 ± 0.4	6.5 ± 0.2	1.7 ± 0.1
4	26.9 ± 0.3	9.9 ± 0.5	7.1 ± 0.5	2.3 ± 0.1
5	25.3 ± 0.3	11.9 ± 0.5	8.8 ± 0.3	3.4 ± 0.2
6	21.8 ± 0.5	14.3 ± 1.5	11.8 ± 0.6	8.4 ± 0.3
7	21.4 ± 0.3	16.3 ± 0.9	13.7 ± 0.4	5.9 ± 0.2
8	20.1 ± 0.5	16.5 ± 1.5	13.9 ± 0.7	9.3 ± 0.8
9	18.0 ± 0.4	18.4 ± 1.1	13.1 ± 0.6	14.4 ± 0.9
10	18.0 ± 0.4	18.6 ± 1.0	12.2 ± 0.6	15.1 ± 0.7

rium from the methyl position to the other three positions differ markedly from one another, especially at the initial stage, and the following order of transfer rate is found irrespective of metals

trans-$CH_3 \cdot CH:CHD >$

$$cis\text{-}CH_3 \cdot CH:CHD > CH_3 \cdot CD:CH_2 \quad (1)$$

In the case of palladium, as Figure 4 indicates, it was found that the transfer from the methyl to the methine position obeys approximately a first order, *i.e.*

$$k = \frac{2.303}{t} \log \frac{C_e}{C_e - C_t} \quad (2)$$

where C_t and C_e are the concentrations of $CH_3 \cdot CD:CH_2$ at time t and when the system reaches equilibrium, respectively. The rate constant k calculated for palladium catalyst was 0.021 (sec^{-1} per gram of catalyst). In the cases of platinum, rhodium, nickel–alumina, and nickel, similar relations can be observed.

Moreover, production of dideuterated propylene is confirmed on platinum (experiment number 2), and the deuterium distribution is shown as follows[14]

$CHD_2 \cdot CH:CH_2$, 1.1% $CH_3 \cdot CH:CD_2$, 0.3%

c-$CH_2D \cdot CH:CHD$ (I), 1.7% *t*-$CH_2D \cdot CH:CHD$ (II), 2.3%

It is noteworthy that *cis*-$CH_3 \cdot CD:CHD$ (III) cannot be detected.[15]

Propylene-3-d_1 Self-Exchange in the Presence of Water. It was reported by one of the authors[3] that in the exchange of propylene with deuterium oxide catalyzed by

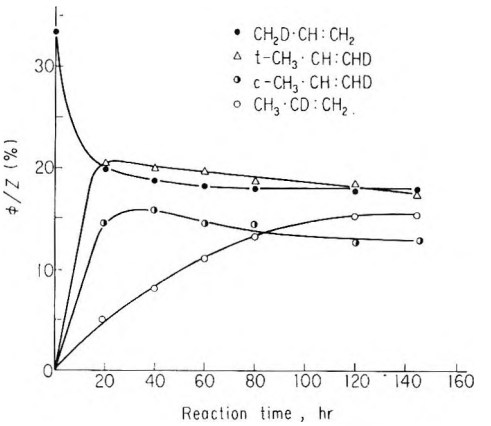

Figure 1. Variation in degrees of isotopic exchange of C_3H_5D subspecies with reaction time for propylene-3-d_1 self-exchange on Pd catalyst at 30° (propylene-3-d_1:Pd, 1.0×10^{-3} M:0.5 g).

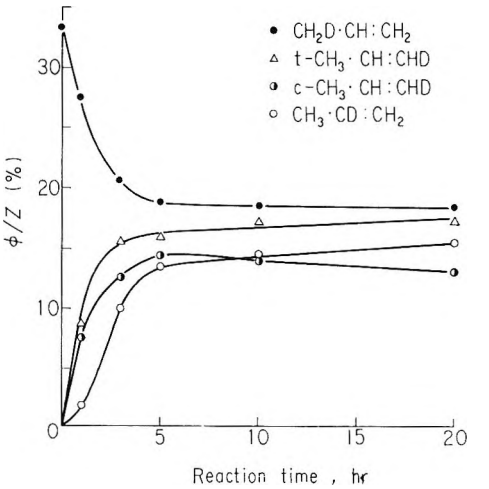

Figure 2. Variation in degrees of isotopic exchange of C_3H_5D subspecies with reaction time for propylene-3-d_1 self-exchange on Rh catalyst at 30° (propylene-3-d_1:Rh, 1.0×10^{-3} M:0.5 g).

(14) Only qualitative analysis was made in the same scale as that for the monodeuterated species.

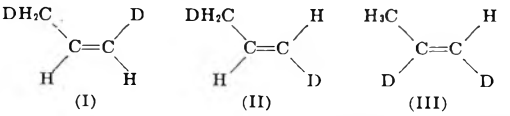

(15) The measurable limit on concentration is 0.1% for each species.

Table III: Propylene-3-d_1 Self-Exchange in the Presence of Water on Ni Catalyst (Propylene-3-d_1: H_2O: Ni, 1.0×10^{-3} M: 5×10^{-4} M: 1.0 g)

Expt no.	Reaction Temp, °C	Reaction Time, hr	Propylene-d_1, % $CH_2D \cdot CH:CH_2$	t-$CH_3 \cdot CH:CHD$	c-$CH_3 \cdot CH:CHD$	$CH_3 \cdot CD:CH_2$	Propylene-d_0, % $CH_3 \cdot CH:CH_2$
S		0	(86.3 ± 0.2)[a]				(13.7 ± 0.3)
11	30	120	95.7 ± 0.6	2.5 ± 0.3	1.8 ± 0.3		
			(81.2 ± 1.1)	(2.2 ± 0.2)	(1.5 ± 0.3)		(15.1 ± 0.8)
12	30	213	82.2 ± 1.3	10.3 ± 0.8	7.5 ± 0.9		
			(64.9 ± 1.5)	(8.1 ± 0.7)	(6.0 ± 0.7)		(21.0 ± 1.1)
13	40	100	91.7 ± 0.4	5.0 ± 0.2	3.3 ± 0.2		
			(75.9 ± 0.7)	(4.1 ± 0.2)	(2.8 ± 0.2)		(17.2 ± 0.5)
14	40	200	85.1 ± 1.0	8.5 ± 0.9	6.4 ± 0.3		
			(70.4 ± 1.5)	(7.0 ± 0.8)	(5.3 ± 0.3)		(17.3 ± 1.2)

[a] Figures in parentheses denote the percentage allotted to propylene-d_1 and -d_0.

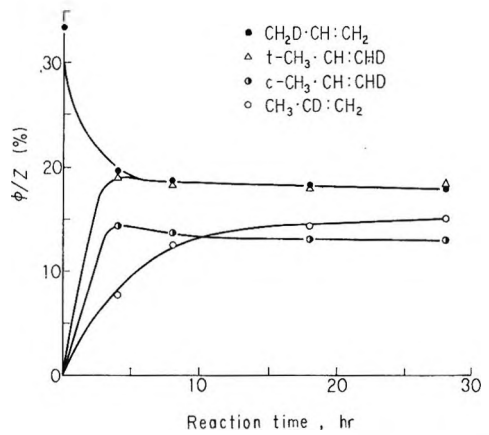

Figure 3. Variation in degrees of isotopic exchange of C_3H_5D subspecies with reaction time for propylene-3-d_1 self-exchange on Ni–Al_2O_3 catalyst at 30° (propylene-3-d_1: Ni–Al_2O_3, 1.1×10^{-3} M: 2 g).

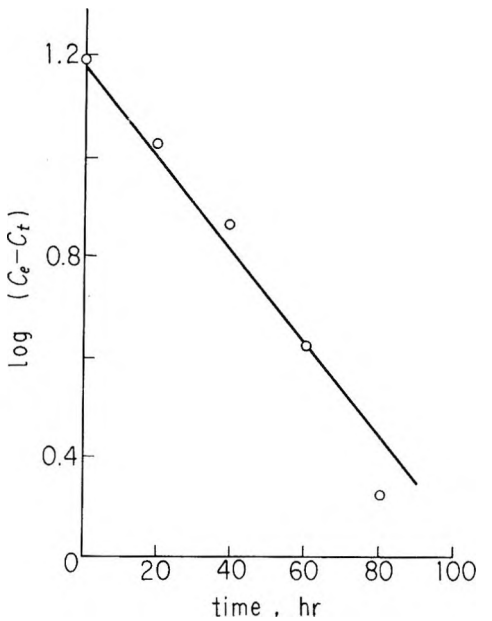

Figure 4. Propylene-3-d_1 self-exchange into propylene-2-d_1 on Pd catalyst at 30°.

nickel, the amount of monodeuterated propylenes is as follows

$$CH_3 \cdot CD:CH_2 \gg \textit{trans}\text{- and } \textit{cis}\text{-}CH_3 \cdot CH:CHD \quad (3)$$

However, an entirely different result was obtained by the present self-exchange, especially at the initial stage (eq 1). Then, in order to investigate the effect of water, the self-exchange in the presence of protium oxide was carried out at the same temperature. The result is summarized in Table III, which shows the percentage compositions of the four isotopic monodeuterated propylenes with or without a nondeuterated propylene.

Decrease of starting propylene-3-d_1 and corresponding increase of *trans*- and *cis*-propylene-1-d_1, shown in Table III, give the evidence of the transfer of deuterium from the methyl to the *trans*- and *cis*-methylene positions in the presence of water. However, the transfer of deuterium to the methine position is still negligible. It may be noticed that the relative transfer rates of deuterium to the methine and methylene positions were unaffected practically by the presence of water. By comparing numbers 7 and 10 of Table II with the corresponding numbers 11 and 13 of Table III, it may be seen that the absolute transfer rates of deuterium from the methyl to the *trans*- and *cis*-methylene positions fairly decrease in the presence of water, although the deuterium percentage in propylene decreases somewhat due to the dilution with water given by eq 4

$$C_3H_5D + H_2O \longrightarrow C_3H_6 + HDO \quad (4)$$

Discussion

In a previous article,[2] it was made clear that the self-exchange of deuterium in monodeuterated toluene is an intermolecular deuterium transfer brought about by the dissociative adsorption of toluene, producing both adsorbed protium and deuterium on the catalyst surface. This conclusion is based on the formation of multiply deuterated species. Such a dissociation process may also be realized in the case of propylene-3-d_1 self-

exchange, because of the detection of dideuterated propylene (d_2). Now it seems to be premised that the dissociation of deuterium from the methyl group in propylene-3-d_1 takes place. Moreover, a significant point is that behavior of the exchangeable hydrogens in propylene differs was found in this reaction; *i.e.*, the transfer rates of deuterium from the methyl to the *trans*- and *cis*-methylene positions were faster at the initial stage than to the methine position in all the catalysts. The above results are explained by considering the dissociative species of propylene, π-allyl (IV), on the catalyst surface in the first step, as shown by eq 5a

$$\underset{*}{H} + \underset{*}{CHD{=}CH{=}CH_2} \longleftarrow$$

(IVa)

$$CH_2D{-}CH{=}CH_2 \longrightarrow \underset{*}{CH_2{=}CH{=}CH_2} + \underset{*}{D} \quad (5a)$$

(IVb)

$$(IVa) + \underset{*}{H} \longrightarrow CHD{=}CH{-}CH_3 \quad (5b)$$

$$(IVa) + \underset{*}{D} \longrightarrow CHD_2{-}CH{=}CH_2,$$

$$CHD{=}CH{-}CH_2D \quad (5c)$$

where the stars represent the bond with the catalysts. If the self-exchange in the absence of water is compared with similar reactions for other reactants, the dissociative adsorption occurs more easily than in other reactions, because there are no other species which retard adsorption. However, this process is hardly found in the presence of water and the reaction rate of self-exchange fairly decreases in the case of nickel catalyst. Nevertheless, it is difficult to elucidate the facts, by the above mechanism alone, that in accordance with the progress of reaction the transfer degree of deuterium to the methine position increased gradually in all the catalysts and especially it was approximately a first-order reaction in the case of palladium catalyst and that in the final state all the hydrogens of methine, methylene, and methyl positions had nearly equal degrees of isotopic exchange in all the catalysts. According to the associative mechanism for ethylene hydrogenation,[16] which was first suggested by Horiuti and Polanyi and since then widely employed by numerous authors, both adsorbed species $\underset{*}{CH_2}{-}\underset{*}{CH_2}$ and half-hydrogenated species $\underset{*}{CH_2}{-}CH_3$ are included in this scheme, but there remains a direct addition mechanism, by which the simultaneous addition of two adsorbed hydrogen atoms to the associatively adsorbed olefin occurs. Judging from the minor production of dideuterated propylene, in which *cis*-$CH_3{\cdot}CD{:}CHD$ was undetected, at the initial stage for platinum catalyst in the present investigation, the self-exchange of propylene-3-d_1 seems to occur mainly in the stepwise mechanism. Therefore, the above findings are explained by considering the half-hydrogenated states of propylene as intermediate under the plausible assumption that hydrogen and deuterium atoms have been produced by dissociation of propylene-3-d_1. This is the reason why nondeuterated propylene has also been made in a large amount (Table III). The whole reaction may proceed by eq 6

$$CH_2D{-}HC{=}CH_2 \longrightarrow \underset{*\ *}{DH_2C{-}HC{-}CH_2} \xrightarrow{+H}$$

(Va)

$$\underset{*}{DH_2C{-}HC{-}CH_3} \xrightarrow{-H} \underset{*\ *}{DHC{-}CH{-}CH_3} \longrightarrow DHC{=}CH{-}CH_3, \quad (6a)$$

(VI)

$$C_3H_6 \longrightarrow \underset{*\ *}{H_3C{-}HC{-}CH_2} \xrightarrow{+D}$$

(Vb)

$$\underset{D\ *}{H_3C{-}HC{-}CH_2} \xrightarrow{-H} \underset{*\ *}{H_3C{-}DC{-}CH_2} \longrightarrow CH_3{-}CD{=}CH_2, \quad (6b)$$

(VII)

where the isopropyl species (VI) may be stabler than the *n*-propyl species (VII) and most of the self-exchanges may be caused, proceeding *via* the former as the intermediate at the early stage. Thus, this mechanism is different to some extent from that of the deuterium exchange of propylene with deuterium oxide, because the *n*-propyl species is produced more than the isopropyl one, for instance, in the case of C_3H_6–D_2O exchange for nickel catalyst.[3]

Such being the situation, the propylene-3-d_1 self-exchange is thought to reach the state of isotopic equilibrium with the dissociative and half-hydrogenated adsorbed intermediates (IV, VI, and VII). It should be emphasized that this mechanism is essentially the

(16) M. Polanyi and J. Horiuti, *Trans. Faraday Soc.*, **30**, 1164 (1934); G. C. Bond, "Catalysis by Metals," Academic Press, London, 1962, p 253.

same on the nickel, nickel–alumina, palladium, platinum, and rhodium catalysts in spite of some differences between their physical properties[17] such as lattice constant, percentage *d*-character, work function, etc., though π-allyl intermediate is produced more easily in rhodium catalyst than in platinum and nickel catalysts, because it was found that in the propylene-3-d_1 self-exchange into propylene-2-d_1 the rhodium catalyst is the most active of all the metals.

Finally, it can be pointed out that the dissociative species of propylene is probably produced also in its hydrogenation, though this species may play a minor role for the reaction in the presence of hydrogen.

Acknowledgment. The authors wish to express their gratitude to Professor Yonezo Morino and Professor Eizi Hirota, the University of Tokyo, and Mr. Naomu Morimiya, for their advice and help concerning the construction of the microwave spectrometer, and to Dr. Kazunori Tanaka for very helpful discussion of the present work.

(17) G. C. Bond, ref 16, Chapter 2.

Infrared Absorbance by Water Dimer in Carbon Tetrachloride Solution[1]

by Lawrence B. Magnusson

Chemistry Division, Argonne National Laboratory, Argonne, Illinois 60439 *(Received October 27, 1969)*

Water dimer was detected by double-beam cancellation of the monomer absorbance in the 2700-nm stretching region. The dimerization constant is estimated to be 2.2 l. mol^{-1} at 25° in carbon tetrachloride solution. Only two OH stretching frequencies with ϵ_{max} values at 3693 and 3552 cm^{-1} are observed, which implies that the structure is cyclic with two bent H bonds in contrast to the open structure reported from nitrogen matrix studies. Under equilibrium conditions cyclic polymers appear to be the rule for water with no strong preference for linear H bonds, which supports the idea of Bernal that the ring size in liquid water may not be restricted to the hexameric ring of the ice structure.

Introduction

The process of polymerizing H_2O molecules at ordinary temperatures and saturation pressures leads ultimately to the enigma of liquid water. The water problem will be solved when the individual and cooperative behavior of H bonds is fully understood and formalized. Many workers have simplified the liquid system by studying the small polymers in inert, condensed phases.[2] Current interest is centered on linear *vs.* cyclic configurations and the relative influence of H bond bending with its associated distortion energy. The structure of the dimer would appear to have been settled by recent high-resolution ir work with a solid nitrogen matrix.[3] Four OH stretching bands were observed which would be characteristic of an open dimer with one linear H bond. Other experimental work, notably on alcohols and phenols,[4] is in accord with the idea that a cyclic dimer with two very bent H bonds would be unstable. The properties of water vapor have been correlated with some success by assuming an open dimer.[5] Theoretical studies predict an open structure for the dimer, and cyclic structures for the trimer and larger polymers.[6]

Water in carbon tetrachloride and hydrocarbon solvents appears from solubility data to be monomeric.[2,7] In attempting to determine equilibrium constants from ir spectra for H_2O–*p*-dioxane complexes in carbon tetrachloride solution, it was noted that the spectrum of the presumed monomeric H_2O was dependent on the total water concentration.[3] The resolution of the problem is presented here.

Experimental Section

Materials. Matheson Coleman and Bell Spectroquality carbon tetrachloride was washed four times with distilled water, dried by stirring under flowing nitrogen, and stored under dry nitrogen on a silica gel column.

(1) Based on work performed under the auspices of the U. S. Atomic Energy Commission.

(2) S. D. Christian, A. A. Taha, and B. W. Gash, *Quart. Rev.*, **24**, 20 (1970).

(3) A. J. Tursi and E. R. Nixon, *J. Chem. Phys.*, **52**, 1521 (1970).

(4) L. J. Bellamy and R. J. Pace, *Spectrochim. Acta*, **22**, 525 (1966).

(5) J. P. O'Connell and J. M. Prausnitz, *Ind. Eng. Chem., Fundam.*, **8**, 453 (1969).

(6) J. DelBene and J. A. Pople, *Chem. Phys. Lett.*, **4**, 426 (1969).

(7) J. R. Johnson, S. D. Christian, and H. E. Affsprung, *J. Chem. Soc., A1*, 77 (1966).

(8) L. B. Magnusson, unpublished results.

Prior to use, the carbon tetrachloride was drawn from the column and again stirred under nitrogen. The treatment removed water (to $<10^{-6}$ M), chloroform (absorption band at 2370 nm) which was usually present at several thousandths molar in the commercial solvent, carbon dioxide (absorption bands at 2710 and 2785 nm), and an unidentified trace impurity absorbing at 2490 nm. Reagent grade lithium chloride, magnesium chloride, potassium nitrate, and sodium chloride were recrystallized under nitrogen from triply distilled water.

Spectrophotometry. Absorbance (A) and wavelength in the 2700-nm fundamental stretching region were measured with a Cary Model 14 CMRI spectrophotometer. Undispersed illumination was used as the dispersed mode of operation has a variable nonlinearity from chopper radiation. The instrument was flushed continuously with nitrogen, and the residual water vapor had no discernible effect on double-beam operation. Temperature control consisted of a water-jacketed cell compartment (Cary No. 1445100) enclosed in a box made of Micarta sheet with suitable holes for the beams and nitrogen and water supplies. The nitrogen was brought to the water temperature before entering the compartment. The standard aluminum compartment lids were replaced by Micarta lids carrying mercury thermometers, the bulbs of which were positioned close to the sample cells. The thermometers were calibrated to 0.01° by comparison with a platinum resistance thermometer.

Solutions were measured in 1.00-, 2.00-, 5.00-, and 10.00-cm cylindrical quartz cells with Infrasil windows and Teflon stoppers. Cell plus solvent backgrounds were determined before and after the water measurements. Base line shift, usually zero, was monitored with a third cell plus solvent in the extra track in the sample compartment.

The wavelength scale was calibrated to within 1 cm^{-1} with the vacuum values for resolved water vapor lines given by Gates, *et al.*[9] The absorbance linearity (lead sulfide detector) was determined over the 0–0.2 and 0–2.0 scales by measuring 12 samples (5-cm cell) of weighed dilutions of aqueous $NiSO_4$ at the broad 722-nm band maximum. Least-squares treatment of the observed absorbances, weighted by estimated uncertainties, yielded $A_{true} = (1.0017 \pm 0.0019)A_{obsd}$ at the 95% confidence level. The nonlinearity factor was supported near the spectral region of interest by measuring the peak height at 2642 nm (ϵ 0.762, 23-cm^{-1} full width at half-height, FWHH) in eight samples of 1,1,2,2-tetrachloroethane in carbon tetrachloride solution. Cell length was 2 cm, and the calculated spectral band width was 1 cm^{-1}. Above 0.7 M the molar absorptivities of the 2642-nm band and other nearby bands began to change markedly, indicating solute association. Least-squares treatment of the data for A less than unity gave $A_{true} = (1.0016 \pm 0.0035)A_{obsd}$. The water bands are similar in width to the 1,1,2,2-tetrachloroethane bands, and Beers' law is assumed from this calculation to hold exactly.

Procedures. Reproducible water- and CO_2-free cell plus solvent backgrounds were obtained by placing a glass collar with a side arm for rapid nitrogen flushing over the neck of the cell. Carbon tetrachloride was pressurized from the nitrogen storage flask through a tip inserted through the collar and into the cell. The cells were dried on a nitrogen jet prior to filling. All flexible connections in a glass system for the nitrogen shielding were made with Fluran F-5000 tubing (U. S. Stoneware) to avoid the volatile constituents found in most elastomer tubing. The nitrogen is off-gas from the house supply of liquid nitrogen and has no water or CO_2.

Although it is useful to know the total concentration of a component in an equilibrium study, the rapid exchange of water between vapor and solution makes this information difficult to obtain with the accuracy required for the determination of stoichiometry in the carbon tetrachloride system. Sufficing for the present purpose, relative concentrations were determined from the absorbances of the asymmetric vibration (ν_3) of monomer H_2O at 2696 nm and from the ratios of absorbances at a selected wavelength to the 2696-nm absorbance. Stock solutions of water for the relative absorbance measurements were prepared in a cylinder by stirring water and carbon tetrachloride phases magnetically. The cylinder was purged with nitrogen during mixing. The carbon tetrachloride phase was sampled by a technique similar to that of Johnson, *et al.*,[7] except that the carbon tetrachloride was pressurized into the optical cell.

Solutions of known water activity were prepared by equilibrating carbon tetrachloride with aqueous salt solution. A 2-cm cell was filled to the neck with carbon tetrachloride, either dry or containing somewhat less than the equilibrium concentration of water. A layer of aqueous phase, including crystals for the saturated phases, was placed over the carbon tetrachloride, and the cell was tightly capped with a Teflon stopper. The cell was placed in the thermostated compartment of the spectrophotometer, and the absorbance was monitored at intervals over periods of several days. Equilibrium was closely approached within about 15 hr for the originally dry carbon tetrachloride phases. The instrument was on continuously, but the tungsten lamp was on only for a 10-min warmup with the beam shutters closed and brief absorbance measurement to avoid temperature fluctuation in the sample. The same 2-cm cell was used for all measurements to avoid path length variation. Observations of saturated solutions with a

(9) D. M. Gates, R. F. Calfee, D. W. Hansen, and W. S. Benedict, "Line Parameters and Computed Spectra for Water Vapor Bands at 2.7 μ," National Bureau of Standards Monograph 71, U. S. Government Printing Office, Washington, D. C., 1964.

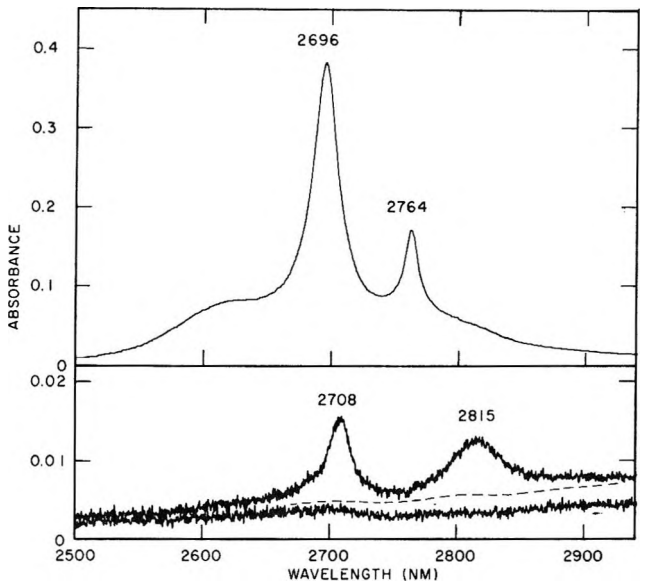

Figure 1. Absorbance spectra of water species in carbon tetrachloride solution. Upper trace: *ca.* 0.008 *M* solution of water in 1-cm cell, 0–1 absorbance scale. Middle trace: difference spectrum between the solution in 1-cm cell and dilute, compensating solution in 5-cm cell, 0–0.1 scale. Bottom trace: cells plus solvent background. Dashed line is estimated sample background consistent with those observed for other preparations.

pure water phase in the cell over the carbon tetrachloride were not accurately reproducible. On prolonged equilibration the water tends to spread throughout the cell forming emulsions and depositing on the cell windows.

A cancellation technique, similar to that of Bellamy and Pace,[4] was used for the difference between two solution spectra. The Infrasil window absorbance is neither negligible nor constant between cells, however, and it was necessary to select two cells for each beam to secure a decent base line. A typical arrangement was a 1-cm cell plus dry CCl_4, 5-cm cell plus dilute H_2O in CCl_4 in the reference beam; 1-cm cell plus nearly saturated H_2O in CCl_4, 5-cm cell plus dry CCl_4 in the sample beam.

Results

The existence of two species of water in carbon tetrachloride solution is shown by the recorder tracings of Figure 1. The upper spectrum is that of a 1-cm cell filled with carbon tetrachloride nearly saturated with water measured on the 0–1 absorbance scale, the fundamental stretching bands of monomeric water appearing with Q band maxima at 2695.8 and 2763.8 nm. Unresolved rotational branches are seen at wavelengths above and below the maxima. The lower spectrum, recorded on the 0–0.1 scale, is a difference spectrum obtained with the cancellation technique. Water was added by bubbling wet nitrogen in a 5-cm cell in the reference beam until the 2696- and 2764-nm peaks in the 1-cm cell were canceled. Two new bands appear, centered at 2708 and 2815 nm. The spectral band widths at these wavelengths were 2 and 4 cm^{-1}, respectively. Ten such difference spectra were obtained with 1- or 2-cm cells in the sample beam using both dispersed and undispersed modes of operation. No significant difference in intensity could be observed with a 0.1-cm–1-cm cell combination which is evidence against water being adsorbed on the cell windows. The intensity of the difference spectrum was roughly proportional to the cell length, indicating that the absorbing species is in solution. A complexing impurity in the carbon tetrachloride is ruled out because a complex spectrum would be canceled between two cells carrying the same amount of water.

The base line for the difference spectrum (lowest trace, Figure 1) was the same before and after the difference measurement. The difference spectrum, however, shows a slight increase in background toward the red, amounting to *ca.* 0.002 absorbance at 2815 nm. The effect was not reproducible, some preparations showing zero absorbance in the 2920-nm region. A similar effect is observed when water droplets are suspended in solution or are on the windows, but the solution for Figure 1 was not saturated and the spectrum did not change during an hour of observation. The cause is believed to be scattering by dust particles in the solution.

The stoichiometry of the polymeric species was deduced from measurements of total absorbances at 2710, 2815, and 2845 nm relative to the absorbance at 2696 nm as functions of the water concentration. The equilibrium constant for a given polymeric species is denoted by

$$K_p = \frac{(H_2O)_p}{(H_2O)^p} \tag{1}$$

in units of liters^{p-1} mole^{1-p}. For the small water concentrations involved here ($<10^{-2}$ *M*) Henry's law is assumed. The assumption is supported for the monomer by the work of Johnson, *et al.*[2,7] Substituting spectrophotometric units in eq 1, one has

$$K_p = \frac{A_p \epsilon_m{}^p}{A_m{}^p \epsilon_p} \tag{2}$$

where A_p and A_m are the absorbances (cm^{-1}) of polymer and monomer, respectively, and ϵ_p and ϵ_m are the corresponding molar absorptivities. For the relative measurement eq 2 is arranged to

$$\frac{A_p}{A_m} = \frac{K \epsilon_p A_m{}^{p-1}}{\epsilon_m{}^p} \tag{3}$$

Observed absorbances at wavelengths 1 and 2, chosen for maximum contributions for monomer and polymer, respectively, are the sums of monomer and polymer absorbances (see eq 4 and 5).

$$ {}_1A = {}_1A_m + {}_1A_p \quad (4)$$

$$ {}_2A = {}_2A_m + {}_2A_p \quad (5)$$

Wavelength 1 is 2696 nm, the position of maximum absorbance for the monomer. As a first approximation ${}_1A_p$, the polymer absorbance at 2696 nm, is assumed to be negligible with respect to the monomer absorbance. Equation 3 is rearranged with eq 4 and 5 to

$$ \frac{{}_2A}{{}_1A} = \frac{K_p \epsilon_p {}_1A_m{}^{p-1}}{{}_1\epsilon_m{}^p} + \frac{{}_2A_m}{{}_1A_m} \quad (6)$$

where ${}_2A_m/{}_1A_m$ is constant and the notation ${}_1A$ is a reminder of the approximation. Equation 6 is a linear relation between ${}_2A/{}_1A$ and ${}_1A_m{}^{p-1}$ provided p is a constant integer. Figures 2 and 3 show tests of the data for dimer and trimer formation according to eq 6. The samples were prepared by dilutions of CCl_4 saturated with water or by "diluting" by allowing water vapor to escape for a few minutes from an uncapped cell in the nitrogen atmosphere of the spectrophotometer compartment. The agreement in the relative values for different cell lengths rules out the possibility of species adsorbed on the windows. The data in Figure 2 are seen to be linear in first approximation showing that a dimer exists in very low concentrations in CCl_4 solutions. The 2710-nm data in Figure 3 with p set equal

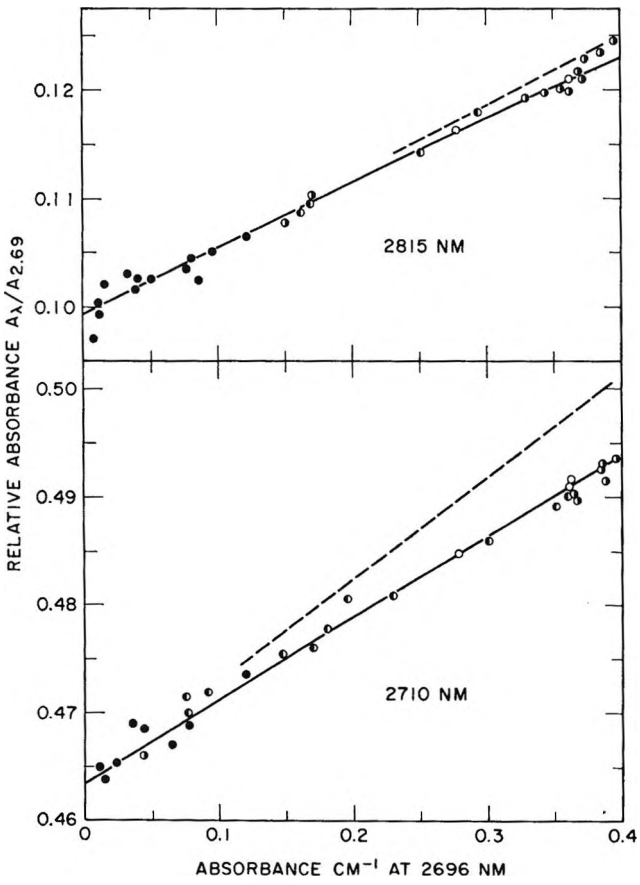

Figure 2. Test for dimer formation (eq 6 with p equal to 2). Absorbances relative to the absorbance at 2696 nm as functions of the relative water monomer concentration: ○, 1-cm cell; ◑, 2-cm cell; ◐, 5-cm cell; ●, 10-cm cell. Dashed lines result from correcting 2696-nm absorbance for dimer contributions.

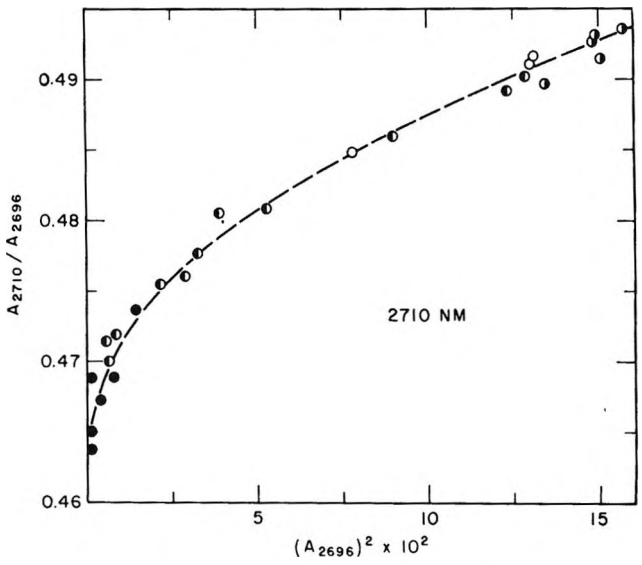

Figure 3. Test for trimer formation (eq 6 with p equal to 3). Absorbance at 2710 nm relative to the absorbance at 2696 nm as a function of the square of the relative water monomer concentration. Same data as in Figure 2.

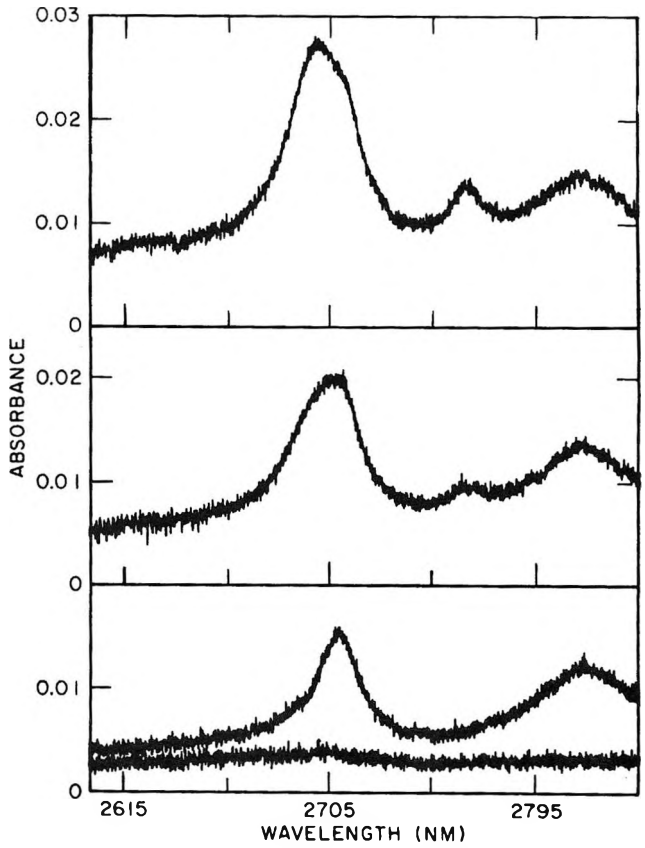

Figure 4. Difference spectra showing approach to cancellation of the monomer absorbance starting from top spectrum. Monomer absorbance is completely cancelled in bottom spectrum which is from the same pair of solutions as in Figure 1 and as in the third spectrum from top in Figure 5.

to 3 are not linear, ruling out the trimer as an important species. A similar curvature was obtained for the 2815-nm data with p equal to 3. The dashed lines in Figure 4 have been corrected for dimer contribution at 2696 nm as will be explained later. The curves through the points were calculated from the parameters for the dashed lines.

The results from the equilibrations of carbon tetrachloride with solutions of known water activity (Table I)[10-15] were used to determine the contributions of

Table I: Aqueous–CCl_4 Equilibria at 25.00°; Water Activities and Absorbances at 2696 nm in the CCl_4 Phase

Aqueous	a_w[a]	f_m[b]	A (2 cm)$^{-1}$[c]
$LiCl \cdot H_2O$ (satd)	0.11065[d]	0.003458	0.0867
			0.0868 ± 0.0002
			0.0867
$MgCl_2 \cdot 6H_2O$ (satd)	0.3298[e]	0.010300	0.2588 ± 0.0005
			0.2593
KNO_3 (satd)	0.9248[f]	0.028864	0.734
			0.734 ± 0.002
			0.734
0.7438 m NaCl	0.9755[f]	0.030443	0.775
			0.776 ± 0.002
			0.775
H_2O	1.00[g]	0.031207	0.796[h]
			0.798[i]
			0.899[j]

[a] Relative water vapor pressures for solutions under water vapor pressure only. The change in water activity by the *ca.* 1 atm total pressure of the present work is negligible. [b] Fugacity of monomer in atm, calculated from vapor pressure with second virial coefficient equal to 1165 cc mol^{-1} atm^{-1} (ref 10). [c] Duplicate and triplicate samples. Observed absorbance corrected for background but not corrected for nonlinearity of detector. Absorbance uncertainties are estimated. [d] Best value estimated from the data given in ref 11, 12, and 13. [e] Best value estimated from ref 11, 13, and 14. [f] Ref 11. [g] Vapor pressure of water, 23.753 mm (ref 15). [h] Equilibration for 9 hr with CCl_4 phase nearly saturated at start. [i] Equilibration for 29 hr. [j] Equilibration for 39 hr.

monomer and dimer to the absorbance spectra. The activity scale in the literature[10-15] is based on the relative vapor pressures of the salt solutions and pure water, the standard state of unit activity. An activity scale for the monomeric species is required for the present purpose. The fugacity of monomer (f_m) is obtained by correcting the known vapor pressures, P, of water and of the solutions with the second virial coefficient, B, and

$$\ln f_m = \ln P + \frac{BP}{RT} \tag{7}$$

With P in atmospheres and with appropriate units for the coefficients, the standard state for the monomer is unity which is equivalent to 1 atm of ideal gas pressure. The water activities and monomer fugacities are given in the second and third columns of Table I.

The thermodynamic equilibrium constant for the dimerization is

$$K_d^\circ = \frac{f_d}{f_m^2} \tag{8}$$

with f_d being the fugacity of the dimer. From Henry's law

$$f = kM = \frac{kA}{\epsilon} \tag{9}$$

eq 8 may be written as

$$K_d' = \frac{A_d}{f_m^2} \tag{10}$$

where

$$K_d' = \frac{K_d^\circ \epsilon_d}{k_d} \tag{11}$$

A is absorbance per centimeter of cell length and k_d is the Henry's law constant for the dimer. From eq 10 the absorbance of dimer at any monomer fugacity is related to the absorbance, A_{ds}, of dimer in carbon tetrachloride saturated with water by

$$A_d = \frac{f_m^2}{f_{ms}^2} A_{ds} \tag{12}$$

where f_{ms} is the fugacity of monomer water in pure water (0.031207 atm, Table I). The total absorbance at 2696 nm from eq 4 becomes

$$A = \frac{f_m}{f_{ms}} A_{ms} + \frac{f_m^2}{f_{ms}^2} A_{ds} \tag{13}$$

Rearranging to a linear form gives

$$\frac{f_{ms}}{f_m} A = A_{ms} + \frac{f_m}{f_{ms}} A_{ds} \tag{14}$$

The data in Table I for the salt solutions only were computed according to eq 14 by least squares to obtain the intercept (A_{ms}), which is the absorbance of monomer water in saturated carbon tetrachloride, and slope (A_{ds}) at the ν_3 peak position (2696 nm). The observed absorbances were corrected for the nonlinearity measured with the $NiSO_4$ solutions, averaged for each solution and weighted by estimated absorbance uncertainties (Table I, column 4) which are considerably larger than the errors in the water activities and somewhat larger than

(10) F. G. Keyes, *J. Chem. Phys.*, **17**, 923 (1949).
(11) R. H. Stokes and R. A. Robinson, *Ind. Eng. Chem.*, **41**, 2013 (1949).
(12) R. A. Robinson, *Trans. Faraday Soc.*, **41**, 756 (1945).
(13) W. F. Giauque, E. W. Hornung, J. E. Kunzler, and T. R. Rubin, *J. Amer. Chem. Soc.*, **82**, 62 (1960).
(14) R. H. Stokes, *Trans. Faraday Soc.*, **41**, 637 (1945).
(15) H. F. Stimson, *J. Res. Nat. Bur. Stand., Sect. A*, **73**, 493 (1969).

those which would be applied for the error in the nonlinearity. The results at the 95% confidence level are

$$A_{ms} = 0.3911 \pm 0.0005 \text{ cm}^{-1}$$

$$A_{ds} = 0.0069 \pm 0.0007 \text{ cm}^{-1}$$

The total absorbance for carbon tetrachloride in equilibrium with pure water (Table I) tended to increase with equilibration time and to exceed the value (0.796, 2-cm cell) calculated from the salt solutions as noted in the section on procedures.

The cancellation of the monomer contribution to obtain the dimer spectrum may now be calculated from the saturation values. The total absorbance at 2696 nm in the 1-cm cell of Figure 1 was 0.3786 including the small correction for nonlinearity. The fugacity of the monomer in the solution was 0.02971 from eq 13. Putting this value in eq 12 gives 0.0063 for the dimer absorbance at 2696 nm. The difference spectrum will show somewhat less absorbance because the compensating cell (5 cm for Figure 1) contains dimer at 0.04 times the concentration in the 1-cm cell (eq 10). The greater cell length raises the dimer absorbance in the 5-cm cell to 0.20 times that in the 1-cm cell. The difference spectrum should then show an absorbance of 0.0050 at 2696 nm. Good agreement was obtained to within the *ca.* 0.0010 uncertainty in the background on examination of an expanded wavelength scale tracing in the 2696-nm region (not shown) of the difference spectrum shown in Figure 1. The dashed straight lines in Figure 2 result from correcting ${}_1A$ of eq 6 for dimer contribution.

The stepwise approach to cancellation as water was added to the 5-cm cell is seen on expanded wavelength scale tracings in Figures 4 and 5. As in Figure 1, a trace over the peak of the ν_1 monomer absorbance at 2764 nm is included in Figure 5, displaced upwards slightly for clarity. The top difference spectra in Figures 4 and 5 are from the same pair of solutions (1- and 5-cm cells) and similarly for the second from the top. The third spectra down in Figures 4 and 5 and the spectrum in Figure 1 are from the same pair of solutions. The bottom two traces in Figure 5 show overcompensation with a net monomer absorbance appearing in the back, or reference, beam. The absorbance at 2696 nm for the pair of solutions showing the difference spectrum which is second from the top in Figures 4 and 5 was 0.013.

These spectra were actually obtained before the quantitative determination of the monomer and dimer contributions from the equilibrations at known water activities. In addition to isolating the previously observed 2708- and 2815-nm bands, the purpose of the stepwise approach was to see if other bands near the monomer frequencies had escaped detection. As may be seen in Figures 1, 4, and 5, no other bands are apparent. The agreement between the quantitative determination and the absorbance difference at 2696 nm indicates that Figure 1 is a reliable representation of the OH stretching region for pure dimer, as it exists in carbon tetrachloride solution. The valley between the two bands does not go to zero absorbance but appears to be just the overlapping of broad distributions assuming each band to be more or less symmetrical on the high and low energy sides. The energies and widths of the water bands in carbon tetrachloride solutions and in the nitrogen matrix are summarized in Table II.

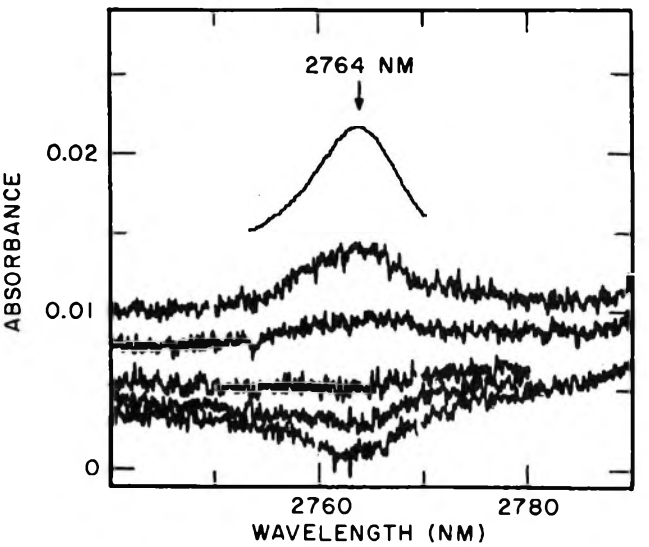

Figure 5. Difference spectra with expansion of ν_1 region showing approach to cancellation of monomer absorbance and overcancellation. Monomer absorbance is completely canceled in third (difference) trace from top. The top trace is a wavelength marker using the ν_1 absorbance of the monomer.

Discussion

The interpretation of the nitrogen matrix work[3] is persuasive, and there are no apparent reasons for questioning the conclusion that the dimer is formed with an open structure during deposition of the matrix. In the present work, with a considerably different environment and temperature for the water, a dimer has been proved by the equilibrium stoichiometry, but only two OH stretching bands have been resolved. The monomer and dimer bands are much wider in the liquid, presumably in part from collisional interactions with the solvent. If we assume that the overall effect of the medium and temperature on monomer and dimer frequencies is the same, the dimer frequencies for an open structure in carbon tetrachloride solution can be predicted from the frequencies in the nitrogen matrix. The ratios of the ν_1 and ν_3 monomer frequencies in the two media are 0.9952 and 0.9954, respectively (Table II). Applying the average ratio gives the dimer frequencies in column 4 of Table II.

A synthetic spectrum consisting of the Gaussian intensities of the two predicted bands at 3697 and 36 [illegible] arbitrarily assumed widths of 25 cm^{-1}

Table II: Water Monomer and Dimer Stretching Frequencies

	Nitrogen matrix, 20°K[a]			CCl_4 soln, 25°			
	Assignment[b]	cm^{-1}	Rel peak intensity	Predicted,[c] cm^{-1}	Obsd, cm^{-1}	$w_{1/2}$[d]	Rel. peak intensity
Monomer	ν_3	3725.7	1.0	...	3708	27[f]	1.0
	ν_1	3632.5	0.32[e]	...	3616	18[f]	0.43
Dimer	ν_3	3714.4	1.0	3697	...		
	ν_f	3697.7	0.38[e]	3680	3693	29	1.0
	ν_1	3625.6	0.25[e]	3609	...		
	ν_b	3547.5	0.62[e]	3531	3552	65	0.66

[a] Reference 3. The matrix bands appeared to have full widths at half-height of 3–4 cm^{-1}. [b] Symmetric ν_1 and asymmetric ν_3 notations retained as though left half of open dimer were an entity

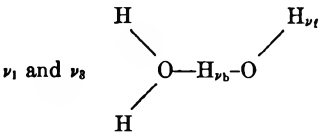

[c] For open dimer from average ratio $\nu(CCl_4)/\nu$(matrix) = 0.9953 for ν_1 and ν_3 monomer frequencies. [d] Full width at half-height (FWHH). [e] Estimated from spectra in ref 3. [f] Measured at 0.8 full height but calculated for FWHH assuming Gaussian.

indicated that these bands, if present, would not be resolved in the solution measurements. The only evidence for two bands would be a small asymmetry on the low energy side. The width of the observed band at 3693 cm^{-1} (2708 nm) is more than 25 cm^{-1}, but there is no way of predicting the band width. The width of the Q branch of the ν_1 vibration of the monomer, for example, is considerably less than that of ν_3.

The ν_1 band for an open dimer, predicted to be at 3609 cm^{-1} (2771 nm) in solution, is not observed. Its peak intensity should be about 0.0025 absorbance unit in Figure 1 and the corresponding difference spectra in Figures 4 and 5 (third from top), if the relative matrix intensities apply and the observed peak intensity at 3693 cm^{-1} is considered to be largely that of ν_3. The upper limit for any band in the ν_1 region is estimated to be 0.0010 absorbance unit in the difference spectrum. The intensity ratio of ν_1 to ν_3, at least for the Q branches of the monomer, is actually larger in carbon tetrachloride solution than in the nitrogen matrix (Table II), and one would expect an absorbance near 0.004 for the ν_1 vibration of an open dimer.

The dimer spectrum in solution is very similar to spectra of 1–1 complexes in which one hydrogen of the water is H-bonded to an electron donor and the other hydrogen is free.[8,16] A relatively narrow band is seen for the free hydrogen with frequency a few reciprocal centimeters less than that of ν_3. A broad band is observed for the H-bonded OH vibration with energy dependent upon the H-bond strength. The H bonds in these complexes are probably linear since the difference in frequency between ν_f and ν_b is typically 170–200 cm^{-1} for the ether homologs[16] of water as compared to 150 cm^{-1} for the linear water dimer (Table II) seen in the matrix.[3] The molar absorptivity (ϵ_{max}) of ν_f for H_2O in the 1–1 *p*-dioxane complex is about the same as that for ν_3 of the monomer.[8] The ratio of ν_f to ν_3 in the matrix dimer is about 0.4 (Table II).[3] These ratios may simply reflect the freezing out (depletion) of the rotational Boltzmann distribution as the monomer becomes complexed in solution or dimerized in the matrix.

Another point of difference between the matrix and solution spectra would be the relative intensities of ν_b and ν_f. If we suppose that the band observed in solution at 3693 cm^{-1} is an unresolved composite of ν_3 and ν_f in the intensity ratio of about 3 as given by the matrix spectrum, the ratio of intensities (ν_b/ν_f) integrated over the bands would be 4.5 in contrast to the matrix ratio of 1.6. If we suppose that all of the band at 3693 cm^{-1} is ν_f, the integrated intensity ratio (ν_b/ν_f) is 1.5 in agreement with the matrix ratio.

The indication from the present work is that the structure of the water dimer is cyclic with two bent hydrogen bonds in carbon tetrachloride solution. The band at 3693 cm^{-1} (ν_f) is the excitation of either of the two indistinguishable free OH groups, and the broad band centered at 3552 cm^{-1} (ν_b) is the excitation of either of the two indistinguishable H-bonded OH groups. The ν_b frequency predicted from the matrix frequency for an open dimer in solution is 3531 cm^{-1}, but the higher frequency of 3552 cm^{-1} is observed which is evidence for the weaker, bent H bond of the cyclic structure. The difference is not large, however, and possibly reflects a cooperative strengthening of the bent bonds. The cyclic dimer differs from a 1–1 complex only in that each water molecule in the dimer is acting both as electron donor and acceptor.

There is no conflict between the matrix and solution results if the energy difference between the open and

(16) S. C. Mohr, W. D. Wilk, and G. M. Barrow, *J. Amer. Chem. Soc.*, **87**, 3048 (1965).

cyclic structures is small so that the configuration depends on the environment, including temperature. Alternatively, there remains a question as to whether the dimer species in the nitrogen matrix is an equilibrium form. It is known from rare gas matrix studies[17] that water monomer is irrotationally bound in the nitrogen matrix. If dimer formation is by capture of monomers one at a time rather than by condensation of dimers from the vapor, it would seem likely that the first monomer would be partially buried by nitrogen before being found by a second monomer, resulting in a single attachment (linear dimer). In rare gas matrices where monomer rotation occurs, dimer bands have been reported,[17] but there seems to be no correspondence to the four-band vibrational pattern in the nitrogen matrix.

There is a conflict between the solution result and theoretical studies which have predicted the linear dimer.[6] Carbon tetrachloride certainly does not interact strongly with water because the rotational branches of the monomer are prominent even though the lines are broadened beyond resolution. The solution result leads to the expectation that the trimer and higher n-mers would also be cyclic by virtue of forming the additional H bond, the energy of which overrides the penalty of any bond nonlinearity. The bond distortion energy would appear to be overemphasized in the theoretical treatment. The solution result supports the idea[18] that the ring size in liquid water may not be restricted to the hexameric ring of the ice structure.

One of the incomplete aspects of the continuum model of liquid water[19] is the lack of a detailed account of the phenomena near and at the melting point. It is difficult to see in Pople's description,[20] for example, how H-bond bending alone could cause an abrupt breakdown of long-range structure at the constant temperature of the melting point. Supercooling of a network of distorted hexameric rings is inexplicable because there seems to be no way to take energy out without removing the distortion. The behavior of water rings projected from that of the small polymers suggests a melting mechanism which could be compatible with the continuum model. One may suppose that the entropy increase results from the formation and mixing of new "species" by the collapse of some of the 12-membered (O plus H) rings of the ice structure to smaller rings. The mechanism meets the requirement of reducing the void space of the ice structure without decreasing the nearest-neighbor distance and, if bending is not a severe restriction, four H bonds can be retained about each oxygen nucleus. The formation of smaller rings would imply a range of bent H bonds even in a static picture of the mixture. Dynamic bending and distortion would probably be required, however, for the continuum which is inferred from infrared and Raman spectra.[19] The ring mechanism provides the barrier necessary for the supercooling phenomenon in which freezing would be described as the breaking of many hydrogen bonds in the smaller rings, expanding against the internal pressure of the water, and re-forming the stronger bonds of the hexameric ice rings.

An estimate of the dimerization constant can be made from the present data and the solubility of water in carbon tetrachloride (0.0087 M) reported by Johnson, *et al.*[2,7] The molar absorptivity for ν_f (per single OH oscillator) is assumed to be the same as ϵ for ν_3, as appears to be approximately true for the 1–1 complex of water with p-dioxane.[8] The assumption leads to 3.6% of the total water molecules in saturated carbon tetrachloride being present as dimer. The Henry law measurements of Johnson, *et al.*,[2,7] appear not to be accurate enought to detect less than about 5% dimer content. The dimerization constant (eq 1) becomes 2.2 l. mol^{-1}. Masterton and Gendrano derived a dimerization constant of 0.54 l. mol^{-1} for water in 1,2-dichloroethane solution.[21] The value is probably an upper limit since the trimer seems to be present,[2,22] but it is consistent with the present value in carbon tetrachloride. Water is about 15 times more soluble in 1,2-dichloroethane than in carbon tetrachloride, and one expects larger polymerization constants in the latter solvent according to the correlation of Christian, *et al.*[2,23]

Acknowledgment. The author is grateful for the thermometer calibrations provided by Dr. Felix Schreiner.

(17) R. L. Redington and D. E. Milligan, *J. Chem. Phys.*, **39**, 1276 (1963).

(18) J. D. Bernal, *Proc. Roy. Soc., Ser. A*, **280**, 299 (1964).

(19) J. Schiffer and D. F. Hornig, *J. Chem. Phys.*, **49**, 4150 (1968).

(20) J. A. Pople, *Proc. Roy. Soc., Ser. A*, **205**, 163 (1951).

(21) W. L. Masterton and M. C. Gendrano, *J. Phys. Chem.*, **70**, 2895 (1966).

(22) C. Jolicoeur and A. Cabana, *Can. J. Chem.*, **45**, 567 (1968).

(23) S. D. Christian, J. R. Johnson, H. E. Affsprung, and P. J. Kilpatrick, *J. Phys. Chem.*, **70**, 3376 (1966).

Nuclear Magnetic Resonance Studies of Molecular Complexes

by W. R. Carper,* C. M. Buess, and Gary R. Hipp

Department of Chemistry, Wichita State University, Wichita, Kansas 67208 *(Received March 13, 1970)*

A Scatchard-type equation has been derived that allows the determination of complex formation constants by nmr spectroscopy. The primary advantage of this equation is that K is determined directly from the slope of an experimental plot rather than from the intercept. In addition, it is possible to use the molar and molal versions of the same equation and to determine the molar volume of the pure donor component of the complex. A series of trinitrobenzene (TNB) complexes with sulfoxides, sulfides, and a disulfide have been analyzed by this technique. The complexes were studied in carbon tetrachloride, carbon disulfide, and 1,2-dichloroethane at 10, 20, and 30°. Complex formation constants and thermodynamic properties were determined.

Introduction

Despite the large number of papers dealing with molecular complexes, only a small percentage of these studies use nmr spectroscopy as a means of determining complex formation constants and thermodynamic data. More recent papers include the work of Strom,[1] Hanna,[2,3] Foster,[4,5] and their coworkers.

In particular, Hanna and Ashbaugh[2] noted that equilibrium constants in hydrogen-bonding systems had been successfully determined by nmr spectroscopy[6] and that π-complex equilibria between donors and acceptors are similar to those found in hydrogen-bonding systems. Nmr spectroscopy is a successful detection tool for these diamagnetic molecular complexes as it is extremely sensitive to small changes in the electronic environment of a magnetic nucleus.

It is the purpose of this present investigation to apply molar and molal versions of a Scatchard-type[7] nmr equilibrium equation to a series of trinitrobenzene (TNB) complexes. The donor molecules include certain sulfoxides, sulfides, and a disulfide. Complex formation constants, thermodynamic parameters, and molar volumes are obtained in three solvents at 10, 20, and 30°.

Experimental Section

Materials. Methyl phenyl sulfide, bp 80° (18 mm), diphenyl sulfoxide, mp 70° (petroleum ether), diphenyl sulfone, mp 125–125.5° (ethanol), and di-*p*-tolyl sulfoxide, mp 95–95.5°, were obtained from the K & K Laboratories and distilled or recrystallized as indicated. Methyl phenyl sulfoxide, bp 95° (0.8 mm), and methyl phenyl sulfone, mp 88–88.5°, were prepared by oxidation by methyl phenyl sulfide with hydrogen peroxide in acetic acid.[8] Diphenyl sulfide and tetramethylene sulfoxide were highly pure samples obtained from the Aldrich Chemical Co. and were used without further purification. Eastman 1,3,5-trinitrobenzene was recrystallized from chloroform to yield a product which melted at 121°. Dimethyl sulfoxide (DMSO) was triply recrystallized and used immediately thereafter. Carbon tetrachloride (CCl_4), carbon disulfide (CS_2), and 1,2-dichloroethane (1,2-DCE) were either reagent grade or spectrophotometric grade and were used without further purification.

Procedure. Equipment used was a Varian A-60A nmr spectrophotometer equipped with a Varian temperature controller. Sweep width calibrations were done with a signal generator and a Hewlett-Packard frequency counter Model 524B on a monthly basis, while daily sweep width calibrations were done on the basis of a reference sample (part no. 943346-07) of chloroform with 6% tetramethylsilane which was supplied by Varian Associates for this purpose.

Temperature calibration of the Varian V-6040 temperature controller was accomplished by following the separation of the two major peaks (signals) of methanol. The alcohol sample (Part No. 943346-06) and the calibration curve were supplied by the manufacturer.

The samples were prepared by weighing the donor compounds in 10-ml volumetric flasks and then reweighing the flasks after filling so that the weight of both donor and solvent would be known. After initial preparation of the samples some of the aliquot was transferred to nmr sample tubes (4.28 mm i.d.; 5 mm o.d.) and a small amount of tetramethylsilane (TMS) was added as an internal standard. The sample tubes were then sealed with "parafilm M" (American Co.), capped with plastic tops, and the spectra were done as soon as possible to avoid undue evaporation.

* To whom correspondence should be addressed.

(1) E. T. Strom, W. L. Orr, B. S. Snowden, and D. E. Woessner, *J. Phys. Chem.*, **71**, 4017 (1967).

(2) M. W. Hanna and A. L. Ashbaugh, *ibid.*, **68**, 811 (1964).

(3) H. A. Sandoval and M. W. Hanna, *ibid.*, **70**, 1203 (1966).

(4) R. Foster and C. A. Fyfe, *Trans. Faraday Soc.*, **61**, 1626 (1965).

(5) R. Foster and C. A. Fyfe, *ibid.*, **62**, 1400 (1966).

(6) P. J. Berkely, Jr., and M. W. Hanna, *J. Phys. Chem.*, **67**, 846 (1963).

(7) G. Scatchard, *Ann. N. Y. Acad. Sci.*, **51**, 660 (1949).

(8) C. C. Price and J. J. Hydock, *J. Amer. Chem. Soc.*, **74**, 1943 (1952).

The sample concentration ranges included from 5×10^{-3} to 10^{-3} M in trinitrobenzene and from 0.1 to 1.6 M in the various sulfur-containing donor molecules.

A simple average of four to six scans (±0.3-cps range) for each sample was computed and used for the calculation of Δ. The plots were computed on the basis of the least-mean-square method and indicated an average of 5% error in the value of either K_M or K_m. A sample set of data for the phenyl disulfide–trinitrobenzene study is included in Table I. In

Table I

Sample data for phenyl disulfide–TNB complex in CCl_4 (see Figure 1). [TNB] = 8.0×10^{-3} M/l. at 20°

Phenyl disulfide concn (20°)		Δ, cps		
Molar	Molal	10°	20°	30°
0.110	0.071	5.8	5.0	4.2
0.204	0.134	9.8	8.6	7.2
0.496	0.346	19.2	17.1	15.2
0.753	0.548	24.4	22.6	20.5
1.002	0.770	28.0	26.6	24.4
1.33	1.10	32.0	30.5	28.5

Sample data for phenyl disulfide–TNB complex in 1,2-dichloroethane. [TNB] = 8.0×10^{-3} M/l. at 20°

Phenyl disulfide concn (20°)		Δ, cps		
Molar	Molal	10°	20°	30°
0.201	0.167	2.8	2.7	2.6
0.518	0.457	6.7	6.5	6.4
0.751	0.698	9.4	9.1	8.7
1.008	0.989	12.1	11.7	10.9
1.302	1.362	15.0	14.3	13.5
1.502	1.662	16.9	16.0	15.0

Sample data for phenyl disulfide–1,2-dichloroethane complex in CCl_4. [1,2-DCE] = 8×10^{-3} M/l.

Phenyl disulfide concn (20°)		Δ, cps		
Molar	Molal	10°	20°	30°
0.254	0.168	2.9	2.8	2.6
0.494	0.342	5.4	5.2	4.8
0.754	0.547	7.9	7.5	7.1
0.999	0.768	10.1	9.6	9.2
1.261	1.034	12.3	11.9	11.2
1.497	1.301	Ppt formed	13.6	12.9

all cases the experimental data were checked by using identical solutions and repeating the experiment at least once. The relative shifts were seen to be constant within 0.2 cps for separate runs of the same experiment. Given in Figure 1 is a plot of the data for the phenyl disulfide–TNB complex in carbon tetrachloride.

Derivation of the Nmr Equilibrium Equation.[2-12] For the ideal case assume that the equilibrium condition implied by 1

$$\text{acceptor (A)} + \text{donor (D)} \rightleftharpoons \text{complex (C)} \quad (1)$$

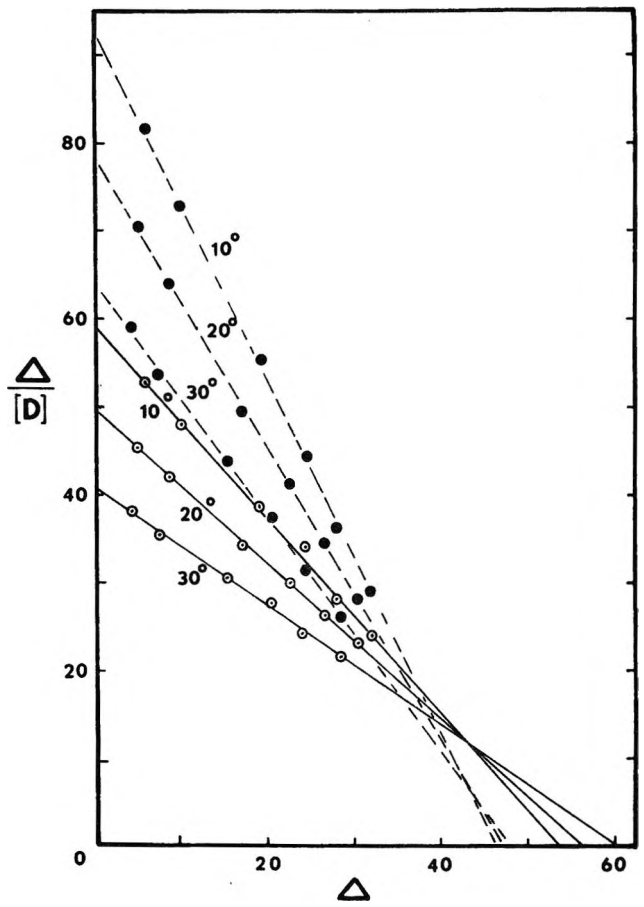

Figure 1. Plot of Δ/D *vs.* Δ for phenyl disulfide–TNB complex in carbon tetrachloride at 10, 20, and 30°; both molal (●) and molar (⊙) plots are given.

denotes the formation of a 1:1 molecular complex by an acceptor and a donor molecule. Furthermore, assume the activity coefficients are either unity or constant throughout the concentration ranges used, and let A_0 and D_0 represent the initial concentrations of acceptor and donor, respectively. Now, if $D_0 \gg A_0$, then C will be small and comparable in magnitude to A_0 and consequently[12]

$$K = \frac{C}{D_0(A_0 - C)} \quad (2)$$

To relate the nmr measurements to the equilibrium it is assumed that the free and complexed forms of the acceptor each have characteristic precessional frequencies (γ_{ref} and γ_c, respectively) and that the observed resonance frequency (γ_{obsd}) is the weighted arithmetic mean.

(9) D. A. Deranleau, *J. Amer. Chem. Soc.*, **91**, 4044 (1969).

(10) C. M. Huggins, G. C. Pimental, and J. N. Shoolery, *J. Chem. Phys.*, **23**, 1244 (1955).

(11) M. I. Foreman, R. Foster, and D. R. Twiselton, *Chem. Commun.*, 1318 (1969).

(12) P. J. Trotter and M. W. Hanna, *J. Amer. Chem. Soc.*, **88**, 3724 (1966).

Table II: Sulfide–, Disulfide–TNB Complexes

Donor	Solvent	Temp, °C	K_M, l./mol	K_m, kg/mol	Molar vol, l./M Calcd	Molar vol, l./M Exptl
Methyl phenyl sulfide	CCl_4	10	1.00	1.75	0.114	0.117
		20	0.92	1.63	0.114	
		30	0.78	1.40	0.114	
	CS_2	10	0.72	1.05	0.117	
		20	0.66	0.98	0.117	
		30	0.62	0.93	0.117	
	1,2-DCE	10	0.14	0.32	0.117	
		20	0.15	0.34	0.117	
		30	0.13	0.31	0.117	
Phenyl sulfide	CCl_4	10	1.04	1.91	0.164	0.167
		20	0.95	1.76	0.165	
		30	0.89	1.68	0.165	
	CS_2	10	0.74	1.14	0.164	
		20	0.66	1.04	0.164	
		30	0.58	0.94	0.164	
	1,2-DCE	10	0.15	0.39	0.168	
		20	0.12	0.36	0.168	
		30	0.12	0.36	0.168	
Phenyl disulfide	CCl_4	10	1.10	2.01	0.174	0.161
		20	0.88	1.65	0.174	
		30	0.67	1.33	0.174	
	1,2-DCE	10	0.19	0.46	0.183	
		20	0.20	0.48	0.183	
		30	0.25	0.54	0.183	

Table III: Sulfoxide–TNB Complexes

Donor	Solvent	Temp, °C	K_M, l./mol	K_m, kg/mol	Molar vol, l./M Calcd	Molar vol, l./M Exptl
Phenyl sulfoxide	CCl_4	10	4.78	7.22		
		20	4.28	6.52		
		30	3.71	5.85		
	CS_2	10	3.43	4.52	0.168	
		20	3.21	4.25	0.168	
		30	3.02	4.01	0.167	
p-Tolyl sulfoxide	1,2-DCE	10	0.03	0.25	0.173	
		20	0.02	0.21	0.151	
		30	0.00	0.00	...	
DMSO	CCl_4	10	5.59	8.96	0.068	0.071
		20	5.79	9.28	0.069	
		30	5.96	9.53	0.069	
TMSO	CCl_4	10	9.15	14.66	0.088	0.088
		20	6.90	11.1	0.088	
		30	5.66	9.11	0.088	
	CS_2	10	5.76	15.7		
		20	4.97	15.3		
		30	4.07	15.1		

$$\gamma_{obsd} = \left(\frac{C}{A_0}\right)\gamma_c + \left(\frac{A_0 - C}{A_0}\right)\gamma_{ref} \quad (3)$$

which leads to

$$\frac{\Delta}{D_0} = -K(\Delta - \Delta_0) \quad (4)$$

Equation 4 is the experimental one where Δ/D_0 is plotted *vs.* Δ and yields $-K$ as the slope and Δ_0 as the x intercept.

Equation 4 has been recently suggested by Deranleau[9] and is a type of Scatchard plot.[7]

Equation 4 can also be written in the form of a molal plot

$$\frac{\Delta}{m_d} = -K(\Delta - \Delta_m) \quad (5)$$

where $\Delta_m = \Delta_0$. For the x intercept let $\Delta/m_d \rightarrow 0$, then $\Delta = \Delta_m$ or the shift of the acceptor in pure donor.

Table IV: 1,2-DCE Complexes

Donor	Solvent	Temp, °C	K_m, l./mol	K_m, kg/mol	Molar vol, l./M Calcd	Molar vol, l./M Exptl
DMSO	CCl_4	10	0.61	1.10	0.069	0.071
		20	0.70	1.22	0.073	
		30	0.74	1.29	0.069	
Phenyl sulfide	CCl_4	10	0.09	0.40	0.165	0.167
		20	0.07	0.37	0.165	
		30	0.04	0.32	0.164	
Phenyl disulfide	CCl_4	10	0.18	0.57	0.179	
		20	0.14	0.52	0.183	
		30	0.15	0.53	0.183	

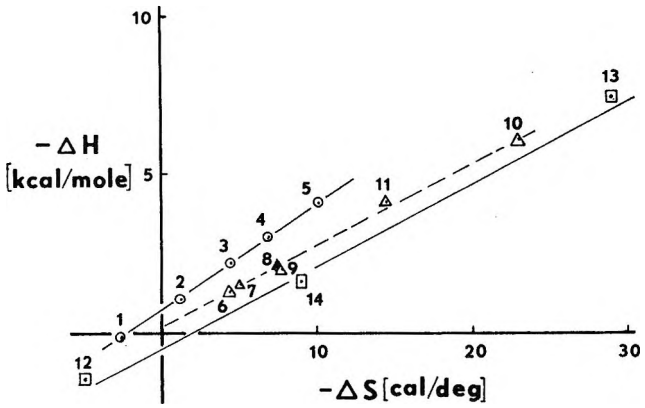

Figure 2. Thermodynamic data on the various molecular complexes of TNB and 1,2-DCE: 1, DMSO + TNB complex in CCl_4; 2, phenyl sulfoxide + TNB complex in CS_2; 3, phenyl sulfoxide + TNB complex in CCl_4; 4, TMSO + TNB complex in CS_2; 5, TMSO + TNB complex in CCl_4; 6, phenyl sulfide + TNB complex in CCl_4; 7, methyl phenyl sulfide + TNB complex in CS_2; 8, methyl phenyl sulfide + TNB complex in CCl_4; 9, phenyl sulfide + TNB complex in CS_2; 10, phenyl sulfide "eff" + TNB in 1,2-DCE; 11, phenyl disulfide + TNB complex in CCl_4; 12, DMSO + 1,2-DCE complex in CCl_4; 13, phenyl sulfide + 1,2-DCE in CCl_4; 14, phenyl disulfide + 1,2-DCE complex in CCl_4.

Calculation of Molar Volume of Pure Donor. Equation 6 denotes the molar equation with its characteristic parameters; now if $\Delta_m = \Delta$ in eq 6

$$\frac{\Delta}{[D_0]} = -K_M[\Delta - (\Delta_0)_M] \quad (6)$$

$$\frac{1}{[D_0]} = \frac{K_M[(\Delta_0)_M - \Delta_m]}{\Delta_m} \quad (7)$$

Equation 7 permits the calculation of the molar volume of the undiluted donor from three experimental parameters, and the result can then be compared to literature values.

Results and Discussion

A recent study by Foreman, *et al.*,[11] indicates that nonequivalent nuclei give different K's for the same complexes. This suggests a degree of uncertainty in cases where the complex is weak and where the molecule serving as the nmr probe is an unsymmetrical one. In our case, TNB possesses D_{3h} symmetry and presents no such problem.

Table V: K_M (l./mol) Values of TNB–Donor Complexes in 1,2-Dichloroethane *vs.* K_M' (l./mol) Values of TNB–Donor ("Effective") Complexes in 1,2-Dichloroethane

Donor	Temp, °C	K_M, l./mol	K_M', l./mol
Phenyl sulfide	10	0.15	0.52
	20	0.12	0.38
	30	0.12	0.25
Phenyl disulfide	10	0.19	1.13
	20	0.20	0.99
	30	0.25	1.14

Table VI: Molar and Molal Values of Δ_0 for TNB Complexes of Sulfides and Disulfide

Donor	Solvent	Temp, °C	$-(\Delta_0)_M$, cps	$-\Delta_m$, cps
Methyl phenyl sulfide	CCl_4	10	52.9	47.5
		20	50.4	44.8
		30	51.1	44.5
	CS_2	10	38.5	45.8
		20	34.5	44.2
		30	31.1	41.9
	1,2-DCE	10	88.0	47.9
		20	77.2	43.8
		30	85.1	44.2
Phenyl sulfide	CCl_4	10	51.6	44.5
		20	50.8	43.2
		30	49.4	41.7
	CS_2	10	53.9	44.0
		20	53.6	42.9
		30	53.3	41.5
	1,2-DCE	10	82.3	38.5
		20	92.1	38.1
		30	87.6	36.1
Phenyl disulfide	CCl_4	10	53.8	46.4
		20	56.8	47.4
		30	60.4	48.1
	1,2-DCE	10	76.9	38.7
		20	68.1	35.9
		30	54.9	31.6

The results of this investigation are contained in Tables II–VIII and Figure 1. All of the data obtained during this investigation have been analyzed by both the "molal" and "molar" equations given previously as (5) and (6). The molal value of K is consistently higher than the molar value as it should be.[12] Furthermore the ratios of K's at 30 and 10° for any particular complex are quite similar for each method; thus it would appear that enthalpy of complex formation will be the same regardless of the approach used to evaluate the data.

Table VII: Molar and Molal Values of Δ_0 for TNB Complexes of Sulfoxides

Donor	Solvent	Temp, °C	$-(\Delta_0)_M$, cps	$-\Delta_m$, cps
Phenyl sulfoxide	CCl_4	10	21.7	19.5
		20	20.9	21.3
		30	20.7	20.7
	CS_2	10	25.6	24.4
		20	24.5	23.3
		30	23.6	22.4
p-Tolyl sulfoxide	1,2-DCE	10	295.5	47.8
		20	578.3	57.1
		30	...	...
DMSO	CCl_4	10	9.18	9.07
		20	8.50	8.40
		30	7.75	7.66
TMSO	CCl_4	10	9.67	9.58
		20	9.31	9.19
		30	8.82	8.69
	CS_2	10	15.5	15.7
		20	15.0	15.3
		30	14.8	15.1

Table VIII: Molar and Molal Values of Δ_0 for 1,2-Dichloroethane Complexes in CCl_4

Donor	Temp, °C	$-(\Delta_0)_M$, cps	$-\Delta_m$, cps
DMSO	10	−8.80	−7.90
	20	−7.70	−7.06
	30	−8.40	−7.68
Phenyl sulfide	10	100.2	34.8
	20	120.5	34.9
	30	198.4	35.7
Phenyl disulfide	10	66.0	33.1
	20	76.7	33.9
	30	70.7	31.7

Returning to eq 5 and 6, let us consider the consequences of each approach. When Δ/m_D is plotted *vs.* Δ the slope is seen to be $-K_m$. Trotter and Hanna[12] have recently shown that if one uses a Benesi–Hildebrand[13] (BH) molal equation to evaluate K from the intercept, there still may be a significant error. Unfortunately, they[12] also indicate that any method used can give linear plots which may all disagree with one another. While the Scatchard[7] method may still contain the same inherent errors, it nevertheless provides a means of determining the K from the slope rather than from the intercept. Furthermore, K is determined as a single function rather than a composite one as is the case in BH approaches.

Equation 6 represents the molar version of eq 5, and once again allows us to evaluate K from the slope. It would seem that eq 6 is a linear function, and in practice our observations are that it appears to be so. Unfortunately, it is much harder to experimentally approach the x intercept in eq 6 than it is to approach the x intercept in eq 5. This may lead to additional uncertainties in the determination of the shift of the pure complex (Δ_0).

An examination of Tables VI–VIII indicates different values of Δ_0 for each method. As an evaluation of Δ_0 we decided to use the molal values to calculate donor molar volumes from eq 7. The results obtained from using the molal Δ_0 values are given in Tables II–IV. As indicated therein, the results are quite satisfactory with the exceptions of phenyl sulfoxide in CCl_4 and TMSO in CS_2.

The complexes in question were studied at 10, 20, and 30°. In certain cases solubility prevented a complete study. The donor molecules include methyl phenyl sulfide, phenyl sulfide, phenyl disulfide, phenyl sulfoxide, *p*-tolyl sulfoxide, dimethyl sulfoxide, tetramethylene sulfoxide, diphenyl sulfone, and methyl phenyl sulfone. The sulfones exhibited little, if any, molecular association, and as a consequence are not included in this report.

The solvent effects are consistent and suggest that CCl_4 is the least interfering of the three solvents. In the case of the phenyl disulfide–TNB complex it is obvious that some interaction occurs between phenyl disulfide and 1-2,dichloroethane. The same general effect is also seen for dimethyl sulfoxide and phenyl sulfide. Consequently, an analysis of 1,2-dichloroethane complexes was also completed, and the results are given in Table IV.

The results in Table IV were used to recalculate the K's that are listed in Tables II and III. The initial and final versions are given in Table V. While the K's in Table V represent an improved value they are not, necessarily, the true values. This is due to the possible association between TNB and each of the three solvents. While we were unable to detect any measureable chemical shift when TNB–solvent mixtures were diluted, there was a slight upfield shift with decreasing temperature. Furthermore, Johnston, *et al.*,[14] reported a K of 0.09 l./mol for the TNB–CCl_4 complex at 40°. As-

(13) (a) H. A. Benesi and J. H. Hildebrand, *J. Amer. Chem. Soc.*, 71, 2703 (1949); (b) W. Lin and S. Tsay, *J. Phys. Chem.*, 74, 1037 (1970).

(14) M. D. Johnston, Jr., F. P. Gasparro, and I. D. Kuntz, Jr., *J. Amer. Chem. Soc.*, 91, 5715 (1969).

suming that donor–solvent competition does exist, then this suggests that our "corrected" K_M' values are slightly lower than what they should be.

A final examination of our results suggests that the donor properties exist in the following order: sulfoxide > disulfide > sulfide > sulfone. This is somewhat different than might be expected. In particular, Drago, *et al.*,[15] studied complexes between alkyl sulfoxides, sulfides, sulfones, and either iodine or phenol and determined the order: sulfide > sulfoxide > sulfone. Similarly, Good, *et al.*,[16] studied iodine complexes of alkyl sulfides and disulfides. In the latter[16] investigation, the sulfide complexes were seen to be slightly stronger than those of the disulfides.

These results suggest that the phenyl group may be involved in different inductive effects as one goes from a sulfur atom to a sulfoxide group or that perhaps that steric effects are somewhat different in each case. A final suggestion is that both effects are present simultaneously.

A plot of $-\Delta H$ *vs.* $-\Delta S$ is given in Figure 2. The TNB complexes can be grouped into two classes: (a) the sulfoxides, and (b) the sulfides and disulfide. The 1,2-dichloroethane complexes, generally, do fit into the same class as the TNB–sulfide and –disulfide complexes. This would suggest that the sulfide and disulfide complexes are formed through a similar mechanism. A possible conclusion is that the sulfoxides donate electrons from the sulfur–oxygen group, while the other donors donate a lone-pair electron from the sulfur atom.

(15) R. S. Drago, B. Wayland, and R. L. Carlson, *J. Amer. Chem. Soc.*, **85**, 3125 (1963).

(16) M. Good, A. Major, J. Nag-Chaudhuri, and S. P. McGlynn, *ibid.*, **83**, 4329 (1961).

A Spectroscopic Study of the Excited States of Coumarin[1]

by Pill-Soon Song[2] and William H. Gordon, III[3]

Department of Chemistry, Texas Tech University, Lubbock, Texas 79409 *(Received June 10, 1970)*

The luminescence emission and polarization spectra of coumarin have been investigated in both polar and nonpolar solvents at 77°K. Lifetime measurements and the method of photoselection have been employed in order to determine spectroscopic assignments of the molecular luminescence. The triplet–singlet emission shows a broad structured band at *ca.* 450–550 nm and is negatively polarized with respect to $\pi \rightarrow \pi^*$ excitations, indicating that phosphorescence originates from the lowest π,π^* triplet. The fluorescence spectrum in ethanol glass at 77°K is broad and unstructured. On the basis of the observed positive polarization values, the fluorescence at 77°K is assigned to $^1(\pi,\pi^*)$. In a nonpolar solvent, however, the fluorescence spectrum is red-shifted (*ca.* 30 nm) and becomes significantly more intense at the expense of the phosphorescence intensity. The polarization values remain significantly positive, indicating that the fluorescent state is of $^1(\pi,\pi^*)$ character. Theoretical transition energies and direction of polarizations calculated by the P–P–P SCF MO CI method have been used for the interpretation of the observed results. In addition, the electronic structures of the singlet and triplet excited states of coumarin have been obtained theoretically in an attempt to correlate them with the photochemical reactivity of coumarin.

Introduction

Coumarins are well known in photobiology as photosensitizing agents in photodynamic actions. Coumarin itself is also known to show interesting photochemical behavior, particularly dimerization,[4] in polar and nonpolar solvents. In polar solvents such as ethanol, the cis heat-to-head dimer is formed presumably *via* interaction of excited singlet coumarin with its ground state, while in nonpolar solvents such as benzene, trans head-to-head dimer is formed *via* the triplet state. The purpose of this communication is to describe theoretical and experimental results on the excited states of coumarin obtained through MO computations and luminescence techniques. It is hoped that a better understanding of the versatile reactivity of the excited coumarin molecule and its role in photobiology will be gained from the type of study described herein.

(1) Supported by the Robert A. Welch Foundation (Grant No. D-182) and by the National Science Foundation (Grant No. GB-21266).

(2) To whom correspondence and reprint requests should be addressed.

(3) The Robert A. Welch Foundation predoctoral fellow, 1970.

(4) G. S. Hammond, C. A. Stout, and A. A. Lamola, *J. Amer. Chem. Soc.*, **86**, 3103 (1964).

Experimental Section

Materials. Coumarin (1,2-benzopyrone), crystalline form, was obtained from Matheson Coleman and Bell and was recrystallized. It was found to be free of luminescent impurities at a desired sensitivity setting of the detector unit. Ethanol was spectrograde and was obtained from U. S. Industrial Co. Isopentane, spectrograde, was purchased from Matheson Coleman and Bell and was dehydrated by treatment with anhydrous sodium sulfate.

Methods. Unless indicated otherwise, fluorescence and phosphorescence emission and excitation and the polarization spectra were recorded as described previously.[5] Polarization of luminescence excitation and emission bands was determined by means of Glan–Thompson polarizing and analyzing prisms, and polarization spectra were corrected using the Azumi–McGlynn formula.[6] The light source was a xenon Hanovia compact arc lamp (150-W) and the detector was an EMI 9558QA photomultiplier tube with an S-20 response photocathode. No spectral correction of the output and detector response to wavelength has been made in the recorded spectra. Absorption spectra were recorded on a Cary 14 spectrophotometer.

Phosphorescence lifetimes were determined as follows. The Aminco–Keirs phosphoroscope was replaced with a similar cylindrical shutter with a wide window. This shutter is spring loaded and will rotate 90° when released from a cocked position. When the shutter is in the cocked position, the sample is exposed to the exciting light and the steady emission intensity is detected by a PM tube. When the spring is released, the shutter rotates 90° so that the exciting light is cut off and the sample phosphorescence emitted into the emission monochromator and PM tube begins to decay. The signal from the PM tube is fed into an Analab oscilloscope with a type 700 dual channel plug-in. A microswitch on the shutter assembly triggers the sweep as the shutter is released. The decay curve is then photographed with a type 3000 single frame oscilloscope camera. With this attachment, lifetimes longer than 10^{-3} sec can be accurately measured. Lifetimes shorter than 10^{-3} sec can be measured using the rotating phosphoroscope on our instrument. 1,2-Benzanthracene was used as a standard to check the lifetime accessory. Its measured lifetime was found to be 0.3 sec in EPA at 77°K and in agreement with the known lifetime of 0.3 sec.[7] Alternatively, the lifetimes were measured on an X–Y recorder equipped with a time-base scan operation.

Molecular Orbital Computations. The Pariser–Parr–Pople SCF MO CI computations in the restricted[8,9] and unrestricted[10] Hartree–Fock–Roothaan schemes are carried out in order to calculate the excited states of coumarin. The unrestricted scheme assumes different orbitals for different spins (DODS). Table I lists semiempirical integrals used for the P–P–P MO computations. The two-center electron repulsion integrals of the form (rr|ss) are estimated according to the Mataga–Nishimoto formula,[11] unless otherwise indicated.

Table I: Values of Semiempirical Integrals in eV

Atom	Bond	$-W_{2p}$	(rr|rr)	β_{rs}^{core}
C		11.16	11.13	
—O—		32.90	21.53	
=O		17.70	15.23	
	C=C			−2.39
	=C—C=			−2.39
	C—O—			−2.12
	C=O			−3.00

The configuration interaction (CI) matrix elements are evaluated for 12 singly excited configurations for coumarin and 9 singly excited configurations for pyrone. These configurations are constructed using the SCF closed-shell and virtual orbitals.

The extended Hückel MO calculations have been performed using approximations and parameters originally proposed by Hoffmann.[12] The LCAO MO SCF CNDO/2 method was also used withs emiempirically evaluated parameters reported by Pople and Segal.[13] All computations were performed on an IBM 7040 and were repeated on a CDC 1604.

Results and Discussion

Singlet Excited States. Absorption, fluorescence and phosphorescence excitation, fluorescence and phosphorescence emission, and polarization spectra are shown in Figures 1 and 2. In order to aid assignment of these spectral bands, singlet–singlet transitions will be considered first. Table II and Figure 3 show theoretical predictions of the transition energies and directions of their polarizations, respectively. An excellent agreement between the predicted and observed transition energies can be seen. The lowest $\pi \rightarrow \pi^*$ transition is polarized nearly along the long molecular axis, but it is mainly localized in the 1,2-pyrone ring. This is consistent with the observed transition at 300 nm (ϵ 5000 in ethanol) in 5-methyl-1,2-pyrone.[14,15] We calculated

(5) P.-S. Song and W. E. Kurtin, *J. Amer. Chem. Soc.*, **91**, 4892 (1969).
(6) T. Azumi and S. P. McGlynn, *J. Chem. Phys.*, **37**, 2413 (1962).
(7) D. S. McClure, *ibid.*, **17**, 905 (1949).
(8) R. Pariser and R. G. Parr, *ibid.*, **21**, 466, 767 (1953).
(9) J. A. Pople, *Trans. Faraday Soc.*, **49**, 1375 (1953).
(10) J. A. Pople and R. K. Nesbet, *J. Chem. Phys.*, **22**, 571 (1954).
(11) N. Mataga and K. Nishimoto, *Z. Phys. Chem.* (*Frankfurt am Main*), **13**, 140 (1957).
(12) R. Hoffman, *J. Chem. Phys.*, **39**, 1397 (1963).
(13) J. A. Pople and G. A. Segal, *ibid.*, **44**, 3289 (1966).
(14) J. Fried and R. C. Elderfield, *J. Org. Chem.*, **6**, 566 (1941).

Table II: The P–P–P SCF MO CI Calculations of (π,π^*) States Arising from Low Energy Configurations. The Mataga-Nishimoto Formula was Used for (rr|ss) Terms

Molecule	Transition[a]	Energy, nm (obsd)	Oscillator strength (obsd)	CI wave functions (Ψ)[b]
Coumarin	$^1(\pi,\pi^*)$			
	6 → 7	306 (310)[c]	0.377 (6000)[d]	$0.82\phi(6 \rightarrow 7) + 0.43\phi(5 \rightarrow 7) + 0.22\phi(6 \rightarrow 8) + \ldots$
	5 → 7	273 (274)	0.415 (10500)	$0.66\phi(5 \rightarrow 7) - 0.54\phi(6 \rightarrow 7) + 0.47\phi(6 \rightarrow 8) + \ldots$
	6 → 8	224 (238)[e]	0.139	$0.55\phi(6 \rightarrow 8) - 0.58\phi(5 \rightarrow 7) - 0.34\phi(5 \rightarrow 8) + \ldots$
	6 → 9	212 (210)	0.508 (11700)	$0.66\phi(6 \rightarrow 9) - 0.51\phi(6 \rightarrow 8) - 0.50\phi(5 \rightarrow 8) + \ldots$
	$^3(\pi,\pi^*)$			
	6 → 7	490[f] (457)		$0.92\phi(6 \rightarrow 7) - 0.20\phi(4 \rightarrow 9) + 0.18\phi(4 \rightarrow 8) + \ldots$
	5 → 7	331		$0.66\phi(5 \rightarrow 7) + 0.51\phi(5 \rightarrow 8) + 0.37\phi(5 \rightarrow 9) + \ldots$
	5 → 8	300		$0.57\phi(6 \rightarrow 8) - 0.56\phi(5 \rightarrow 7) + 0.44\phi(5 \rightarrow 8) + \ldots$
	6 → 9	280		$0.59\phi(6 \rightarrow 9) - 0.54\phi(4 \rightarrow 7) + 0.52\phi(5 \rightarrow 8) + \ldots$
1,2-Pyrone	$^1(\pi,\pi^*)$			
	4 → 5	290 (300)	0.374 (5000)	$0.98\phi(4 \rightarrow 5) + 0.11\phi(2 \rightarrow 6) - 0.08\phi(3 \rightarrow 5) + \ldots$
	4 → 6	225	0.129	$0.86\phi(4 \rightarrow 6) + 0.48\phi(3 \rightarrow 5) + 0.11\phi(2 \rightarrow 5) + \ldots$
	3 → 5	186	0.565	$0.64\phi(3 \rightarrow 5) + 0.48\phi(4 \rightarrow 7) - 0.49\phi(2 \rightarrow 5) + \ldots$
	$^3(\pi,\pi^*)$			
	4 → 5	678		$0.95\phi(4 \rightarrow 5) - 0.19\phi(3 \rightarrow 6) - 0.15\phi(3 \rightarrow 7) + \ldots$
	4 → 6	368		$0.84\phi(4 \rightarrow 6) - 0.38\phi(3 \rightarrow 5) - 0.27\phi(2 \rightarrow 5) + \ldots$
	3 → 5	313		$0.63\phi(3 \rightarrow 5) - 0.52\phi(4 \rightarrow 7) - 0.47\phi(2 \rightarrow 5) + \ldots$

[a] The first and last numbers represent indices of the closed shell and virtual orbitals, respectively, in order of increasing orbital energy. [b] Important CI contributions. [c] Observed values from Figure 2. [d] Extinction coefficients in ethanol. [e] A shoulder in isopentane (Figure 2). [f] A constant deviation of 0.5 eV added to the triplet energy levels.

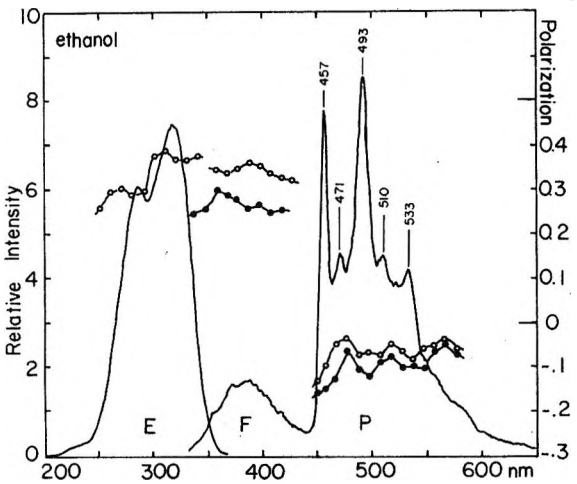

Figure 1. Spectra of coumarin (5.7×10^{-5} M) in ethanol at 77°K: E, excitation spectrum and polarized fluorescence excitation with respect to λ_{em} 384 nm (-○-); F, fluorescence spectrum and polarization with respect to λ_{ex} 330 nm (-○-) and λ_{ex} 255 nm (-●-), and P, phosphorescence spectrum and polarization with respect to λ_{ex} 331 nm (-○-) and λ_{ex} 278 nm (-●-).

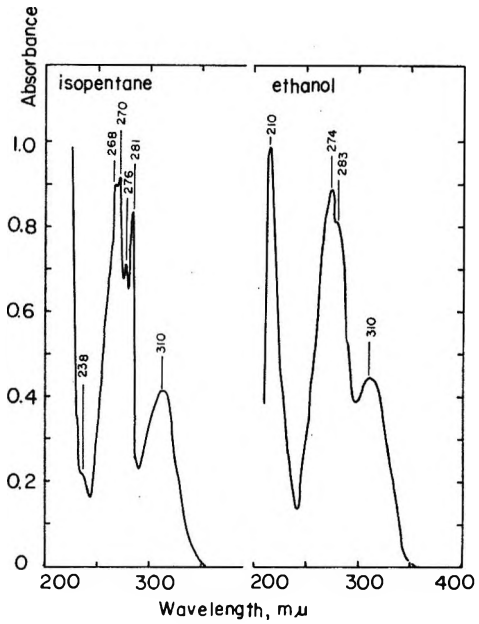

Figure 2. Absorption spectra of coumarin in isopentane and in ethanol at 298°K.

the transition energy in 1,2-pyrone with the P–P–P SCF MO CI, and results are presented in Table II. In general, agreement is satisfactory in both coumarin and pyrone. We will designate the lowest singlet state as $^1(\pi,\pi^*)_1$, and the second lowest as $^1(\pi,\pi^*)_2$, etc.

The polarized fluorescence spectrum of coumarin in ethanol at 77°K is shown in Figure 1. On the basis of the positive values of polarization, the fluorescent state is assigned to the $^1(\pi,\pi^*)_1$ state. The fluorescence polarization with respect to 255 nm excitation is less positive, and this is internally consistent with the polarized fluorescence excitation spectrum. In addition, Figure 3 shows an angle of 60 or 16° between the two

(15) Dezelic, *et al.* [M. Dezelic, M. Trkovnik, and M. Zovko, *Glasnik Hemicara Technol. Bosne Hercegovine*, 12, 17 (1963); *Chem. Abstr.*, 63, 17846 (1965)] have studied electronic spectra of a series of coumarins and concluded that the long wavelength absorption at 300 nm is localized in the pyrone ring. However, we are unable to obtain the original reference for further details.

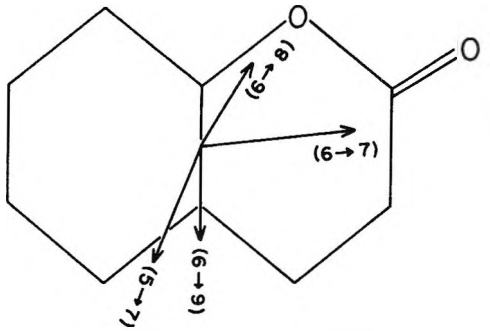

Figure 3. Polarizations of $\pi \rightarrow \pi^*$ transitions predicted by the P–P–P SCF MO CI method. Pertinent spectroscopic quantities are tabulated in Table I. Angle (θ) between (6 → 7) and (5 → 7) moments reduces to 16° after configuration interactions.

lowest $\pi \rightarrow \pi^*$ transition moments. It appears that mutual orientations of the two polarizations are not clearly revealed, possibly owing to overlapping $^1(\pi,\pi^*)_1$, $^1(n,\pi^*)$ and $^1(\pi,\pi^*)_2$ bands, a situation analogous to the case of indole in which ^1L_a and ^1L_b bands overlap.[5] We suggest, therefore, that there is a reasonable agreement between the polarized fluorescence spectrum in Figure 1 and calculated transitions shown in Figure 3.

Figure 4 shows spectra of coumarin in dry isopentane. In contrast to the ethanol glass, the phosphorescence intensity is very weak and is observable only at reasonably high concentrations of coumarin ($>10^{-4}$ M). However, at these concentrations of coumarin, its fluorescence begins to show a self-quenching. It is also apparent that the fluorescence polarization is significantly less positive in isopentane than in ethanol. The reason for the depolarization is not certain at this time. However, vibrational structure appears in the absorption band of coumarin in isopentane. Whether the appearance of the structure corresponds to a solvent-shifted n → π^* band in isopentane cannot be answered from the observed spectral data. Furthermore, it is essential to have information on the location and polarization of the n → π^* transition in order to explain the anomalous fluorescence polarization in the nonpolar solvent. Some discussion pertinent to this point is offered below.

The sharp decrease in the degree of fluorescence polarization at longer wavelengths in isopentane shown in Figure 4 may be ascribed to negatively polarized phosphorescence which begins to contribute to some extent in the longer wavelength region. More likely, the fluorescence polarization is low because the excitation is not monochromatic in isopentane. It should be noted that the blue edge of the fluorescence emission band and red side of the fluorescence excitation spectrum show a trend toward higher polarization. On this basis, the fluorescent state is assigned to $^1(\pi,\pi^*)_1$. Vibronic activity involving out-of-plane vibrations and energy transfer may also account for the sharp decline of the fluorescence polarization in isopentane.

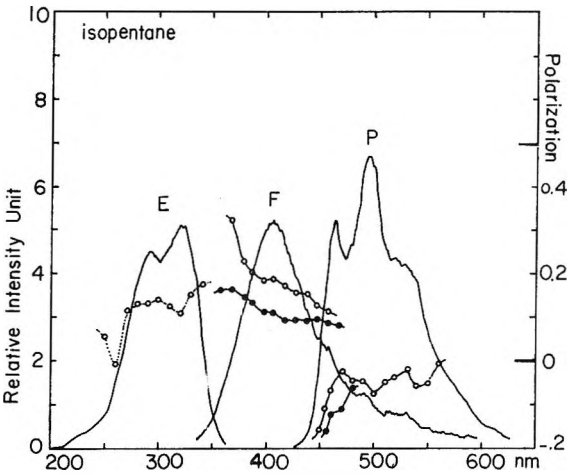

Figure 4. Spectra of coumarin (9×10^{-5} M) in dry isopentane at 77°K: E, excitation spectrum and polarized fluorescence excitation with respect to λ_{em} 407 nm (···○···); F, fluorescence spectrum and polarization with respect to λ_{ex} 340 nm (–○–) and λ_{ex} 270 nm (–●–); and P, phosphorescence spectrum and polarization with respect to λ_{ex} 345 nm (–○–) and λ_{ex} 290 nm (–●–). The phosphorescence emission was very weak, as evidenced by residual emission in curve F. Curve P is obtained at magnified sensitivity and slit width and with a phosphoroscope to eliminate the intense fluorescence.

We rule out the $^1(n,\pi^*)$ state as the lowest singlet and fluorescent state on empirical and theoretical grounds. It is generally observed that $^1(n,\pi^*)$ states are not usually fluorescent. Theoretically, the extended HMO predicts the lowest n → π^* transition to be higher in energy by 0.126 eV (31 nm) than the lowest $\pi \rightarrow \pi^*$. The CNDO also predicts that the n,π^* state is not the lowest singlet state. In this case, the energy gap is 1.012 eV, a value obviously too large. Nevertheless, the extended HMO and CNDO predictions are still meaningful regarding the relative ordering of the n,π^* and π,π^* states.

We have examined the fluorescence emission in ethanol and isopentane at room temperature. Within the concentration range of 0.3×10^{-4} to 3×10^{-4} M, no detectable fluorescence was observed at a sensitivity of the instrument so high as to give an intolerable signal to noise ratio. Petrovich and Borisevich[16] were also unable to obtain the fluorescence spectrum of coumarin at room temperature. However, a fluorescence band with maximum at 358 nm was reported for a concentrated solution (0.02 M) in ethanol at room temperature.[4] It is not certain whether the decreased fluorescence, or lack of it, is due to the enhanced intersystem crossing at room temperature. However, both intersystem crossing and radiationless transition to the ground state may have been thermally enhanced.

Triplet Excited States. Figures 1 and 4 show that polarization of the phosphorescence emission, particu-

(16) P. I. Petrovich and N. A. Borisevich, *Izv. Akad. Nauk SSSR, Ser. Fiz.*, 27, 703 (1963).

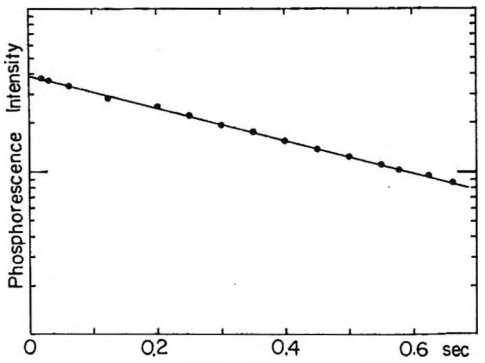

Figure 5. A typical exponential decay of phosphorescence of coumarin in ethanol. The average lifetime is 0.45 sec. The lifetime in dry isopentane is 0.47 sec.

larly in the 0–0 region, is negative with respect to two excitation wavelengths which are predominantly of $\pi \rightarrow \pi^*$ intensity. This implies that the major portion of the emission intensity is attributed to the out-of-plane component and that the lowest triplet state is $^3(\pi,\pi^*)_1$. As shown in Figure 5, this assignment is consistent with a relatively long lifetime of 0.45–0.47 sec in either ethanol or in isopentane and with the epr results for the coumarin triplet (π,π^*).[17] The negative polarization of the 0–0 phosphorescence can be ascribed to the spin–orbit (SO) coupling between n,π^* and π,π^* states; $\beta = \langle ^1n,\pi^*|H_{so}|^3\pi,\pi^*\rangle$ or $\langle ^1\pi,\pi^*|H_{so}|^3n,\pi^*\rangle$. As a crude estimate of the spin–orbit coupling matrix element between lowest n,π^* and π,π^* states, Table III[18]

Table III: Absolute Squares of the One-center Spin-Orbit Matrix Element Between n,π^* and π,π^* States in Coumarin, Calculated with the Procedure and with Atomic Spin-Orbit Coupling Constant of 47.7 cm^{-1} for Oxygen Adopted by Plotnikov[18]

Method for MO expansion coefficients	$\lvert\beta\rvert^2$, cm^{-2}
Simple Hückel MO	1009
P–P–P with Pariser–Parr two-center electron repulsion integrals	410
P–P–P with Mataga–Nichimoto two-center electron repulsion integrals	451
Extended Hückel MO	58
CNDO/II	603

lists absolute squares $|\beta|^2$ of the one-center contribution of the carbonyl oxygen to the spin–orbit coupling between n,π^* and π,π^* states. Except for the extended Hückel result, the one-center spin–orbit contribution appears to be substantial. However, it is not possible to estimate the intensity contribution, since location of the lowest (n,π^*) state in coumarin is at present unknown. Of course, other out-of-plane transition dipoles may also contribute either directly (first-order) or vibronically.

Figures 1 and 4 show some vibronic activities in the phosphorescence band. Although the polarized phosphorescence spectrum shown in Figure 1 is of low resolution, it is apparent that the 0–0 band at 21880 cm^{-1} (457 nm), and other peaks at 20280 cm^{-1} (493 nm) and 18760 cm^{-1} (533 nm) are more negatively polarized than weaker peaks at 21230 cm^{-1} (471 nm) and 19600 cm^{-1} (510 nm). The more negatively polarized vibronic peaks may be assigned either to carbonyl stretching or to C=C stretching in the pyrone moiety, the latter (1600–1650 cm^{-1}) being more likely than the former (1731 cm^{-1} in pyrone).[19,20] The less polarized vibronic peaks may be assigned to a CH out-of-plane bending. However, these assignments are only tentative until better resolution can be achieved in the polarization measurements.

Electronic Structure of the Excited States. After having assigned the fluorescent and phosphorescent states to $^1(\pi,\pi^*)_1$ and $^3(\pi,\pi^*)_1$, respectively, we will now attempt to describe the electronic structure of these excited states. Figure 6 illustrates changes in π-electron densities and mobile bond orders upon excitation to the lowest singlet and triplet (π,π^*) states. It is interesting to note that the carbonyl oxygen loses its π-electron density in the excited states, unlike many other aromatic carbonyls. It is also remarkable that the mobile bond order for C=C in the pyrone moiety experiences a 50% reduction in the excited triplet state. The triplet coumarin yields trans head-to-head dimer with a high efficiency.[4] The lengthening of the C=C bond appears to be closely associated with the appearance of C=C stretching in the phosphorescence and the process of photodimerization at this site. This relationship is further confirmed in Figure 7, which shows that positions 3 and 4 carry extremely high α spin densities. The CNDO/II in its unrestricted formulation (DODS) also yields similar spin density distribution, except for the significant σ contribution to the spin density at carbonyl oxygen. No significant dimerization has occurred during the measurements in rigid matrices, as judged by constancy of phosphorescence intensity with time.

A significant red shift (30 nm) of the fluorescent band and a small red shift (7 nm) of the phosphorescent band of coumarin is observed in going from ethanol to isopentane matrices. However, the absorption and excitation spectra remain essentially unchanged in both solvents. In order to understand the abnormal solvent dependence of the fluorescent and phosphorescent (π,π^*) states, interactions between solvent molecules and the solute in its ground and excited states must be

(17) D. R. Braber, M. W. Grimes, and A. Haug, *J. Chem. Phys.*, **50**, 1623 (1969).

(18) V. G. Plotnikov, *Opt. Spectrosk.*, **20**, 735 (1966).

(19) L. J. Bellamy, "Advances in Infrared Group Frequencies," Methuen & Co., London, 1968, pp 27–29, 164.

(20) Y. Kamano, *J. Jap. Chem.*, **24**, 421 (1970).

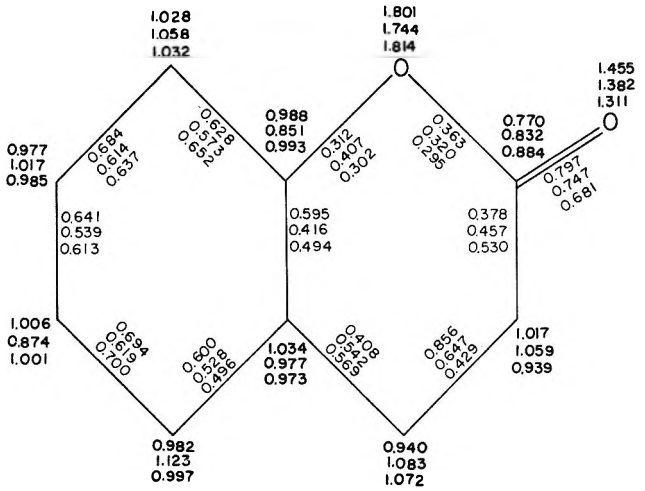

Figure 6. π-Electron densities and mobile bond orders in coumarin. The lowest triplet state charges and bond orders are from the restricted P–P–P calculations. Top, middle, and bottom numbers at each atom refer to the ground, singlet, and triplet (π,π^*) states, respectively.

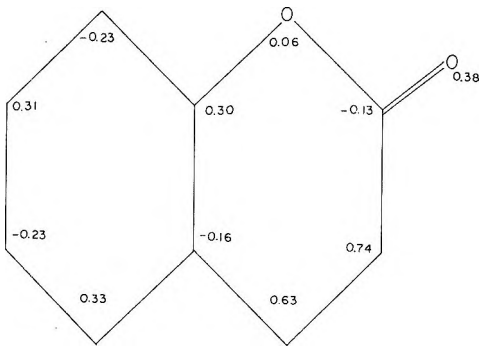

Figure 7. Spin densities in the triplet (π,π^*) coumarin without annihilation, as calculated by the unrestricted Hartree–Fock–Roothaan formulation within the P–P–P approximations. Note the high densities at the pyrone double bond position.

elucidated. At present, semiquantitative treatments of such intermolecular interactions involving dipole–dipole and dispersion forces are available in the literature. For example, effect of dipole–dipole interactions between solute and solvent molecules on the fluorescence frequency has been discussed by several authors.[21-25] Abe[24] has included the contribution of the isotropic polarizability in the ground and excited states to the fluorescence frequency, in addition to the dipole–dipole contribution. However, all of these treatments are based on the assumption that solute and solvent molecules do not experience strong dipole orientation strains in solution. In the case of rigid glass, this assumption is only partly valid. The direction of the solvent shift in room temperature solutions parallels with that of the rigid matrices, and the magnitude of the shift (fluorescence) is larger in the former than in the latter. Therefore, the observed red shift of the emission bands of coumarin in isopentane can be accounted for in terms of the change in polarizability[24] and in dipole moment[21,24] upon excitation. It is difficult to estimate polarizabilities and dipole moments of the excited coumarin molecules in a rigid matrix, since a series of glass-forming organic solvents at 77°K is not readily available. In this respect, results on the change in dipole moment calculated by MO methods (Table IV) may be useful to account for the solvent shift of coumarin at least in part.

Table IV: The Calculated Permanent Dipole Moments (in Debye Unit) of Coumarin in its Ground (A) and Excited States

State	Observed[a]	Calculation I[b]	II[c]	III[d]
A	4.61	4.07	5.18	4.62
$^1(\pi,\pi^*)_1$		4.37	2.59	3.02
$^3(\pi,\pi^*)_1$		2.60	2.50	1.55[e]

[a] In dioxane. V. S. Griffiths and J. B. Westmore, *J. Chem. Soc.*, 4941 (1963). [b] The P–P–P calculation with Mataga–Nishimoto formula for (rr|ss). See ref 11. [c] The P–P–P calculation with Pariser–Parr formula for (rr|ss). See ref 8. [d] The CNDO/II calculation. [e] Using unrestricted DODS scheme.

Table IV presents the calculated dipole moments. It is predicted that the $(\pi,\pi^*)_1$ states possess lower dipole moments than the ground-state coumarin. Therefore, the abnormal solvent shift can be explained on the basis of a decrease in dipole moment upon excitation and a certain amount of relaxation encountered during the lifetime of the excited states. Decrease in dipole moment for the $(\pi,\pi^*)_1$ states is a reflection of reduced charges on carbonyl oxygen (Figure 6), since the ground-state moment is directed along the carbonyl axis. This also weakens the hydrogen bonding with hydroxyl solvents.

As described earlier, the phosphorescence intensity substantially decreases in going from ethanol to isopentane matrix. At present, information concerning location of upper triplet states, particularly the $^3(n,\pi^*)$ state, is not available. Nevertheless, it is tempting to speculate that the dramatic reduction of the phosphorescence intensity in isopentane is a result of the blue shift of the $^3(n,\pi^*)$ state above the $^1(\pi,\pi^*)_1$ state. This situation reduces the spin–orbit contribution to the phosphorescence intensity. In other words, the unfavorable energy denominator in the first-order singlet–triplet transition probability decreases the intersystem cross-

(21) E. G. McRae, *J. Phys. Chem.*, **61**, 562 (1957).
(22) E. Lippert, W. Lüder, F. Moll, W. Nägele, H. Boos, H. Prigge, and I. Seibold-Blankenstein, *Angew. Chem.*, **73**, 695 (1961).
(23) T. Abe, *Bull. Chem. Soc. Jap.*, **38**, 1314 (1965).
(24) T. Abe, *ibid.*, **40**, 1571 (1967).
(25) W. Liptay, *Angew. Chem. Int. Ed. Engl.*, **8**, 177 (1969).

ing. The observation that the phosphorescence lifetime in ethanol and isopentane matrices is about the same is not inconsistent with this suggestion. The lack of fluorescence at 298°K in the concentration range examined can then be explained in terms of thermally enhanced intersystem crossing and internal conversion at the expense of emission.

Whether raising of the (n,π^*) energy is brought about by an increase in dipole moment upon excitation cannot be decided owing to the lack of pertinent data. It is generally realized that direction of the charge polarization in an (n,π^*) configuration is opposite to that of a (π,π^*) configuration. For example, the dipole moment of $^1(\pi,\pi^*)$ states of some organic molecules shows a larger increase[26] than $^1(n,\pi^*)$ states with respect to the ground states.[27,28] The $^1(n,\pi^*)$ states of some nitrogen heterocylics possess substantially lower dipole moments than their ground states.[27,28] Whether the opposite is true in the case of coumarin $^{1,3}(n,\pi^*)$ states remains to be investigated. Theoretical studies may be helpful in illuminating this point, since experimental studies of the upper excited states are not accessible in conventional luminescence spectroscopy.

Conclusions. The fluorescent and phosphorescent states of coumarin have been assigned to (π,π^*) on the basis of their polarization spectra, lifetimes, theoretical transition energies, and direction of transitions. Theoretical dipole moments of the singlet and triplet (π,π^*) states are predicted to be lower than those of the ground state. This is consistent with the observed red shift of the emission bands in nonpolar solvents. Both the spectroscopic results and theoretical calculations of the electronic structures of the excited states of coumarin indicate that the excitation is substantially localized in the pyrone moiety. This conclusion is useful in understanding photoreactivity of coumarin[4] and in its role of photomutagenic reaction with DNA bases.[29] However, a further study is needed for a complete description of the chemistry of the excited state of coumarin and its derivatives.

Acknowledgments. Technical assistance of Thomas Moore is greatly appreciated. We also acknowledge the staff of the Texas Tech University Computer Services for a gift of computing time and their assistance.

(26) G. Weber, *J. Chem. Phys.*, **43**, 521 (1965).

(27) H. Baba, L. Goodman, and P. C. Valenti, *J. Amer. Chem. Soc.*, **88**, 5410 (1966).

(28) C. Mugiya and H. Baba, *Bull. Chem. Soc. Jap.*, **40**, 2201 (1967).

(29) L. Musajo, *Ann. Ist. Super. Sanita*, **5**, 376 (1969), and references therein.

Experimental Investigations on the Light Scattering of Colloidal Spheres. VIII. Brief Survey of Problems in Angular Light-Scattering Measurements and Performance of a New Type of Reflection-Free Scattering Cell

by Wilfried Heller* and Jack Witeczek

Chemistry Department, Wayne State University, Detroit, Michigan 48202 *(Received October 27, 1969)*

The various problems arising in measurements of the angular variation of dissymmetric light scattering by means of conventional scattering cells are reviewed, including several problems to which only scant attention had been paid previously. Above all, a new type of scattering cell, provided with both a terminal Rayleigh horn and a "wide angle horn" is described which eliminates all complications due to reflections of primary and scattered beams. Results obtained with the new cell agree very well with the theoretical data calculated for the scattering system used, a monodisperse Dow latex. The results are also compared with those obtained with a conventional scattering cell after correcting the data, in the latter instance, by means of an improved version of the Kratohvil correction equation.

It was shown in three preceding publications in this series that the spectra of certain light-scattering quantities can be used successfully for determining size distribution curves in heterodisperse systems.[1] It was found that spectra of the "scattering ratio" ("σ spectra")[2] are particularly suitable for this purpose. The only angle of observation with respect to the incident beam considered so far was 90°. At this angle, a series of complications which arise at other angles in the case of dissymmetric radiation are avoided. In the case of strong heterodispersion, the spectra of the scattering ratio obtained at a single angle may not give a single valued answer.[3] The same problem arises on using turbidity spectra[1] or the angular variation of scattering or of the "polarization ratio" in monochromatic light,[4] alternate techniques available for determining size distribution curves. In the case of strongly heterodisperse systems, it is therefore desirable to combine two or all of these techniques. The resulting increase in the number of experimental data increases the conclusiveness of the results. This was shown for the combination of σ spectra and turbidity spectra.[1,3] The alternate and potentially more powerful combination of σ spectra and angular variation of scattering yielding the angular dispersion of σ spectra had thus far not been considered in this laboratory on account of the well-known complications which arise in measurements of the angular variation of light scattering in the case of dissymmetric radiation.

These complications were analyzed recently by Tomimatsu and Palmer[5] and by Kratohvil,[6] who also developed correction equations for the purpose of compensating for some of these complications. The present paper is concerned with an improvement in the technique of angular measurements of light scattering which makes the application of correction equations unnecessary and therefore enhances considerably the attractiveness of measurements of the angular dispersion of scattering in the case of dissymmetric radiation and the promise of measurements of the angular dispersion of σ spectra.

It appears useful to precede the discussion of the new technique by a brief critical review of other complications which one has to contend with in studies on the angular variation of light scattering including some on which information available and explanations given in the literature appear incomplete.

I. Survey of Complications in Results on the Angular Variation of Light Scattering in the Case of Dissymmetric Radiation Envelopes

The factors affecting the angular variation of light scattering can, for convenience, be subdivided into

* To whom correspondence should be addressed.

(1) W. Heller and M. Wallach, *J. Phys. Chem.*, **67**, 2577 (1963); **68**, 924 (1964); **68**, 931 (1964).

(2) The scattering ratio, σ, is the ratio of the total intensities, I, scattered at a given angle of observation from an incident linearly polarized beam vibrating once parallel ($\|$) and another time perpendicular ($\perp$) to the plane of observation, *viz.*, $\sigma = (I_\| / I_\perp)$.

(3) Results of B. Greene to be published.

(4) Various papers by M. Kerker and associates, see, *e.g.*, *J. Phys. Chem.*, **71**, 514 (1967), and by J. P. Kratohvil and associates, see, *e.g.*, *J. Polym. Sci.*, **B5**, 1139 (1967).

(5) Y. Tomimatsu and K. J. Palmer, *J. Phys. Chem.*, **67**, 1720 (1963).

(6) J. P. Kratohvil, *J. Coiloid Interface Sci.*, **21**, 498 (1966).

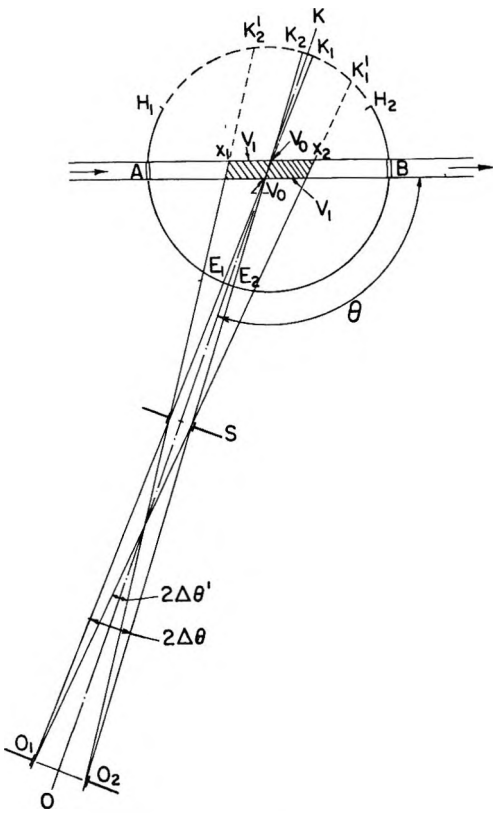

Figure 1. Schematic representation of complications arising in angular light scattering measurements (see text).

two types: those that are largely independent of the type of scattering cell used and those that depend significantly on it. Complications pertinent to the former shall be reviewed first.

1. Problem of the Optically Effective Scattering Volume. In Figure 1, it is assumed that a Brice-Phoenix instrument[7] and a cylindrical cell are used. The primary beam is assumed to be parallel[8] to exclude unnecessary complications in addition to those to be discussed here. It enters the cell at A and leaves it at B. It produces a light-scattering effect recorded at O between O_1 and O_2. The effect originates in the optically effective volume of the cell whose cross section is indicated. The narrow fully black central section of the volume, V_0, makes the main contribution to the radiant energy which passes through the slit S and is received at the aperture of the recording instrument, at O, while the hatched additional volume, V_1, makes a contribution which decreases from V_0 radially towards both x_1 and x_2. The optically effective volume consists,[9] therefore, of volume elements which make contributions of widely differing statistical weight, to the scattering effect observed at a given angle of observation with respect to the direction of the primary beam, θ. This fact defeats any attempt—and there have been such attempts—to define the optically effective volume for the purpose of "absolute" measurements of laterally scattered light intensities. Introduction of a double slit into the path of the scattered light and increase in the optical path between scattering cell and observer—two possible improvements to the design shown in Figure 1—can significantly reduce the problem of the optically effective volume but cannot eliminate it. The best solution therefore is the use of a calibration constant for lateral measurements of scattered light intensities. This calibration constant varies with θ since the optically effective volume varies in direct proportion to sin θ if the cell is perfectly cylindrical and free of flaws. Such a calibration constant is, however, not necessary for measurements of intensity ratios, *e.g.*, of the scattering ratio, σ, an important advantage of σ measurements.[10]

2. The Effect of Concentration upon the Angular Variation of Light Scattering. The concentration of the light-scattering system can profoundly affect the angular variation of individual light-scattering intensities and of intensity ratios such as the scattering ratio. If the concentration is not sufficiently small (how small it should be depends, at a given wavelength and for a given medium, very much on the refractive index and the size of the scatterers), both turbidity and multiple scattering, *i.e.*, rescattering, by a particle, of light scattered previously by another particle, begin to cause complications. Some of these complications have been discussed previously,[11] but only limited attention has been paid to the factors involved. Using Figure 1 as a guide and considering first the effect of concentration upon the *intensity* of scattered light, one has to contend with (1) an intensity loss (turbidity loss) of the primary beam, between A and x_1 due to scattering in the optically unused portion of the cell; (2) an intensity loss (turbidity loss) of the scattered beam, emerging from $V_0(V_1)$, due to the production of secondary scattered light (see below) before its arrival at E_1E_2; (3) a reduction of the intensity loss (1) by primary scattered light propagated, at small angles θ, from the irradiated volume, between A and x_1, into V_1; (4) an attenuation of the intensity loss (2) by primary (and secondary)

(7) For other types of instruments, the situation would not be essentially different except for the possibility that the double cone drawn, which defines the primary irradiated volume, V_0, may have to be replaced by a single cone whose apex is directed either towards the observer or away from him. The double cone, which assumes circular apertures and circular slits, represents that part of the scattered beam which makes the principal contribution to the light intensity recorded by the measuring instrument. The Brice-Phoenix instrument is considered here since the measurements connected with the use of the new cell described below were carried out with a suitably modified version of this instrument.

(8) To maintain its parallelity within the cell, it is assumed furthermore that the cell contains at A and B inserts of plane parallel glass plates, thus excluding a lens effect of the cell.

(9) Various problems regarding the optically effective volume were discussed by M. Kerker, J. P. Kratohvil, and E. Matijevic, *J. Polym. Sci.*, **A2**, 303 (1964).

(10) W. Heller and R. Tabibian, *J. Phys. Chem.*, **66**, 2059 (1962).

(11) (a) R. M. Tabibian and W. Heller, *J. Colloid Interface Sci.*, **12**, 25 (1957); **13**, 6 (1958); (b) various papers by M. Kerker, *et al.*; see M. Kerker, "The Scattering of Light," Academic Press, New York, N. Y., 1969.

scattering from the cell volume between $V_0(V_1)$ and E_1E_2 into O_1O_2. The latter two complications are more prominent the larger the scatterers are relative to the wavelength due to the increase, in this direction, in the importance of small angle scattering. These four factors are operative, of course, also *within* the volume $V_0(V_1)$. Consequently, the contribution, of the individual volume elements within $V_0(V_1)$, to the scattered intensity received at O decreases from x_1 toward x_2 and from the back (facing K) to the front (facing O) of $V_0(V_1)$. (5) The last factor which complicates matters is the secondary scattered light for which the primary scattered light is the source.[12] Although the intensity of secondary scattered light is, per unit volume of scattering system, very weak relative to that of primary scattered light, this is in part offset by the much larger volume from which secondary scattered light (which is produced throughout the entire optical cell) reaches O. The lateral cross section of the truncated cone involved is defined in Figure 1 by E_1, K_2', K_1', E_2. Major complications result from the presence of this secondary scattered light in spite of its low intensity, due to the fact that it, obviously, may pertain to any angle θ from 0 to 180°. The most important ones are the following two.

(a) Since it contains contributions from all angles θ, it tends to smoothen out the radiation envelope if angular maxima and minima are present. The reason for this is, as previously shown (Figures 5 and 6 in ref 11a), that the intensity of scattered light, per unit concentration, *increases* with concentration (prior to reaching a maximum due to eventually predominating turbidity losses) if the angle of observation is at or very near to an angular scattering minimum. For all other angles, increasing concentration produces the inverse change. The resulting decrease, with increasing concentration, in the amplitude of angular oscillations of the specific scattered intensities, reflects itself also in a corresponding decrease in the amplitude of angular oscillation of *intensity ratios*. Figure 2 illustrates this for the scattering ratio. The scattering system used is a "monodisperse" polystyrene latex with a modal diameter of 894 mμ. The fully drawn curve I is the theoretical scattering ratio expected on taking into account a slight degree of heterodispersion determined by electron-microscopic analysis, by using the heterodispersity parameters $q = 0.7$ and $p = 6.2$.[13] Those of the experimental data which pertain to a polymer concentration of $1.95 \times 10^{-4}\%$ and a solid angle of 54×10^{-4} steradian give curve II, using a cylindrical cell with plane parallel inserts at the entrance and exit of the primary beam. On the other hand, the data indicated by black circles are the results of extrapolations to zero concentration at the same solid angle. It is apparent from this figure that even at the relatively modest polymer concentration used for this comparison, the amplitude of oscillations is reduced.[14] This concentration effect upon σ, to which the factor discussed under (b) also contributes, invites the erroneous conclusion that the scattering system is very heterodisperse while, in reality, it is not.

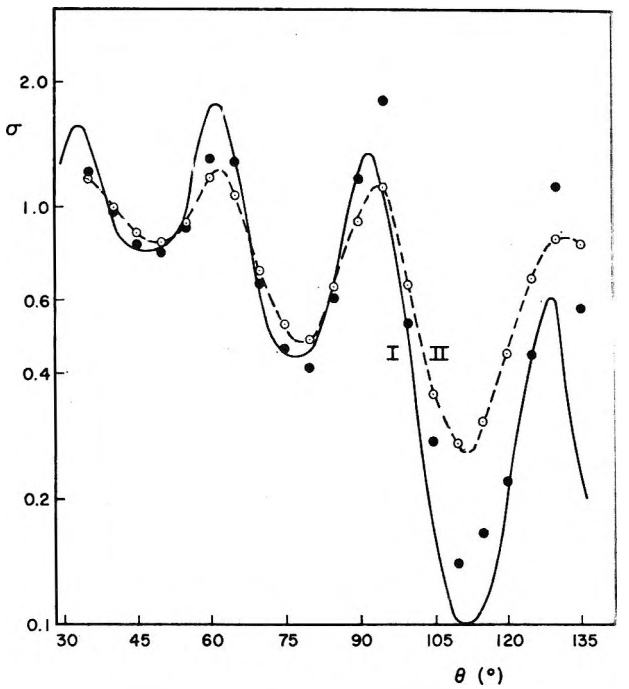

Figure 2. Effect of concentration on angular variation of scattering ratio, σ. Polystyrene latex; modal particle diameter: 894 mμ; distribution parameters: $q = 0.7$; $p = 6.2$; vacuum wavelength, λ_0 5461 Å; relative refractive index, $m = 1.20$; cylindrical cell. Curve I, theoretical variation of σ with θ; curve II (open circles), experimental variation at polymer concentration $c = 1.95 \times 10^{-4}$ g/100 ml; full circles, experimental data extrapolated to zero concentration and corrected for reflections.

(b) The secondary scattered light received at a given angle θ is not representative of it. Therefore, the above complications in the concentration dependence of the intensity of scattered light are accompanied by complications in the concentration dependence of its quality. This phenomenon is well known for scattering at θ =

(12) The complications due to tertiary (multiply) scattered light can, in general, be neglected in solutions and in dilute dispersed systems.

(13) The quantity q is a measure of the degree of heterodispersion and the quantity p is representative of the size of the smallest particles which are present in the system in significant numbers. For further details, see ref 1.

(14) It is useful at this point, for the sake of clarity, to recall a few definitions. If the incident beam is *unpolarized* light and an analyzer is used to determine the intensity of that component of the scattered beam which vibrates in the plane of observation, $I_\parallel$, and perpendicular to it, respectively, $I_\perp$, then the intensity ratio of the two components, $(I_\parallel/I_\perp)_u = \rho$, is defined as depolarization if $\theta = 90°$. If $\theta \neq 90°$, it is generally referred to as "polarization ratio." If, on the other hand, the total intensity of a scattered beam is determined on interposing between incident beam and scattering cell a polarizer with the plane of polarization parallel and perpendicular, respectively, to the plane of observation, then the ratio of the two total scattered intensities $(I_\parallel/I_\perp)_p = \sigma$ represents the scattering ratio. If the scattering objects are isotropic spheres, $\rho = \sigma$; if they are nonspherical, $\rho \neq \sigma$.

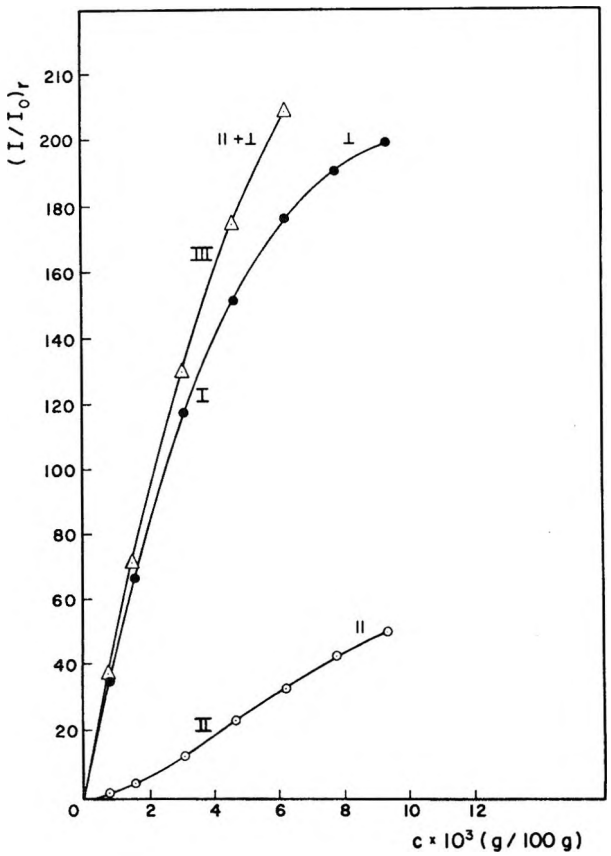

Figure 3. Variation, with concentration, of the relative intensity of light scattered at $\theta = 90°$ (data by R. Tabibian). Monodisperse polystyrene latex; average particle diameter: 238 mμ; λ_0 5461 Å; cell used: see ref 11a. Curve I, electric vector of incident linearly polarized beam is perpendicular (⊥) to plane of observation; curve II, it is parallel (||) to plane of observation; curve III, incident beam is unpolarized.

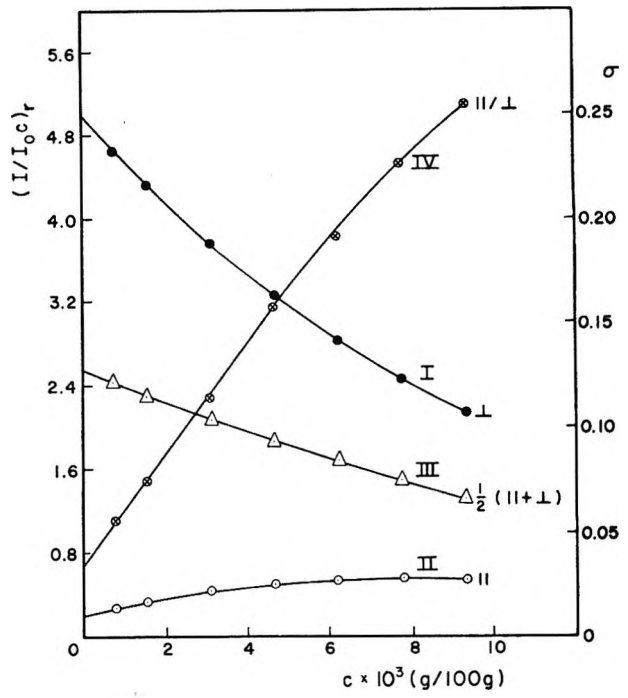

Figure 4. Variation, with concentration, of the specific intensity of light scattered and of σ at $\theta = 90°$. System and experimental conditions are the same as in Figure 3; curve IV, σ.

90°. Known as "depolarization[14] by multiple scattering," it is observed at finite concentration of solutions or dispersed systems if the theory predicts none (isotropic spheres), or it is larger than the predicted value (anisotropic or anisometric scatterers). In either case, depolarization always increases with increasing concentration. At angles θ other than 90°, the situation is similar inasmuch as the state of polarization expected from theory in a given case is altered by the finite concentration and changes with it. The fundamental phenomenon involved is quite simple; most of the primary scattered light is propagated in directions which form a finite angle with the plane of observation. Some of it travels in that plane orthogonal to the plane of observation which also contains the primary beam. Concentrating on this orthogonal plane, for the sake of argument only, and assuming, for the same reason, that the electric vector of an incident linearly polarized beam vibrates in the plane of observation, it is immediately evident that the particular fraction of secondary scattered light which originates in this plane and is received at O (Figure 1), represents, in the case of spheres, a mixture of apparently unpolarized and elliptically polarized light. In light received from other planes containing the primary beam, elliptically polarized secondary scattering will be particularly pronounced. The ellipticity, however, will not be recognized as such on using a simple analyzer. Its contribution will then go in part to the account of the linearly polarized fraction and in part to that of the apparent unpolarized fraction of scattered light. An example of the consequences is given in Figure 3 for $\theta = 90°$ and the simplest possible case, that of a radiation diagram which does not exhibit as yet any angular minima and maxima for $I_\perp$.[15] Curve I represents the (relative) values of the total intensity of light scattered at $\theta = 90°$ from an incident linearly polarized beam of unit intensity and whose electric vector is ⊥ to the plane of observation. Curve II applies to the relative total intensity scattered from an incident polarized beam whose electric vector is || to the plane of observation. (Curves I and II also represent the relative intensities of the scattered components vibrating ⊥ and ||, respectively, to the plane of observation if the incident beam is unpolarized.) Curve III, finally, represents twice the intensity scattered from an incident unpolarized beam of unit intensity. Curve I shows a "normal" variation of $I_\perp$ with c. Here, the rate at which $I_\perp$ increases with c decreases steadily due to increasing turbidity

(15) These data and also those of Figure 4 are from unpublished work carried out in this laboratory by R. Tabibian using another light-scattering instrument.[10]

losses. Curve II, on the other hand, is dominated, at low c, by a scattering increment which exceeds the effect of turbidity losses. This increment results from secondary scattering and it leads to an increase, with c, in the absolute intensity scattered per unit solid angle from the unit volume by an incident beam of unit intensity (Figure 4). As regards an explanation of this increase, it will be noted that, in absence of multiple scattering ($c \rightarrow 0$), the total specific intensity scattered from the primary beam vibrating perpendicular ($\perp$) to the plane of observation is about 20 times stronger than that scattered from the beam vibrating parallel ($\parallel$) to it. Therefore, it appears that the secondary scattered light contributes most to the total intensity of that component which is scattered the least in the O direction (Figure 1). These complications are not apparent from the concentration dependence of the scattering ratio σ (curve IV in Figure 4)[16] which exhibits the simple, easily extrapolated curve typical for radiation envelopes which are free from angular maxima and minima.

The situation becomes considerably more complicated if the particle size is so large that angular maxima and minima appear. In that case, the values of $(I_{\parallel})$ and $(I_{\perp})$ at angles near to the angle θ considered become also very important both for the intensities and intensity ratios (σ or ρ) at θ. This is illustrated by Figure 5. It represents the variation, with c, of σ at 4 particularly interesting angles θ, for the same polystyrene latex considered in Figure 2. Comparison with the theoretical curve in Figure 2 shows that σ decreases with increasing c at or near a σ maximum and, inversely, increases with c at or near a σ minimum.[17] Consequently, at θ, the total amount of light scattered, from an incident polarized beam, decreases with increasing concentration relative to the total amount scattered from an orthogonally polarized beam if a slight change in θ leads to a decrease in the total intensity scattered from the former relative to that of the latter. Considering the polarization ratio, *i.e.*, incident natural light, the results in Figure 5 mean alternately the following. The light scattered at θ acquires, with increasing c, a relative excess of that polarized component which, at constant c, is stronger at nearby angles θ.

The regularities derived from Figure 5 are confirmed by Figure 6 which applies to the Hg line λ_0 4358 Å. Due to the angular shift of maxima and minima with λ_0, one now observes a maximum near 45 and 90° and a minimum at 60°. Of particular interest is the nearly straight line of zero slope obtained at 75°. At this angle, one is, at 4358 Å, midway between a maximum and minimum. Thus, the component which decreases in relative intensity between $\theta + \Delta\theta$ increases in relative intensity between θ and $-\Delta\theta$, so that the concentration effect upon σ cancels. Table I summarizes the relationships discussed.

The preceding discussion leads to the following conclusion. To obtain significant results on the angular

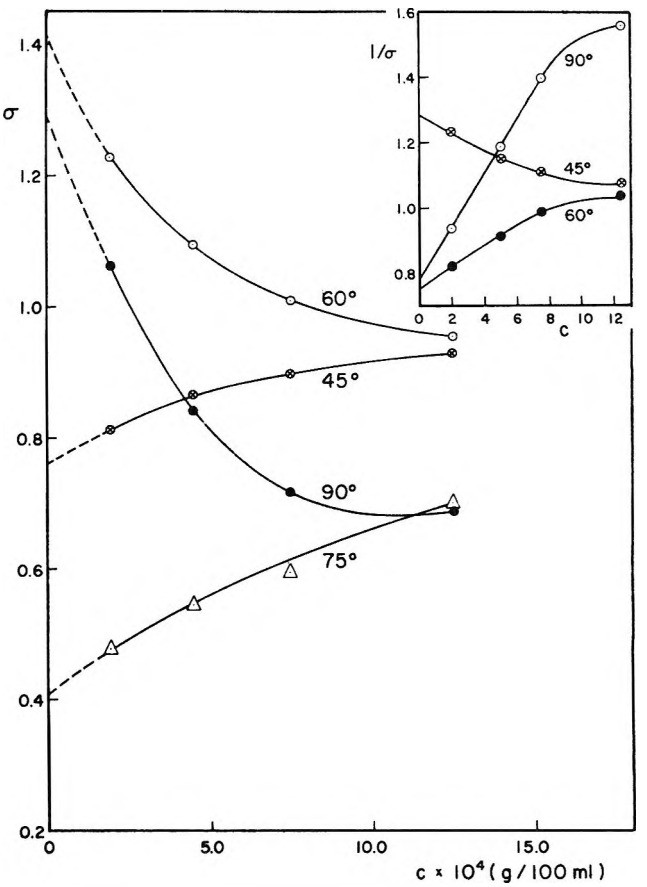

Figure 5. Variation, with concentration, of σ at or near angular minima (45°, 75°) or maxima (60°, 90°); λ_0 5461 Å. Polystyrene latex, mean diameter: 894 mμ; distribution parameters: $p = 6.2$, $q = 0.7$; solid angle, $\omega_0 = 5.4 \times 10^{-3}$ steradians; double horn cell.

variation of the intensity of light scattering or of σ (or ρ), the concentration of the systems should be made as low as is compatible with the collection of reasonably precise results, or, preferably, the data should be extrapolated to zero concentration. Such an extrapolation should lead to precise data whenever the scattering diagram does not exhibit steep maxima and minima (Figures 3 and 4). The latter applies when-

(16) Since $\sigma = \rho$ in the case of spheres (see footnote 14), curve IV alternately represents the variation, with concentration, of the polarization ratio at $\theta = 90°$, *i.e.*, of the depolarization. As regards the positive slope of curve I in Figure 4, it means, in this alternative interpretation, that the light scattered, at $\theta = 90°$, from an unpolarized incident beam contains, due to multiple scattering, an excess in intensity for that component which, in absence of secondary scattering, is the weakest (which here is that vibrating in the plane of observation).

(17) In evaluating the significance of these regularities, it must be borne in mind that the concentration effect considered in Figures 5 and 6 is that characteristic for relatively dilute systems. At higher concentrations, where tertiary (multiple) scattering should become significant, one would expect, as pointed out previously,[10] that σ eventually approaches the value 1.0. Therefore, the descent of σ to values <1.0 should be followed eventually by a minimum with subsequent asymptotic approach of 1.0. This was found in one instance at a concentration in excess of those used here (Figure 3, ref 10). Still, even in the present investigation, limited to lower concentrations, a shallow minimum seems to be reached in one instance (90° curve in Figure 6).

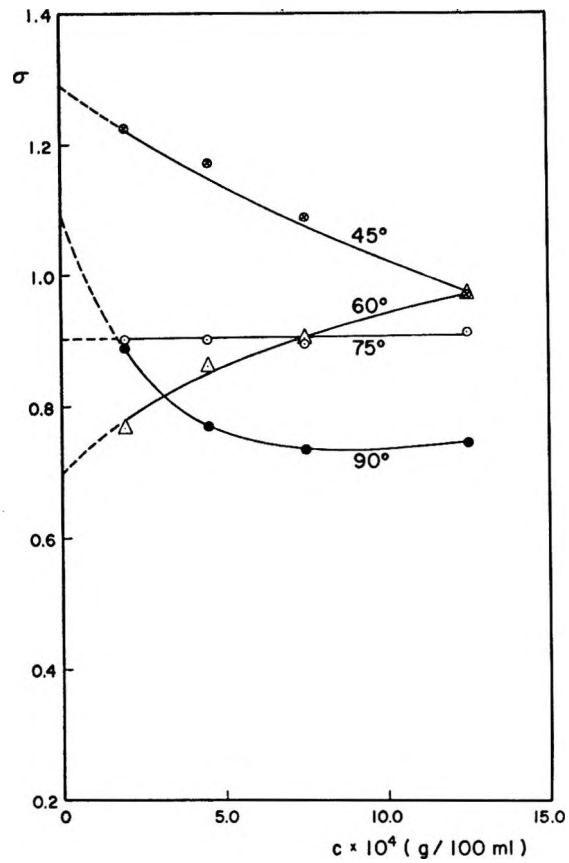

Figure 6. Variation, with concentration, of σ at or near angular minimum (60°) or maxima (45°, 90°) or at midpoint (75°); λ_0 4358 Å. System and experimental details are the same as in Figure 5 (except for λ_0).

Table I

	45°	60°	75°	90°
		λ_0 5461 Å		
$d\sigma/dc$	−	+	−	+
$\sigma(\theta)$	Min	Max	Min	Max
		λ_0 4358 Å		
$d\sigma/dc$	+	−	~0	+
$\sigma(\theta)$	Near max	Min	Near mid-point	Near max

ever the particle size in monodisperse systems is sufficiently small (the diameter of the spheres should not exceed ~300 mμ on using visible light if the relative refractive index, m, is 1.20). It applies, in addition, at any average particle size, whenever the systems are sufficiently heterodisperse. If there are steep maxima and minima, extrapolations to $c \rightarrow 0$ encounter at certain angles θ difficulties as is apparent from Figures 5 and 6. There are three possible methods to reduce these difficulties of extrapolation. (1) One may use $1/\sigma$ as the abscissa instead of σ. This reduces the rate of change of the slope, here of $1/\sigma$ (c), as c decreases (see insert to Figure 5) while in the σ *vs.* c plot the rate of change increases with decreasing c. If the latter type of plot does not give a secure intercept either, the average of the two extrapolated values should be satisfactory. (2) One may interpolate the σ value from a curve giving the extrapolations to $c \rightarrow 0$ as a function of the wavelength using both larger and shorter wavelengths than that of interest. The reason for this is apparent from a comparison of Figures 5 and 6. (3) One may appreciably reduce the concentration dependence of the scattered intensities and, therefore, the attendant complications by operating with as small a solid angle as possible. This is evident from the discussion of the curves in Figures 5 and 6 in ref 10 and will be treated more fully in the next section.

3. Problems Resulting from the Finite Solid Angle at Which Measurements Are Carried Out. Theoretical data on light scattering pertain to a specific angle θ. Experimental data, on the other hand, pertain to an angular range $\theta \pm \Delta\theta$, a fact which is apparent from Figure 1. Consequently, even in the limiting case of a very small volume, $(V_0 + V_1)$, or of a very large photometric distance, V_0–O, the scattered light received at O would be representative of the radiation scattered within a finite solid angle, ω_0 of which Figure 1 shows the planar projection, $2\Delta\theta$. If these limiting conditions do not apply, then the solid angle itself is ill defined since it varies from volume element to volume element. The extreme solid angle ω_0' would then be defined by the planar equivalent $2\Delta\theta' > 2\Delta\theta$ (see Figure 1). This problem is best taken care of by carrying out measurements at various "average" solid angles and by extrapolating the results to a suitably small standard solid angle. If the measured quantity is the intensity of light scattered per unit concentration of the scattering system, it is found to vary, as one would expect, in direct proportion with the solid angle as long as the latter is sufficiently small and no scattering maxima or minima occur at or near the angle θ considered. In that case, therefore, "the scattered intensity, *per unit solid angle*, will be essentially independent of the solid angle,"[18] a result recently again confirmed by Kratohvil and Smart.[19]

Intensity measurements can be seriously falsified on operating with too large a solid angle whenever scattering maxima or minima are close to the angle θ considered, particularly if they occur within $\omega_0(\omega_0')$. The result will be a flattening out of angular scattering maxima and minima. This, in turn, will lead to the

(18) Quotation from: R. M. Tabibian and W. Heller, *J. Colloid Sci.*, 13, 6 (1958). See Figure 10 of this reference.

(19) J. P. Kratohvil and C. Smart, *J. Colloid Interface Sci.*, 20, 875 (1965). These authors unfortunately contrast their small variation, with ω_0, of the specific scattered intensity, *per unit solid angle*, with the obviously large variation, with ω_0, of the specific intensity itself, as shown in Figure 8 of ref 11. They evidently should have compared their results instead with those in Figures 9 or 10 of ref 11.

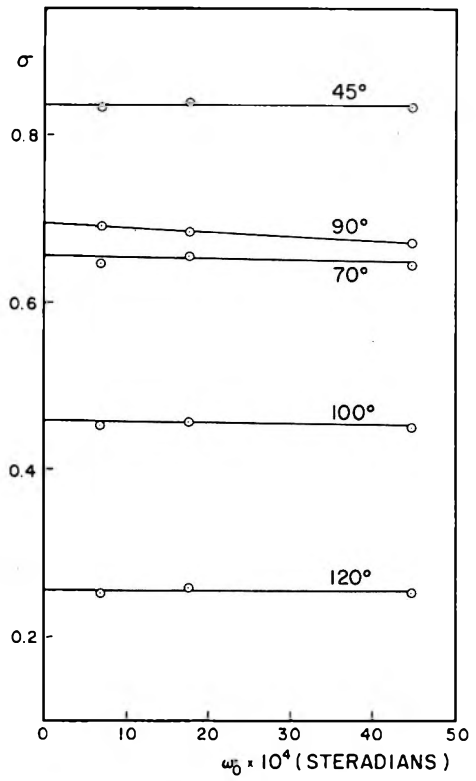

Figure 7. Variation of σ with solid angle at various angles θ. System and experimental details are the same as in Figure 5; polymer concentration: 5.45×10^{-4} g/100 ml.

erroneous impression that the respective system is more heterodisperse than it is in reality.[20] An increase in solid angle has therefore, qualitatively, the same effect as an increase in concentration.

There is clearly no general answer possible to the question as to how small a solid angle has to be for reliable intensity measurements since this depends both on the system and its concentration. In absence of steep angular maxima and minima, a solid angle not in excess of 1×10^{-3} steradian should be safe in view of results reported earlier.[11a] In all other cases, it is advisable to use smaller solid angles even when exploratory results seem to make this unnecessary. The reason is that the effect of changes in the solid angle is apt to be masked by multiple scattering if the concentration is not sufficiently small (see also pertinent remarks at the end of this section).

The situation is simpler if one determines, instead of the specific scattered intensity, rather intensity ratios, such as the scattering ratio or polarization ratio. Here, the results which are obtained at sufficiently low concentration, or are extrapolated to zero concentration (and, obviously, are not referred to unit solid angle), are numerically independent of the size of the solid angle as long as one operates at reasonably small solid angles and at angles θ at which no steep maxima or minima occur. Figure 7 shows on one typical set of examples that even at $\omega_0 \simeq 5 \times 10^{-3}$ steradian, no variation of σ with ω_0 has become evident as yet at the concentration used (1.95×10^{-4} g/100 ml) except at $\theta = 90°$ where a σ maximum is located (see Figure 2). In agreement with expectation, σ increases in the latter case with decreasing ω_0. The theoretically expected opposite trend at $\theta = 45°$ does not manifest itself, most likely because the minimum at $\theta = 45°$ has become washed out already at the above concentration. On evaluating the significance of the results in Figure 7, it must, therefore, be borne in mind that the concentration, though small, was already large enough to attenuate the variation of σ with ω_0 significantly. This follows immediately on comparing curve II in Figure 2 (which is pertinent to the results in Figure 7) with curve I which would apply at infinite dilution.

In conclusion, it is clear that optimum σ results can be expected on extrapolating, whenever this seems advisable, experimental data to both zero concentration and zero solid angle.[10]

4. Complications Due to Reflections of Incident and Scattered Beams. The problems discussed thus far can be resolved readily, for any type of conventional scattering cell, by the use of the proper experimental procedure. This is not so for the problems which arise from reflections of incident and scattered beams. Among these, the following two are important.

(a) The incident beam produces scattering in the volume $V_0(V_1)$ (Figure 1) on entering it and additional scattering after being reflected into it from exit window B. The latter increment, though observed at the angle $\theta \pm \Delta\theta$, will represent an effect pertinent to the complimentary angle, $[180° - (\theta \pm \Delta\theta)]$.[21] This applies to any kind of cell in which the beam enters and leaves it through a window perpendicular to the direction of the beam.

(b) If the cell is cylindrical, as in Figure 1, then the scattered beam received at O contains still another increment, characteristic for the angle $(180° - \theta)$, namely the entire portion of the scattered beam reflected at the surface of the cell between K_1 and K_2, and a fraction of the portion of the beam reflected between K_1 and K_1' and between K_2 and K_2', respectively.[22]

How important these "parasite" effects are depends on the refractive indices involved (those of the cell and of the media on either side) and on the degree of dissymmetry of the radiation envelope. Assuming the practically important case that the cell made of Pyrex

(20) The angular range $2\Delta\theta$, pertinent to a given θ, depends, of course, also on the degree of parallelity of the incident beam. If the incident beam is not strictly parallel as is assumed here, then the value of $2\Delta\theta$ and, therefore, of ω_0 is increased still further.

(21) An additional increment of the same type, after a second reflection at B, following reflection at A, is quantitatively negligible.

(22) A third increment (c) results from scattering produced by the fraction of the primary beam which, at B, is reflected back into the cell. The respective scattered beam, which is characteristic for the angle θ, reaches O_1O_2 after reflection at K_1K_2. Since this scattering increment is numerically 20 times smaller than either of the two other increments, it may, in most cases, be neglected.

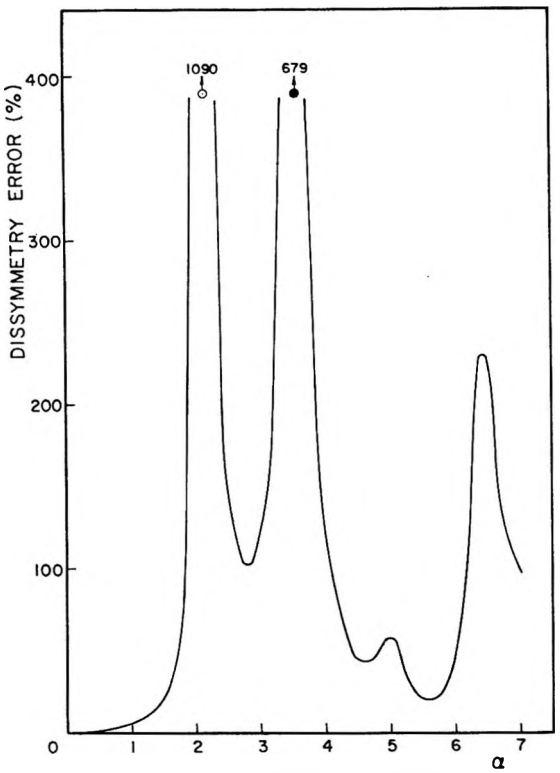

Figure 8. Variation with the relative particle size, α, of the per cent error in dissymmetry measurements if reflection phenomena in a cylindrical cell are disregarded. $\alpha = (2r\pi/\lambda)$, where r is the radius of scattering spherical particles and λ is the wavelength in the medium; the angles of observation, θ, considered are 45 and 135°; λ_0; 5461 Å.

glass is surrounded by air and contains an aqueous system, one obtains for the middle of the visible spectrum and by using the Fresnel equations a reflection coefficient of approximately 4% at room temperature. Consequently, in case a and, in a first approximation, also in case b, the scattering increment at $(180° - \theta)$ is, in the middle of the visible spectrum and at room temperature, 4% of the intensity scattered at θ. How serious the numerical errors due to these reflections can be may be illustrated by Figure 8. It shows the total error expected on failing to correct dissymmetry data (obtained with a cylindrical cell from measurements at $\theta = 45°$ and $\theta = 135°$) for reflection effects. The calculations are based on published theoretical dissymmetry data.[23] (The numerical values given in Figure 7 apply, of course, to the idealized case of zero solid angle.)

The two scattering increments a and b will falsify the experimentally determined radiation diagram also *qualitatively* if it contains maxima and minima. This applies particularly to the θ range from 90 to 180°, where "ghost maxima" may be observed.

The importance of these complications depends to a certain extent on the scattering cell used, and it is, therefore, useful to consider briefly the situation also for square and semioctagonal cells which are favorite alternatives to the cylindrical cell. If in either of these alternate types of cell the measurements are carried out over the entire angular range, then one has to contend with the problem that the mean scattering angle θ and, particularly $\Delta\theta$ and $\Delta\theta'$, pertinent to scattering increment b are ill-defined. This disadvantage is mitigated in part by the fact that the quantitative contribution of the scattering increments is smaller than in the case of the cylindrical cell. On the other hand, a new complication arising with both types of cells compared to the cylindrical cell is that now the refraction corrections for the scattered beam emerging from the cell also vary with θ. Moreover, the solid angle pertinent to a given measurement is now only an apparent quantity and has to be corrected by taking into account the refraction of the beam emerging from the cell, excepting only observations at 90° and at 45, 90, and 135° in the case of the square and the semioctagonal cell, respectively.

II. Elimination of the Complications Due to Reflections by the Use of Correction Equations

Tomimatsu and Palmer[5] and Kratohvil,[6] who discussed these problems extensively, tried to exclude scattering increments a and b by calculation introducing to that effect correction equations. These equations require that the effect at $(180° - \theta)$ is measured in addition to that at θ and that the refractive indices of the cell material and of the scattering system are known. In addition, the dispersion of both must be known if angular scattering is to be studied at several wavelengths. We shall discuss here only the more recent expression, that of Kratohvil.[6] It assumes an incident parallel beam. It can, however, be quantitatively correct only in the limiting case that the cell dimensions (the radius, r, in the case of a cylindrical cell) are negligibly small compared to the photometric distance, r_0, in the apparatus used. The reason for this is that the author overlooked the fact that the solid angle operative for increment a differs from that operative for increment b. On taking this difference into account, one obtains a revised Kratohvil equation which differs from the original one in that the quantity A is replaced by[24]

$$\left(1 + \frac{r_0^2}{(r_0 + 2r)^2}\right)A$$

On using the Brice-Phoenix instrument and a cylindrical cell of 17-mm radius (the cell used in the present work), the resulting overall correction is 22% smaller than on using the original Kratohvil equation. This "over correction" resulting from the use of the original Kratohvil equation is, of course, significant only if the scattering increments exceed 25% of the effect to be measured (since the precision in this type of measurement is defined by an uncertainty of no less than 5%).

(23) W. Heller and M. Nakagaki, *J. Chem. Phys.*, 31, 1188 (1959).
(24) A further simple correction is to be added if the incident beam is not parallel.

Unless light-scattering data are obtained on highly dilute systems, it is necessary, as discussed above, to extrapolate results to $c \rightarrow 0$. One has therefore two alternatives for the introduction of reflection corrections: (1) the individual specific scattered intensities, obtained at various concentrations, are corrected for reflections and the results are extrapolated to $c \rightarrow 0$; (2) the individual uncorrected data are extrapolated to $c \rightarrow 0$ and the result obtained is corrected for reflections. Similarly, intensity ratios, such as σ or ρ, may be derived from the individual specific intensities obtained by either of the two alternatives. The σ data given in this paper for $c \rightarrow 0$ are based upon procedure (1). Whichever procedure is chosen, it must be kept in mind that at, or very near to, steep maxima (or minima) the uncertainty of extrapolation, to $c \rightarrow 0$, of intensity data and of the derived σ (or ρ) data may be increased by application of the reflection corrections. Consequently, a corrected and extrapolated σ (or ρ) value may actually appear to deviate more from the theoretical value than that not corrected for reflections. Two such instances follow from a comparison of the cylindrical cell data in Figures 11 and 12.

It follows from the preceding discussion that the application of reflection corrections is indicated, in spite of the inconveniences referred to above, whenever one has to operate with scattering cells in which reflections are not eliminated and whenever scattering does not exhibit steep angular maxima and minima. It furthermore follows that the elimination of scattering increments a and b would be a much better solution of the problem. This requires the use of scattering cells of special construction.

III. Elimination of Complications Due to Reflections by the Use of a New Type of Cell

The idea of excluding reflections of both primary and scattered light is not new and several specially constructed cells have been proposed for this purpose. By far the best solution is that provided by the well-known Rayleigh horn. In it, all stray light is trapped completely (for a schematic representation of the light path, see Figure 1 in ref 11a). It can be used, however, only at a single angle θ. Generally 0 or 90° is selected. If angular measurements are limited to $\theta = 90°$, one may, as done by many authors, resolve the problem completely by using two Rayleigh horns, one at $\theta = 0°$ and the other at $\theta = 90°$. In none of the other more recent principles of cell construction used is a 100% elimination of stray light possible. The best solution among the latter is the double cell, introduced by Zimm[25] and modified by several later authors. A small light scattering cell is immersed in a large Erlenmeyer-type vessel filled with a liquid which has the same refractive index as the solution in the small cell. This cell has the advantage over the Rayleigh horn in that it is effective at any angle θ. Since the reflecting wall of the outer vessel forms an angle $\neq 90°$ with the incident beam, the latter is not reflected back directly in the scattering cell. It is, however, not eliminated completely, in contradistinction to the situation in a Rayleigh horn. Therefore, there is a risk that stray light resulting from imperfect reflections or from reflections at imperfect portions of the Erlenmeyer may reach the scattering cell again. If this is not avoided by proper measures, a serious error may result since the total intensity of scattered light is 10^{-5} to 10^{-10} that of the incident beam. Therefore, a very large number of reflections of the latter would be needed to reduce its intensity to the same level. For the present work, a cell was constructed which, while being as effective as a cell provided with a Rayleigh horn, avoids the limitation in its use to a single angle θ.

The scattering increment a is eliminated completely by attaching at the end of the scattering cell (at the exit B in Figure 1) a conventional Rayleigh horn. Scattering increment b, which cannot be eliminated by the use of such a "terminal" Rayleigh horn, is excluded by attaching at the rear of the cell a second horn similar to a Rayleigh horn, but differing from it by its having a very wide and curving aperture. This type of horn shall be referred to as a "wide angle horn." Its ideal aperture would comprise all values of θ from 0 to 180°. An aperture covering the angles $\theta = 30$–150° retaining the terminal Rayleigh horn, was found to be more practical and was realized in the scattering cell shown in Figures 9 and 10. The angular range encompassed by it is also shown in Figure 1 by the dotted lines between H_1 and H_2. It will be noted from Figures 9 and 10 that the new wide angle horn slopes downward while the conventional Rayleigh horn slopes upward. The advantage of the downward slope is that the cell

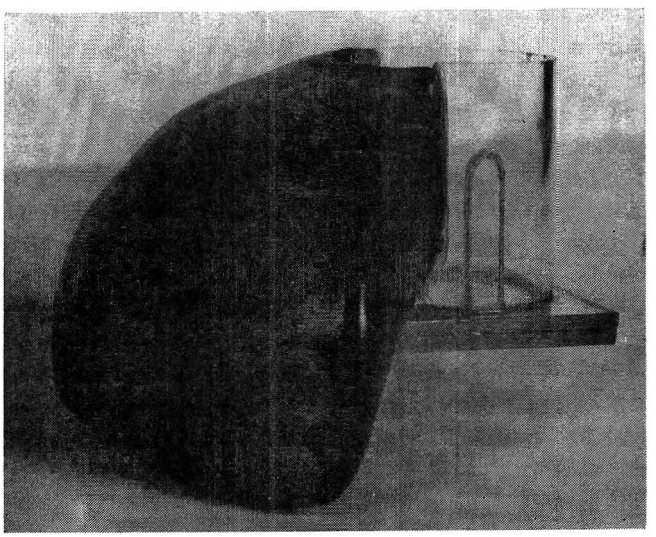

Figure 9. New double horn cell; side view.

(25) B. H. Zimm, *J. Chem. Phys.*, 16, 1099 (1948).

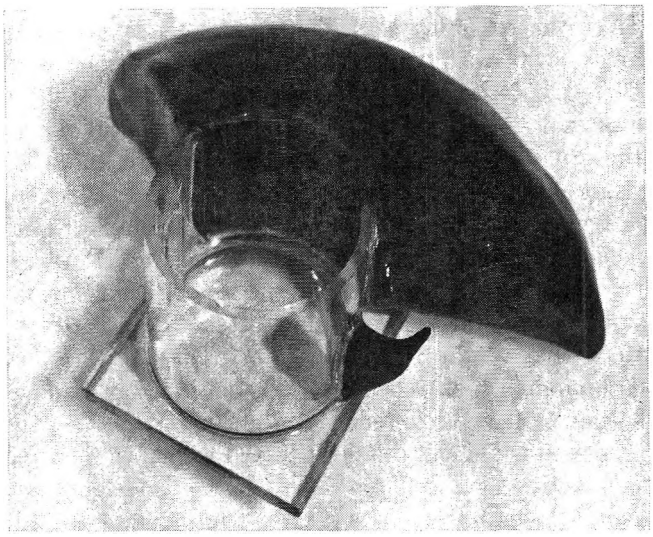

Figure 10. New double horn cell; top view.

can be filled easily, and above all, that the formation of a liquid–air surface within the horn is avoided. This is important since a liquid–air surface produces reflections which would partially defeat the purpose of a horn. (In a simple Rayleigh horn, the precaution of a downward curvature is not imperative because it is easier to fill, and therefore the risk of one's leaving an air bubble in the top of the horn is relatively small.)

The wide angle horn was produced from dull-black epoxy resin reinforced with Fiberglas.[26] The downward curvature to be given to such a wide horn is, of course, critical if any light entering the horn within the angular range defined is to be completely trapped in the narrow end of it. In view of the somewhat irregular appearance of the outside of the horn, it is therefore important to mention that the inside of the horn has the smooth and rigid geometrical contours of the wooden mold used in its production. It is clear from Figures 9 and 10 that the cell, except for the wide angle horn, is made of glass (Pyrex) and is covered with dull-black paint wherever this seemed to be advisable.

Use of the "double horn cell" (a cell containing the stated combination of a wide angle horn and a terminal Rayleigh horn, at B, as shown in Figures 9 and 10) turned out to be the ideal solution in order to eliminate both scattering increments a and b for systems which exhibit a dissymmetrical radiation diagram. Use of the double horn cell is, therefore, indicated in all instances except those in which angular scattering measurements and measurements of turbidity are to be combined. In the latter case, the terminal Rayleigh horn has to be omitted which, of course, introduces the inconvenience of having to apply corrections for scattering increment a.

The cell shown in Figures 9 and 10 is, of course, a pilot type, attention having been paid neither to appearance nor size, but only to performance. Much smaller cells using the same principle can readily be constructed if sample size and/or cell size are important considerations. If the samples are very small (1 ml or less), the double horn cell may be used as the outer cell to be filled with liquid of the same refractive index as that of the sample in a small inner cell.

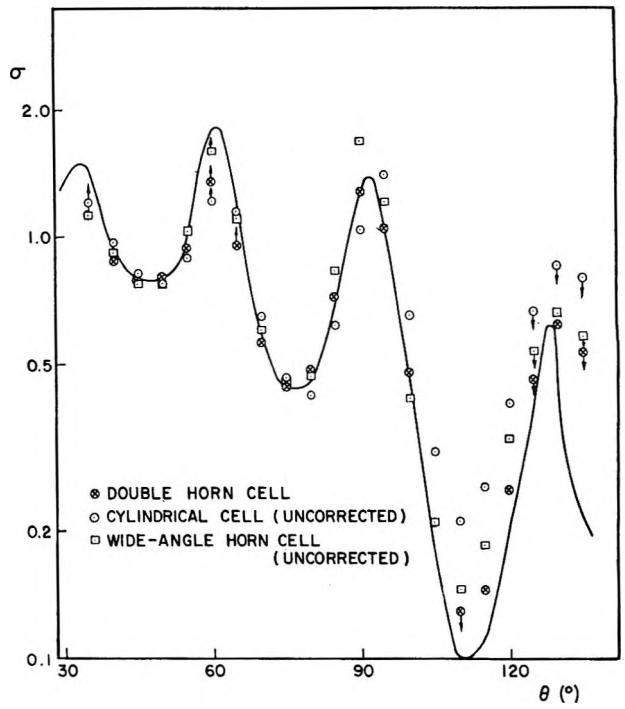

Figure 11. Comparison of experimental results (points) on the angular variation of the scattering ratio, σ, obtained with conventional cells and with the double horn cell, with the theoretically expected results (fully drawn curve). Same latex as in Figure 2; λ_0 5461 Å. No corrections are applied except for the angular variation of the optically effective volume. All data pertain to $c \rightarrow 0$. Whenever extrapolation to $c \rightarrow 0$ was difficult (see *e.g.*, Figure 5), an arrow was attached to the point obtained indicating the direction of alternate possibilities of extrapolation. These uncertainties were smallest for the double horn cell.

IV. Comparison of the Performance of Conventional Cylindrical Cells, Single Horn Cells, and Double Horn Cells

The fully drawn curve in Figure 11 reproduces the theoretical variation of the scattering ratio, σ, for the latex already considered in Figure 2. The experimental data are this time exclusively those obtained by extrapolation to zero concentration, excluding complications due to secondary scattering. They were obtained using (a) a cylindrical cell, (b) a wide angle horn cell (without terminal Rayleigh horn at B, and (c) the double horn cell of Figures 9 and 10.[27] In each instance, the smallest solid angle of 6.9×10^{-4} steradian is considered.

(26) The wide angle horn was kindly produced from our plans by Duralastic, Inc., Detroit, Mich.

(27) The conventional single horn cell where one uses only a Rayleigh horn at B was not considered in the present work.

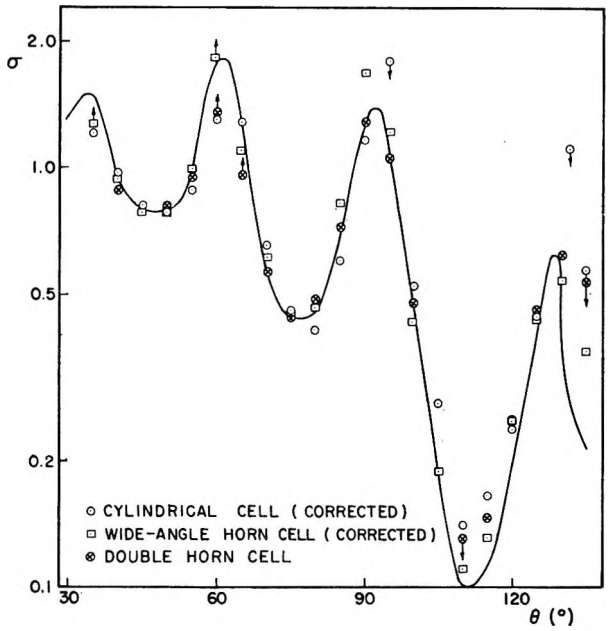

Figure 12. Comparison of experimental results on the angular variation of σ (points) with the theoretical variation (fully drawn curve). Same latex as in Figure 2; λ_0 5461 Å. The experimental results are pertinent to $c \rightarrow 0$. Reflection corrections are applied for the cylindrical cell (two corrections) and wide angle horn cell (one correction).

It is apparent that the data obtained with the cylindrical cell without corrections deviate at $\theta > 90°$ very strongly from the theoretical data. If these data were used for the calculation of distribution curves, one would obtain an erroneous degree of heterodispersion although the error would clearly be far smaller than on considering data directly obtained without extrapolating to $c \rightarrow 0$ (curve II in Figure 2). The data pertinent to the wide angle horn cell, uncorrected for scattering increment a, are, at large θ values, much closer to the theoretical results but are still not satisfactory. Finally, the data obtained with the double horn cell, which obviously did not require reflection corrections, are seen to agree, with very few exceptions, very well with the theoretical curve. Those points to which an arrow is attached pertain to insecure extrapolations to zero concentration.

Finally, it is of interest to compare, by means of Figure 12, the results obtained with the double horn cell (Figure 11) with those obtained with the conventional cylindrical cell or with a wide angle horn cell without terminal Rayleigh horn after applying in the two latter cases the corrections for reflections discussed in section II using the revised Kratohvil equation. It is seen that the corrections improve most of the results[28] in the two latter instances. However, their agreement with the theoretical results is clearly less good than that of the uncorrected data obtained with the double horn cell. Table II, finally, indicates the standard deviation

Table II: Standard Deviation of the Experimental Scattering Ratio from the Theoretical Data (Polystyrene Latex; $q = 0.7$; $p = 6.2$)

		Wide angle horn cell		Cylindrical cell (Figure 2)	
λ_0, Å	Double horn cell	Corrected	Uncorrected	Corrected	Uncorrected
5461	0.143	0.147	0.154	0.178	0.207
4358	0.194	0.213	0.298	0.237	0.352

of the data from the theoretical data. It follows from these data, once more, that the use of the double horn cell is the most satisfactory and also the simplest way of avoiding complications in the determination of the angular dispersion of scattering data.

A subsequent paper will deal with the application of the double horn cell for the determination of the size distributions in heterodisperse latices from the angular variation of the scattering ratio at several wavelengths.

Acknowledgments. This work was supported by the Office of Naval Research. We are indebted to Dr. John H. L. Watson, Director of the Physics Department of the Edsel B. Ford Institute for Medical Research, for the electron microscopic data, and to Dr. John W. Vanderhoff of the Dow Chemical Company for providing the polystyrene latices used in this investigation.

(28) The correction in the case of the wide angle horn cell covers, of course, only scattering increment a.

Optical Spectra of Chromium(III), Cobalt(II), and Nickel(II) Ions in Mixed Spinels

by R. D. Gillen[1a] and R. E. Salomon[1b]

Department of Chemistry, Temple University of the Commonwealth System of Higher Education, Philadelphia, Pennsylvania 19122 *(Received March 20, 1970)*

$LiAl_5O_8$, $ZnAl_2O_4$, and $MgAl_2O_4$ spinels, in pure form, as solid solutions with each other, and with sodium ion added, were used as host lattices for Cr^{III}, Co^{II}, and Ni^{II} ions. The diffuse optical reflectance spectra and lattice constants of these solutions were measured and compared with predictions based on crystal field theory.

Introduction

Numerous attempts have been made in the past to relate crystal field parameters, particularly $10Dq$ and in some cases the Racah parameter B, to the central ion ligand distance in oxides containing transition metal ion impurities. Changes in this interatomic distance have been achieved by application of pressure,[2] by changes in temperature,[3] and by changes in composition.[4] From data presently available in the literature it appears that the variables which determine optical transition energies are in many cases not the host cation–host anion interatomic distances but either the impurity ion–anion interatomic distances (which may be different) or impurity ion–host cation interactions. The point charge approximation of crystal field theory leads to the prediction that $10Dq$ should vary inversely as the fifth power of the interatomic distance. An extreme example, cited by Ferguson, *et al.*,[5] of deviation from this prediction, is that of Cr^{III} ion in K_2NaCrF_6 and CrF_3, for which Dq values are 1650 and 750 cm^{-1}, respectively, even though the chromium to fluorine distances are very nearly the same and the chromium ions are octahedrally surrounded by fluoride ions in both cases. Of course, in this example, the chromium ions are not dilute, and resonance interactions may be significant.

The environment of an impurity ion in a host lattice will be determined by the geometry of the pure lattice, the size of the impurity ion, the nature of bonding between the impurity ion and the surrounding species, and the ease with which the host lattice can be distorted. The latter is related to the effective force constants and the degree to which stress relief mechanisms (vacancies, dislocations) can occur.

The spinels are particularly suitable as a model host for understanding the nature of the accommodation of foreign impurity ions. They are noted for simplicity of structure[6] (the oxygens form a face-centered cubic lattice with the metal ions distributed among the tetrahedral and octahedral interstices), ease of preparation in pure and mixed form, and the fact that the metal to oxygen distances can be continuously varied by ion substitution.

The basic spinels used in this study were $LiAl_5O_8$, $ZnAl_2O_4$, and $MgAl_2O_4$. They were used in pure form, in combination with each other, and in combination with sodium ion. When sodium ion was used, the composition of the other ions was adjusted to preserve spinel stoichiometry.

The transition metal ions chosen to probe the impurity ion environments were Cr^{III}, Co^{II}, and Ni^{II}. The large body of information available concerning the optical transitions that these ions undergo in various systems facilitated the correlation of results.

Experimental Section

Each spinel composition was prepared by weighing dry CP or reagent grade oxides, or compounds decomposable by heat into oxides, mixing them dry, then wet-mixing them with mortar and pestle until well homogenized. After the raw materials were well mixed, they were dried and sintered at temperatures up to 1250° in an electric furnace in an air atmosphere. The samples were allowed to cool with the furnace, then finely ground with mortar and pestle before measurements were made.

Lattice constants were calculated from powder dif-

(1) (a) This research is part of a dissertation submitted by R. D. Gillen to the Temple University Graduate Board in partial fulfillment of the requirements for the degree of Doctor of Philosophy. (b) To whom correspondence should be addressed.

(2) H. G. Drickamer, *Solid State Phys.*, **17**, 1 (1965); D. R. Stephens and H. G. Drickamer, *J. Chem. Phys.*, **34**, 937 (1960); **35**, 424, 427, 429 (1961); R. W. Parsons and H. G. Drickamer, *ibid.*, **29**, 930 (1958).

(3) M. Dirfford, *C. R. Acad. Sci., Paris, Ser. B*, **266**, 561 (1968).

(4) T. Sakuri, M. Ishigame, and H. Arashi, *J. Chem. Phys.*, **50**, 3241 (1969); J. Graham, *J. Phys. Chem. Solids*, **17**, 18 (1960); J. Graham and D. E. Schaife, *Nature*, **192**, 161 (1961); C. P. Poole, Jr., and J. F. Itzel, Jr., *J. Chem. Phys.*, **39**, 3445 (1963); O. Schmitz-DuMont and H. Fendel, *Monatsch.*, **96**, 495 (1965); O. Schmitz-DuMont and D. Grimm, *ibid.*, **96**, 922 (1965).

(5) J. Ferguson, K. Knox, and D. L. Wood, *J. Chem. Phys.*, **35**, 2236 (1961).

(6) R. L. Harvey, I. J. Hegyi, and H. W. Leverenz, *RCA Rev.*, **11**, 321 (1950); R. K. Datta and R. Roy, *J. Amer. Ceram. Soc.*, **46**, 388 (1963).

fraction data obtained with General Electric X-RD-6 X-ray diffraction equipment. For calibration, finely ground KBr powder was mixed with the spinel powders. Diffraction peaks were identified by comparison with A.S.T.M. Diffraction Data cards for Zn and Mg spinels and with the data of Hummell[7] on $LiAl_5O_8$.

Diffuse reflectance spectra were recorded, at wavelengths from 2000 to about 7400 Å, in a Cary Model 14 spectrophotometer with a Model 1411 diffuse reflectance attachment. Reflectance of the spinels containing no transition metal ion impurities was also recorded. Most measurements were at room temperature, but the spectra of several compositions were recorded at liquid nitrogen temperature, 77°K, using apparatus previously described by Meehan.[8] These low-temperature measurements were made to see if there were any differences in peak positions or sharpness of the bands, or if any new lines or bands not present in the room temperature spectrum would arise.

Fluorescence emission measurements were made on a Hitachi Perkin–Elmer fluorescence spectrophotometer, Model MPF-2A. Excitation was by white light and by light at 2000, 2500, 3000 Å, etc.

Experimental Results

A. Lattice Constants. The lattice constants, obtained by X-ray diffraction measurements of polycrystalline powdered samples sintered at 1250° for $LiAl_5O_8$ containing small amounts of Cr^{III}, Co^{II}, and Ni^{II} ions are shown in Table I. Also included are data

Table I: Lattice Constants, Spinels Sintered at 1250°

$LiAl_5O_8$	7.907	±0.002 Å
$Li_5Cr_{0.036}Al_{2.464}O_4$	7.911	±0.002 Å
$Li_{0.492}Co_{0.015}Al_{2.463}O_4$	7.908	±0.002 Å
$Li_{0.485}Ni_{0.03}Al_{2.485}O_4$	7.913	±0.002 Å
$Li_4Na_{0.1}Al_{2.5}O_4$	7.894	±0.004 Å
$Li_{0.3}Na_{0.2}Al_{2.5}O_4$	7.910	±0.004 Å
$ZnAl_2O_4$	8.082	±0.002 Å
$Na_{0.1}Zn_{0.8}Al_{2.1}O_4$	8.080	±0.001 Å
$Na_{0.2}Zn_{0.6}Al_{2.2}O_4$	8.077	±0.005 Å

for $LiAl_5O_8$ in which part of the lithium is replaced by sodium, and for $ZnAl_2O_4$ in which part of the zinc is replaced by equal amounts of sodium and aluminum ions. The possibility that Na or Li might be lost during the sintering is ruled out by the lack of any X-ray diffraction lines corresponding to corundum.

In Table II are the lattice constants for the $LiAl_5O_8$–$ZnAl_2O_4$—Co^{II} system, sintered 6 hr at 1200°, and for the $LiAl_5O_8$–$MgAl_2O_4$—Co^{II} system, sintered 10 hr at 1250°. Between the compositions $LiAl_5O_8$ and $ZnAl_2O_4$, the deviations from Vegard's law are positive; for compositions between $LiAl_5O_8$ and $MgAl_2O_4$, the deviations from Vegard's law are positive at the $MgAl_2O_4$ end of the series and negative at the $LiAl_5O_8$ end.

Table II

(a) Lattice constants in LiZn spinels sintered at 1200°

$ZnAl_2O_4$–Co^{II}	a_0 = 8.087 ± 0.001 Å
$Li_{0.1}Zn_{0.8}Al_{2.1}O_4$–$Co^{II}$	8.074 ± 0.001 Å
$Li_{0.2}Zn_{0.6}Al_{2.2}O_4$–$Co^{II}$	8.061 ± 0.001 Å
$Li_{0.3}Zn_{0.4}Al_{2.3}O_4$–$Co^{II}$	8.024 ± 0.002 Å
$Li_{0.4}Zn_{0.2}Al_{2.4}O_4$–$Co^{II}$	7.960 ± 0.002 Å
$LiAl_5O_8$–Co^{II}	7.907 ± 0.002 Å

(b) Lattice constants in LiMg spinels sintered at 1250°

$MgAl_2O_4$–Cr^{III}	a_0 = 8.085 ± 0.005 Å
$Li_{0.1}Mg_{0.8}Al_{2.1}O_4$–$Co^{II}$	8.058 ± 0.001 Å
$Li_{0.2}Mg_{0.6}Al_{2.2}O_4$–$Co^{II}$	8.031 ± 0.004 Å
$Li_{0.3}Mg_{0.4}Al_{2.3}O_4$–$Co^{II}$	7.976 ± 0.006 Å
$Li_{0.4}Mg_{0.2}Al_{2.4}O_4$–$Co^{II}$	7.934 ± 0.002 Å
$LiAl_5O_8$–Co^{II}	7.908 ± 0.002 Å

B. Diffuse Reflectance Spectra. 1. Chromium(III). In the case of Cr-containing $LiAl_5O_8$, it was necessary to leach the spinel powder with a dilute solution of hydrochloric acid to remove a yellowish surface compound probably a chromate) on the particles. A second acid leaching did not change the positions of the optical spectral peaks. The leached $LiAl_5O_8$–Cr^{III} is reddish violet in color. A comparison of spectra for leached and unleached spinels containing cobalt and nickel ions indicated that no acid leaching was necessary for spinels containing those two metal ions. Table III lists the energies of the principal reflectance peaks ($10Dq$ and T_F) for Cr^{III}, representing the transitions $^4A_{2g}(F) \rightarrow {}^4T_{2g}(F)$ and $^4A_{2g}(F) \rightarrow {}^4T_{1g}(F)$, respectively, together with the value of the Racah parameter B calculated according to an equation given by Poole,[9] for spinels in the LiZn and LiMg series, and in Na-substituted $LiAl_5O_8$ and $ZnAl_2O_4$. In each case the chromium concentration is 1.2 atom % of the metal ions present.

In addition to the major peaks representing the energies $10Dq$ and T_F, the room temperature spectrum of $LiAl_5O_8$–Cr^{III} also has weak peaks at 14,000, 14,300, 15,100, and 15,300 cm^{-1}; at 77°K, there is a sharp peak at 16,800 cm^{-1} and some very weak peaks at about 21,400 cm^{-1}. By comparison, there is in the room temperature spectrum of $ZnAl_2O_4$–Cr^{III} a shoulder on the T_F band at about 23,800 cm^{-1}, and a strong peak in the 77°K spectrum at 29,400 cm^{-1}.

2. Cobalt(II). Cobalt was incorporated to the extent of 0.5 atom % into spinels of the LiZn and LiMg series and into Na-substituted $LiAl_5O_8$ and $ZnAl_2O_4$. The Co-containing spinels were blue in all cases. A tabulation of the diffuse reflectance peak positions is given in Table IV. Spectral peaks for $LiAl_5O_8$–Co^{II}

(7) F. A. Hummell, *J. Amer. Chem. Soc.*, **34**, 235 (1951).

(8) J. Meehan, Ph.D. Dissertation, Temple University, Philadelphia, Pa., 1965.

(9) C. P. Poole, Jr., *J. Phys. Chem. Solids*, **25**, 1169 (1964); eq 1.

Table III

(a) Diffuse reflectance peak positions for Cr^{III} in $Li_xZn_{1-2x}Al_{1.964+x}Cr_{0.036}O_4$, sintered 6 hr at 1200°, leached with dilute hydrochloric acid

x	$10Dq$,[a] cm^{-1}	T_F, cm^{-1}	B, cm^{-1}
0	18,700	25,300	640
0 (77°K)	18,700	25,600	680
0.1	18,600	25,500	710
0.2	18,400	25,500	700
0.3	18,200	25,400	720
0.4	17,800	25,000	720
0.5	17,600	25,300	800
0.5 (77°K)	17,600	25,400	810

(b) Diffuse reflectance peak positions for Cr^{III} in $Li_xMg_{1-2x}Al_{1.964} + {}_xCr_{0.036}O_4$, sintered 6 hr at 1250°, leached with dilute hydrochloric acid

x	$10Dq$, cm^{-1}	T_F, cm^{-1}	B, cm^{-1}
0	18,300	25,200	680
0.1	18,000	26,000	830
0.2	17,800	26,600	970
0.3	17,800	26,400	940
0.4	17,700	25,700	840
0.5	17,600	25,300	800

(c) Diffuse reflectance peak positions for Cr^{III} in Na-substituted $LiAl_5O_8$ and $ZnAl_2O_4$, sintered 6 hr at 1250°, leached with dilute hydrochloric acid

Composition	$10Dq$, cm^{-1}	T_F, cm^{-1}	B, cm^{-1}
$Li_{0.5}Al_{2.5}O_4$-Cr^{III}	17,600	25,400	810
$Li_{0.4}Na_{0.1}Al_{2.5}O_4$-$Cr^{III}$	17,600	25,800	870
$Li_{0.3}Na_{0.2}Al_{2.5}O_4$-$Cr^{III}$	17,500	26,700	1060
$ZnAl_2O_4$-Cr^{III}	18,700	25,600	670
$Na_{0.1}Zn_{0.8}Al_{2.1}O_4$-$Cr^{III}$	18,700	25,600	670
$Na_{0.2}Zn_{0.6}Al_{2.2}O_4$-$Cr^{III}$	18,600	25,700	700

[a] In this table, and those following, the approximate uncertainty in value of peak position is ±100 cm^{-1}.

were much less sharp than in $ZnAl_2O_4$-Co^{II}. Positions of the peaks were essentially the same for the two compositions, and in the Na-substituted products and where there were any differences the peaks for $LiAl_5O_8$-Co^{II} were at slighter shorter wavelengths (higher energies). The 77°K reflectance spectrum of $LiAl_5O_8$-Co^{II} had one additional line, at about 14,300 cm^{-1}, not present in the room temperature spectrum.

3. Nickel(II). Nickel was added to $LiAl_5O_8$ and to other spinels to the extent of 1% of the cations present. Except for $ZnAl_2O_4$-Ni^{II}, which is green in color, all Ni-containing spinels were blue in color. Table V lists major diffuse reflectance peak positions for these Ni-containing spinels, all sintered 6 hr at 1250°. There are also broad weak bands at about 21,500 and 32,100 cm in $LiAl_5O_8$-Ni^{II}. In the 77°K spectrum of $LiAl_5O_8$-Ni^{II}, the only line not present in the room temperature spectrum is a low level double peak at about 15,200 cm^{-1}, on the low energy side of the $^3T_2(F) \rightarrow {}^3T_1(P)$ (tetrahedral) band.

C. Fluorescence Emission Spectra. Fluorescence lines for $LiAl_5O_8$-Cr^{III} were found at 14,045 and at 14,330 cm^{-1}, the former line being much more intense. These lines are fairly sharp, corresponding in position to two of the minor reflectance peaks, and are slightly lower in energy than the chromium R lines in ruby and in $MgAl_2O_4$-Cr^{III}.[10] The most favorable excitation wavelength for fluorescence of the $LiAl_5O_8$-Cr^{III} sample was 4000 Å. In the case of Co- and Ni-containing $LiAl_5O_8$, there were numerous small peaks on the recording chart, but no well-defined fluorescence peaks were obtained.

Discussion of Results

The lattice constant of the $LiAl_5O_8$ prepared in this work indicates that it is the low-temperature stable form, $LiAl_5O_8$-II, described by Datta and Roy, in which $a_0 = 7.907$ Å and in which cations are distributed in an ordered fashion among the tetrahedral and octahedral interstices of the face-centered cubic oxygen lattice. There is very little difference between the lattice constant of the $LiAl_5O_8$ itself and the same compound containing small amounts of the transition ions chromium, cobalt, and nickel, nor would any large increase be expected considering the small amounts of the impurity ions and the similarity of ionic radii. It is of interest to note that substitution of sodium into $ZnAl_2O_4$ and $LiAl_5O_8$ causes very little change in the lattice constant, even though the ionic radius of the Na(I) ion is larger than for either Zn^{II}, Al^{III}, or Li^{I}.

The diffuse reflectance spectrum of $LiAl_5O_8$-Cr^{III} shows that $10Dq$ is lower and the Racah parameter B higher than for either $ZnAl_2O_4$-Cr^{III} or $MgAl_2O_4$-Cr^{III}. The high value of B may be in part a result of a greater ionic character of $LiAl_5O_8$, resulting from lower electronegativity of lithium as compared to other spinel-forming cations. The lower value of $10Dq$ is unexpected from the viewpoint of crystal field theory because $LiAl_5O_8$ has a lower lattice constant than $ZnAl_2O_4$ or $MgAl_2O_4$, and a lower lattice constant usually implies a smaller cation–anion interatomic distance. The compositions of $ZnAl_2O_4$-Cr^{III} having part of the Zn^{II} ions replaced by Na^{I} and Al^{III} ions had essentially the same lattice constant and reflectance peaks as $ZnAl_2O_4$-Cr^{III} (see Tables I and III). Apparently there is little or no change in cation–cation interactions as a result of this substitution. It is then reasonable to suppose that there will be no changes in cation–cation interactions as Li^{I} ions (having a similar electronic configuration to that of Na^{I} ions) and Al^{III} ions replace Zn^{II} ions. Therefore, the entire change in $10Dq$ between $ZnAl_2O_4$-Cr^{III} and $LiAl_5O_8$-Cr^{III} may be attributed to the change in Cr–O distance. As the decrease in $10Dq$ is

(10) P. M. Jaffe, *J. Electrochem. Soc.*, 115, 1203 (1968).

Table IV

(a) Diffuse reflectance peak positions (cm^{-1}) for Co^{II} in $Li_xZn_{1-2x}Al_{2+x}O_4$-Co^{II}, sintered 6 hr at 1200°

x	$T_P(^4A_2(F) \rightarrow {}^4T_1(P))$			^2G levels	
0.1	16,200	16,800	18,300	21,000	24,700
0.1	16,100	16,900	18,300	21,000	24,700
0.2	16,100	16,900	18,300	21,000	24,700
0.3	16,100	17,100	18,300	21,000	24,700
0.4	16,000	17,300	18,300	20,900	24,700
0.5	16,000	17,300	18,400	20,800	24,500

(b) Diffuse reflectance peak positions (cm^{-1}) for Co^{II} in $Li_xMg_{1-2x}Al_{2+x}O_4$-Co^{II}, sintered 10 hr at 1250°

x	T_P			^2G levels	
0	15,900	16,900	18,500	20,900	24,500
0.1	16,000	17,200	18,300	20,800	24,700
0.2	16,000	17,200	18,400	20,900	24,600
0.3	16,000	17,200	18,300	20,900	24,500
0.4	16,000	17,200	18,400	20,900	24,700
0.5	16,000	17,300	18,400	20,900	24,600

(c) Diffuse reflectance peak positions (cm^{-1}) for Co^{II} in Na-substituted $LiAl_5O_8$ and $ZnAl_2O_4$, sintered 6 hr at 1250°

Composition	T_P			^2G levels	
$LiAl_5O_8$-Co^{II}	16,000	17,200	18,300	20,900	24,600
$Li_{0.4}Na_{0.1}Al_{2.5}O_4$-$Co^{II}$	16,000	17,200	18,300	20,900	24,700
$Li_{0.3}Na_{0.2}Al_{2.5}O_4$-$Co^{II}$	16,000	17,200	18,300	21,000	24,600
$ZnAl_2O_4$-Co^{II}	16,100	16,800	18,300	21,000	24,600
$Zn_{0.8}Na_{0.1}Al_{2.1}O_4$-$Co^{II}$	16,100	16,900	18,300	21,000	24,600
$Zn_{0.6}Na_{0.2}Al_{2.2}O_4$-$Co^{II}$	16,100	16,900	18,300	21,000	24,700

Table V: Diffuse Reflectance Peak Positions (cm^{-1}) for Ni-Containing Spinels

Composition	T_P (tetrahedral)		T_P (octahedral)
$LiAl_5O_8$-Ni^{II}	15,900	16,700	27,400
$Li_{0.4}Na_{0.1}Al_{2.5}O_4$-$Ni^{II}$	15,900	16,800	27,800
$Li_{0.3}Na_{0.2}Al_{2.5}O_4$-$Ni^{II}$	15,900	16,900	27,800
$ZnAl_2O_4$-Ni^{II}	15,900	16,900	24,400
$Na_{0.1}Zn_{0.8}Al_{2.1}O_4$-$Ni^{II}$	15,900	17,100	26,300
$Na_{0.2}Zn_{0.6}Al_{2.2}O_4$-$Ni^{II}$	15,900	16,900	26,300
$MgAl_2O_4$-Ni^{II}	15,700	16,800	24,700
$Li_{0.25}Zn_{0.5}Al_{2.25}O_4$-$Ni^{II}$	15,900	16,800	27,400
$Li_{0.25}Mg_{0.5}Al_{2.25}O_4$-$Ni^{II}$	15,900	16,900	27,400

about 6%, the increase in Cr–O distance, on the basis of the inverse fifth (or sixth) power law, would be about 1%. A longer Cr–O bond distance in $LiAl_5O_8$–Cr^{III}, in spite of the shorter lattice constant, could be explained by a distortion of the cubic spinel lattice. Such a distortion of the spinel lattice has been suggested by Jaffe,[10] who found a lower energy value for the chromium R line in the cathode luminescence spectrum of $LiAl_5O_8$–Cr^{III} than for $MgAl_2O_4$–Cr^{III} or Al_2O_3–Cr^{III}.

The two weak peaks near 14,000 cm^{-1} are probably a result of the spin-forbidden transitions $^4A_{2g}(F) \rightarrow {}^2T_{1g}(G)$ and $^4A_{2g}(F) \rightarrow {}^2E_g(G)$, which occur in ruby as the R lines. In $LiAl_5O_8$-Cr^{III} there are also two low intensity peaks at about 15,000 cm^{-1}. These cannot be explained by any spin-allowed transition to the quartet ground state, but they may be the $^2E_g(t^3) \rightarrow {}^2A_{1g}(t^2e)$ and $^2T_{1g} \rightarrow {}^2A_{1g}$ transitions, which, according to Naiman, Di Bartolo, and Linz,[11] can occur in ruby at energies near the $^4A_{2g} \rightarrow {}^4T_{2g}$ band. In the 77°K spectrum of $LiAl_5O_8$, there are some very weak peaks at about 21,000 cm^{-1}. This is very close to $MgAl_2O_4$–Cr^{III} peaks assigned by Ford and Hill[12] to the $^4A_{2g}(F) \rightarrow {}^2T_{2g}(G)$ transition. The strong peak at about 29,000 cm^{-1}, found in the 77°K spectrum of $ZnAl_2O_4$–Cr^{III}, and probably a result of the $^4A_{2g}(F) \rightarrow {}^2A_{1g}(G)$ transition as in ruby,[13] was not observed in the $LiAl_5O_8$–Cr^{III} spectrum. The sharp peak at 16,850 cm^{-1} found only in the 77°K spectrum of $LiAl_5O_8$–Cr^{III} may be one of the spin-orbit split components of the $^4A_{2g}(F) \rightarrow {}^4T_{2g}(F)$ band, or it could be a result of the $^4A_2(F) \rightarrow {}^4T_1(F)$ transition of tetrahedrally coordinated Cr^{III} ion, a transition for which Drifford and Charpin[13] found a line at 16,200 cm^{-1} in nonstoichiometric Mg spinel.

Co^{II} occurs in spinels in tetrahedral interstices. Its d electron configuration ($3d^7$) is, by the electron–hole reciprocity, related to that of Cr^{III} ($3d^3$). The Co^{II} ion has the same ^4F ground state as does Cr^{III}. In a

(11) C. S. Naiman, B. Di Bartolo, and A. Linz, "Physics of Quantum Electronics," McGraw-Hill, New York, N. Y., 1966, pp 315-321.

(12) R. A. Ford and O. F. Hill, *Spectrochim. Acta*, **16**, 318 (1960).

(13) M. Drifford and P. Charpin, *C. R. Acad. Sci., Paris, Ser. AB*, **264**, 64 (1967).

tetrahedral field Co^{II} has the same crystal field splittings and qualitatively the same energy level diagram as does the Cr^{III} ion in an octahedral field. The first three peaks of the Co^{II} spectrum belong largely to the $^4A_2(F) \rightarrow {}^4T_1(P)$ transition. The other two peaks are spin-forbidden transitions to components of the split ^2G level from the $^4A_2$ ground state. From Table IV it may be seen there is very little change in peak positions with changes in host lattice composition. This means that $10Dq$ is probably the same in $LiAl_5O_8$–Co^{II} as in the other spinels, but this was not verified by determination of $10Dq$ because the spectral bands for this transition are in the infrared, beyond the range of the spectrophotometer. In the 77°K diffuse reflectance spectrum of $LiAl_5O_8$–Co^{II}, the new line at about 14,300 cm^{-1} is most likely the transition from the ground state to the $^2T_1$ and ^2E branches of the ^2G level, the energy of these branches being almost independent of Dq/B according to the Tanabe–Sugano diagram.[14] If this is so, this line would correspond to the R line of the Cr^{III} ion. Recently the crystal field spectra, at liquid helium temperature, of Co^{II} in $ZnAl_2O_4$ spinel has been reported.[15]

The Ni^{II} ion has the electron configuration $3d^8$, and ground state ^3F. In spinels, the Ni^{II} occupies both tetrahedral and octahedral sites. In the diffuse reflectance spectrum of $LiAl_5O_8$–Ni^{II}, the double peak at 16,000 and 16,800 cm^{-1} (Table V), corresponds to the $^3T_1(F) \rightarrow {}^3T_1(P)$ transition of the tetrahedrally coordinated Ni^{II} ion. The band peaking at 27,600 cm^{-1} represents the $^3A_{2g}(F) \rightarrow {}^3T_{1g}(P)$ transition of the octahedrally coordinated Ni^{II} ion. The weak band at about 21,000 cm^{-1} in $LiAl_5O_8$–Ni^{II} corresponds approximately to the energy expected for the spin-forbidden $^3A_{2g}(F) \rightarrow {}^1A_{1g}(G)$ transition of the octahedrally coordinated Ni^{II} ion, and the weak band at 32,000 cm^{-1} is probably a result of the $^3A_{2g}(F) \rightarrow {}^1T_{2g}(G)$ transition, the $^3A_{2g}(F) \rightarrow {}^1E_{2g}(G)$ transition, or the sum of the effect of both of these transitions.

For both Co^{II} and Ni^{II} in tetrahedral surroundings, the transition energies differ very little for different host crystal compositions, which suggests that there is no appreciable change in the crystal field strength even though lattice constant (and presumably interatomic distances as well) are different. While it is theoretically possible for both Dq and B to change in such a manner that certain transition energies would remain unchanged, this seems an unlikely possibility. In the case of the Ni^{II} ion in an octahedral environment (Table V), both $ZnAl_2O_4$–Ni^{II} and $MgAl_2O_4$–Ni^{II} have considerably lower values for the T_P transition than does $LiAl_5O_8$–Ni^{II}. Such a lower T_P value for these compositions, having greater lattice constants than $LiAl_5O_8$–Ni^{II}, would correspond to a lower value of $10\,Dq$, assuming B to be reasonably constant.

Conclusions

Optical transition energies for chromium, cobalt, and nickel ions in spinels indicate that crystal field parameters cannot be correlated to lattice constants by the predictions of crystal field theory. Whereas in $LiAl_5O_8$–Cr^{III} one would expect a higher $10Dq$ value than in $ZnAl_2O_4$ or $MgAl_2O_4$ (because of lower lattice constant), the actual value obtained, 17,600 cm^{-1}, is less than in either of the other two spinels. This is probably more a result of lattice distortion and a longer Cr–O distance than of cation–cation interactions. In the case of Co- and Ni-containing spinels, there is very little change in transition energies with composition of lattice constants, and the small changes which do occur are nowhere near that required by the inverse fifth power law of the point charge approximation. Probably for both Co^{II} and Ni^{II} ions in tetrahedral coordination, the crystal field strengths in these spinels are very nearly the same, in spite of the changing lattice constant.

(14) B. N. Figgis, "Introduction to Ligand Fields," Wiley, New York, N. Y., 1966.

(15) J. Ferguson, D. L. Wood, and L. G. Van Uitert, *J. Chem. Phys.*, **51**, 2904 (1969).

Force Constants and Thermodynamic Properties of the Unstable Linear Triatomic Molecules HCP, DCP, and FCN

by H. F. Shurvell

Department of Chemistry, Queen's University, Kingston, Ontario, Canada *(Received April 22, 1970)*

Force constants and thermodynamic quantities have been calculated for the unstable linear triatomic molecules HCP, DCP, and FCN. For FCN the relationships between the CF and CN stretching force constants and the interaction constant of the valence force field have been studied.

Introduction

We have recently studied[1] the ultraviolet and infrared absorption spectra of the phosphorus analog of hydrocyanic acid, HCP, and the deuterated molecule, DCP. Cyanogen fluoride, FCN, has been studied by Dodd and Little,[2] and force constants have been calculated previously for this molecule.[2-5] No previous force constant calculations have been made for HCP. The thermodynamic properties of FCN were predicted[6] before the molecule was isolated, and the infrared[2] and microwave spectra[7] were recorded.

Calculations

We have used the Wilson FG matrix method[8] for the force constant calculations and an iterative procedure to refine an initial set of force constants. A modified[9] version of the Fortran program written by Schachtschneider[10] was used for these calculations. Thermodynamic properties were calculated using the methods described by Herzberg.[11] All calculations were carried out on an IBM 360/50 computer.

The internal coordinates used for linear XYZ molecules are the changes in the XY and XZ bond lengths and the change in the angle $\widehat{XYZ}$. The valence force constants are XY stretching (f_{xy}), YZ stretching (f_{yz}), $\widehat{XYZ}$ bending (f_{xyz}), and an interaction constant between the two stretching modes ($f_{xy,yz}$).

The G matrices were set up in the usual way[8] using the bond lengths for HCP reported by Tyler[12] of 1.067 Å for C–H and 1.542 Å for C–P and for FCN reported by Sheridan, *et al.*,[7] of 1.260 Å for C–F and 1.165 Å for C–N.

Results and Discussion

HCP and DCP. These are relatively unstable molecules prepared by passing phosphine or PD_3 through a carbon arc.[13] The compounds are stable at liquid nitrogen temperatures but have a lifetime of only a few hours at room temperature.

The three fundamental vibration frequencies of HCP were observed in the infrared spectrum.[1] However, only the CD stretching and DCP bending fundamentals (ν_1 and ν_3) were observed for DCP.[1] The structure was determined from the microwave spectrum.[12]

For these molecules it is possible to calculate a unique set of force constants of the general valence force field (GVFF) and to predict the CP stretching frequency of DCP. The results are shown in Table I. The HCP bending force constant is determined by ν_3 only, and the best value for this force constant gives calculated values for ν_3 for HCP and DCP which are, respectively, 8.1 cm^{-1} low and 7.4 cm^{-1} high. This may be due in part to the uncertainty in ν_3 of DCO[1] or to the effects

Table I: Force Constants and Frequencies (in cm^{-1}) for HCP and DCP

Force constants, mdyn/Å			HCP		DCP	
			Obsd	Calcd	Obsd	Calcd
f_{CH}	5.525	ν_1	3216.9	3216.8	2419.4	2419.3
f_{CP}	9.040					
f_{HCP}	0.145[a]	ν_2	1276.2	1276.2	...	1214.1
$f_{CH,CP}$	−0.3965	ν_3	674.7	666.6	510	517.4

[a] The $\widehat{HCP}$ bending constant has been divided by $(r_{CH} \cdot r_{CP})$.

(1) J. W. C. Johns, H. F. Shurvell, and J. K. Tyler, *Can. J. Phys.*, **47**, 893 (1969).

(2) R. E. Dodd and R. Little, *Spectrochim. Acta*, **16**, 1083 (1960).

(3) E. E. Aynsley and R. Little, *ibid.*, **18**, 667 (1962).

(4) H. Siebert, "Anwendungen der Schwingungsspektroskie in der anorganischen Chemie," Springer-Verlag, Berlin, 1966, p 47.

(5) E. J. Williams and J. A. Ladd, *J. Mol. Structure*, **2**, 57 (1968).

(6) M. W. Luft, *J. Chem. Phys.*, **21**, 1900 (1953).

(7) J. Sheridan, J. K. Tyler, E. F. Aynsley, R. E. Dodd, and R. Little, *Nature*, **185**, 96 (1960).

(8) E. B. Wilson, Jr., J. C. Decius, and P. C. Cross, "Molecular Vibrations," McGraw-Hill, New York, N. Y., 1955.

(9) W. V. F. Brooks, private communication.

(10) J. H. Schachtschneider, Technical Report No. 57-65, Shell Development Co., 1965.

(11) G. Herzberg, "Infrared and Raman Spectra," Van Nostrand, Princeton, N. J., 1945.

(12) J. K. Tyler, *J. Chem. Phys.*, **40**, 1170 (1964).

(13) T. E. Gier, *J. Amer. Chem. Soc.*, **83**, 1769 (1961).

Table II: Heat Content $H°$, Free Energy $G°$, Entropy $S°$, and Heat Capacity $C_p°$ in Calories per Degree per Mole, for the Ideal Gaseous State of HCP and DCP at 1 atm Pressure for Several Temperatures T

T, °K	$(H° - E_0°)/T$[a] HCP	$(H° - E_0°)/T$[a] DCP	$(G° - E_0°)/T$ HCP	$(G° - E_0°)/T$ DCP	$S°$ HCP	$S°$ DCP	$C_p°$ HCP	$C_p°$ DCP
100	6.95	6.96	36.07	36.48	43.04	43.44	6.97	7.02
200	7.11	7.15	40.94	41.35	48.04	48.49	7.71	7.69
273.16	7.38	7.36	43.19	43.60	50.57	50.97	8.58	8.21
298.16	7.50	7.44	43.84	44.25	51.34	51.69	8.87	8.38
300	7.51	7.45	43.89	44.30	51.39	51.75	8.89	8.39
400	7.98	7.76	46.11	46.48	54.09	54.24	9.87	8.98
500	8.44	8.06	47.94	48.25	56.38	56.30	10.61	9.49
600	8.85	8.33	49.51	49.74	58.36	58.07	11.17	9.94
800	9.54	8.83	52.16	52.21	61.69	61.03	11.98	10.66
1000	10.09	9.25	54.35	54.22	64.43	63.47	12.56	11.19
1500	11.08	10.04	58.64	58.13	69.72	68.18	13.49	11.97
2000	11.75	10.58	61.92	61.10	73.68	71.68	13.99	12.33

[a] $E°_0$ is the energy per mole of the perfect gas at $T = 0°K$.

of anharmonicity, which have been ignored in the present calculation. The CH and CP stretching constants, together with the interaction constant, have been varied to produce a fit between observed and calculated frequencies.

The magnitudes of the CP stretching and $\widehat{HCP}$ bending constants are about one-half of the CN stretching and $\widehat{HCN}$ bending constants of HCN,[8] while the CH stretching constant is similar to the corresponding constant of HCN. The interaction is larger for HCP than for HCN but has the same sign. The CP single bond stretching constant in molecules such as $(CH_3)_3P$ is about 3.0 mdyn/Å,[14] so that in HCP the CP bond order probably approaches 3.

Thermodynamic Properties. Using the three fundamentals of HCP and DCP together with the rotational constants from the microwave work of Tyler,[12] the thermodynamic properties—heat content, free energy, entropy, and heat capacity—have been calculated for 12 temperatures from 100 to 2000°K for the ideal gaseous state at 1 atm pressure. The rigid-rotor harmonic oscillator approximation was used. The results of the calculations are given in Table II.

FCN. Cyanogen fluoride is an unstable molecule prepared by high-temperature pyrolysis of cyanuric fluoride $(FCN)_3$ under reduced pressure[15] or by fluorination of cyanogen.[2]

Orville-Thomas[16] predicted CN and CF stretching constants for FCN of 17.5 and 8.07 mdyn/Å, respectively, prior to the preparation of the compound, and Luft[6] calculated thermodynamic functions from the theoretical frequencies and structure extrapolated from other XCN molecules. Other force constant calculations for FCN have been reported in four previous papers.[2-5] The results are summarized in Table III. We have used these sets of force constants to calculate the stretching frequencies of FCN, and in the two cases noted in the table we could not reproduce the experimental frequencies. The bending constant is determined uniquely as 0.379 mdyn Å or 0.258 mdyn/Å, from the bending fundamental. However, the two

Table III: Previous Stretching and Interaction Constants (mdyn/Å) for FCN

	Reference 16[a]	Reference 2		Reference 3	Reference 4	Reference 5
f_{CF}	8.07	9.2	9.3[b]	8.70[b]	7.95	8.41
f_{CN}	17.5	16.3	17.6[b]	17.44[b]	19.2	17.92
$f_{CF, CN}$	0.45	0.0	1.3[b]	0.45[b,c]	1.66	0.83

[a] Force constants predicted theoretically. [b] These sets are incorrect (see text). [c] This value has been incorrectly quoted as 0.70 mdyn/Å by Williams and Ladd.[5]

Table IV: Stretching and Interaction Force Constants (in mdyn/Å) for FCN

$f_{CF, CN}$	f_{CF}	f_{CN}
0.00	9.18	16.31
0.25	8.90	16.82
0.45	8.71	17.20
0.50	8.67	17.30
0.75	8.47	17.74
0.83	8.41	17.88
1.00	8.30	18.16
1.30	8.12	18.64
1.50	8.02	18.94
1.66	7.95	19.18
1.75	7.91	19.31

(14) H. Siebert, *Z. Anorg. Allg. Chem.*, **273**, 161 (1953).

(15) F. S. Fawcett and R. D. Lipscomb, *J. Amer. Chem. Soc.*, **86**, 2576 (1964).

(16) W. J. Orville-Thomas, *J. Chem. Phys.*, **20**, 920 (1952).

Table V: Heat Content $H°$, Free Energy $G°$, Entropy $S°$, and Heat Capacity $C_p°$ in Calories per Degree per Mole for the Ideal Gaseous State of Cyanogen Fluoride at 1 atm Pressure for Several Temperatures T

	$(H° - E°_0)/T$[a]		$-(G° - E°_0)/T$		$S°$		$C_p°$	
T,°K	This work	Ref 6	This work	Ref 6	This work	Ref 6	This work	Ref 6
100	6.99	...	37.43	...	44.42	...	7.21	...
200	7.49	...	42.40	...	49.89	...	8.78	...
273.16	7.97	...	44.81	...	52.77	...	9.72	...
298.16	8.12	8.28	45.51	45.69	53.64	53.97	9.98	10.18
300	8.14	8.29	45.56	45.74	53.70	54.03	10.00	10.20
400	8.71	8.88	47.98	48.21	56.70	57.09	10.84	11.01
500	9.21	9.36	49.98	50.24	59.19	59.60	11.48	11.59
600	9.63	9.77	51.70	51.99	61.33	61.76	11.98	12.08
800	10.32	10.45	54.57	54.89	64.89	65.34	12.75	12.80
1000	10.86	10.97	56.93	57.68	67.79	68.65	13.28	13.32
1500	11.81	...	61.53	...	73.34	...	14.03	...
2000	12.41	...	65.01	...	77.43	...	14.37	...

[a] $E°_0$ is the energy per mole of the perfect gas at $T = 0$°K.

stretching constants and the interaction cannot be determined from the stretching frequencies alone.

Williams and Ladd[5] have calculated sets of force constants for the cyanogen halides. In the case of ClCN and BrCN they were able to make use of centrifugal distortion constants to fix the value of the interaction constants for these molecules. However, they were unable to apply this method to FCN because the centrifugal distortion constant was insensitive to the force constants. They estimated f_{CF} and $f_{CF,CN}$ by assuming a value of 17.92 mdyn/Å for f_{CN}.

We have investigated how the values of the CF and CN stretching constants vary with the value of the interaction constant. These calculations have been carried out using the Wilson FG matrix method, which lends itself to a perturbation calculation in which f_{CF} and f_{CN} are adjusted to give an exact fit between observed and calculated frequencies for a series of values of the interaction constant.

In fact the interaction can take on a large number of reasonable values and still give reasonable values for the CN and CF stretching constants. We have calculated the stretching constants, when the interaction was given a series of values in the range 0.0 to 1.75 mdyn/Å. The results of these calculations are shown in Table IV.

In Table IV we have included sets of stretching constants determined by fixing the interaction at 0.45, 0.83, 1.3, and 1.66. The second and last of these agree with previous calculations,[4,5] whereas the first and third sets are not in agreement with previous work.[2,3]

Thermodynamic properties have been calculated for FCN using the frequencies and the rotational constant from the work of Dodd and Little.[2] The results are given in Table V together with the estimated values of Luft.[6] It is seen that the agreement is close.

Solubility Phenomena in Dense Carbon Dioxide Gas in the Range 270–1900 Atmospheres

by Joseph J. Czubryt, Marcus N. Myers, and J. Calvin Giddings*

Department of Chemistry, University of Utah, Salt Lake City, Utah 84112 *(Received May 18, 1970)*

A high-pressure gas chromatographic instrument has been used to measure the density dependent solubility of Carbowax 4000, Carbowax 1000, 1-octadecanol, and stearic acid in compressed CO_2 at 40°. It is shown that maxima exist in all these solubility curves at between 300 and 2500 atm, depending on the solute. This result is consistent with a form of regular solution theory developed for dense gaseous solvents. A comparison of theory and experiment relative to a number of parameters shows generally excellent qualitative agreement and in some instances a quantitative predictability.

Introduction

The enhancement of volatility caused by the presence of a dense gaseous atmosphere has been noted on many occasions.[1-13] Compression appears to give to the gas a positive solvent power not possessed in its normal, low-pressure state. This solvent power increases substantially with increasing compression. Studies of the phenomenon, which extend back to the last century,[1] are mainly limited to solute molecules of small and medium size and to pressures under 200 atm. Recently we have reported data on the solubility of biochemicals and polymers (molecular weight to 4×10^5) in dense NH_3 gas at 200 atm and dense CO_2 gas at pressures to 1560 atm.[12,13] Here we extend this work by obtaining solubilities as a function of CO_2 density for Carbowax 4000, Carbowax 1000, 1-octadecanol, and stearic acid in CO_2 in the pressure range 270–1900 atm at 135-atm intervals. We show that there are maxima in the solubility curves not seen before and indeed not present in the low-pressure range. In our cases, the maxima for different solutes occur anywhere from 300 to 2040 atm. The existence of the maxima is predicted, and their locations well approximated, by the application of a form of regular solution–solubility parameter theory.

The impetus for recent studies in dense gas solubility comes from the realization that these gaseous "solvents" may be of unique value in enhancing the volatility of complex molecules so that they can be gas chromatographed.[10-14] The sensitivity of solubility to pressure provides a rapid mechanical means for manipulating solubility both in chromatographic and in other systems. Experiments have borne out the fruitfulness of this approach.

Efforts to describe the solvent power of nonideal gases in quantitative, mathematical form have almost entirely used the virial approach. This direction has been followed for both chromatographic[11,15-22] and nonchromatographic[23-27] work. The virial treatment is rigorous, but is inapplicable at pressures much beyond 100 atm because of difficulties in evaluating higher virial coefficients and series convergence problems.[9] Hence

* To whom correspondence should be addressed.

(1) J. B. Hannay and J. Hogarth, *Proc. Roy. Soc.*, **29**, 324 (1879).

(2) E. Ingerson, *Econ. Geol.*, **29**, 454 (1934).

(3) D. Iu. Gamburg, *Neft. Khoz.*, **25** (No. 9), 46 (1947).

(4) G. A. M. Diepen and F. E. C. Scheffer, *J. Amer. Chem. Soc.*, **70**, 4085 (1948).

(5) H. S. Booth and R. M. Bidwell, *Chem. Rev.*, **44**, 477 (1949).

(6) S. Robin, *J. Chim. Phys.*, **48**, 501 (1951).

(7) S. Robin and B. Vodar, *Discussions Faraday Soc.*, **15**, 233 (1953).

(8) G. W. Morey, *Econ. Geol.*, **52**, 225 (1957).

(9) J. S. Rowlinson and M. J. Richardson, "Advances in Chemical Physics," Vol. 2, I. Prigogine, Ed., Interscience, New York, N. Y., 1959, p 85.

(10) E. Klesper, A. H. Corwin, and D. A. Turner, *J. Org. Chem.*, **27**, 700 (1962).

(11) S. T. Sie, W. Van Beersum, and G. W. A. Rijnders, *Separation Sci.*, **1**, 459 (1966).

(12) J. C. Giddings, M. N. Myers, L. McLaren, and R. A. Keller, *Science*, **162**, 67 (1968).

(13) J. C. Giddings, M. N. Myers, and J. W. King, *J. Chromatog. Sci.*, **7**, 276 (1969).

(14) J. C. Giddings, "Gas Chromatography, 1964," A. Goldup, Ed., Elsevier, Amsterdam, 1965, p 3.

(15) D. H. Desty, A. Goldup, G. R. Luckhurst, and T. W. Swanton, "Gas Chromatography, 1962," M. van Swaay, Ed., Butterworths, Washington, D. C., and London, 1962, p 67.

(16) D. C. Locke and W. W. Brandt, "Gas Chromatography," L. Fowler, Ed., Academic Press, New York, N. Y., 1963, p 55.

(17) D. H. Everett and C. T. H. Stoddart, *Trans. Faraday Soc.*, **57**, 746 (1961).

(18) D. H. Everett, *ibid.*, **61**, 1637 (1965).

(19) A. J. B. Cruickshank, M. L. Windsor, and C. L. Young, *Proc. Roy. Soc., Ser. A*, **295**, 259 (1966).

(20) A. J. B. Cruickshank, M. L. Windsor, and C. L. Young, *ibid.*, **295**, 271 (1966).

(21) A. J. B. Cruickshank, B. W. Gainey, and C. L. Young, *Trans. Faraday Soc.*, **64**, 337 (1968).

(22) A. J. B. Cruickshank, B. W. Gainey, C. P. Hicks, T. M. Letcher, R. W. Moody, and C. L. Young, *ibid.*, **65**, 1014 (1969).

(23) A. H. Ewald, W. B. Jepson, and J. S. Rowlinson, *Discussions Faraday Soc.*, **15**, 238 (1953).

(24) J. S. Rowlinson, F. H. Sumner, and J. R. Sutton, *Trans. Faraday Soc.*, **50**, 1 (1954).

this method, which approaches dense gases from the ideal gas side, is not valid for the high densities studied here.

More likely to succeed, under the circumstances, would be an approach based on liquid solubility phenomena. Densities of practical interest are usually in the range 0.3–0.9 times the equivalent liquid density, while gases at 1 atm pressure, already showing measurable nonideal effects, are removed in density by several hundredfold from this range.

The principal difficulty with following the general path of liquid solution is that the latter are themselves imperfectly understood.[28] However, it is clearly more suitable to use approximate methods where the approximations are in accord with the physical situation than to stretch an exact theory (virial) far beyond its reasonable limit of application.

For the above reasons, we previously suggested and developed approximate methods for applying solubility parameter concepts to dense gaseous solutions.[13] Some aspects of this approach will be tested here.

The key results of the theory are given in the following two equations. First the solubility parameter is a function only of density ρ, approximated by the linear relationship

$$\delta_g = \delta_{liq}[\rho/\rho_{liq}] \quad (1)$$

and therefore reaches the value, δ_{liq}, characteristic of the parent liquid when the gas is compressed to the liquid density, ρ_{liq}. Solubility enhancement is related to this by

$$\ln I = (V_0\delta_0^2/RT)\Delta(2 - \Delta) \quad (2)$$

where I is the solubility enhancement, the solute concentration at saturation relative to its ideal gas value, V_0 and δ_0 are solute molar volume and solubility parameter, respectively, and Δ is the reduced solubility parameter of the compressed gas, δ_g/δ_0.

The direct measurement of I is impractical for large solute molecules since ideal vapor pressures are immeasurably low (estimates of I will be given later). Instead, solubility relative to the maximum value is more appropriate here. From eq 2 this is

$$\ln (I/I_{max}) = -(V_0\delta_0^2/RT)(\Delta - 1)^2 \quad (3)$$

The above equations are approximations which do not adequately allow for density-dependent entropy effects, pressure–volume effects, and the various molecular subtleties which render regular solution theory itself inexact. They are looked to more as a guide to qualitative effects and to rough quantitative estimates, both presently needed in this field.

Experimental Section

The high-pressure apparatus used in this study was basically like that described elsewhere.[12,29] A schematic diagram which helps illustrate the procedure is given in Figure 1. Modifications to the previous apparatus are as follows.

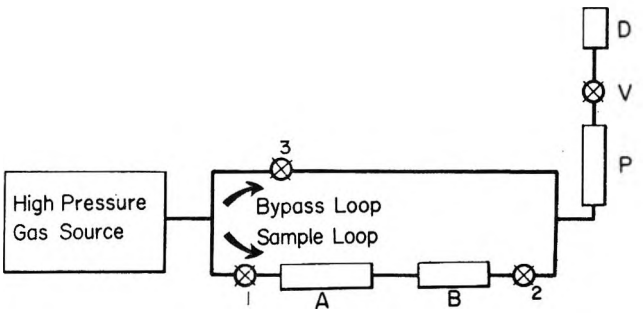

Figure 1. Schematic of high-pressure unit: 1, 2, 3, on–off valves; A, B, sample chambers; P, pyrolysis unit; V, pressure reducing valve; D, detector.

Pyrolysis Unit. It has been pointed out often that the dissolved molecules become thermodynamically unstable upon decompression and tend to condense out.[7,8,12,30] This leads to line clogging and consequently to alteration or stoppage of flow to the detector. It was suggested that pyrolysis at the downstream end of the column prior to decompression may eliminate this difficulty.[12] For this reason a pyrolysis unit was incorporated into the system.

The structure of the pyrolysis unit is shown in Figure 2. It consists of approximately 20 cm of 0.015-cm i.d. stainless steel tubing which is heated to about 650°. The outer tubing acts both as a form on which the heating wire is wound and also as a guard in the event of rupture of the inner tubing. From our experience, such a unit can withstand pressures up to 30,000 psi without failure. This, however, is not true for ammonia, where a few leaks have been encountered.

Pressure Reducing Valve. A new type of valve has been constructed which maintains very stable flow for long periods of time. A detailed description of this valve will appear elsewhere.

Splitter. The splitter and the back pressure regulator have been eliminated because of the availability of controlled flow. Under these conditions the entire sample is swept into the detector.

Detection System. The detector was a Beckman GC-4 flame ionization detector. Provisions were made to ensure constant air and hydrogen supply to the detector. The detector signal was fed into a Cary Model 31 electrometer which was coupled to a Speedomax Type G

(25) G. C. Najour and A. D. King, Jr., *J. Chem. Phys.*, **45**, 1915 (1966).

(26) H. Lehman and E. Ruschitzky, *Chem. Teck.* (Leipzig), **18**, 280 (1966).

(27) A. D. King, *J. Chem. Phys.*, **49**, 4083 (1968).

(28) R. L. Scott and D. V. Fenby, "Annual Review of Physical Chemistry," Vol. 20, H. Eyring, C. J. Christensen, H. S. Johnston, Ed., Annual Reviews, Inc., Palo Alto, Calif., 1969, p 111.

(29) M. N. Myers and J. C. Giddings, *Separation Sci.*, **1**, 761 (1966).

(30) L. McLaren, M. N. Myers, and J. C. Giddings, *Science*, **159**, 197 (1968).

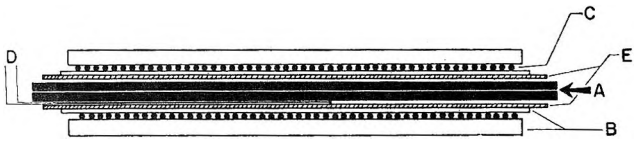

Figure 2. The pyrolysis unit: A, stainless steel tube, 0.006 in. i.d.; B, Fiberglas insulation; C, heating wire; D, thermocouple; E, outer tubing.

recorder. The voltage to the detector was supplied by a 300-V battery. All experiments were carried out at 40 ± 1°.

Solutes. The stearic acid was obtained from Merck and Co., Inc., and the 1-octadecanol from Eastman Kodak. These compounds were recrystallized three times from hot water; only the first portion of solute to crystallize was used. The solutes were then dried, melted, and cooled under vacuum.

The two Carbowaxes (1000 and 4000) were supplied by Applied Science Laboratory.

Experimental Procedure. Prior to each experiment, sample chambers A and B and the tubing between valves 1 and 2 (see Figure 1) were washed with organic solvents, ethanol, and finally distilled water. After drying, the sample chambers were installed and pressurized to 1900 atm. By using valves 1, 2, and 3, the gas was directed through the sample loop and finally into the detector. When the recorder signal dropped to the limit of detectability, it was assumed that organic impurities were adequately purged. The sample chambers were then removed from the system for charging with solute. The sample chambers were filled to capacity, this requiring about 1 cm^3 of solute. They were then returned to the system and pressurized to 1900 atm. Extreme care was taken to avoid contamination during filling.

A plug of solute vapor can be obtained by momentarily routing the gas flow through the sample loop. Plug sampling, however, introduced too much uncertainty into the data. Even with considerable care the peak size varied ±6%.

A superior way for determining solute concentration in the dense gas is by the constant plateau method. Here the carrier gas is flowed steadily through the sample loop for 15–20 min. The recorder trace showed a steep rise followed by a constant plateau. The height of the plateau is proportional to the solute concentration in the carrier gas and to the flow rate, and thus can be used to measure equilibrium concentrations.

The plateau method can be used to check on and correct for the presence of impurities and the possible lack of solubility equilibrium.

Impurities (light hydrocarbons, etc.) were apparent on several occasions, particularly with octadecanol. They were observed and allowed for as follows. Following 30 min of static equilibration, flow causes a steep signal rise, a short plateau, and a slow signal decay to a new plateau. With repetition of this process the initial rise becomes progressively smaller until a true and reproducible plateau trace is obtained. Apparently at this point the volatile impurities have been extracted. This repetition test was made for all systems.

Lack of solubility equilibrium is indicated by a sharp rise, a short plateau, and a decay. Repetition does not lead to a steady plateau. Saturation could be improved by reducing the flow, but this reduces the detector signal. One could also increase the size or length of the sample chamber and sample, thus giving a longer contact time with the carrier gas. It is for this reason that two sample chambers were joined in series in the present study. Sample chamber A can be thought of as a presaturator. Satisfactory saturation was thus achievable with all compounds attempted except Carbowax 6000; the latter was thus not studied further.

Calibration Procedure. To estimate the absolute values of solubilities in compressed gases, the signal size requires calibration. Since the detector responses for the compounds used in this work are unknown, approximate calibration is achieved using the principle that the signal from a flame ionization detector is roughly proportional to the flux of carbon atoms into the flame. A relative response factor, or equivalently, an effective carbon atom number, which accounts for the bonding of carbon atoms to noncarbon atoms, must be employed.

Propane was used as the reference compound. Ten 60-μl peaks were passed through the detector. Assuming the ideal gas law, each peak contained 2.10×10^{-6} mol of propane or 6.29×10^{-6} g-atoms of carbon. From this and the mean area per peak, it was determined that the number of effective gram-atoms of carbon in unit time was equal to

$$\frac{m}{t} = 0.90 \times 10^{-2} R \times E \qquad (4)$$

where R is the recorder response in tenths of an inch and E the electrometer setting in millivolts. The outlet gas flow rate was held constant at 39 cc/min. Assuming the CO_2 to be ideal under outlet (atmospheric) conditions, this corresponds to a CO_2 flux of 2.3×10^{-5} mol/sec. Thus the mole fraction of solute in the dense gas is simply

$$X_2 = 3.0 \times 10^{-8} R \times E/\theta \qquad (5)$$

where θ is the number of effective carbon atoms in the molecule in relationship to detector response.

Pyrolysis Products. The products of the high pressure pyrolysis of Carbowax 4000 were examined by sampling the column effluent into a low-pressure Poropak Q-S column. Pyrolysis constituents were identified by relative retention times.

Results and Discussion

Density Dependence of Solubility. The accurate mea-

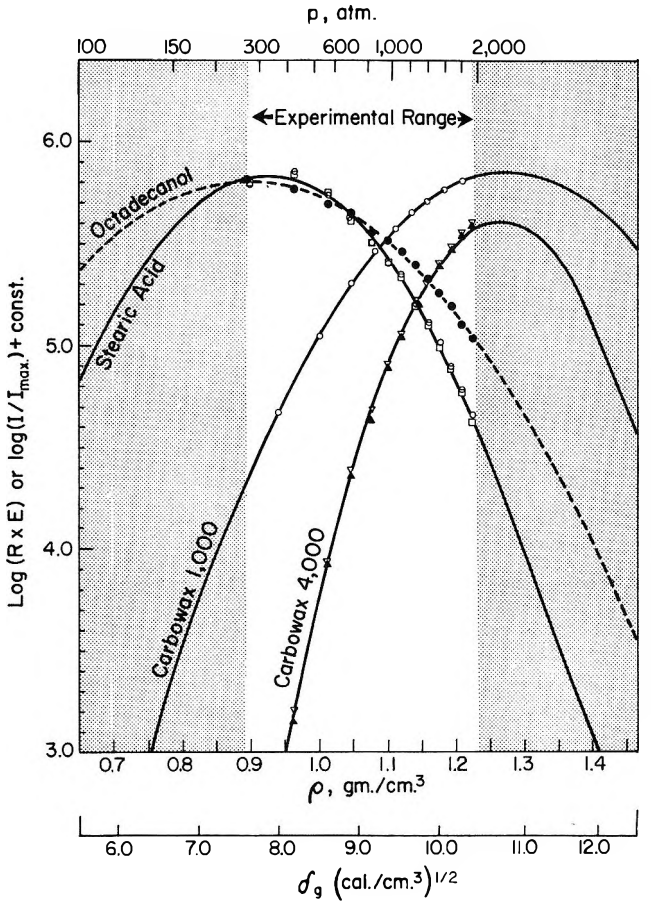

Figure 3. Detector response ($R \times E$) and relative solubility ($X_2/X_{2,max}$) at 40° as a function of CO_2 density, ρ, solubility parameter, δ, and pressure, P.

surement of relative solubility changes in dense gases by our procedure hinges on the assumption that essentially all the solute reaches the detector in some form. However, without pryolysis or with only partial pyrolysis, the dissolved solute would be inclined thermodynamically to condense upon decompression and would perhaps not reach the detector. This tendency has been observed many times.[5,7] Evidence against any significant condensation in our case is the failure of the small flow lines to the detector to plug after prolonged use, including that with a continuous 2-hr, high level Carbowax 4000 plateau at 1900 atm. However, with the pyrolyzer unit unheated the detector signal was very small and the flow fell off rapidly, presumably due to clogging. Thus we conclude that, with pyrolysis, the solute reaches the detector in some form in nearly quantitative amounts.

Figure 3 shows the logarithmic variation of detector response ($R \times E$) with CO_2 density for the four compounds. The curves are also shown as log (I/I_{max}) + constant, equivalent to log ($X_2/X_{2,max}$) + constant, where ($X_2/X_{2,max}$) is the mole fraction of solute relative to its maximum volume and the constant represents vertical displacement depending on θ, eq 5. The heights at the signal maxima are seen to be fairly close to one another.

Also on the abscissa of Figure 3 is a solubility parameter scale and entries for pressure. The pressure–density conversion was made using data for CO_2 found in the literature.[31-35]

The gaseous solubility parameter was calculated from eq 1. When δ_{liq} is approximated by $1.25P_c^{1/2}$ (with P_c in atmospheres) the value 10.7 $(cal/cm^3)^{1/2}$ is obtained. With ρ_{liq} = 1.25 g/cm^3, we have $\delta = 8.54\rho$. This coefficient may be in error up to 10% due to uncertainties in δ_{liq} and ρ_{liq}.

The reproducibility and precision of the data were checked by obtaining two independent sets of data for Carbowax 4000 and stearic acid. As shown in Figure 3, the duplicated experiments yield points lying essentially on top of one another. This is in accord with our observation that the solubility plateau was steady with little tendency to drift.

Equations 2 and 3 are effective expressions for solubility (or solubility enhancement) in volume concentration while our experiments, because a constant mass flux of solvent gas is employed, lead directly to mole fraction solubilities. While the two are not exactly proportional to one another because of variable gas density, a virtual proportionality exists within experimental limits. This occurs because a hundredfold solubility change is induced by a density change of only 5–30%. Therefore we expect, providing solubilities remain fairly small, a parabolic expression for log ($E \times R$) or log (X_2), *i.e.*

$$\log X_2 = a\delta^2 + b\delta + C \tag{6}$$

This equation has been fit to the data, yielding the solid lines in Figure 3. The function seems certainly of the right general form. A comparison of coefficients in eq 2 and 6 yields the apparent molar volume and solubility parameter for solute

$$V_0 = -2.3RTa \tag{7}$$

$$\delta_0 = -b/2a \tag{8}$$

In Table I these experimentally derived quantities are shown in comparison with values obtained independently. This comparison is of some significance and will be discussed at length in the next subsection.

The most novel feature of the results in Figure 3 is the decrease in the solubility of octadecanol and stearic

(31) E. W. Washburn, C. J. West, N. E. Dorsey, F. R. Bichowsky, and A. Klemenc, "International Critical Tables," Vol. 3, McGraw-Hill, New York, N. Y., 1928, p 11.

(32) A. Michels and C. Michels, *Proc. Roy. Soc., Ser. A*, **153**, 201 (1935).

(33) A. Michels, C. Michels, and H. Wouters, *ibid.*, **153**, 214 (1935).

(34) G. C. Kennedy, *Amer. J. Sci.*, **252**, 225 (1954).

(35) A. Michels, A. Botzen, and W. Schuurman, *Physica*, **23**, 95 (1957).

Table I: Solubility Properties of the Four Solutes in CO_2 at 40°

Solute	δ_0(eq 8), (cal/cm³)$^{1/2}$	δ_0(calcd), (cal/cm³)$^{1/2}$	V_0(exptl), cm³	V_0(calcd), cm³	$\epsilon = \frac{V_0(\text{exptl})}{V_0(\text{calcd})}$	I_{max}	X_{max}	Mol wt	P^*, atm	P^* (previous), atm
Carbowax 4000	10.8	10.7 ± 0.9	520	2800	0.186	5.6×10^{54}	2.4×10^{-4}	3350	162	190
Carbowax 1000	10.9	10.7 ± 0.8	206	865	0.238	1.1×10^{21}	1.5×10^{-3}	1000	91	115
Stearic acid	7.9	8.5	257	329	0.780	1.7×10^{17}	1.6×10^{-3}	284	76	
1-Octadecanol	7.6	8.6	136	328	0.416	6.7×10^{8}	1.5×10^{-3}	270		

acid with increasing pressure. This effect, consistent with eq 2 and 3, has not been previously observed.

The apparent existence of maxima in the continuous solubility–density curves of Figure 3 which lead to this peculiar phenomenon are, in fact, analogous to the formation of maxima in solubility–polarity plots with liquid mixtures. The explanation is presumably the same. The excess energy of mixing is a minimum when the cohesive energy densities are roughly equal for solute and solvent. Therefore the dense gas solubility parameter at a given maximum should equal the solubility parameter of the particular solute. This is in accord with eq 2 and 3, and, as we shall see in the next subsection, can be broadly confirmed for our specific group of solutes. Since these solutes have different solubility parameters, the maxima in Figure 3 are horizontally displaced from one another.

Although the present experimental pressure range, 270–1900 atm, is rather broad, it covers a relatively incompressible region well above the critical pressure. Thus the density and solubility parameter vary only about 25% in our experiment. While this has a very large effect on solubility, as Figure 3 illustrates, the limited range makes it difficult to show a clear solubility maximum with both descending branches distinctly exhibited. Nonetheless, the existence of a maximum is rather certain from (a) the shape of the curves in the experimental range, and (b) the fact that octadecanol and stearic acid are effectively nonvolatile at low pressures and must therefore have a descending branch on the left to complement the observed one on the right. In fact, previous work has been done with octadecanol on other instrumentation which shows a threshold pressure of 98.7 atm.[13] This is equivalent to another point (actually a cluster of points) on the plot at (0, 4.8). Such an addition clearly requires a maximum in the solubility curve.

Figure 3 shows that the solubility peaks differ in width. From eq 2 it can be shown that the half-width is

$$\delta_2 - \delta_{2,max} = \left[\frac{2.3RT}{V_0}(\log I_{max} - \log I)\right]^{1/2} \quad (9)$$

so that the width at any level below the peak maximum is related to solute mole volume as $V_0^{-1/2}$. Thus larger molecules have narrower solubility peaks, as strikingly confirmed by the Carbowax 4000 and 1000 peaks in Figure 3. This is another instance where liquid and dense gas solubility phenomena follow parallel trends.

Solubility Enhancement. The enhancement in solubility (or volatility) relative to that for the ideal gas reaches very large proportions. At the solubility maximum it is given by

$$I_{max} = \exp(V_0\delta_0^2/RT) \quad (10)$$

Values of I_{max} are tabulated in Table I. For Carbowax 4000 the maximum enhancement is seen to be in excess of 10^{50}, reflecting mainly its extremely low vapor pressure under ideal conditions.

Absolute Solubility. The absolute magnitude of the equilibrium solute concentration can be approximated using the calibration procedure mentioned earlier. However, some uncertainty exists because of the need to estimate effective carbon numbers (θ in eq 5). For stearic acid and octadecanol we assumed θ as the number of carbon atoms in the molecule minus one, the excluded one corresponding to a carbon presumably tied up in nondetectable form (CO_2 or CO) in the pyrolysis products. For Carbowax 4000 (mean molecular weight, 3350) we assumed $\theta = 75$, the other half of the carbon atoms again presumably tied up in nondetectable form.

The results for the mole fraction of solute at the solubility peak, X_{max}, calculated from eq 5, are shown in Table I. Solubilities at other δ values may be calculated from eq 6 or obtained from the relative solubility plots in Figure 3.

Threshold Pressures. Of great experimental importance, particularly to gas chromatography, is the threshold pressure, P^*, the applied pressure which is barely sufficient to bring volatility to a measurable level. Since the solubility is an extremely steep function of pressure for large molecules, this parameter is nearly constant with reasonable variations in the sensitivity of the detection device.

For the present system, $R \times E = 1$ serves as the lowest limit of detection. Since none of the measurements was made near the threshold level, the latter was calculated assuming a parabolic dependence of the solubility signal on δ as in eq 6. Conversion from the obtained δ value to density and then to pressure yields the P^* values shown in Table I. Values obtained pre-

viously on a different apparatus are shown in the subsequent column. The agreement is satisfactory.

It is interesting that the present theory predicts two threshold pressures, only the lower of which has been observed. Gas densities necessary to reach the upper threshold are impractical with most systems, but clearly exceptions exist which should be experimentally tractable.

Pyrolysis Products. Methane was the major detectable pyrolysis product for Carbowax 4000. The methane peak was followed by ethane and ethylene peaks in slightly smaller amounts. There were then several minor peaks of propane, propylene, etc. Only slight shifts in the pyrolysis pattern were noted with a twofold change in flow. The pattern was also rather stable with changes in the age of the pyrolyzer.

Effective Solubility Parameters and Volumes. The solubility parameters in columns 2 and 3 of Table I are obtained from eq 8 in combination with the experimental data and from independent calculations, respectively. The calculated δ_0 for stearic acid was obtained from data given by Beerbower and Dickey;[36] values for 1-octadecanol and the Carbowaxes were calculated by known procedures.[37,38] The Carbowax δ_0's appear as a range because of the uncertainty in the oxygen contribution. Small suggests a contribution of 70 (cal ml)$^{1/2}$.[37] Available V_0 and δ_0 values[37-39] suggest that the ether oxygen contribution varies drastically with molecular size and shape. Molecules such as dioxane and triethylene glycol suggest values in the neighborhood of 140 (cal ml)$^{1/2}$. Use of 70 and 140 (cal ml)$^{1/2}$ gives the lower and upper limits, respectively, of δ_0(calcd) for the Carbowaxes in Table I. The agreement between experimental and calculated δ_0 values is excellent considering the inherent uncertainties in both values and in the underlying theory. In particular the relative displacement of the Carbowax maximum upscale from that for 1-octadecanol and stearic acid in Figure 3 is exactly as predicted.

The agreement on molar volume, columns 4 and 5 of Table I, is far less satisfactory. To a degree such discrepancies are consistent with studies of liquid mixtures. "Effective volume" parameters have been used to account for molecular shape differences. Martire defines the parameter ϵ where $\epsilon = V_0^*/V_0$, the ratio of effective to actual volumes.[40,41] His ϵ values for several solutes were in the range 0.74–1.0. Values less than unity also occur for our solutes, column 6.

A plot of log ϵ *vs.* (mol wt)$^{-1}$, shown in Figure 4, yields a straight line, again with the exception of stearic acid. If stearic acid were "normal" on this plot its ϵ value would be 0.390 and its "experimental" volume thus 129 cm^3. Actual values are twice this, suggesting dimer formation in the dense gas phase. The stearic acid points in Figure 4 are based on the assumption of dimer formation.

The reason for the considerable departure of ϵ from unity is not clear. Martire[40] found this parameter to be independent of the particular solvent in a given class. He also attempted to correlate the ϵ values with the solution process. From solution–density measurements carried out at various concentrations, he showed that the partial molar volumes at infinite dilution were close to the pure solute molar volumes and that no apparent correlation existed with the ϵ values.

The present results, Figure 4, indicate that the ϵ values do not vary in a random manner for the large solute species dealt with here, and that they can be related to the molecular weight. However there is no obvious theoretical basis for the empirical straight line correlation between log ϵ and (mol wt)$^{-1}$.

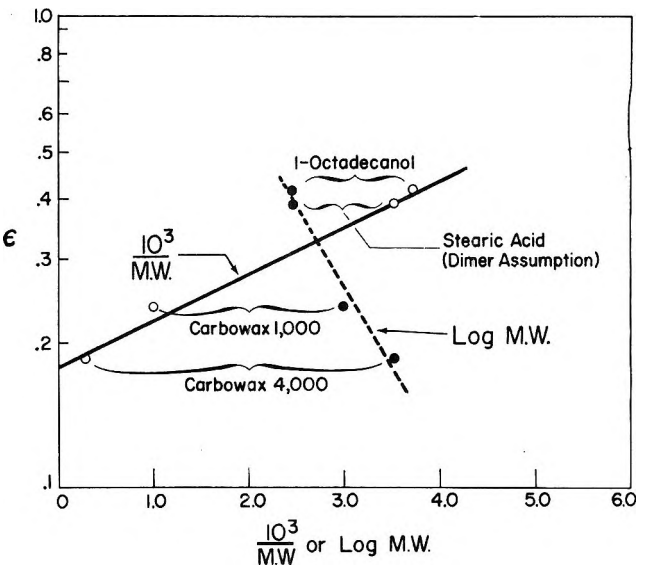

Figure 4. Correlation of $\epsilon = [V_0(\text{exptl})/V_0(\text{calcd})]$ with molecular weight.

It is possible that ϵ is consistently less than unity for large molecules because the latter, in a poor solvent, will tend to form intramolecular contacts in place of solute–solvent contacts. A reduced energy of mixing will be associated with the reduced number of contacts, leading to enhancement of the expected solubility. This is precisely the effect of $\epsilon < 1$. In the limit the solute molecules will assume a spherical form, and since intermolecular energy can be associated with inter-

(36) A. Beerbower and J. R. Dickey, ASLE Preprint, Lubrication Conference, Oct 8–10, 1968.

(37) P. A. Small, *J. Appl. Chem.*, **3**, 71 (1953).

(38) J. L. Gardon, "Encyclopedia of Polymer Science and Technology," Vol. 3, H. F. Mark, N. G. Gaylord, and N. M. Bikales, Ed., Interscience, New York, N. Y., 1965, p 833.

(39) A. E. Rheineck and K. F. Lin, *J. Paint Technol.*, **40**, 611 (1968).

(40) D. E. Martire, "Gas Chromatography," L. Fowler, Ed., Academic Press, New York, N. Y., 1963, p 33.

(41) D. E. Martire, "Gas Chromatography, 1966," A. B. Littlewood, Ed., Institute of Petroleum, London, 1967, p 21.

(42) P. J. Flory, *J. Amer. Chem. Soc.*, **87**, 1833 (1965).

facial contacts,[42] ϵ may approach the ratio of the respective surface areas of a sphere and an extended chain. In this case ϵ should be in proportion to (mol wt)$^{-1/3}$ and a plot of log ϵ *vs.* log M should form a straight line of slope $-1/3$. Figure 4, in which the dashed line has $-1/3$ slope, demonstrates reasonable agreement with this hypothesis. However, more evidence is needed before any firm conclusions about the phenomenon can be made.

Acknowledgment. This work was supported by Public Health Service Research Grant GM 10851-13 from the National Institutes of Health. J. J. C. acknowledges support from the National Research Council of Canada for a postdoctoral fellowship.

The Adsorption of Anions at the Solid–Solution Interface. An Ellipsometric Study

by Woon-kie Paik, Marvin A. Genshaw, and John O'M. Bockris*

The Electrochemistry Laboratory, The University of Pennsylvania, Philadelphia, Pennsylvania 19104
(Received April 14, 1970)

Effects of adsorbed anions at the metal–electrolyte interface on the polarization state of reflected light were observed by means of ellipsometry. The systems studied include aqueous solutions of sodium salts of Cl^-, Br^-, ClO_4^-, SO_4^{2-}, and OH^- with Ag, Au, Rh, and Ni as electrodes. Degrees of adsorption of ions were calculated from the observed optical effects as functions of potential. In the calculation, a correction for the effect of electrode charge on the optical properties of metals was included. The adsorption of anions on all metals increased in the order: $ClO_4^- < SO_4^{2-} < Cl^- < Br^-$. The halide ions were observed to adsorb strongly on silver and gold electrodes. The nature of forces involved in ionic adsorption is discussed.

Introduction

There has been recently an interest in the employment of ellipsometry for the study of electrode processes. Ellipsometry has been used in the investigations of oxidation–passivation phenomena for metals.[1-5]

More recently, Chiu and Genshaw have shown that this technique can also be applied to the quantitative measurement of contact (specific) adsorption of ions on mercury[6] and platinum[7] electrodes. Contemporaneously, Stedman[8] also calculated the effect of adsorbed ions in the electrical double layer, including the diffuse part of the double layer, on the optical parameters measurable by ellipsometry.

Measurement of ionic adsorption in the double layer is needed as a basis of knowledge of the electrical double layer at solid–solution interfaces. The ellipsometric method has fewer limitations than do other methods[7,9,10] for this measurement. In ellipsometry, a complication is due to an effect of electric charge on the metal and the concentration of electrons near the interface.[11] However, it is possible to correct for this effect.

The purpose of the present work is to apply ellipsometric measurement to the adsorption of Cl^-, Br^-, OH^-, SO_4^{2-}, and ClO_4^- from solution onto gold, silver, nickel, and rhodium.

Theory of the Calculations

1. Ellipsometry of Adsorption. When plane-polarized light is reflected from a film-covered metal surface, the two components of the light, perpendicular and parallel to the plane of incidence, are reflected with different amplitude reductions and phases. The ratio of the complex reflection coefficients of the parallel

* To whom correspondence should be addressed.

(1) A. K. N. Reddy and J. O'M. Bockris in "Ellipsometry in the Measurement of Surfaces and Thin Films, Symposium Proceedings, Washington, 1963, U. S. Department of Commerce," E. Passaglia, R. R. Stromberg, and J. Kruger, Ed., National Bureau of Standards Miscellaneous Publication 256, U. S. Government Printing Office, Washington, D. C., 1964, p 229.

(2) J. Kruger, ref 1, p 131.

(3) J. O'M. Bockris, A. K. N. Reddy, and B. Rao, *J. Electrochem. Soc.*, 113, 1132 (1966).

(4) A. K. N. Reddy, M. A. Genshaw, and J. O'M. Bockris, *J. Chem. Phys.*, 48, 671 (1968).

(5) R. S. Sirohi and M. A. Genshaw, *J. Electrochem. Soc.*, 116, 910 (1969).

(6) Y. C. Chiu and M. A. Genshaw, *J. Phys. Chem.*, 72, 4325 (1968).

(7) Y. C. Chiu and M. A. Genshaw, *ibid.*, 73, 3571 (1969).

(8) M. Stedman, *Chem. Phys. Lett.*, 2, 457 (1968).

(9) N. A. Balashova and V. E. Kazarinov, *Usp. Khim.*, 34, 1721 (1965).

(10) S. Gilman, *J. Phys. Chem.*, 68, 2098 2112 (1964).

(11) W. N. Hansen and A. Prostak, *Phys. Rev.*, 174, 500 (1968).

($R_{||}$) and perpendicular ($R_{\perp}$) components of light defines the relative amplitude reduction tan Ψ and the relative phase retardation Δ as

$$\tan \Psi \cdot e^{i\Delta} = \frac{R_{||}}{R_{\perp}} \tag{1}$$

Ψ and Δ are the experimentally measured quantities.

This ratio is related to the refractive index, n_1, of the ambient medium (electrolyte solution in the present case); the complex refractive indices of the film and the substrate metal, $\hat{n}_2$ and $\hat{n}_3$; the thickness of the film, τ; wavelength, λ; and angle of incidence, ϕ.

$$\tan \Psi \cdot e^{i\Delta} = f(n_1, \hat{n}_2, \hat{n}_3, \lambda, \tau, \phi) \tag{2}$$

The functional form of f can be found, *e.g.*, in McCrackin and Colson[12] or Heavens.[13] In the case of a dielectric film (of which refractive index is real and, hence, denoted by n_2) covering the metal surface (as in the case of ionic adsorption), by computing Ψ and Δ from eq 2 using different set of film parameters, n_2 and τ, it is possible to correlate n_2 and τ with the experimentally observed Ψ and Δ.

However, when τ is very small (a few ångstroms) and n_2 not very different from n_1, as in the case of an adsorbed ion layer on the electrode in solution, it would be necessary, in order to determine τ and n_2 from eq 2, to have extremely accurate values of Ψ and Δ, along with other parameters beyond the practical limitations of present experimental techniques.

But by using a modified technique,[6,7] which is described in the Experimental Section, it is possible to measure small changes in one of the parameters, Δ or Ψ, with a precision of $\sim$0.002°. In an optical model for calculating adsorption in the submonolayer region, the thickness of the submonolayer can be taken as a constant, determined by geometry of the adsorbing ions or molecules, only n_2 being changed as a function of the relative coverage.

Thus, if a change in Δ or Ψ is measured as adsorption takes place, n_2 can be obtained with the assumed value of τ. In this paper, Δ is chosen as the observable quantity since it is changed more rapidly by a thin film than is Ψ.

To correlate n_2 to the amount of adsorption, one proceeds as follows. The Lorenz–Lorentz equation can be written in the form

$$NR = \frac{n^2 - 1}{n^2 + 2} \tag{3}$$

where N is the number of moles in unit volume of a medium with molar refraction R.

It is assumed that molar refraction of the layer of adsorbed ions (i) and water (w) can be taken as a linear combination of the molar refractions of the ions (R_i) and water (R_w), thus

$$N_i R_i + N_w R_w = \frac{n_2^2 - 1}{n_2^2 + 2} \tag{4}$$

where N_i and N_w are the numbers of moles of the two species in unit volume of the mixture layer. n_2 is the resultant refractive index of the adsorbed layer which is composed of ions and water molecules.

If the fraction of surface covered by ions is denoted by θ

$$N_i = \theta N_i', \; N_w = (1 - \theta) N_w' \tag{5}$$

where N_i' and N_w' are the N_i and N_w values for $\theta = 1$ and $\theta = 0$, respectively. If S_i is the covered area of the electrode per ion, N_A is the Avogadro's number, V_w is the molar volume of water, and τ_i is the thickness of the adsorbed layer, one has

$$N_i' = \frac{1}{S_i \tau_i N_A} \text{ (mol cm}^{-2}\text{)}$$
$$N_w' = \frac{1}{V_w} \text{ (mol cm}^{-3}\text{)} \tag{6}$$

Then

$$\frac{\theta R_i}{S_i \tau_i N_A} + (1 - \theta)\frac{R_w}{V_w} = \frac{n_2^2 - 1}{n_2^2 + 2} \tag{7}$$

We also have, when there are anions as adsorbate

$$\theta = q_-/q_{-,\text{sat}} \tag{8}$$

where q_- is the amount of adsorbed anions in units of charge, $q_{-,\text{sat}}$ is the value of q_- at the full coverage, which can be equated to e/S_i, e being the electronic charge. S_i and τ_i are calculated for individual ions in the Appendix. Equations 7 and 8 enable us to obtain q_-.

In deriving eq 7, we used a model in which all the adsorbed ions are assumed to be in a layer of thickness τ_i which is the layer in which the contact adsorption occurs, but any surface excess of ions, regardless of its degree of separation from the metal, will contribute to the over-all effect on the reflected light. A suitable optical model for the entire double layer would be an inhomogeneous film in which the index of refraction varies in the direction perpendicular to the plane of the film. McCrackin and Colson[12] showed that for such an inhomogeneous film the ellispometer readings are directly related to the integral $\int \Delta n \, d\tau$ where Δn is the difference between the refractive index of a layer of thickness $d\tau$ and the refractive index of the surrounding medium. Since Δn is proportional to the excess concentration of adsorbed ions, Δc, the above integral is proportional to the integral $\int \Delta c \, d\tau$, which is the total amount of the surface excess per unit area of the surface. [Equation 7 does not contradict this proportionality as

(12) F. L. McCrackin and J. P. Colson, ref 1, p 61.

(13) O. S. Heavens, 'Optical Properties of Thin Solid Films,' Butterworths, New York, N. Y., and London, 1955, pp 125, 126.

Table I: Electromodulation Coefficients of Metals, b (Eq 14), for the Reflection of Light of 5500 Å

Metal	Au	Ag	Pt	Ni	Rh	Hg
ϕ, deg	64.20	64.20	72.12	64.20	72.12	68.20
n	0.331	0.055	2.45	1.685	1.62	1.21
k	2.324	3.32	3.46	3.130	4.63	4.02
$-b$, deg μC^{-1} cm^2	0.0042	0.0029	0.0010	0.0017	0.0017	0.0021

can be shown by expanding (7) into the polynomial $n_2 = f(\theta)$, the term in θ^2 is negligibly small.] Therefore, the ellipsometer readings are determined by this total surface excess, not by the manner in which the excess is distributed along the axis perpendicular to the surface. Hence, the ellipsometer readings that would result from the actual distribution of surface excess ions would be very close to those calculated assuming that all the ions are located in the contact adsorption layer.

Therefore, q_- calculated from the ellipsometric reading ($\delta\Delta$) as outlined above using eq 2, 7, and 8 is approximately the total amount of the adsorbed anions. Thus

$$q_- = q_-^{s} + q_-^{d} \tag{9}$$

where q_-^{s} and q_-^{d} are the amounts of ions adsorbed in the contact and the diffuse layers, respectively.

2. Electromodulation of Metals. In the above treatment there has been a tacit assumption that the intrinsic properties of the metal do not change with change of the excess electrostatic charge upon it. However, there have been reports of changing optical properties of metal electrodes due to changing potential.[11,14] Hansen[11] interpreted this phenomenon in terms of changes in electron density in the surface layer. He predicted this "electromodulation" effect would be large for metals such as Au, Ag, and Cu. From the electron theory of matter the dielectric constant $\hat{\epsilon}$, of a metal at a frequency ω is given by[15,16]

$$\hat{\epsilon} \equiv \hat{n}^2 = 1 + \frac{4\pi N_e e^2/m}{-\omega^2 + i\beta\omega} + \sum_j \frac{4\pi N_j e^2/m}{\omega_j^2 - \omega^2 + i\beta_j\omega} \tag{10}$$

where N_e is the number of free electrons per cubic centimeter, e is the electronic charge, m is the mass of the electrons, and β is the "friction coefficient due to the scattering of electrons. [The conventions adopted here for the mathematical formulation are $\hat{n} \equiv n - ik$; $E = E_0 e^{+i(\omega t - \hat{n}\,\omega/c\,x)}$. Note: β terms in eq 10 have a + sign with these conventions.] N_j, ω_j, and β_j stand for the number of electrons per cubic centimeter, resonance frequency, and friction coefficient, respectively, of the jth bound electron and the summation is over all the bound electrons. The second term in eq 10, which is the contribution from the free electrons, is changed on charging the metal electrically because the charge will alter N_e. The effect of this charge on $\hat{\epsilon}$ and, hence, on Δ or Ψ, can be calculated. Such calculations are made for the metals of interest in the following way. Using the identity $\hat{n} = n - ik$, eq 10 can be written in the form

$$(n - ik)^2 = 1 - \frac{4\pi N_e e^2/m}{\omega^2 - i\beta\omega} + Z \tag{11}$$

where Z replaces the summation over the bound electrons. Equating real and imaginary parts we obtain

$$n^2 - k^2 = 1 - \frac{4\pi N_e e^2/m}{\omega^2 + \beta^2} + Z_{\text{real}}$$
$$2nk = \frac{4\pi N_e e^2\beta/m}{\omega^3 + \beta^2\omega} + Z_{\text{imag}} \tag{12}$$

Suppose a surface layer of arbitrary thickness of the metal attains a charge density σ; then the optical constants of this layer, n' and k', will be related, from eq 12, to the corresponding constants of the uncharged metal, n and k, by

$$n'^2 - k'^2 = n^2 - k^2 - \frac{4\pi e^2/m}{\omega^2 + \beta^2}\delta N_e$$
$$2n'k' = 2nk + \frac{4\pi e^2\beta/m}{\omega^3 + \beta^2\omega}\delta N_e \tag{13}$$

where $\delta N_e = \sigma/e$. An approximate value of β can be obtained from the n and k values of the metal using eq 12 neglecting Z_{real} and Z_{imag} terms. σ is q_M/d where q_M is the charge per square centimeter of metal surface and d is the thickness of the surface layer of the metal. In reality, σ will be a complicated function of distance from the surface. As a trial a slab of arbitrary thickness on the surface is assumed to contain all the excess charge. Thus, n' and k' of this slab were calculated from eq 13 (*cf.* Table I). The effect of this slab on Δ (and Ψ) of the reflected light is obtained through the ellipsometric calculations using eq 2 with $\hat{n}_2$ replaced by $n' - ik'$ (disregarding the adsorption for this calculation). Different thicknesses ranging from 3 to 50 Å for the

(14) J. Feinleib, *Phys. Rev. Lett.*, **16**, 1200 (1966).

(15) R. K. Wangsness, "Introduction to Theoretical Physics, Classical Mechanics and Electrodynamics," Wiley, New York, N. Y., 1963, p 360.

(16) (a) C. Kittel, "Introduction to Solid State Physics," 3rd ed, Wiley, New York, N. Y., 1966, pp 228–398; (b) A. V. Sokolov, "Optical Properties of Metals," American Elsevier, New York, N. Y., 1967, pp 65–77.

excess charge on the metal were tried, and there was little dependence on thickness (less than 20% of change on going from 3 to 50 Å). Thus the actual distribution of the excess charge inside the metal does not make a significant difference to the effect on Δ (denoted by $\delta\Delta_{\text{modln}}$), only the total amount of charge being important.

It was found that Δ_{modln} is nearly a linear function of q_M for the range of values of q_M from -20 to 100 μC

$$\delta\Delta_{\text{modln}} = b\delta q_M \tag{14}$$

cm^{-2}. The calculated values of b's are tabulated in Table I, along with the unmodulated n and k values.

From the values of b in Table I it is evident that for none of the metals would $\delta\Delta_{\text{modln}}$ be negligible for δq_M of, say, 10 μC cm^{-2}. $\delta\Delta_{\text{modln}}$ would be particularly large for Au and Ag, and whenever the double layer capacitance is large.

A $\delta\Delta$ value that is experimentally obtained from the electrolyte–metal interface would be a sum of this electromodulation effect and the ion adsorption effect

$$\begin{aligned}\delta\alpha_{\text{obsd}} &= \delta\Delta_{\text{ads}} + \delta\Delta_{\text{modln}} \\ &= \delta\Delta_{\text{ads}}(q_-) + b\delta q_M\end{aligned} \tag{15}$$

Both the terms in the above are negative. Thus, if the correction is not made for the electromodulation effect, an increasingly positive charge upon the electrode may indicate a negative error in the $\delta\Delta$ values, *i.e.*, may introduce a positive error in the amount of adsorption as measured ellipsometrically. Therefore, $\delta\Delta_{\text{ads}}$ must be separated for use in eq 2 to calculate n_2. Then θ and q_- are obtained by eq 7 and 8 using n_2.

Experimental Section

Gold and silver electrodes were prepared by vacuum deposition of the metals onto microscope slides. Rhodium could not practically be evaporated and was prepared by the technique of deposition by "sputtering"[17] *in vacuo*. Sputter-deposited nickel electrodes did not have desirable electrochemical and optical properties, probably due to porosity, and hence, mechanically polished electrodes were used. The electrochemical cleaning of the electrode was carried out after polishing by applying an anodic, succeeded by a cathodic, potential. The electrolytes studied were sodium salts of chloride, bromide, perchlorate, sulfate, and hydroxide of concentrations in the range of 10^{-3} to 10^{-1} N in conductance water, the pH of which was adjusted to 3.0 with perchloric or sulfuric acid, except for the solution of NaOH. Sodium was chosen as the cation because it is nonadsorbable on mercury and even adsorbed sodium ions would probably not cause a significant change in the optical properties of the double layer because of the low value of their molar refractivity.[18,19] The experimental setup of the cell and the ellipsometer was arranged as shown in Figure 1. It was aimed to make

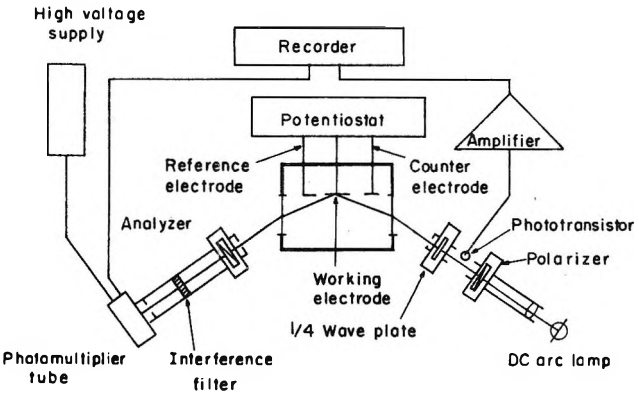

Figure 1. Experimental setup for the ellipsometric study of ion adsorption.

precise measurements of $\delta\Delta$ beyond the resolution of the classically arranged ellipsometer (0.02°).

When the polarizer and the analyzer are set to the extinction positions, P_0 and A_0, respectively, the intensity of light reaching the photomultiplier tube is minimal. If the polarizer is off the extinction position by a few degrees, the intensity changes with changing P_0.[20] Since $\delta\Delta = \pm 2\delta P_0$, it is possible to measure small changes in Δ by the measurement of the corresponding change of intensity.

[This relation holds for the arrangement of ellipsometer in which the $^1/_4$ wave plate is oriented at 45° in the path of the incident light beam.]

The method used was similar to that of Chiu and Genshaw for measurement on platinum electrode,[7] but in the present work an improvement has been made which was necessitated by a sporadic variation in the intensity produced by the tungsten arc source. The modification is shown in Figure 1 and consists of a phototransistor, in the path of the incident light beam, linked with an amplifier. By recording the difference between the signals from the two light detectors after proper amplification, only the changes in the light wrought by the interaction of the light with the substrate are seen, the fluctuation of the source light being completely compensated. In this way it was possible to resolve 0.002° of $\delta\Delta$.

A wavelength of 5500 Å was selected by an interference filter. Observations were made after a few cycles of potential sweep in which the electrode was oxidized and then reduced to eliminate possible organic contaminations and surface oxides. The electrode potential was changed manually by steps of 100 mV in anodic and cathodic directions, avoiding oxide-forming or dissolution-causing potentials and the hydrogen evolution

(17) B. D. Cahan, Thesis, University of Pennsylvania, 1968.
(18) A. Heydweiller, *Phys Z.*, **26**, 526 (1925).
(19) T. C. Waddington, *Trans. Faraday Soc.*, **62**, 1482 (1966).
(20) V. Brusic, M. A. Genshaw, and B. D. Cahan, *J. Appl. Opt.*, **9**, 1634 (1970).

Table II: Relative Phase Retardation with an Ag Electrode in ClO_4^- and Cl^- Solutions; Angle of Incidence, 64.20°

Potential, V vs. nhe	$-\delta\Delta_{obsd}$, deg					
	10^{-3} N ClO_4	10^{-2} N ClO_4	10^{-1} N ClO_4	10^{-3} N Cl^-	10^{-2} N Cl^-	10^{-1} N Cl^-
−0.385	0	0.002	0	0.008	0.010	0.018
−0.285	0.002	0.010	0.018	0.016	0.034	0.061
−0.185	0.024	0.036	0.038	0.045	0.076	0.130
−0.085	0.041	0.059	0.061	0.099	0.155	0.206
+0.015	0.070	0.082	0.086	0.166	0.233	0.284
0.115	0.098	0.108	0.111	0.23	0.308	0.361
0.215	0.132	0.138	0.140	0.286	0.381	0.474
0.315	0.15	0.159	0.17	0.35	0.457	
0.415	0.172	0.182	0.201	0.413		
0.515	0.198	0.206				

region. After each step of potential, about 1 min was allowed for attaining a steady state.

During measurements, solutions were stirred by bubbling with prepurified nitrogen, which also served to reduce the oxygen content of the solution.

Results and Analysis

A typical set of relative phase retardation data, $\delta\Delta$, is presented in Table II.

In most systems there was hysteresis in the value of Δ depending on the direction of potential change corresponding to adsorption and desorption conditions. This is in accordance with the observations on platinum by Chiu and Genshaw.[7] Averages are taken from the Δ values obtained with increasing and decreasing potentials.

$\delta\Delta$'s obtained with rhodium electrode in ClO_4^-, SO_4^{2-}, and OH^- solutions and with all metals in OH^- solutions are not taken as the results of ionic adsorption for the reasons discussed later and, hence, are not used in calculating the amount of ionic adsorption.

The nickel electrode in perchlorate, sulfate, and hydroxide solutions did not show appreciable change in Δ within the potential range available for the double layer study, which is limited by hydrogen evolution at and oxidation of the electrode.

For the calculation of the amount of adsorption of ions by means of eq 2, 7, 8, and 15, it is necessary to have double-layer capacitance data for the systems of interest because the $\delta\Delta_{modln}$ term includes q_M (eq 15) while the experiment was carried out under controlled potentials instead of controlled charge on the electrodes. Available double-layer capacitance data are very limited for most solid–electrolyte systems. For nickel and rhodium electrodes, the potential ranges studied were narrow because of the proximity of oxidation and hydrogen evolution potentials. $\delta\Delta$ values in these ranges were small. Thus, neither of the terms in eq 15 can be large; *i.e.*, both adsorption and electromodulation are small on these electrodes. Therefore, a constant capacitance of 14 μF cm^{-2} was assumed. R_i's of individual ions are found in ref 18. The resultant q_- values are plotted against potential in Figure 2.

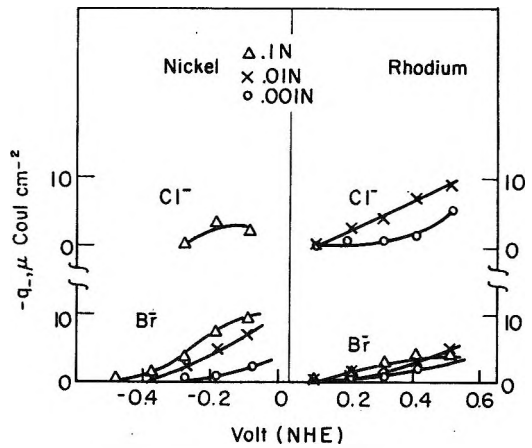

Figure 2. Anion adsorption on Ni and Rh electrodes.

For gold and silver electrodes, however, such an assumption of constant capacitance independent of potential cannot be justified, even as a crude approximation, because of the wider ranges of potential studied and the fact that capacitance can change drastically with anions present in the anodic potential regions. Therefore, on these two metals the following scheme of approximation was adopted.

In the concentration range studied the change in q_M will approximately parallel that of q_- with the sign changed. Thus

$$\delta q_M = -\alpha \delta q_- \qquad (16)$$

α being constant. It is not unreasonable to expect that α values of the solid metal–electrolyte systems would be close to those of mercury–electrolyte systems. α of mercury electrode in chloride,[21] bromide,[22] sulfate,[23] and

(21) (a) H. Wroblowa, Z. Kovac, and J. O'M. Bockris, *Trans. Faraday Soc.*, **61**, 1523 (1965); (b) Z. Kovac, Thesis, University of Pennsylvania, 1964.

(22) J. Lawrence, R. Parsons, and R. Payne, *J. Electroanal. Chem.*, **16**, 193 (1968).

(23) D. C. Grahame and B. A. Soderberg, *J. Chem. Phys.*, **22**, 449 (1954).

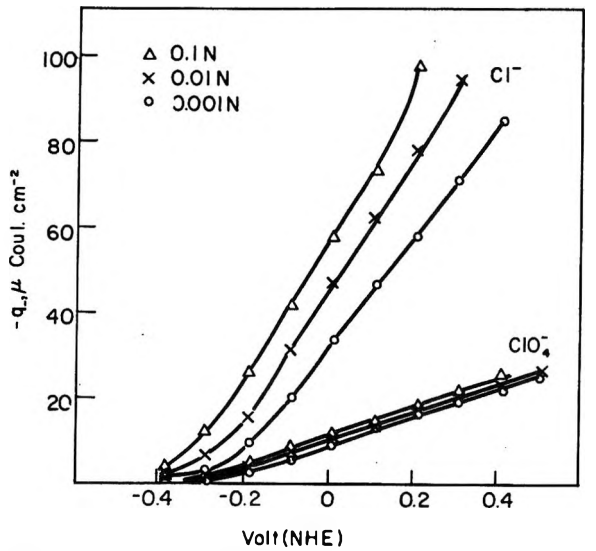

Figure 3. Adsorption of Cl^- and ClO_4^- ions on Ag electrode.

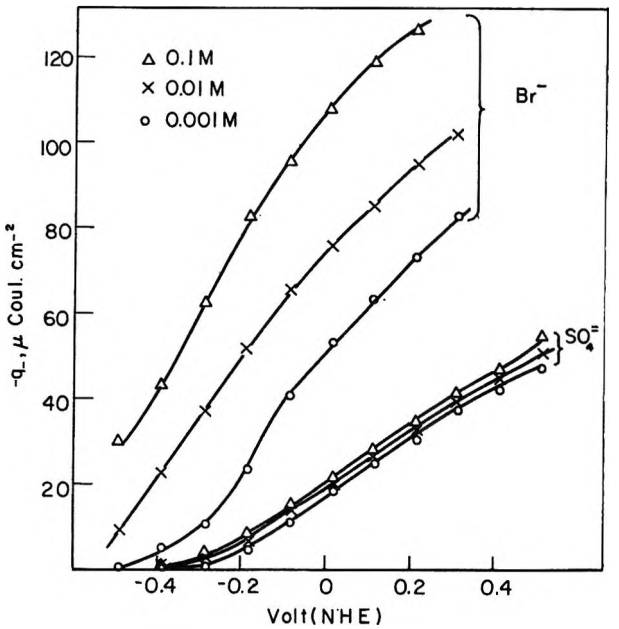

Figure 4. Adsorption of SO_4^{2-} and Br^- ions on Ag electrode.

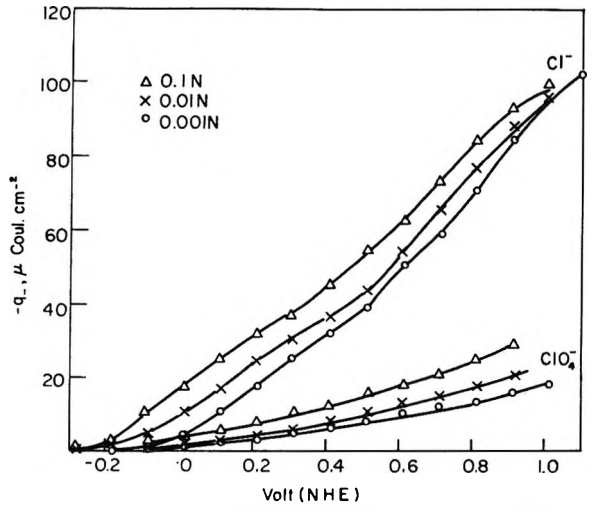

Figure 5. Adsorption of ClO_4^- and Cl^- ions on Au electrode.

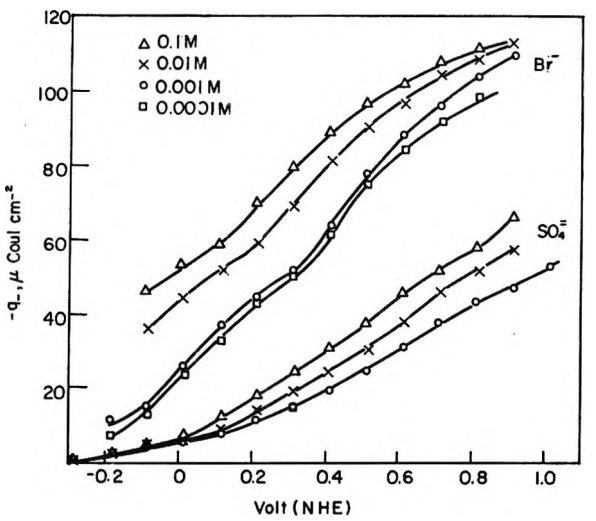

Figure 6. Adsorption of SO_4^{2-} and Br^- ions on Au electrode.

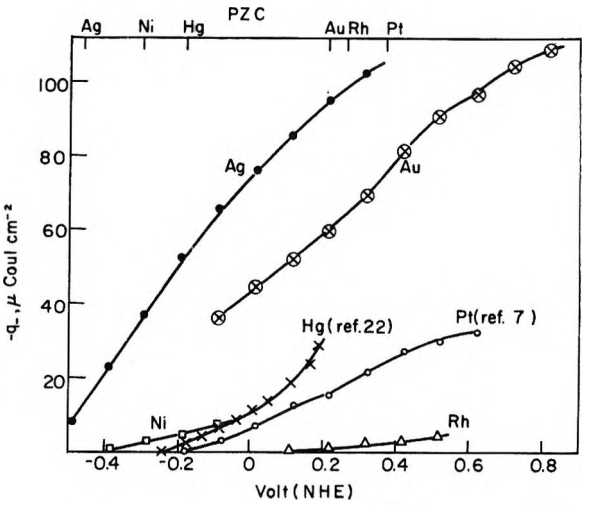

Figure 7. Adsorption of Br^- ions from 10^{-2} M Br^- solutions on different metals.

perchlorate[21] solutions are 1.0, 0.77, 1.1, and 2.0, respectively (they vary little with concentration). These values of α were used to compute the adsorption for gold and silver electrodes. The results are shown in Figures 3–6.

Some of the features of these results can be summarized as follows (for comparison, facts known for Hg and Pt electrodes are included). (1) Anions adsorb on different metals to very different degrees (see Figures 7, 8, and 9). (2) The potentials of electrodes (on the nhe scale) of different metals at which anions adsorb to an appreciable extent increase in the order Ag < Au < Ni < Hg < Pt < Rh (Figures 7, 8, and 9). (3) Adsorbability of anions as measured by $(q_-)_v$ increases in the order $ClO_4^- < SO_4^{2-} < Cl^- < Br^-$ (Figures 10 and 11) (If the number of ions per square centimeter, instead of charge per square centimeter, is used as the measure of adsorption then the order would be $ClO_4^- \cong SO_4^{2-} \ll Cl^- < Br^-$.) (4) At low degrees of

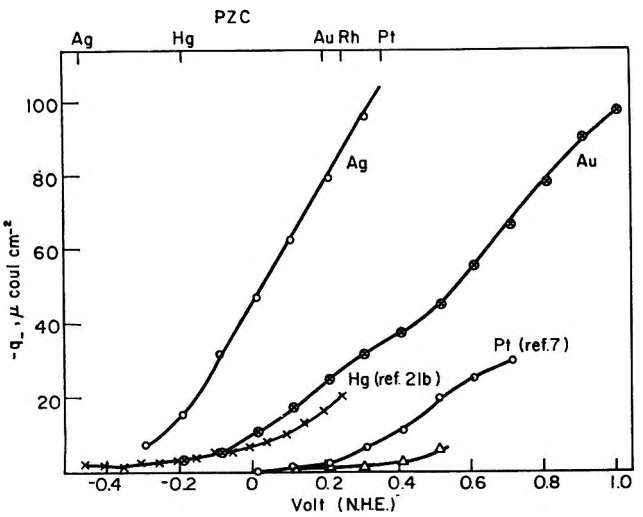

Figure 8. Adsorption of Cl^- ions from 10^{-2} M Cl^- solutions on different metals.

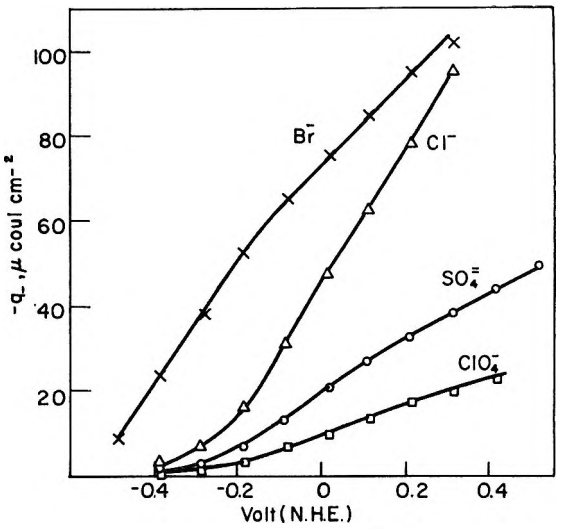

Figure 10. Adsorption of anions from 10^{-2} M solutions on silver electrode.

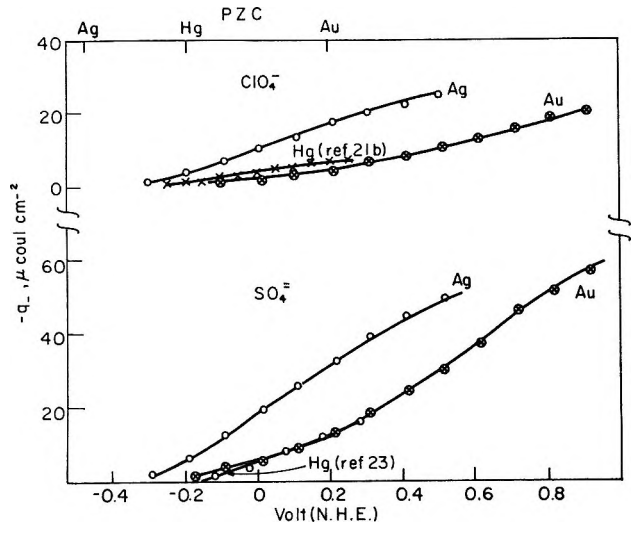

Figure 9. Adsorption of SO_4^{2-} and ClO_4^- ions from 10^{-2} M solutions on different metals. (SO_4^{2-} on Hg data are for 10^{-1} M solution.)

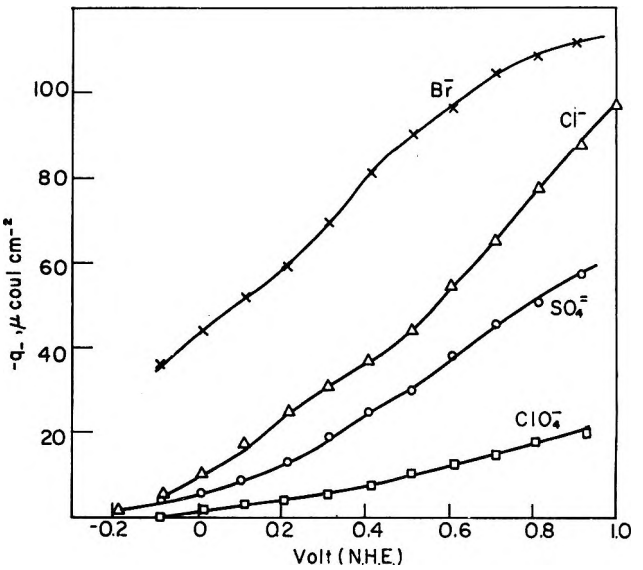

Figure 11. Adsorption on anions from 10^{-2} M solutions on gold electrode.

adsorption there is usually an exponentiallike rise of adsorption with increasingly positive potential, followed by one or more inflections of the curve (Figures 2–6). (5) $(q_-)_v$'s plotted against log c follow straight lines in most systems (Figures 12, 13, and 14). (6) For the less adsorbing anions (SO_4^{2-} and ClO_4^-), $(\partial q_-/\partial \log c)_v$ is small and increases with increasingly positive potential and with the adsorbability of the anions, $ClO_4^- < SO_4^{2-}$. For strongly adsorbing anions (Cl^- and Br^-), $(\partial q_-/\partial \log c)_v$ is large and either increases or decreases with potential (Figures 12–14). (7) Ag and Au electrodes can adsorb halide ions to large extents ($\gtrsim$100 μC cm^{-2}). [The possibility of such a large adsorption was established by the works of Balashova[9] and Gilman[10] for platinum.] (8) There is an indication of greater contact adsorption of anions on Au and Pt than on the other metals (Figures 7 and 8; see section 2 of Discussion).

Discussion

A Δ–potential plot for any of the systems analyzed above shows a very sharp rise in $(-\Delta)$ as the potential reaches the oxide-forming potentials of the metals. However, in hydroxide solution such a sharp change was not observed. $(-\Delta)$ values start to rise at relatively lower potentials and continue to rise rapidly with potential (Figures 15 and 16).

The molar polarizability of OH^- (4.42 cm^3) is close to that of water (3.72 cm^3). The molar volumes of OH^- and H_2O differ little. Hence, the refractive index of an OH^- layer, if such a layer exists, would be close to that of water. Even a monolayer of OH^- ions would

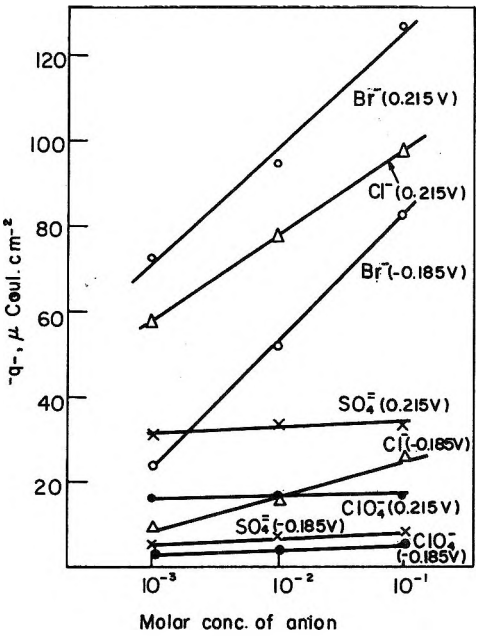

Figure 12. Adsorption isotherms on Ag electrode.

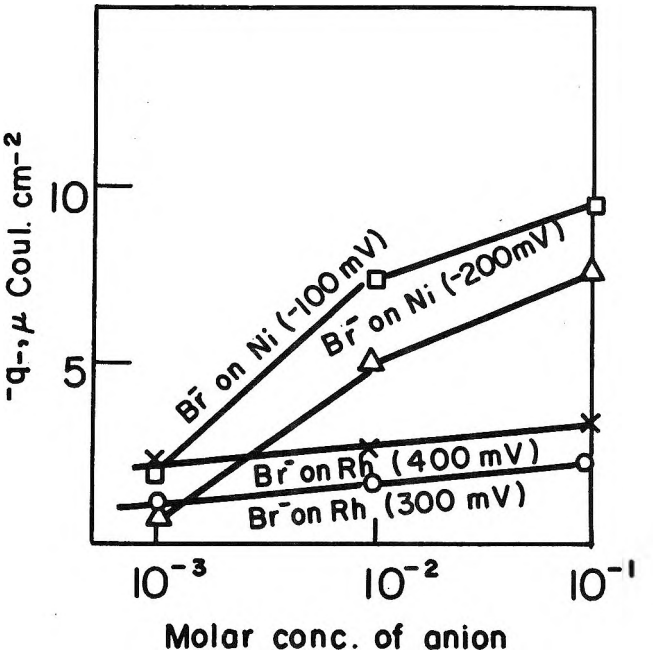

Figure 14. Adsorption isotherms on Ni and Rh electrodes.

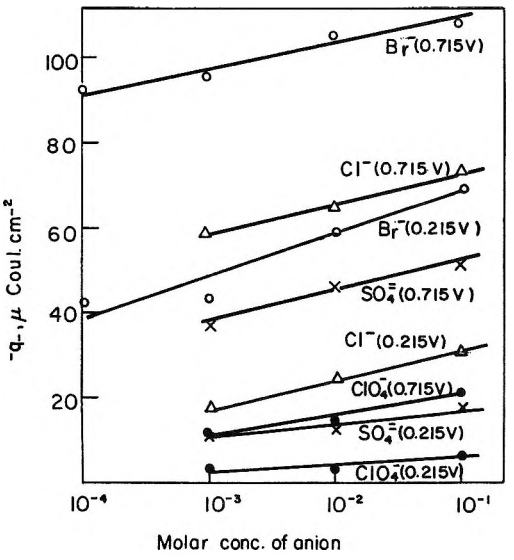

Figure 13. Adsorption isotherms on Au electrode.

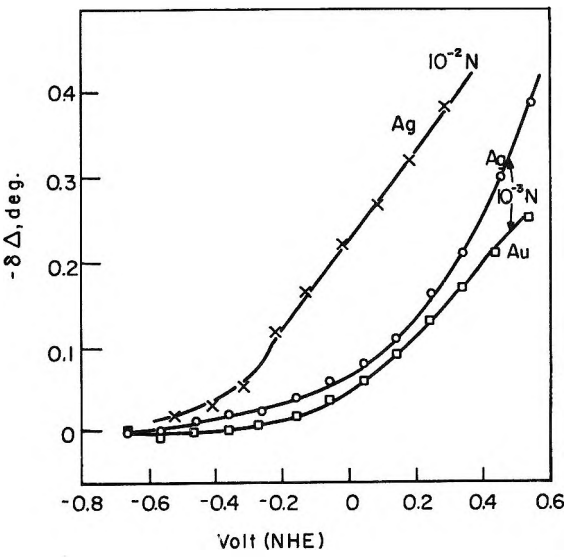

Figure 15. $\delta\Delta$ *vs.* potential of Ag and Au electrodes in OH^- solutions (angle of incidence 64.20°).

not cause a change in Δ as large as that observed. Thus, probably the sharply rising Δ–potential plots observed for hydroxide solutions are not due to the *adsorption* of OH^- ions, and may represent the formation of a new *phase* of hydroxide or oxide on the metal surface, analogous to the indication of a new oxide phase found on Pt at 0.9 V.[4] On rhodium electrode the ClO_4^- solution gave identical result with that of SO_4^{2-}, which is shown in Figure 16. The results were independent of the concentrations of these anions. The curves for these solutions are identical with that of OH^- solution (Figure 16), except that they are separated along the potential axis by RT/F times the difference in the pH units for the respective solutions (*i.e.*, 0.059 V × 8). This similarity between the OH^- and SO_4^{2-} or ClO_4^- curves for Rh electrode further suggests that the changes in Δ with Rh in OH^-, SO_4^{2-}, or ClO_4^- solutions are not due to the adsorption of these anions, but due to formation of anodic film of hydroxide or oxide. The presence of Cl^- or Br^- seems to prohibit the hydroxide formation, ionic adsorption being measurable in these systems.

Another anomaly of the rhodium electrode in SO_4^{2-}, ClO_4^-, or OH^- solutions is that each of the Δ–potential curves (Figure 16) rises on the negative side of the potential as well as on the positive side at which it was concluded that oxide or hydroxide formation occurs.

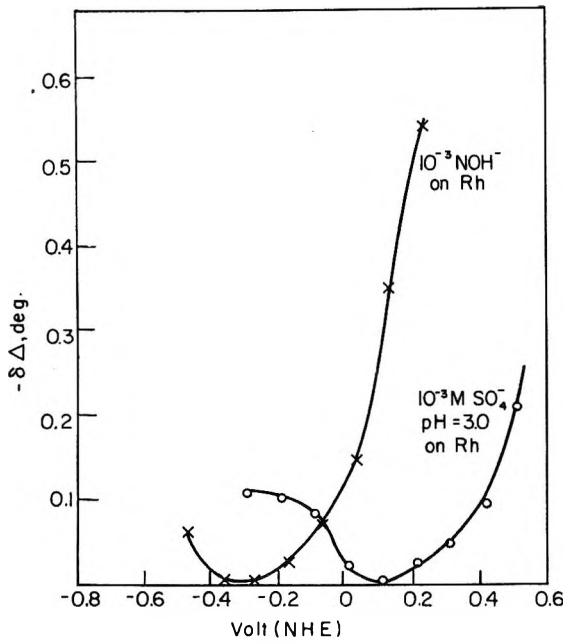

Figure 16. $\delta\Delta$ *vs.* potential of Rh electrode in SO_4^{2-} and OH^- solutions. ClO_4^- solutions gave identical result as SO_4^{2-} solutions (angle of incidence 72.12°).

Adsorption of atomic or molecular hydrogen would not cause such a large change in Δ. The question of specific adsorption of cations arises, although there does not seem to be any evidence for specific adsorption of Na^+ ion on rhodium. An alternative possibility concerns the absorption of atomic hydrogen into the metal causing changes in the optical properties of the metal.

1. On Models. Our optical model for the adsorption resulted in the formula for the calculation of θ from n (eq 7), which differs from that used in the work of Chiu and Genshaw,[7] in which a linear combination of refractive indices of individual species was used

$$n_{film} = n_a\theta_a + n_b(1 - \theta_a) \qquad (17)$$

The present model, and hence eq 7, is adopted here in preference to eq 17 because the present model has a better physical parentage, although both formulas would give numerically similar results.

For gas phase adsorption of single components a relationship

$$\frac{n^2 - 1}{n^2 + 2} = \theta_a \frac{n_a^2 - 1}{n_a^2 + 2}$$

was tested by Bootsma and Meyer[24] to give good agreement with experiment. Equation 7 can be thought of as a two-component version of this equation. An equation similar to eq 4, the starting point for the derivation of eq 7, was used by Debye.[25] It was there shown that the linear combination of the individual polarizabilities is a good approximation for calculation of dielectric constant of solutions.

The scheme of the calculation of the correction for the electromodulation effect as described in section 2 of Theory is different from that of Hansen.[11] In the present work the assumption of a shift of optical spectra made in Hansen's work[11] is avoided. Whichever approach is taken, such a calculation can be only approximate. The electron model of the metal used may not be perfect for the optical phenomena involved. The unavailability of accurate experimental data of electrode charge or double-layer capacitance and the unknown charge distribution profile inside the metal are also responsible for the uncertainties in the final values of the calculated q_-.

2. Experimental Accuracy. Our data might have a further source of error from the fact that only *changes* in Δ could be accurately measured as functions of potential, not its absolute values. Usually, the point at which the Δ–potential curve rises from a flat region was taken as the reference point of zero adsorption. Extrapolation of the Δ–potential plot was necessary in some cases when the Δ–potential curve does not level off even at a potential at which significant hydrogen evolution occurs. The change of Δ observed on introducing the ions in the solutions was also used as a guide.

3. Forces Governing Adsorption of Ions. To consider the effect of the electric field strength on ionic adsorption, the potential dependence of the ionic adsorption on different metals was compared in reference to the potentials of zero charge (pzc) of these metals. Pzc values found in the literature[26-29] are marked on the upper edges of Figures 7–9. The marked values are averages of those pzc's selectively chosen from the literature for solutions of weakly adsorbing electrolytes.

A comparison of these pzc's and the relative positions of the adsorption–potential curves reveals that (i) for Ag, Ni, Hg, and Rh there is a direct correlation between the pzc's and the relative positions of adsorption curves along the potential axis. Also q_-'s are small at the pzc's (<10 μC cm^{-2} for Br^- (Figure 7); <4 μC cm^{-2} for Cl^- (Figure 8); <2 μC cm^{-2} for SO_4^{2-} and ClO_4^- (Figure 9)). (ii) For Au and Pt, the adsorption curves rise at more cathodic potentials than one would expect from their pzc's alone. The q_- values at pzc's are already large (>20 μC cm^{-2} for Br (Figure 7); >10 μC cm^{-2} for Cl^- (Figure 8)).

The dependence of adsorption on pzc (i), and the strong dependence of adsorption on the applied poten-

(24) G. A. Bootsma and F. Meyer, *Surface Sci.*, 14, 52 (1969).

(25) P. Debye, "Polar Molecules," Dover Publications, New York, N. Y., p 44.

(26) S. D. Argade, Thesis, University of Pennsylvania, 1968.

(27) A. N. Frumkin, *Sv. Kem. Tidskr.*, 77, 300 (1965).

(28) R. S. Perkins, R. C. Livingston, T. N. Andersen, and H. Eyring, *J. Phys. Chem.*, 69, 3329 (1965); R. S. Perkins, Thesis, University of Utah, 1967.

(29) D. D. Bode, Jr., T. N. Andersen, and H. Eyring, *J. Phys. Chem.*, 71, 792 (1967); D. D. Bode, Jr., Thesis, University of Utah, 1966.

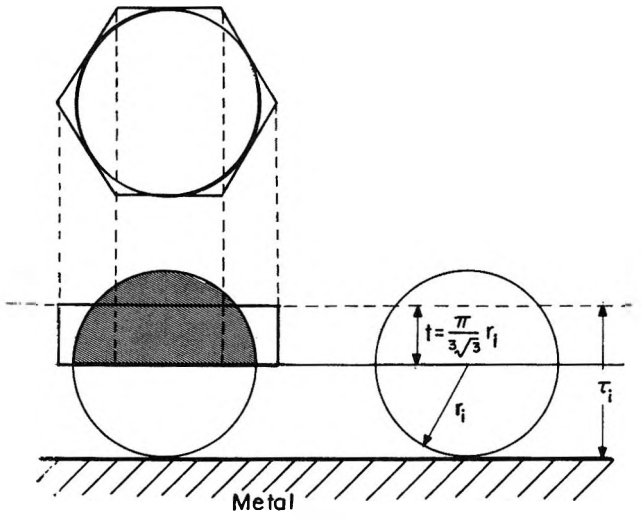

Figure A-1. Calculation of τ_i of spherical ions.

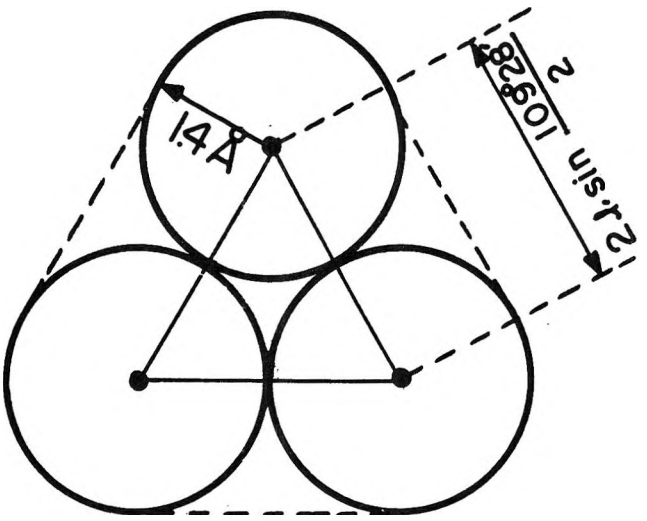

Figure A-2. Calculation of S_i of adsorbed layer of tetrahedral ions.

tial of every electrode, would suggest that the nature of the force governing ionic adsorption is largely electrostatic. However, the fact that on Au and Pt electrodes the adsorptions of the anions are already large at the pzc's, as pointed out above (ii), would indicate that there is more super-equivalent (contact) adsorption on Au and Pt electrodes than on the rest of the metals. Also the observed hysteresis with the adsorption–desorption processes would indicate significant activation energies for the adsorption or desorption processes. No such hysteresis is observed for Hg.

The data are as yet too sparse for a more mature discussion of this question. In particular, it is necessary to obtain heats and entropies of adsorption of ions and to examine if there is any charge transfer accompanying the adsorption.

Acknowledgments. The authors wish to express their gratitude to Dr. H. Wroblowa and Dr. T. Emi for helpful discussions, to Dr. B. Cahan for his instruction in the operation of vacuum evaporation-sputtering apparatus, and to Mr. D. LaPointe for his help in handling the numerical data. The financial support of NASA (Contract No. NGR-39-010-002) and the American Iron and Steel Institute (Project No. 68-161) is gratefully acknowledged.

Appendix

Calculation of S_i and τ_i. 1. Simple Spherical Ions, Cl^- and Br^-. S_i was taken as the area of surface occupied by an anion when it is in a hexagonal array. Thus, $S_i = 2\sqrt{3}r_i^2$, where r_i denotes the radius of the ion.

τ_i was taken as the thickness of the layer of spheres, as shown in Figure A-1, taken up to the plane (dotted line) defining the phase boundary between the surrounding medium (taken uniform) and the spheres. As the averaging process, the volume of the upper half sphere (shaded) is equated to that of a hexagonal column of height t

$$^2/_3\pi r_i^3 = t \cdot S_i$$
$$= 2\sqrt{3}r_i^2 t$$

Then

$$\tau_i = r_i + t$$
$$= \left(1 + \frac{\pi}{3\sqrt{3}}\right)r_i$$

2. Tetrahedral XO_4-Type Anions, SO_4^{2-} and ClO_4^-. The ions are assumed to sit on the electrode surface with three O atoms touching the electrode (Figure A-2). The distance between the centers of two oxygen atoms is $2l \sin 109° 28'/2$ where l is the X–O distance. S_i is taken as the area of the triangle that is rounded at the corners as in Figure A-2.

$$S_i = 1.40^2\pi + 3 \times 1.40 \times 2 \times l \sin\frac{109° 28'}{2} + 3l^2 \sin^2\frac{109° 28'}{2} \tan 30°$$
$$= (6.157 + 6.86l + 1.154l^2)\ \text{Å}^2$$

The thickness due to the oxygen atoms on the bottom is 2×1.40 Å. The fourth oxygen on the top adds $l(1 + |\cos 109° 28'|)$. However, the population in the layer of the fourth oxygen is one-third of the layer at the base. Therefore, we obtain

$$\tau_i = 2 \times 1.40\ \text{Å} + {}^1/_3 l(1 + |\cos 109° 28'|)$$

l is 1.48 Å for ClO_4^- and 1.51 Å for SO_4^{2-}.

Gravimetric Adsorption Studies of Thorium Oxide. V. Water Adsorption between 25 and 500°[1a]

by R. B. Gammage, E. L. Fuller, Jr., and H. F. Holmes[1b]

Reactor Chemistry Division, Oak Ridge National Laboratory, Oak Ridge, Tennessee 37830 *(Received April 22, 1970)*

Reversible and irreversible adsorptions of water vapor on thorium oxide surfaces have been studied gravimetrically between 25 and 500°. On an oxide with fine pores the water which became irreversibly bound between these two temperatures was equivalent in weight to 40 hydroxyls/100 Å², an amount far in excess of the 12.8 hydroxyls/100 Å² required to completely hydroxylate the 100 face. The excess is attributed to molecular water strongly associated with the surface hydroxyls. Between 300 and 500° the irreversible adsorption involves only surface hydroxyls (mass equivalent) and poses no kinetic barrier to obtaining equilibrium isotherms. The irreversible binding of molecular water below 300° is so kinetically complicated and slow that there is considerable difficulty in establishing the equilibrium isotherms. Measurements were also made on a nonporous sample of thorium oxide. The irreversible adsorption of 36 hydroxyls/100 Å² (mass equivalent) is close to that observed with the porous sample. The capacity of the open surface for reversible adsorption is considerably lower than that of the finely porous oxide, so much so that above 350° it was not detectable. Reversible adsorption on the porous oxide could be measured at temperature up to, and including, 500°.

Introduction

The complex interactions of water with the surface of thorium oxide have previously been studied at 25° using porous and nonporous samples.[2-7] The following picture has emerged. The clean surface is initially hydrolyzed to form a layer of surface hydroxyl groups.[7] Further water can then be irreversibly adsorbed as molecules hydrating the surface hydroxyl groups to form "a strongly associated layer of molecular water."[3] This latter process, however, is a difficult one to accomplish from the vapor phase. Adsorption–desorption cycling and prolonged exposure to water vapor are necessary before an equilibrium isotherm is obtained.[2] Reversible physical adsorption is, of course, a constant companion to the irreversible processes. All of these processes have been identified as surface events since immersion in liquid water at 25° indicated an absence of any bulk hydration.[6] The major purpose of this paper is to explore the nature of water adsorption on thorium oxide between 25 and 500°. A careful attempt has been made to obtain equilibrium isotherms over the entire temperature range using samples of finely pored and nonporous thorium oxide. Previously an equilibrium isotherm has been obtained at 25° only for a sample with large pores.[2]

Additional incentive for the present study is the fact that adsorption isotherms for water on oxide surfaces at elevated temperatures are relatively scarce. Significantly, three of the reported studies have dealt with thorium oxide as an adsorbent.[8-11]

Experimental Section

Details of the adsorption apparatus, incorporating a vacuum microbalance and capacitance manometer, have appeared previously.[4,12] Two separate adsorption systems were operated simultaneously over a period of 2 years, each with only a single specimen of one of the two types of thorium oxide. Once evacuated, the two specimens remained on the vacuum microbalance pans without reexposure to the atmosphere.

Adsorbents. Two oxalate-derived thorium oxides were examined; sample B,[5] calcined at 800°, was porous while sample I,[6] having been calcined at 1200°, was nonporous. These oxides were members of a series fired at temperatures ranging from 650 to 1600°. The samples

(1) (a) Research sponsored by the U. S. Atomic Energy Commission under contract with Union Carbide Corp. (b) To whom correspondence should be addressed.

(2) E. L. Fuller, Jr., H. F. Holmes, and C. H. Secoy, *J. Phys. Chem.*, **70**, 1633 (1966).

(3) H. F. Holmes, E. L. Fuller, Jr., and C. H. Secoy, *ibid.*, **72**, 2293 (1968).

(4) H. F. Holmes, E. L. Fuller, Jr., R. B. Gammage, and C. H. Secoy, *J. Colloid Interface Sci.*, **28**, 421 (1968).

(5) H. F. Holmes, E. L. Fuller, Jr., and C. H. Secoy, *J. Phys. Chem.*, **70**, 436 (1966).

(6) E. L. Fuller, Jr., H. F. Holmes, C. H. Secoy, and J. E. Stuckey, *ibid.*, **72**, 573 (1968).

(7) H. F. Holmes, E. L. Fuller, Jr., and C. H. Secoy, *ibid.*, **72**, 2095 (1968).

(8) M. E. Winfield, *Aust. J. Sci. Res.*, **3A**, 290 (1950).

(9) K. L. Sutherland and M. E. Winfield, *Aust. J. Chem.*, **6**, 244 (1953).

(10) A. G. Oblad, S. W. Weller, and G. H. Mills, "Proceedings of the Second World Congress on Surface Activity," Vol. II, Academic Press, New York, N. Y., 1957, p 309.

(11) A. L. Draper and W. O. Milligan, "Structure and Surface Chemistry of Thorium Oxide," The Rice Institute, Houston, Tex., 1959.

(12) E. L. Fuller, Jr., H. F. Holmes, and C. J. Secoy, "Vacuum Microbalance Techniques," Vol. IV, Plenum Press, New York, N. Y., 1965, p 109.

B and I were selected for the present study because on a unit area basis they were, respectively, the most and the least active of the series. These oxides have already been extensively studied.[4-7] The adsorption of nitrogen (after outgassing at 500°) on these samples was measured on the microbalances to give specific surface areas of 11.20 and 2.70 m^2/g for samples B and I, respectively.

Adsorption of Water Vapor. Sample B was subjected to the following experiments. Initially the oxide was outgassed *in vacuo* (10^{-6} to 10^{-7} Torr) at 500°. While this temperature was maintained, adsorption–desorption cycles were conducted in water vapor up to a pressure of 24 Torr. After achieving equilibrium the temperature was lowered to 400° and the adsorption–desorption cycling repeated. This procedure was repeated for decrements of 100° with the final measurements being made at 25°. On attaining a stable, reproducible weight *in vacuo* at each of these temperatures the adsorptions of nitrogen and argon were measured at 77°K. The nitrogen and argon data will be reported separately.[13]

The same experiments were performed on sample I but in a reverse order with respect to temperature. Liquid water was used to satiate the oxide while in the balance pan at room temperature. The first isotherm was measured at 25°, others following for temperature increments of 50° from 100 to 500°.

Contamination always deserves careful consideration, and this is especially true of this study which extended over 2 years. As stated previously, the atmosphere was excluded after the initial evacuation. However, both the diffusion pump oil and the stopcock grease were hydrocarbons. Their vapors can crack on the oxide surfaces at the higher outgassing temperatures and contaminate the surfaces with carbon. To overcome this problem, treatment with oxygen was carried out at 400 and 500° to burn off any carbon. More details of this procedure can be found in one of the earlier papers.[2]

Irreversible Adsorption. This term needs to be defined clearly for the experimental conditions which we have used. The vacuum system, containing a liquid nitrogen trap, easily pumped down to a pressure of 10^{-6} to 10^{-7} Torr as measured by an ion gauge. The water which was irreversibly adsorbed at a particular temperature (25–500°) was that which could not be removed by evacuation, the experimental criterion being that overnight evacuation produced a weight change of less than 2 μg.

Results

The adsorption–desorption cycles measured on approximately 200 mg of sample B are shown in Figure 1. The arrows at zero pressure indicate the equilibrium weights of the sample *in vacuo*. The right ordinate shows the amount of water irreversibly bound in excess of the 500° vacuum weight, in terms of equivalent hydroxyls on the arbitrarily chosen 100 face. The chemisorptive capacity of the 100 face is 192 $\mu g/m^2$,[2] or 12.8 hydroxyls/100 Å^2.

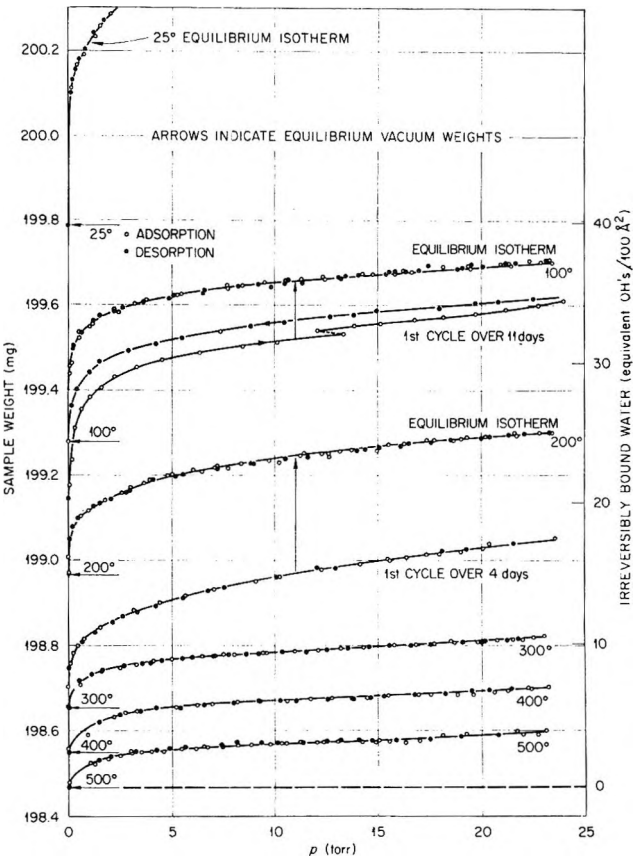

Figure 1. Adsorption of water vapor on porous thorium oxide B.

Reversible isotherms were easy to construct in the temperature range of 500 to 300° with no unduly slow kinetic effects. On dropping the temperature to 200°, however, the onset of laboriously slow kinetics was observed together with a marked increase in both the irreversible retention and the reversible adsorptive capacity. Twenty adsorption–desorption cycles were conducted at 200° over a period of 3 months before a reversible isotherm was obtained. The irreversible binding process was accelerated more by adsorption–desorption cycling than by exposure to water vapor at constant pressure. This phenomenon has previously been seen at 25°.[3] Laboriously slow kinetics were also observed on lowering the temperature to 100° where ten adsorption–desorption cycles completed the irreversible binding of water. Before cycling at 25° the oxide was left exposed, over a 2-month period, to water vapor at near saturation vapor pressure. Several more adsorption–desorption cycles produced the final equilibrium isotherm, a small portion of which is shown in

(13) Presented in part at the Symposium on Surface Area Determination, Bristol, England, July, 1969; arranged by the I.U.P.A.C. and S.C.I.

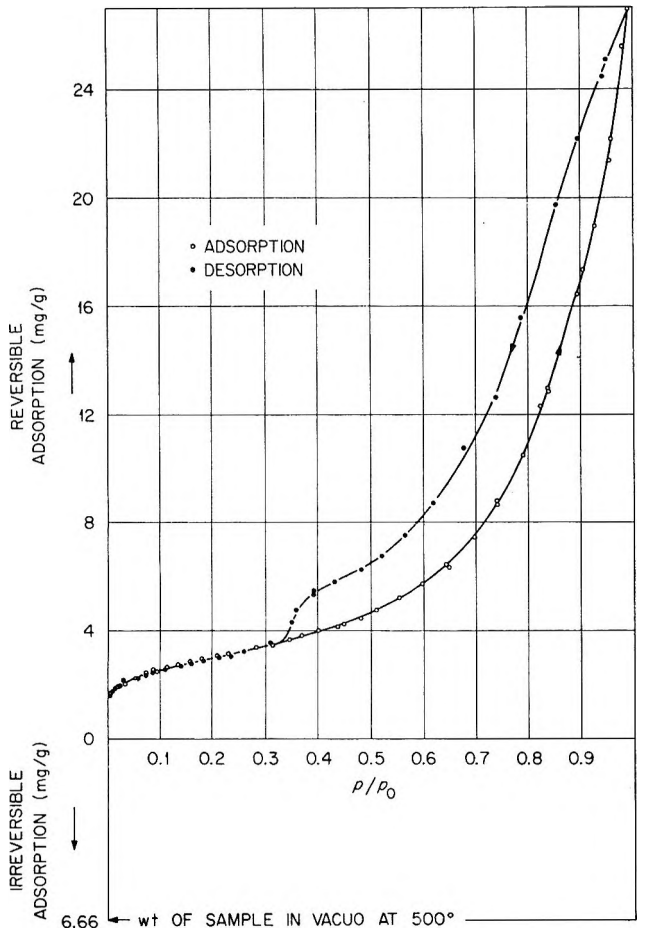

Figure 2. Equilibrium isotherm of water adsorbed at 25° on porous thorium oxide B.

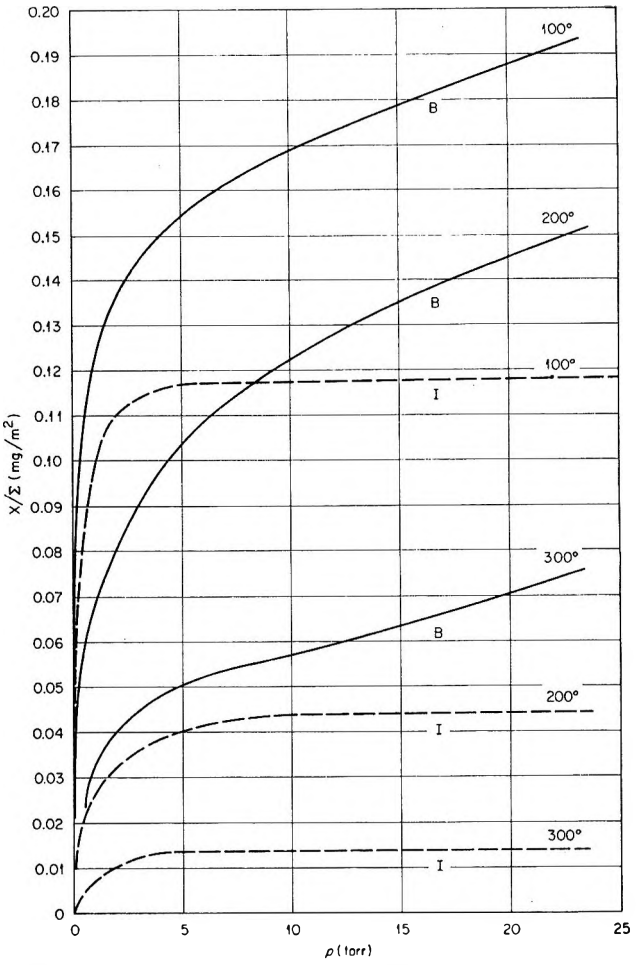

Figure 3. Adsorption of water vapor by porous thorium oxide B and nonporous thorium oxide I.

Figure 1. Figure 2 shows this entire isotherm presented as the amount reversibly adsorbed at 25° per unit mass of oxide. It is worth stressing that this reversible physisorption is taking place on a surface which has already irreversibly adsorbed 6.66 mg of water per gram of thorium oxide.

Exposure of sample I to water vapor at successively higher temperatures gave decreasing amounts of reversibly adsorbed water. No reversible adsorption could be detected at temperatures above 350°. Irreversible adsorption was observed, however, over the entire temperature range of 25 to 500° as evidenced by the monotonically decreasing sample weight *in vacuo*. The amount of water irreversibly adsorbed by sample I from 500 to 25° was equivalent to 36 hydroxyls/100 Å² (assuming 100 faces). Figure 3 is useful for comparing reversible adsorption on the two types of oxide, samples B and I, between 100 and 300°, the data having been reduced to a unit area based on the nitrogen specific surface areas.

Discussion

The adsorption of water on a thorium oxide surface is far too complex a process to be treated simply as chemisorption (surface hydroxyls) or reversible physisorption (water molecules). Intermediate stages of binding must also be considered. The large amount of water which becomes irreversibly bound to the porous thorium oxide surface below 500° is testimony to this fact. The equivalent of nearly 40 hydroxyls/100 Å² is far in excess of the 12.8 hydroxyls/100 Å² which the 100 face could accommodate by straightforward hydroxylation. Even on the most densely packed 111 face hydroxylation can account for only 14.7 hydroxyls/100 Å². Once again we lean heavily towards the concept of strongly associated water molecules hydrating the surface hydroxyls. Previous studies have shown that outgassing *in vacuo* at 300° is required to pull off adsorbed molecular water and leave only a layer of surface hydroxyls.[6] Further loss of water between 300 and 1000° occurs through the condensation of surface hydroxyl groups.[6] In this study, the processes of irreversible binding have undeniably different characters above and below 300°. It now requires little imagination to draw a line through the vacuum weight at 300° in Figure 1 and say that only surface hydroxyl groups are involved in the irreversible process above this temperature whereas at lower tem-

peratures one is observing irreversible hydration of the layer of surface hydroxyls. The previous finding[2] that initial hydrolysis of the surface oxide is relatively rapid but that hydration of the surface hydroxyls is a slow process accords well with the rapidity of irreversible binding at 300–500° (no slow kinetics observed) and the difficulties in obtaining reversible isotherms below 300°.

Prior to this study sample D was the only other thorium oxide where a reversible isotherm had been constructed[2] at 25° following an outgassing at 500°. This oxide, calcined at 1200°, contained no pores of radii less than 50 Å. Sample B on the other hand contains much finer pores. Classical treatment of the hysteresis loop in Figure 3 indicates the presence of pores extending down to a radius as low as 10 Å while *t* plots of adsorbed nitrogen reveal the presence of even smaller micropores.[13] The opportunity exists, therefore, for comparing the amounts of water that can be irreversibly bound to related thorium oxides with differing pore structures. The coarsely porous sample D irreversibly adsorbed the equivalent of 32 hydroxyls/100 Å^2 between 500 and 25°.[2] The corresponding value for the nonporous sample I of the present study is 36 hydroxyls/100 Å^2. These figures compare with the 40 hydroxyls/100 Å^2 taken up by sample B. In view of the uncertainty concerning such matters as which crystal face is present, these values are sufficiently close to suggest that the quantity of irreversible adsorbed water on a thorium oxide surface is independent of the porosity of the sample. This should not be taken as implying that the energetics of the irreversible adsorption are independent of porosity. This has clearly been shown not to be true, *e.g.*, in the case of samples B and D.[5]

The situation is entirely different when one is considering the reversibly adsorbed water. From Figure 3 the superior ability of the finely pored oxide to reversibly adsorb water vapor in the temperature range of 100 to 300°, and, of course, from 300 to 500°, is without question. Clearly water is more tightly absorbed on surfaces contained within pores. Oblad, Weller, and Mills,[10] working with high-area thorium oxide (certainly porous since it was prepared by calcining the oxalate at 650°), found reversible adsorption of water vapor in the temperature range of 500 to 700°. A similar result might be expected of our sample B. These results are not without precedent as reported reversible adsorption above the critical temperature of the absorbates generally involve adsorbents which are porous.[14]

Comparison of the present results with previously reported studies of water adsorption on thorium oxide at elevated temperatures is, at best, difficult. Oblad, Weller, and Mills[10] were working at higher temperatures than those used in the present study. As previously mentioned, their results are probably indicative of a porous sample. The experimental arrangement used by Winfield[8] in his high-pressure study precludes the possibility of ascertaining the reversibility of the reported isotherms. A low-pressure study by Sutherland and Winfield[9] was more concerned with transient rates of adsorption than with equilibrium isotherm data. Draper and Milligan[11] state that their isotherms for water adsorption on thorium oxide are not reversible. In fact, they observed an irreversible effect with adsorption–desorption cycles which they attributed to a probable "aging" of the oxide. Their effect is almost certainly the irreversible adsorption of water which we observe on adsorption–desorption cycling. Reversible and irreversible adsorption of water at elevated temperatures has also been observed on aluminum oxide,[10,15,16] magnesium oxide,[15] zinc oxide,[17] and silica–alumina.[18]

Turning our attention to the reversible adsorption isotherm shown in Figure 2, a BET treatment of the data yielded a monolayer capacity of 2.45 mg of water/g of thorium oxide with a *C* constant of 110. Assuming an apparent cross-sectional area of 10.6 Å^2/water molecule, the apparent specific surface area of sample B, in this state of surface hydration, is 8.67 m^2/g. A nitrogen isotherm (after outgassing at 25°) was measured immediately afterwards and gave a specific surface area of 8.56 m^2/g using 16.2 Å^2/nitrogen molecule. A *t* plot of the adsorbed nitrogen indicated disappearance of the micropores,[13] which had been filled by the irreversibly bound water. In the absence of the micropores it thus becomes more reasonable to compare and equate the adsorption of nitrogen and water since the available pores are likely to be reached by each adsorbate. The closely matching specific surface areas point to the water forming a liquidlike monolayer with each water molecule occupying 10.6 Å^2. Precisely this result was predicted for the reversible physisorption of water on a fully hydrated 100 face.[3] While the result does not prove the model previously postulated,[3] or even the predominance of 100 faces on the surface of sample B, it certainly adds more circumstantial evidence to strengthen our ideas of the associatively adsorbed water on the surface of thorium oxide.

A striking comparison can be made between hydrophilic silica and thorium oxide. At 150° silica retains the equivalent of about 5 hydroxyls/100 Å^2,[19] whereas thorium oxide retains the equivalent of approximately 20 hydroxyls/100 Å^2 over the vacuum weight at 500°

(14) A good example is: P. E. Eberly, Jr., *J. Phys. Chem.*, **65**, 68 (1961).

(15) H. Spannheimer and H. Knozinger, *Ber. Bunsenges. Phys. Chem.*, **70**, 570 (1966).

(16) E. B. Cornelius, T. H. Milliken, G. A. Mills, and A. G. Oblad, *J. Phys. Chem.*, **59**, 809 (1955).

(17) Y. Miyahara, *J. Chem. Soc. Jap., Pure Chem. Sec.*, **71**, 153 (1950); *Chem. Abstr.*, **45**, 4522*d* (1951).

(18) G. M. Panchenkov, L. M. Kuvshinnikov, N. M. Saltykova, and L. N. Denisova, *Zh. Fiz. Khim.*, **36**, 641 (1962); *Russ. J. Phys. Chem.*, **36**, 335 (1962).

(19) V. Ya. Davydov, A. V. Kiselev, and L. T. Zhuravlev, *Trans. Faraday Soc.*, **60**, 2254 (1964).

(see Figure 1). The capacity to adsorb water irreversibly seems to be considerably higher for thorium oxide than for silica.

The hydrolysis of the first few molecular layers of a thorium oxide particle is certainly a possible alternate to our explanation of the data.[20] This possibility cannot be excluded on an absolute basis at the present time. The heats of immersion in liquid water[6,7] have led us to believe that the particles suffered no bulk hydrolysis and that only true surface hydration phenomena were occurring. The heat release was completed within a few seconds[6,7] for nonporous or coarsely porous oxides which would virtually exclude slow diffusion-controlled processes. There are probably other remote possibilities but there is no experimental evidence to support these alternatives or to refute our model.

(20) The possibility was suggested by one of the reviewers.

Polymer Content of Sulfur Quenched Rapidly from the Melt[1]

by Jae Chun Koh and William Klement, Jr.*

Department of Engineering, University of California, Los Angeles, California 90024 *(Received April 24, 1970)*

Liquid sulfur has been quenched to room temperature from temperatures in the range 135–300° at rates up to an estimated 10^5 deg sec^{-1}. Runs were made in which the liquid was heated for 5, 15, and 60 min and >3 hr before quenching. Solution of the quenched sulfur in CS_2, very shortly after quenching, yielded insoluble portions, which are identified as the polymeric species S_μ. The weight fraction, $[S_\mu]$, increases monotonically with temperature from <0.01 at 135° to ~0.56 at ~250°, with no further increase up to 300°; there appears to be a very rapid increase in $[S_\mu]$ near $T_\lambda \approx 159°$.

Introduction

By quenching molten sulfur from various temperatures in various ways to room temperature or lower, dissolving the resultant material (after various "preparations") in carbon disulfide and identifying the insoluble portion as S_μ, the proportion of the polymeric species S_μ as a function of temperature has been implied for the liquid at equilibrium. This approach to the problem is rather venerable, dating from Berthelot[2,3] in 1857 up through the most extensive recent work of Schenk.[4] However, Schenk was unable to quenchl iquid sulfur from the 160–250° range of very high viscosity, whereas this could be done with the present techniques, which also offer much higher quenching rates than hitherto.

Experimental Procedures and Results

The present quenching technique is believed to be the most rapid yet employed for the sulfur problem; it is based on the principle of forming a layer of the molten material—the thinner the better—in intimate contact with a good thermal conductor at ambient temperature. Although this principle had been flirted with by several workers, not until 1960[5] was it clearly enunciated and systematically employed,[6,7] mostly thus far with metallic alloys.

The quenching apparatus is schematically depicted in Figure 1. A few cubic centimeters of compressed gas behind a quick-opening solenoid valve impinge upon the molten sulfur globule at the bottom of the aluminum crucible when the valve is opened, thus ejecting the melt onto the substrate.

Temperature within ~1 mm of the sample was monitored with a chromel–alumel thermocouple (Figure 1) to within ±0.5°, there being no greater deviation after the furnace was brought to equilibrium, often some hours before the quench. Since aluminum is an excellent thermal conductor, the temperature of the sulfur globule is sensibly that measured *via* the thermocouple. There is a possible systematic error in temperature since the cold, rapidly expanding gas is impinging upon the sample in the quench; this possible error cannot be estimated but is believed to be negligible insofar as the results obtained (below) approximately agree with those

* To whom correspondence should be addressed.

(1) Submitted by J. C. K. toward an M.S. degree in Engineering, UCLA.

(2) As quoted in ref 3.

(3) A. Smith and W. B. Holmes, *J. Amer. Chem. Soc.*, **27**, 979 (1905).

(4) P. W. Schenk, *Z. Anorg. Allg. Chem.*, **280**, 1 (1955).

(5) P. Duwez, R. H. Willens, and W. Klement, *J. Appl. Phys.*, **31**, 1136 (1960).

(6) W. Klement, Ph.D. Thesis, California Institute of Technology, 1962.

(7) P. Duwez, *Progr. Solid State Chem.*, **3**, 377 (1966).

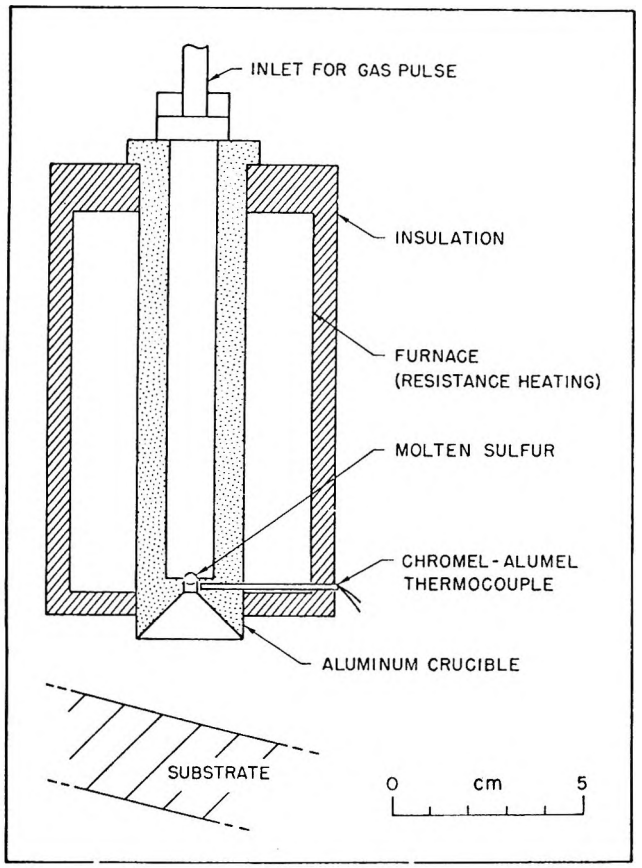

Figure 1. Cross-sectional schematic of quenching apparatus.

of others in appropriate ranges. Temperatures here are believed known to an accuracy of ±1°.

Sulfur of purity 99.999+% from American Smelting and Refining Co. was used in amounts of ~0.1 g, which were put into the crucible, and upon melting, presumably moved into a stable configuration at the hole (Figure 1). The tubing, valve, crucible, substrate, etc., were scrubbed and cleaned with CS_2 before an experiment. There was no visual evidence that the sulfur reacted with the aluminum crucible during heating.

Below ~175° and above ~210°, nitrogen gas pressures of 20–40 bars were sufficient to eject the molten sulfur; in the range ~175–210°, the higher viscosity of the melt necessitated pressures of ~60 bars.

For the requirement of a substrate of high thermal conductivity (in contrast to the glass plate often used by Schenk[4]), copper and also aluminum were used and the surfaces were roughened[6] and cleaned with CS_2 immediately before the quench. Slight darkening of the copper was noted where the sulfur had been quenched, but the results from these samples did not differ noticeably from those quenched onto aluminum.

The main body of data is from these experiments in which the sulfur was heated for about 5, 15, and 60 min, respectively, and for >3 hr.

The quenched samples, all of which adhered firmly to the substrate, may be distinguished as follows: (i) those quenched from below ~170°, which started to harden almost immediately after quenching and were of thickness ~0.007 mm, as measured with a micrometer; (ii) those from ~170 to 210°, which were sticky and of typical thickness 0.033 mm; (iii) those from above ~210°, sticky (noticeable hardening after ~1 day) with a threadlike fabric and of thickness ~0.020 mm.

After the quench, samples were removed almost immediately by scraping with a stainless steel plate (type i) or with forceps (types ii and iii). The samples were not pulverized or ground (in contrast to most previous work) and indeed effort was made to avoid mechanical strain. Within ~5 min, the samples of 0.05 to 0.1 g were weighed directly (to 10^{-5} g) on a Mettler H16 balance and then transferred to a beaker or ceramic crucible. At this stage, it was discovered that traces of water in the containers led to erratically lower S_μ contents (see Schenk[4]).

Then, CS_2 of 99.997% purity was added to the containers and the solutions were allowed to stand for ~30 min at room temperature, becoming light yellow in the process. After about three such extractions, it was found that further repetitions caused only a decrease of ~0.001 to 0.003 in the weight fraction of the insoluble portion. The results (below) also suggest that all portions of the samples were sufficiently accessible to the CS_2 so that the procedures of others of pulverization, grinding, waiting for specimens to harden, etc., could be safely circumvented. After the extractions, the residues were dried in a desiccator at room temperature under artificial light and then removed and weighed after ~30 min. (This weight compared with the weight of the sample after quenching is taken to be the weight fraction, $[S_\mu]$, of the insoluble polymer.) This method suffices for all samples except those of very low $[S_\mu]$, in which cases extractions were made until reaching a constant decline in weight. The overall accuracy is very difficult to estimate because of the several factors involved, but some duplicate runs suggested that the scatter is less than ~0.01 at the higher $[S_\mu]$ contents.

The results, $[S_\mu]$ *vs.* temperature, are shown in Figures 2 and 3 for the various heating times. From Figure 2, there appear to be only small differences between the results from the 5-min period and those for the 15-min heatings; from Figure 3, there is a similar consonance between the results for heatings of 60 min and >3 hr. However, from Figure 4 in which data from other extensive investigations[3,4,8] are also shown, it may be observed that the 5- or 15-min $[S_\mu]$ contents are systematically lower than the 60-min or >3-hr data in the range ~200–280°.

Some experiments were also run to verify Schenk's observations[4] of the pronounced effects of light on "plastic" sulfur. Comparison of sulfur heated for ~5

(8) D. L. Hammick, W. R. Cousins, and E. J. Langford, *J. Chem. Soc.*, 797 (1928).

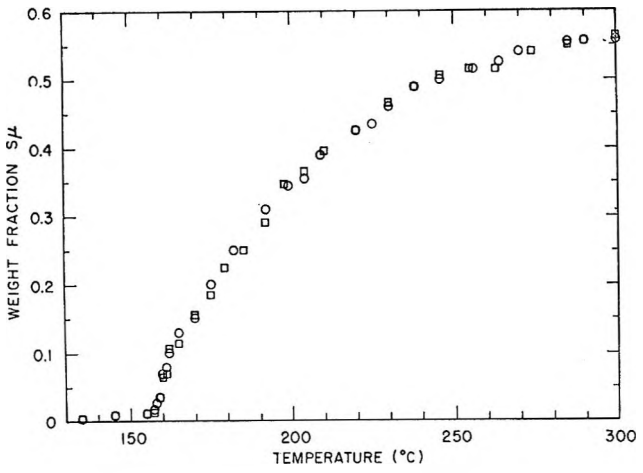

Figure 2. Weight fraction insoluble sulfur *vs.* temperature: circles denote heating period of ~15 min before quench; squares, ~5 min.

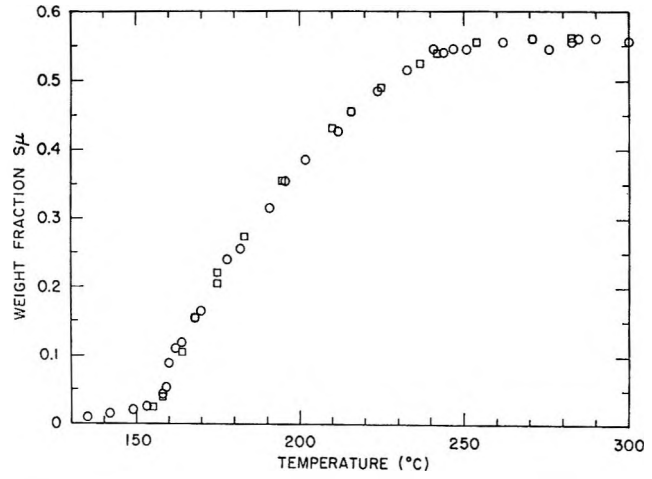

Figure 3. Weight fraction insoluble sulfur *vs.* temperature: circles denote heating period of ~60 min before quench; squares, >3 hr.

min and kept, after quenching, in a dark place and in bright sunlight, respectively, for ~1 hr showed S_μ contents of 0.55 and 0.014, respectively, for 289° and 0.55 and 0.015, respectively, for 295°. Similarly, for sulfur heated for ~5 min and kept in the dark and ~20 cm from a 130-W bulb, respectively, for ~1 hr, the contents were 0.54 and 0.42, respectively, for 269° and 0.55 and 0.44, respectively, for 278°. For samples quenched from 224, 262, and 285°, respectively, the $[S_\mu]$ contents as determined in the usual way, were 0.49, 0.55, and 0.56, respectively; sitting under artificial light for ~1 day yielded, upon extraction, weight fractions of S_μ (referred to the original quenched samples) of 0.43, 0.50, and 0.52, respectively.

Discussion

Quenching Rates. An analysis[6,9] of the cooling rates of the quenched sulfur requires an estimate of h, the coefficient of heat transfer between sample and substrate.

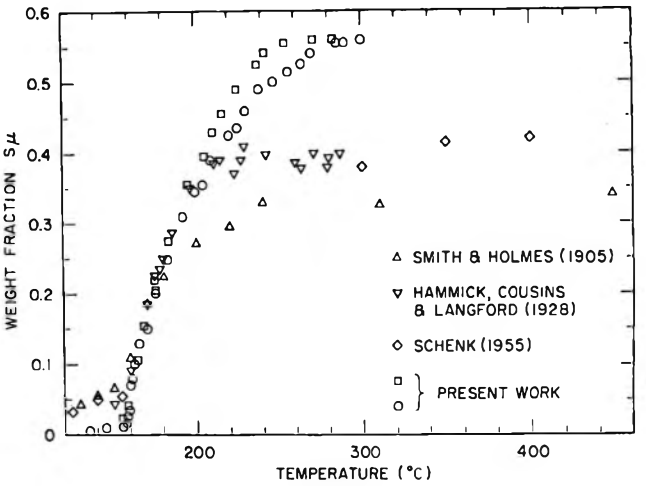

Figure 4. Weight fraction insoluble sulfur *vs.* temperature from from various investigations using various techniques (see text). For data from present work, circles denote heating period of ~15 min before quench (also Figure 2); squares, >3 hr (also Figure 3).

A lower limit is for Newtonian cooling in which the rate is directly proportional to h and inversely proportional to the sample thickness; using data for thermal conductivity,[10] specific heat,[11] density,[12] and the present thickness measurements, *minimum* rates of $\sim 2 \times 10^2$ deg sec^{-1} are estimated.[9] Since the physical contact of sample to substrate was observed to be good, h is perhaps large enough ($h > 10$ J cm^{-2} sec^{-1} deg^{-1}) so that the cooling is nearly "ideal";[9] then the cooling rate is inversely proportional to the square of the sample thickness and might range up to ~10^7 deg sec^{-1}.

For the three regions distinguished above, (i) $\lesssim$170°, (ii) ~170–210°, (iii) $\gtrsim$210°, the cooling rate probably varies by less than two orders of magnitude from ii (low) to i (high). Detailed comparison of the present technique with those used previously can only show the present quenching rates to be much greater. The most pertinent comparison would be with Schenk's technique,[4] but he did not state the thicknesses of his samples. The present quenching rates are estimated to be 10^3 to 10^5 deg sec^{-1}.

Comparison with Previous Quenching Experiments. Below T_λ ($\approx$159°), the present results disagree considerably with most previous experiments[3,4,8,13] (Figure 4). This may arise, in part, from the differences in procedures since, in the present work, there was little waiting before solution in CS_2, no grinding, and little mechanical straining of the quenched specimens. According to Schenk,[4] all of these actions cause transformation of S_π

(9) R. C. Ruhl, *Mat. Sci. Eng.*, 1, 313 (1967).

(10) G. W. C. Kaye and W. F. Higgins, *Proc. Roy. Soc., Ser. A*, 122, 633 (1929).

(11) E. D. West, *J. Amer. Chem. Soc.*, 81, 29 (1959).

(12) F. Fehér and E. Hellwig, *Z. Anorg. Allg. Chem.*, 294, 63 (1958).

(13) P. W. Schenk and U. Thümmler, *Z. Elektrochem.*, 63, 1002 (1959).

(the opened ring[13]) into S_μ. Beckmann and Platzmann[14] have shown that there is a considerable increase in S_μ content the longer one waits before extraction, for samples quenched from the lowest temperatures.

Near T_λ, the present results, derived from similar experimental procedures above and below T_λ, strongly suggest a rapid increase in $[S_\mu]$ near T_λ. The only other extensive data for $[S_\mu]$ very near T_λ appear to be those of Carson, who used a procedure sufficiently different so as to discourage direct comparison. Although Carson apparently[15] concluded that $[S_\mu]$ increased discontinuously at T_λ, such an interpretation is not necessary for either his data [15] or for the present results.

Somewhat above T_λ, to ~180 or 200°, there is fair agreement between the present results and those[3,4] of some previous workers, despite the different procedures for quenching and analysis. At slightly higher temperatures, the results (Figure 4) of Smith and Holmes[3] and of Hammick, *et al.*,[8] would seem to be affected by the quenching media, as shown by Schenk[4] and evident in some of the present experiments in which water was present.

Although the samples in the present experiments were exposed to air during heating before the quench, such was also true in much of the other work. There was no visual evidence of reaction with the aluminum crucible, and it is not easily appreciated how nitrogen may be involved so that the question seems to be one of the effects of oxygen. This is an open question also. One may note that the present results are different from those of Carson[15] and of Smith and Holmes,[3] who saturated their samples with SO_2 before the quench, but the procedures for quenching and analysis also are different.

As seen clearly in Figure 4, the results from the shorter heating periods (Figure 2) show S_μ contents somewhat lower than those from the longer heatings (Figure 3) over the range ~200–280°. If this were to be explained in terms of a more sluggish approach to equilibrium, one would be obligated to point out that the viscosity is greatest in this temperature range only for sulfur with significant impurity contents.[4] Indirectly, from the pressures necessary to eject the molten sulfur and from the appearances of the quenched specimens, it seems that the material in the present experiments exhibited its maximum viscosity in the range ~170–210°, as for the purest sulfur.[4]

Schenk[4] states that the quenching results with his 99.9% material were little different from experiments with highly purified sulfur and that additions of $\geq 0.1\%$ impurities were necessary to produce observable changes in $[S_\mu]$. Further, he[4] states that diminution in $[S_\mu]$ obtained with increased heating time indicates that the impurities are vaporizing, reacting to form impotent compounds, or becoming impotent themselves. (In some contrast, J. Schenk[16] corroborates P. W. Schenk's data[4] for 190–250° only with "purified" sulfur, as quenched in liquid air.) Insofar as the present experiments were with material of higher purity (99.999%) and the effects of heating time on S_μ content no more severe than shown in the comparison of Figure 4, it is believed that the present results are not primarily determined by such large amounts of impurities.

It would appear that the extension of $[S_\mu]$ to the "asymptotic" value of ~0.56 at the higher temperatures is due to the higher quenching rates. One may note that Schenk and Thümmler[17] observed that S_μ decomposes to S_μ and S_λ in the ratio 55 ± 5:45 ± 5, presumably independent of temperature (but at much lower temperatures). Whether this is germane to an interpretation of the present high-temperature quenching data remains to be established, especially since data for the variation of $[S_\pi]$ with temperature are lacking above T_λ. Some of Schenk's experiments[4] appear to offer possible estimates of $[S_\mu]$ from 200–400° but actually are not corroborated in the present work; the fact that he could obtain more S_μ by successive extractions for material put into CS_2 shortly after quenching (without the usual waiting, grinding, etc.) must be attributed to incomplete exposure to the solvent of the massive initial portion.

Kinetics. Although there are still many poorly understood variables, the present work does contribute some new results toward an answer to the question of how the quench product, obtained in a given procedure, is related to the polymeric constitution of the liquid at the temperature of heating. The kinetics of any reaction, on cooling, must almost certainly depend on the quench rate.

The kinetics of the approach to equilibrium before quenching is also of paramount importance here. The present experiments are for given heating times only, and no claim is made that equilibrium is achieved before the quench. Presumably most other workers heated their samples long enough (although heating times are not always stated) so that they considered that they were quenching from the melt at equilibrium. It seems likely that there were significant departures, from equilibrium before the quench only at the lowest temperatures in the present experiments.

After the present experiments were completed, a paper[18] by Wiewiorowski, Parthasarathy, and Slaten (WPS) appeared which dealt with the approach to equilibrium at 130, 140, and 150°. WPS initially heated from the solid to these temperatures, held the melt for certain times, and then observed freezing point depres-

(14) (a) E. Beckmann and C. Platzmann, *Z. Anorg. Allg. Chem.*, 102, 201 (1918); (b) C. R. Platzmann, *Bull. Chem. Soc. Jap.*, 5, 43 (1930).

(15) C. M. Carson, *J. Amer. Chem. Soc.*, 29, 499 (1907).

(16) J. Schenk, *Physica*, 23, 325 (1957).

(17) P. W. Schenk and U. Thümmler, *Z. Anorg. Allg. Chem.*, 315, 271 (1962).

(18) T. K. Wiewiorowski, A. Parthasarathy, and B. L. Slaten, *J. Phys. Chem.*, 72, 1890 (1968).

sions upon cooling—the experiments being neither *in situ* measurements nor involving quenching at high rates. In Smith's classic experiments,[19] a quantitative correlation was suggested between the freezing point depression and the $[S_\mu]$ obtained by quenching from that temperature; WPS[18] use a similar correlation. There are minor discrepancies between the WPS melting temperature (118.8°[18]) and the 119.25° value[19] of the earlier work and in the approximate values cited for the heat on melting. It also seems unlikely that isothermal conditions could be achieved at the given temperatures for the rather large samples (~10 g[18]) (and the low thermal conductivity[10] of sulfur) in less than several minutes. Furthermore, the data[18] corresponding to the freezing point depressions for 240 and 360 min at 130° (as given in their Table I[18]) are not shown in their Figure 1[18] and do not fit the postulated kinetics. If WPS' quantity[18] $(1 - [S_8^R])$ is nominally identified with $[S_\mu]$, some comparisons may be made between the actual WPS data[18] for various times at 130, 140, and 150° and the quenching results. First, for similar heating times and temperatures, WPS' $[S_\mu]$ is ~1.5–2 times greater than the $[S_\mu]$ obtained in the present experiments; there is considerable scatter in this correlation, due partly to the present difficulty in accurately analyzing for small fractions of the small quenched samples. Second, for similar heating times, Carson's quench results[15] for $[S_\mu]$ at 130 and 140° are ~1.5–2 times greater than the WPS results[18] at those temperatures, also with considerable scatter in the correlation. Other work[15] by Carson also suggests a somewhat different approach to equilibrium at 130 and 140° than that described[18] by WPS. It seems clear that the kinetics in the quenched samples at ambient temperature is quite complex, and the current evidence is not that convincing for any appreciably simpler kinetics in the liquid at the lower temperatures.

Acknowledgment. Dr. H. D. Lüdemann is deeply thanked for discussions, especially of Schenk's papers.

(19) A. Smith, *Z. Phys. Chem.* (*Leipzig*), **42**, 469 (1903).

A Study of Interactions between Polyelectrolyte and Neutral Polymer in Aqueous Solutions in Terms of Water Activity[1]

by Tsuneo Okubo and Norio Ise*

Department of Polymer Chemistry, Kyoto University, Kyoto, Japan (*Received June 22, 1970*)

The isopiestic vapor pressure measurements in the ternary systems water–polyelectrolyte–neutral polymer were carried out. Sodium polyacrylate was used as a polyelectrolyte, and the neutral polymers were polyacrylamide (PAAm), polyethylene glycol (PEG), and polyvinylpyrrolidone (PVP). The water activity decreased by the addition of the neutral polymer in the order PVP > PEG > PAAm. The observed depression of water activity was discussed in terms of the water structural influences of the solutes.

Introduction

Recently, the solute and solvent activities of various binary polyelectrolyte solutions have been measured by isopiestic vapor pressure method in this laboratory.[2-7] The relative order of the activity and osmotic coefficients of various salts of polyelectrolytes was accounted for by Gurney's rule[8] found originally for low molecular weight electrolytes. According to this rule, electrolytes composed of ions of dissimilar influence on solvent water structure have larger mean activity and osmotic coefficients than those of ions of similar character. The structural influences of polyelectrolyte to the solvent water molecules were much more remarkable than those found for simple electrolytes such as tetraalkylammonium halide[9] and were discussed in terms of the

* To whom correspondence should be addressed.

(1) Presented at the 18th Discussion Meeting of Polymer Science, Tokyo, Japan, Nov 1969.

(2) N. Ise and T. Okubo, *J. Phys. Chem.*, **71**, 1886 (1967).

(3) N. Ise and T. Okubo, *ibid.*, **72**, 1361 (1968).

(4) N. Ise and K. Asai, *ibid.*, **72**, 1366 (1968).

(5) N. Ise and T. Okubo, *ibid.*, **72**, 1370 (1968).

(6) N. Ise and T. Okubo, *Macromolecules*, **2**, 401 (1969).

(7) N. Ise, K. Asai, and K. Takaya, *J. Phys. Chem.*, **73**, 4071 (1969).

(8) R. W. Gurney, "Ionic Processes in Solutions," McGraw-Hill, New York, N. Y., 1953, Chapter 16.

electrostrictional hydration and hydrophobic iceberg structure formation.

From the above results for the binary polyelectrolyte solutions, it was thought that the presence of additional neutral polymer may further affect the water structure and hence thermodynamic properties. In the present paper, therefore, the isopiestic vapor pressure measurements are carried out for the ternary system water–sodium polyacrylate (NaPAA)–neutral polymer. The neutral polymers investigated are polyacrylamide (PAAm), polyethylene glycol (PEG), and polyvinylpyrrolidone (PVP), which have been often reported as having marked effects on solvent water structure.[10,11]

Experimental Section

Isopiestic Measurements. The isopiestic measurements were carried out at 25 ± 0.005° by using an apparatus described previously.[12] The apparatus consisted of a desiccator containing a copper block in good thermal contact with 14 silver dishes. The time required for the solutions to reach the equilibrium was about 3 days in the present research. The error of our isopiestic measurements was at the highest 3% of the concentration value. The reference electrolyte was sodium chloride. The osmotic coefficients of NaCl solutions were taken from the experiments by Janz and Gordon.[13]

Materials. NaPAA was furnished by the Toa Gosei Chemicals Co., Nagoya, Japan. The weight average degree of polymerization was 640. Dilute solutions of NaPAA were converted to the acid form by passing them through columns of cation- and anion-exchange resins. The molecular weights of PAAm, PEG, and PVP are 128,000, 6,000, and 24,500, respectively. Distilled water, passed through a mixed bed ion-exchange column, was used for the preparation of all solutions. The concentrations of polyelectrolyte and neutral polymers were determined by conductometric titration and by gravimetric method, respectively.

Results

If the ternary solution water–polyelectrolyte–neutral polymer and the binary solution H_2O–NaCl (a reference solution) are in an equilibrium in the isopiestic cell, we have the following equation from the condition of equal vapor pressure

$$-\varphi_{mix}[(1 + z_2)(m_2/z_2) + m_3/P_3] = -2\varphi_{ref}M_{ref} \quad (1)$$

where m_2 and m_3 denote the isopiestic concentrations (monomol/1000 g of water) of polyelectrolyte and neutral polymer, respectively, in the ternary system water–polyelectrolyte–neutral polymer, M_{ref} is the molality of the reference electrolyte (NaCl), and z_2 and P_3 are the stoichiometric valency of the polyelectrolyte and the degree of polymerization of neutral polymer, respectively. The subscripts, 1, 2, and 3, denote solvent (water), polyelectrolyte (NaPAA), and neutral polymer

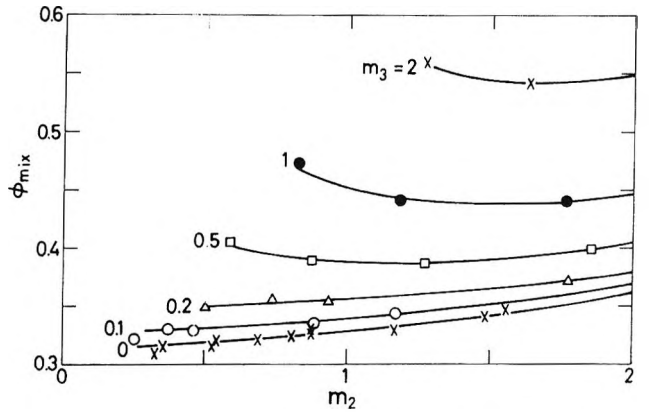

Figure 1. Osmotic coefficient in H_2O–NaPAA–PVP system at 25°.

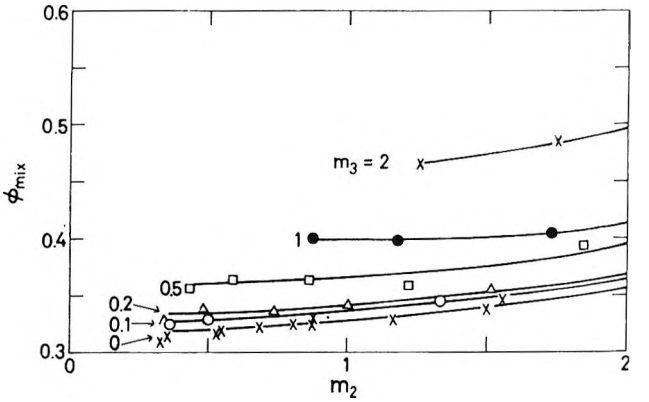

Figure 2. Osmotic coefficient in H_2O–NaPAA–PEG system at 25°.

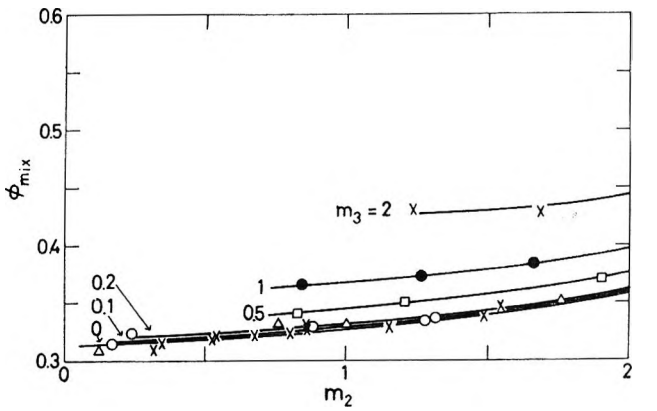

Figure 3. Osmotic coefficient in H_2O–NaPAA–PAAm system at 25°.

(9) See, for example, S. Lindenbaum and G. E. Boyd, *J. Phys. Chem.*, **68**, 911 (1964).

(10) See, for example, P. Molyneux and H. P. Frank, *J. Amer. Chem. Soc.*, **83**, 3169 (1961); J. Eliassaf, *Polym. Lett.*, **3**, 767 (1965).

(11) T. Okubo and N. Ise, *J. Phys. Chem.*, **73**, 1488 (1969).

(12) T. Okubo, N. Ise, and F. Matsui, *J. Amer. Chem. Soc.*, **89**, 3697 (1967).

(13) G. J. Janz and A. R. Gordon, *ibid.*, **65**, 218 (1943).

Table I: Isopiestic Concentrations for the System H_2O–NaPAA(2)–PVP(3) at 25°

Set	M_2	M_{NaCl}	m_2	m_3	Set	M_2	M_{NaCl}	m_2	m_3
1	0.328	0.0538	0.322	0.0148	5	1.164	0.208	1.136	0.0521
			0.313	0.0269				1.124	0.0966
			0.319	0.0359				1.111	0.125
			0.316	0.0676				1.061	0.227
			0.309	0.0832				1.049	0.283
			0.302	0.119				1.011	0.396
			0.290	0.165				0.962	0.546
			0.276	0.235				0.883	0.753
			0.256	0.312				0.807	0.983
			0.237	0.371				0.746	1.167
2	0.529	0.0898	0.519	0.0238	6	1.499	0.276	1.467	0.0672
			0.513	0.0440				1.454	0.125
			0.512	0.0576				1.431	0.161
			0.498	0.107				1.375	0.295
			0.492	0.133				1.355	0.365
			0.480	0.188				1.310	0.513
			0.460	0.261				1.250	0.710
			0.430	0.366				1.148	0.979
			0.397	0.483				1.050	1.280
			0.369	0.577				0.973	1.521
3	0.684	0.118	0.673	0.0308	7	2.132	0.422	2.085	0.0956
			0.665	0.0571				2.071	0.178
			0.661	0.0745				2.037	0.230
			0.637	0.136				1.958	0.419
			0.632	0.170				1.922	0.518
			0.611	0.240				1.859	0.728
			0.585	0.332				1.767	1.003
			0.545	0.465				1.624	1.384
			0.505	0.616				1.482	1.806
			0.473	0.739				1.363	2.132
4	0.876	0.154	0.860	0.0394	8	2.865	0.647	2.826	0.130
			0.847	0.0728				2.796	0.240
			0.841	0.0948				2.037	0.230
			0.807	0.173				2.626	0.563
			0.799	0.215				2.586	0.696
			0.771	0.302				2.499	0.979
			0.736	0.418				2.378	1.351
			0.680	0.580				2.177	1.855
			0.627	0.764				1.985	2.419
			0.584	0.913				1.832	2.864

(PVP, PEG, or PAAm), respectively. φ_{mix} and φ_{ref} indicate the practical osmotic coefficients of the ternary solution and of the reference solution, respectively. When $P_3 \gg 1$, m_3/P_3 is safely neglected compared with $(1 + z_2)(m_2/z_2)$ with the condition that m_3/m_2 is not very large. Thus, we obtain approximately

$$-\varphi_{mix}(1 + z_2)(m_2/z_2) = -2\varphi_{ref}M_{ref} \qquad (2)$$

The determination of the φ_{mix} values in the ternary system is the purpose of our experiments.

The isopiestic concentrations for the ternary systems H_2O–NaPAA–PVP, H_2O–NaPAA–PEG, and H_2O–NaPAA–PAAm are given in Tables I–III. Here M_2 and M_{NaCl} are the concentrations of NaPAA and NaCl in the binary solutions, H_2O–NaPAA and H_2O–NaCl, which are in an isopiestic equilibrium with the ternary solutions. From eq 2, the osmotic coefficients φ_{mix} at various concentrations of NaPAA (m_2) and neutral polymer (m_3) can be derived, and the polymer concentration dependence of φ_{mix} at constant concentrations of neutral polymer is computed. The results for the H_2O–NaPAA–PVP, H_2O–NaPAA–PEG, and H_2O–NaPAA–PAAm are presented in Figures 1–3. As is clearly shown, the osmotic coefficients φ_{mix} increase with increasing concentration of added neutral polymers, and the influence is found to be in the order PVP > PEG > PAAm. For the H_2O–NaPAA–NaCl system previously studied, we found that the mean activity coefficient of NaPAA decreased by the addition of NaCl in dilute concentration regions, and, through a minimum, increased at high concentrations.[12] Our recent study shows that the water activity in the ternary system, H_2O–NaPAA–sodium polystyrenesulfonate (NaPSt) and H_2O–NaPAA–sodium polyethylenesulfonate (NaPES) is raised by an increase of the amount of NaPSt or NaPES.[14] Thus, it is likely that

Table II: Isopiestic Concentrations for the System H_2O–NaPAA(2)–PEG(3) at 25°

Set	M_2	M_{NaCl}	m_2	m_3
1	0.352	0.0590	0.352	0.0702
			0.345	0.0930
			0.342	0.140
			0.339	0.197
			0.327	0.277
			0.318	0.363
			0.302	0.479
2	0.542	0.0928	0.520	0.104
			0.522	0.141
			0.514	0.210
			0.505	0.293
			0.485	0.411
			0.469	0.535
			0.446	0.708
3	0.809	0.141	0.802	0.0601
			0.784	0.104
			0.772	0.154
			0.766	0.207
			0.758	0.310
			0.728	0.422
			0.699	0.593
			0.671	0.765
			0.627	0.996
4	0.875	0.157	0.862	0.114
			0.842	0.168
			0.828	0.223
			0.819	0.335
			0.785	0.455
			0.749	0.635
			0.718	0.819
			0.676	1.073
5	1.555	0.293	1.545	0.0641
			1.535	0.115
			1.510	0.200
			1.489	0.297
			1.472	0.397
			1.395	0.809
			1.331	1.129
			1.279	1.458
			1.193	1.894
6	3.143	0.792	3.117	0.129
			3.108	0.233
			3.032	0.402
			2.994	0.597
			2.942	0.794
			2.772	1.607
			2.627	2.228
			2.490	2.839
			2.311	3.669

Table III: Isopiestic Concentrations for the System H_2O–NaPAA(2)–PAAm(3) at 25°

Set	M_2	M_{NaCl}	m_2	m_3
1	0.326	0.0608	0.341	0.0896
			0.337	0.138
			0.317	0.191
			0.314	0.248
			0.300	0.354
			0.291	0.470
2	0.453	0.0909	0.479	0.0950
			0.481	0.126
			0.473	0.195
			0.441	0.265
			0.435	0.343
			0.408	0.481
			0.401	0.646
3	0.651	0.122	0.667	0.132
			0.668	0.175
			0.653	0.269
			0.627	0.377
			0.616	0.486
			0.579	0.683
			0.568	0.916
4	1.035	0.183	1.028	0.0805
			1.019	0.116
			1.014	0.201
			1.003	0.263
			0.986	0.406
			0.965	0.580
			0.945	0.747
			0.900	1.062
			0.849	1.369
5	1.433	0.261	1.423	0.111
			1.412	0.161
			1.402	0.278
			1.382	0.363
			1.357	0.558
			1.322	0.795
			1.293	1.021
			1.218	1.437
			1.138	1.835
6	2.008	0.389	1.990	0.156
			1.970	0.224
			1.942	0.385
			1.919	0.504
			1.874	0.771
			1.822	1.096
			1.780	1.406
			1.675	1.977
			1.566	2.525

the water activity in the ternary systems is depressed by increasing the amount of coexisting neutral polymer, whereas it is raised by electrolyte addition.[15–19]

Discussion

The increase of the osmotic coefficient, or the decrease of water activity, by addition of neutral polymer (Figures 1–3) can be accounted for as follows. The sodium ions of NaPAA immobilize water molecules as a result of electrostatic ion–solvent interactions[20,21] and thus are

(14) N. Ise and T. Okubo, publication in preparation.

(15) In the ternary system water–glycine–sodium chloride, the activity coefficient of NaCl was reported to decrease with increasing amount of glycine,[16–18] and the activity coefficient of tetraalkylammonium chloride was also depressed by the addition of urea[19] in water–urea–tetraalkylammonium chloride systems.

(16) G. Scatchard and S. S. Prentiss, *J. Amer. Chem. Soc.*, **56**, 2314 (1934).

(17) N. R. Joseph, *J. Biol. Chem.*, **111**, 489 (1935).

(18) V. E. Bower and R. A. Robinson, *J. Res. Nat. Bur. Stand.*, **69**, 131 (1965).

(19) W. Y. Wen and C. L. Chen, *J. Phys. Chem.*, **73**, 2895 (1969).

(20) The hydration number of sodium ions is estimated to be 4–6 by various measurements, *i.e.*, mobility, entropy, compressibility, dielectric constant, density, and ultrasonic method.[21]

regarded as a structure former. The water structural influence of the polyacrylate ion was discussed by several techniques.[7,11,22] From measurements of the partial molal volume,[22] the electrostrictional hydration number of PAA ion was 4 per repeating monomer unit. Furthermore, the Setchenow constant ($k_{32}/2.303$) of NaPAA obtained from the solubility measurements of naphthalene in H_2O–NaPAA–$C_{10}H_8$ was 0.37 (>0) (Table Ib of ref 11), indicating a salting-out effect of NaPAA by the electrostrictional hydration. On the other hand, neutral polymers such as PVP, PEG, and PAAm have more or less hydrophobic effects and enhance the ice-like water structure around their hydrophobic groups. In the ternary solutions, the Setchénow constants of naphthalene ($k_{32}/2.303$) were −1.21, −0.20, and −0.01 for PVP, PEG, and PAAm, respectively,[11] and the order of the strength of the hydrophobic effect of the polymer was

$$\text{PVP} > \text{PEG} > \text{PAAm} \qquad \text{(I)}$$

In the case of aqueous mixtures of NaPAA and PVP, therefore, there are two different kinds of water structure, *i.e.*, the electrostrictional hydration around the NaPAA and the hydrophobic iceberg around the neutral polymer. It is reasonable that the repulsive actions between the two different kinds of water structure cause the increase of the activity of NaPAA (*i.e.*, the decrease of the solute activity), according to Wen, Saito, and Lee.[23] Thus the osmotic coefficient increases by the addition of PVP to the aqueous solution of NaPAA. Since the hydrophobic effect of the neutral polymer decreases in the order (I), the influence on the water activity by PEG for the H_2O–NaPAA–PEG system is smaller than that for the H_2O–NaPAA–PVP system, and the water activity is influenced most slightly by the addition of PAAm having the lowest hydrophobic effect among three neutral polymers.

(21) See, for example, R. A. Robinson and R. H. Stokes, "Electrolyte Solutions," 2nd ed, Butterworths, London, 1959, Chapter 3.

(22) N. Ise and T. Okubo, *J. Amer. Chem. Soc.*, **90**, 4527 (1968).

(23) W. Y. Wen, S. Saito, and C. Lee, *ibid.*, **70**, 1244 (1966).

NOTES

The Extraction of Thallium(III) from Aqueous Chloride Solutions by Tributyl Phosphate in Octane[1a]

by H. Michael Widmer[1b] and R. W. Dodson

Chemistry Department, Brookhaven National Laboratory, Upton, New York 11973 *(Received May 22, 1970)*

In measurements of the stability constants of chloride complexes of thallium(III), Walters and Dodson[2] used tributyl phosphate diluted with hexane to extract the species $TlCl_3$ from aqueous solutions. The present investigation with *n*-octane as diluent extends their work and includes quantitative characterization of the distribution equilibria of $HTlCl_4$ and $TlCl_3$.

As in the earlier work[2] all organic solvents were carefully purified. ^{204}Tl was used as tracer. It was proved that distribution equilibrium was attained. The temperature was 25.0°. Equal phase volumes were used. The ionic strength of the aqueous phase was 0.50 *M*, maintained with suitable mixtures of stock solutions of HCl, $HClO_4$, NaCl, and $NaClO_4$.

The observed distribution ratio *D* is the ratio of the concentration of thallium(III) in the organic phase to that in the aqueous phase. The expected dependence of *D* on the concentration variables is obtained by considering the reactions

$$TlCl_{3\,aq} + m\text{TBP}_{org} = TlCl_3 \cdot m\text{TBP}_{org} \quad (1)$$

$$H^+_{aq} + TlCl_4^-{}_{aq} + n\text{TBP}_{org} = HTlCl_4 \cdot n\text{TBP}_{org} \quad (2)$$

and their equilibrium constants

$$K_{D3} = [TlCl_3 \cdot m\text{TBP}]_{org}/[TlCl_3]_{aq}[\text{TBP}]^m_{org}$$

and

$$K_{D4} = [HTlCl_4 \cdot n\text{TBP}]_{org}/[H^+]_{aq}[TlCl_4^-]_{aq}[\text{TBP}]^n_{org}$$

The omission of activity coefficients of species in the aqueous phase implies the assumption of constant medium, which is a fair approximation at the ionic strength used. The corresponding omission for species in the organic phase limits the constancy of the mass action expressions to a range of TBP concentrations in which the appropriate activity coefficient ratios remain constant. With this limitation the distribution ratio is given by

$$D = \alpha_3 K_{D3}[\text{TBP}]^m_{org} + \alpha_4 K_{D4}[H^+]_{aq}[\text{TBP}]^n_{org} \quad (3)$$

where α_3 and α_4 are the fractions of the thallium(III) in the aqueous phase present as $TlCl_3$ and $TlCl_4^-$, respectively.

Dissociation or polymerization reactions in the organic phase were shown to be unimportant by the finding that *D* is independent of the concentration of thallium(III) in the organic phase under all conditions studied in the present work. The ranges were 4×10^{-9} to 2×10^{-5} and 5×10^{-7} to 2×10^{-3} *M* when the principal extracted species were $TlCl_3$ and $HTlCl_4$, respectively.

With 0.0365 *M* TBP no appreciable change (less than 6%) occurred in *D* as $[H^+]_{aq}$ was varied from 0.002 to 0.50 *M*. These measurements were made at $[Cl^-]_{aq}$ = 0.006, 0.10, and 0.50 *M*. However, a marked effect of acid was found with 0.730 *M* TBP at $[Cl^-]_{aq}$ = 0.50 *M*. The values of *D* were 119, 204, 285, 413, and 475 at $[H^+]_{aq}$ = 0.10, 0.20, 0.30, 0.40, and 0.50 *M*, respectively. These results exhibit the linear acid dependence required by (3). They also show that the TBP solvation number of the extracted $HTlCl_4$ is greater than that of the extracted $TlCl_3$.

Estimates of the solvation numbers *m* and *n* were obtained from the variation of *D* with $[\text{TBP}]_{org}$. Values of log *D* are plotted *vs.* log $[\text{TBP}]_{org}$ in Figure 1. The curve on the left is for the extraction of $TlCl_3$. A straight line of slope 2.0 is a good fit to the data[3] throughout the 100-fold range in concentration. The slope is well established for solutions which are sufficiently dilute that activity coefficient variations can reasonably be neglected. The lack of significant deviations above 0.0365 *M* (1 vol %) TBP suggests that the activity coefficient of $TlCl_3 \cdot 2\text{TBP}$ decreases with TBP concentration in a way which largely cancels the effect of the considerable decrease of the activity coefficient of TBP itself.[4,5] The curve on the right represents the extraction of $HTlCl_4$ from 0.50 *M* hydrochloric acid. The experimental distribution ratios were corrected for the extraction of $TlCl_3$ by subtracting calculated values of the first term on the RHS of (3). The corrections

(1) (a) Research performed under the auspices of the U. S. Atomic Energy Commission. (b) To whom correspondence should be addressed at Department of Chemistry, University of Massachusetts-Boston, Boston, Mass. 02116.

(2) R. M. Walters and R. W. Dodson, "Solvent Extraction Chemistry," D. Dyrssen, J. O. Liljenzin, and J. Rydberg, Ed., North-Holland Publishing Co., Amsterdam, 1967, p 71.

(3) These results agree with observations made earlier by R. W. Dodson and R. M. Walters, which are unpublished except for an allusion in ref 2.

(4) K. Alcock, S. S. Grimley, T. V. Healy, J. Kennedy, and H. A. C. McKay, *Trans. Faraday Soc.*, **52**, 39 (1956).

(5) D. Dyrssen and Dj. Petkovic, *J. Inorg. Nucl. Chem.*, **27**, 1381 (1965).

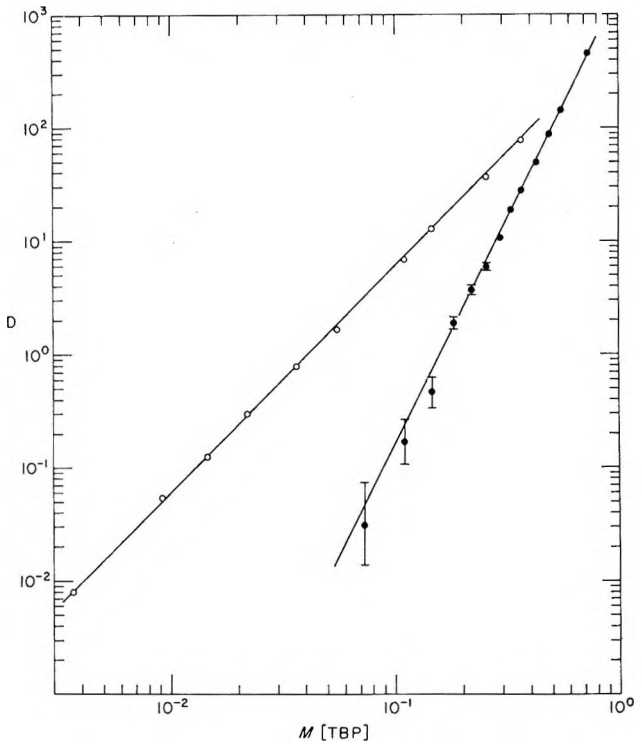

Figure 1. Variation of distribution ratios with concentration of TBP. Left-hand curve, slope 2.0: extraction of $TlCl_3$; $[Cl^-]$ 0.0060 M, $[H^+]$ 0.04 and 0.05 M. Right-hand curve, slope 4.0: extraction of $HTlCl_4$ from 0.50 M HCl. Values corrected for extraction of $TlCl_3$ from this medium.

were calculated from results of Walters and Dodson[2] and the present work. An alternative calculation of the corrections was made using the stability constants of $TlCl_3$ and $TlCl_4^-$ reported by Woods, *et al.*[6] The difference in the corrected values of D obtained by the two methods is taken as a reasonable estimate of the uncertainty in the corrected value and is indicated by the plus and minus error bars. It is remarkable that within these uncertainties the data for the extraction of $HTlCl_4$ are all satisfactorily fit by a straight line of slope 4.0, over a range of 10^4 in the corrected distribution ratio. We provisionally adopt the simplest interpretation of this result, which is that the extracted $HTlCl_4$ is solvated by four molecules of TBP and that the activity coefficient ratio y_T^4/y_4 (where y_T is the activity coefficient of TBP and y_4 is that of the solvated $HTlCl_4$) remains constant up to the highest TBP concentration, 0.73 M. For an ion pair, which the $HTlCl_4 \cdot n$TBP may be supposed to be, it is not surprising that y_4 should vary strongly with increasing polarity of the medium. However, we have no basis for predicting so exact a compensation of effects as appears to prevail.

The distribution equilibrium constants were evaluated with the aid of (3), on the basis that $m = 2$ and $n = 4$. (The stepwise stability constants of $TlCl_3$ and $TlCl_4^-$ involved in the calculations were independently determined in the present work and agreed closely with earlier estimates.[2]) The results were $K_{D3} = 9.7 \times 10^2$ M^{-2} and $K_{D4} = 3.4 \times 10^3$ M^{-5}.

The value 2 found for the TBP solvation number of $TlCl_3$ agrees with the result of Chuchalin, *et al.*,[7] which was obtained by quite different methods. We consider it well established for straight-chain hydrocarbon solutions. Earlier estimates of the TBP solvation number of $HTlCl_4$ differ among themselves and from our provisional value 4. A value 2 was reported[8] for isooctane diluent. Studies with benzene[9,10] gave 3, a value expected on the basis of the model proposed by Tuck and Diamond[11] for the extraction of strong acids. A solvation number 4 was reported by Meyers and McDonald[12] for $HFeCl_4$ in diethyl ether–benzene mixtures. They suggest that in addition to solvation of the hydrated proton there may be a sufficiently strong interaction of extractant molecules with the anions or with the ion pairs that this additional "electrostatic solvation" plays a significant role in the extraction process. We think this is a reasonable point of view and that the $HTlCl_4$–TBP–octane system may also be an example.

Acknowledgments. We are grateful to F. Silkworth for solvent purification, to James R. White for preliminary measurements on this extraction system, and to Karin Karlstrom and Kathleen McLinskey for skillful technical assistance.

(6) M. J. M. Woods, P. K. Gallagher, Z Z. Hugus, and E. L. King, *Inorg. Chem.*, **3**, 1313 (1964).

(7) L. K. Chuchalin, I. A. Kuzin, K. F. Obzherina, T. T. Omarov, and L. S. Chuchalina, *Russ. J. Inorg. Chem.*, **12**, 622 (1967).

(8) K. Henning and H. Specker, *Z. Anal. Chem.*, **241**, 81 (1968).

(9) K. S. Venkateswarlu and P. Chanan Das, *J. Inorg. Nucl. Chem.*, **25**, 730 (1963).

(10) H. Specker and W. Pappert, *Z. Anorg. Allg. Chem.*, **341**, 287 (1965).

(11) D. G. Tuck and R. M. Diamond, *J. Phys. Chem.*, **65**, 193 (1961).

(12) D. A. Meyers and R. L. McDonald, *J. Amer. Chem. Soc.*, **89**, 486 (1967).

Ozone Filter for Selecting 185-nm Radiation from Mercury Vapor Lamps[1]

by L. C. Glasgow and J. E. Willard

Department of Chemistry, University of Wisconsin, Madison, Wisconsin 53706 *(Received June 17, 1970)*

Ninety per cent of the radiation from a low-pressure Hg lamp is emitted in resonance lines at 254 nm and 185 nm, the 254-nm line being typically 4 to 10 times[2]

(1) This work has been supported in part by the U. S. Atomic Energy Commission under Contract AT(11-1)-1715 and by the W. F. Vilas Trust of the University of Wisconsin.

(2) B. T. Barnes, *J. App. Phys.*, **31**, 852 (1960).

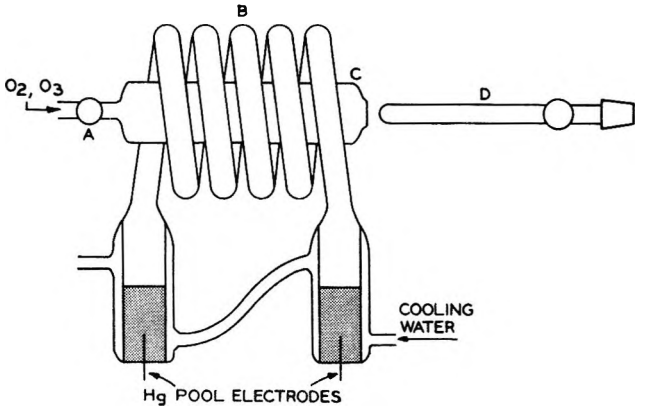

Figure 1. Arrangement for photolysis at 185 nm using flowing O_3 filter.

the intensity of the 185-nm line. For many photochemical studies with the 185-nm line it is necessary to filter out the 254-nm radiation. X- or γ-irradiated LiF,[3] interference filters,[4] and cyclohexane solutions of 9,10-dimethylanthracene[5] have been used for this purpose. All are inconvenient to produce and maintain. Using flowing O_2 containing a few per cent O_3 as a filter for a helical low-pressure mercury lamp (Figure 1), we have obtained higher 185 nm/254 nm ratios at high 185-nm intensities than previously available. The O_3–O_2 mixture made by flowing O_2 through a bank of 5 silent discharge tubes[6] passes through a flow meter (A) and a 28-mm i.d. Suprasil tube (C) positioned in the center of a lamp (B) of the type described by Lossing.[7] Sample tubes (D), up to 9 mm o.d., can be inserted into C for irradiation while surrounded by a flowing O_3–O_2 layer *ca.* 1 cm thick. The extinction coefficients of O_3 reported in the literature are 2.95×10^3 mol^{-1} cm^{-1} at 254 nm[8a] and 3×10^2 mol^{-1} cm^{-1} at 185 nm.[8b] Consistent with these values our measurements indicate a value at least tenfold higher at 254 nm than that at 185 nm.

Tests of the efficiency of the O_3–O_2 filter by HI and HBr actinometry[9] in Suprasil tubes (which transmit both 254 nm and 185 nm) and Vycor tubes (which do not transmit below 210 nm) indicate a 4 to 1 ratio of 254 nm to 185 nm entering the sample without the filter and 0.008 to 1 with the filter. Under the conditions used, the O_3 filter absorbs 99.9% of the 254-nm radiation and transmits about 50% of that at 185 nm. Four cc of HBr at 200 Torr in the 7-mm i.d., 10 cm long tube positioned inside the helical lamp absorbed 1×10^{16} photons sec^{-1} cc^{-1} (nearly 100% of the incident light) during operation of the filter. For comparison, a Hanovia SC2537 lamp with a 25-mm diameter window operated by a 5-kV ballast transformer at a current of 100 mA yields about 10^{13} photons sec^{-1} entering the 2-cm diameter face of a cylindrical reaction cell through a γ-irradiated LiF filter with a lamp to cell distance of 1.5 cm.

The optimum steady-state concentration of O_3 in the

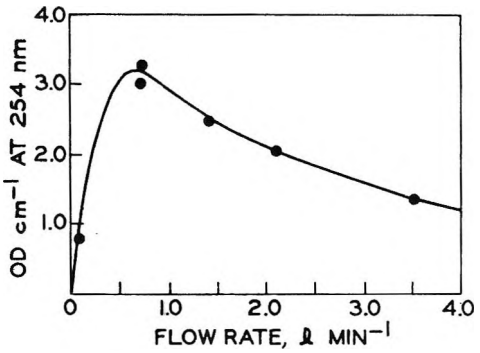

Figure 2. Optical density of 1 cm O_3–O_2 layer as a function of flow rate through ozonizer and irradiation tube C (Figure 1).

filter during illumination is obtained at a flow rate of *ca.* 0.7 l min^{-1} (Figure 2). At lower rates decomposition of O_3 by the 254-nm radiation[10] controls the effluent concentration, while at higher rates it is controlled by the decreased efficiency of production in passing through the ozonizer. The effluent O_3 concentrations were measured spectrophotometrically in optical cells. The O_3–O_2 effluent from the filter is vented to the hood or the O_3 is destroyed by bubbling through aqueous KI to avoid a health hazard.

(3) J. L. Weeks, S. Gordon, and G. M. Meaburn, *Nature*, 191, 1186 (1961).

(4) D. Schroder, *J. Opt. Soc. Amer.*, 52, 1380 (1962).

(5) C. M. Wolff and R. Pertel, *ibid.*, 54, 1168 (1964).

(6) A. C. Jenkins, *Advan. Chem. Ser.*, 21 (1959).

(7) F. P. Lossing, D. G. Marsden, and J. B. Farmer, *Can. J. Chem.*, 34, 701 (1956).

(8) (a) M. Greggs, *J. Chem. Phys.*, 49, 857 (1968); (b) Y. Tanaka, E. C. Y. Inn, and K. Watanabe, *ibid.*, 21, 1651 (1953).

(9) For references see: (a) R. Fass, *J. Phys. Chem.*, 74, 984 (1970); (b) R. Martin and J. E. Willard, *J. Chem. Phys.*, 40, 2999 (1964).

(10) L. T. N. Jones and R. P. Wayne, *ibid.*, 51, 3617 (1969).

Measurement of Thermal Diffusion Factors by Thermal Field-Flow Fractionation

by J. Calvin Giddings,* Margo Eikelberger Hovingh, and Gary H. Thompson

Department of Chemistry, University of Utah, Salt Lake City, Utah 84112 *(Received July 10, 1970)*

The degree of retention of solute peaks in gas–liquid partition chromatography (glpc) is directly dependent on the liquid–gas distribution ratio. In recent years glpc has been increasingly "inverted" in function to obtain meaningful partition coefficients from retention data.[1] This method is noted for its speed, accuracy,

* To whom correspondence should be addressed.

(1) J. C. Giddings and K. L. Mallik, *Ind. Eng. Chem.*, 59, 17 (1967).

and small sample requirements, although there are some limitations (*e.g.*, on volatility).

Thermal field-flow fractionation (TFFF) is a recently devised method for the analytical separation of macromolecules.[2,3] In this case the retention of solute (macromolecule) peaks depends on thermal diffusion parameters. We propose here, with several experimental examples, that the primary purpose of TFFF can be analogously "inverted" to yield the thermal diffusion properties of macromolecular systems.

Thermal diffusion is often characterized by the dimensionless thermal diffusion factor α. In dilute solutions the latter can be defined by the solute flux equation[4]

$$J = -D\left[\frac{dc}{dx} + c\left(\frac{\alpha}{T} + \gamma\right)\frac{dT}{dx}\right] \quad (1)$$

where D is the binary diffusion coefficient for the solute–solvent system, c the solute concentration in moles per unit volume, T the temperature, γ the coefficient of thermal expansion of the solution, and x the coordinate along which transport occurs.

Under steady-state conditions, the solute will be distributed in a near-exponential form, with mean layer thickness l given by[4]

$$l = \left[\left(\frac{\alpha}{T} + \gamma\right)\frac{dT}{dx}\right]^{-1} \quad (2)$$

In the case of constant viscosity, l is related to the TFFF retention ratio R by the equation

$$R = 6(l/w)[\coth(w/2l) - 2l/w] \quad (3)$$

where w is the distance between opposing hot and cold surfaces. A slight correction for the variation of viscosity with temperature, as described in the earlier paper,[4] must be made for accurate results.

In this work polystyrene polymers in toluene solvent were studied with three different temperature increments. These polymers, of narrow molecular weight distribution, were produced using anionic polymerization by the Pressure Chemical Co. of Pittsburgh, Pa. The rectilinear channel apparatus and its operation have been described elsewhere.[3]

Results

The results for α, along with estimated precision, are given in Table I. The temperature T reported for each α value is that at the center of gravity of the solute layer and is usually close to the cold wall temperature. The temperature increment between hot and cold walls is shown as ΔT.

The molecular weight reported in Table I is the manufacturer's weight average value, $\bar{M}_W$. This quantity is used because the refractometer-detector is a sensor for polymer mass, and hence a mass curve is generated. If the weight distribution curve were symmetrical, the retention of the peak center would correspond, to excellent approximation, to the properties of a polymer of molecular weight $\bar{M}_W$. This approximate identity is undoubtedly quite good in any case, and in all likelihood causes less error than the manufacturer's uncertainty in $\bar{M}_W$ itself, the latter uncertainty appearing alongside $\bar{M}_W$ in Table I.

Table I: Values of Thermal Diffuse Factor α as a Function of Temperature and Molecular Weight Parameters

ΔT, °C	T(cold), °C	$\bar{M}_W$	T, °C	α
30 ± 1	18	160,000 (±4%)	26	32 (±13%)
		394,000 (±2%)	23	59 (±6%)
		862,000 (±2%)	22	86 (±7%)
40 ± 1	20	160,000 (±4%)	30	25 (±32%)
		394,000 (±2%)	25	59 (±6%)
		862,000 (±2%)	23	120 (±4%)
74 ± 11	24	50,500 (±4%)	38	19 (±23%)
		160,000 (±4%)	31	41 (±4%)

Comparison of Methods. Several methods have been used for the determination of thermal diffusion factors for macromolecules in solution, in particular for polystyrene in toluene. A thermogravitational column was used by Debye and Bueche[5] and by Taylor.[6] The static cell method was used by Emery and Drickamer[7] and Whitmore,[8] with the concentration distribution determined by withdrawing samples from various positions in the cell. Meyerhoff and Nachtigall[9] also used the static cell. Their optical (schlieren) method of determining the concentration distribution without disturbing the contents of the cell allowed the use of a much shallower cell, which resulted in a significantly shorter time for reaching steady state.

In the moving boundary method, the rate of motion of the boundary between solution and pure solvent in a vertical thermal gradient was studied. The groups who have used this method differ in their means of observing the boundary motion: Hoffman and Zimm[10] used a cathetometer telescope, Herren and Ham[11] a triangle path interferometer, Rauch and Meyerhoff[12] a schlieren-

(2) J. C. Giddings, *Separation Sci.*, **1**, 123 (1966).
(3) G. H. Thompson, M. N. Myers, and J. C. Giddings, *Anal. Chem.*, **41**, 1219 (1969).
(4) M. E. Hovingh, G. H. Thompson, and J. C. Giddings, *ibid.*, **42**, 195 (1970).
(5) P. Debye and A. M. Bueche, "High Polymer Physics," H. A. Robinson, Ed., Chemical Publishing Co., Brooklyn, N. Y., 1948, p 497.
(6) D. L. Taylor, *J. Polymer Sci., Part A*, **2**, 611 (1967).
(7) A. H. Emery and H. G. Drickamer, *J. Chem. Phys.*, **23**, 2252 (1955).
(8) F. C. Whitmore, *J. Appl. Phys.*, **31**, 1858 (1960).
(9) G. Meyerhoff and K. Nachtigall, *J. Polymer Sci.*, **57**, 227 (1962).
(10) J. D. Hoffman and B. H. Zimm, *ibid.*, **15**, 405 (1955).
(11) C. L. Herren and J. S. Ham, *J. Chem. Phys.*, **35**, 1479 (1961).
(12) B. Rauch and G. Meyerhoff, *J. Phys. Chem.*, **67**, 946 (1963).

type optical system, and Norberg and Claesson[13] and Bonner[14] a Rayleigh interference system.

The above studies show that thermal diffusion factor α varies with concentration and temperature, as well as with molecular weight. The concentration dependence has been studied by several investigators. Their conflicting results have been compared and discussed by Norberg and Claesson.[13]

By extrapolating some of the above high-concentration data for polystyrene–toluene to zero concentration, it is possible to compare the results from various laboratories. The moving boundary method[10-14] measures the thermal diffusion coefficient D_T. For comparison, α was calculated from D_T according to $\alpha = D_T \cdot T/D$, using $T = T(\text{cold})$ and D from Meyerhoff and Nachtigall's work.[9] Figure 1 shows a considerable lack of agreement in the dependence of α on molecular weight. Unfortunately, all polystyrene–toluene data could not be shown because the concentration extrapolation was not always meaningful.[5,8,10]

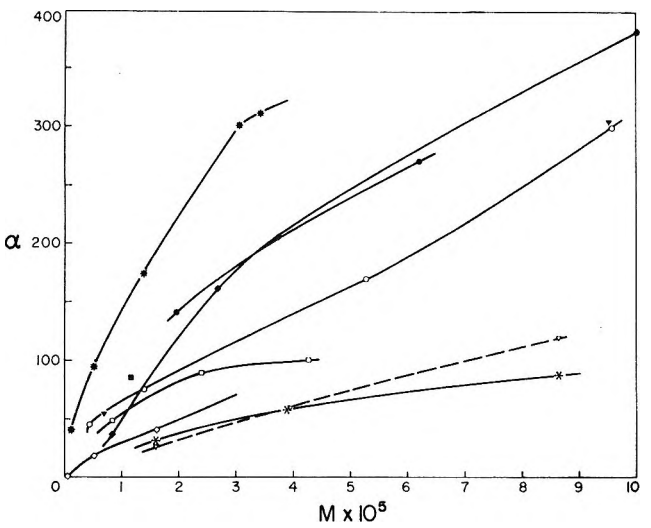

Figure 1. Thermal diffusion factor *vs.* molecular weight for polystyrene in toluene: *, Emery and Drickamer, $T(\text{cold}) = 19°$;[6] ○, Meyerhoff and Nachtigall, $T(\text{cold}) = 20°$;[8] □, Taylor, $T(\text{cold}) = 20°$;[5] ■, Norberg and Claesson, $T(\text{cold}) = 21°$;[12] ▼, Rauch and Meyerhoff, $T(\text{cold}) = 20°$;[11] ●, Bonner, $T(\text{cold}) = 16°$;[13] ◆, Herren and Ham, $T(\text{cold})$ unspecified;[10] *, ▽, ◇, this work, $T(\text{cold}) = 18$, 20, and 24°.

It is difficult to compare with finality the merits of TFFF and other methods used for obtaining thermal diffusion data. First of all, the TFFF device used here was a prototype, yielding less than optimum speed, resolution, and accuracy. Second, existing data show considerable discrepancy, and therefore standard values are unavailable for assessing the accuracy of new methods. Despite these problems, we can suggest certain potential advantages and disadvantages of the TFFF method. The analogous role of glpc in providing physicochemical data serves as a guideline.

Clearly with any fractionation system, including glpc and TFFF, it is possible to separate components and simultaneously measure their properties. Thus unlike other methods, these techniques can be used to characterize immediately the components in a mixture, even if these components exist in trace amounts which are not easy to isolate. Several components can, of course, be handled in a single run. In fact, the potential exists for characterizing the α spectrum of a polydisperse mixture, providing the molecular weight distribution is known.

In general, one can work with minute amounts of solute, although the precise level depends on detector sensitivity. In our case the amount of polystyrene used in each sample varied from 0.4 to 1.0 μg. The mean concentration in the zone was about 4×10^{-4} g/cm^3. Only with the optical method of Meyerhoff, *et al.*,[6] have levels of comparable dilution been reached.

As presently used, TFFF is unsuitable for studying concentration effects. The concentration in the zone varies from zero to some maximum (but usually low) value, and the α obtained reflects some intermediate behavior for this concentration range. However, as with chromatography, tracer pulse and concentration pulse methods could be developed to study the effect of concentration.[15]

An unusual characteristic of TFFF is that the narrow channel leads to rather high temperature gradients, up to 2860°/cm. Most methods utilize gradients of only a few degrees per centimeter.

The time needed for the experimental determination of an α value, depending as it does on sluggish macromolecular transport, is usually excessive. The static cell method of Emery and Drickamer[7] and Whitmore[8] requires between 15 and 60 days. The thermogravitational column of Debye and Bueche[5] and Taylor[6] requires from 3 to 9 hr. The moving boundary method, for which it is unnecessary to wait for steady-state conditions, yields an α value in 2 to 5 hr.

In the present TFFF work, single measurements were made in 2–17 hr. However, in this case the primary goal was the increase in fractionation power, an increase always demanding increased time. From theoretical considerations, the measurement of α for a single component on a shortened TFFF column should require only several "relaxation times" for establishing the steady state in the narrow channel. For our channel thickness of 0.25 mm, calculated relaxation times varied from 0.7 to 2.3 min while empirical relaxation times, possibly reflecting column irregularities, were in the range 1.3–29 min. These values suggest that measurement times could, in favorable cases, be reduced to values as low as 10 min.

(13) P. H. Norberg and S. Claesson, *Acta Imeko*, **4**, 501 (1964).
(14) F. J. Bonner, *Ark. Kemi*, **27**, 115 (1967).
(15) F. Helfferich and D. L. Peterson, *Science*, **142**, 661 (1963).

We conclude that TFFF has considerable potential for the measurement of thermal diffusion parameters and in view of its unique characteristics should prove a useful complement to the established methods.

Acknowledgment. This investigation was supported by Public Health Service Research Grant GM 10851-13 from the National Institutes of Health.

Isothermal Diffusion from a Boundary. Gouy Diffractometry Using Finite Beam Widths

by James A. Bierlein,* Julius G. Becsey, and Nathaniel R. Jackson

Aerospace Research Laboratories, Wright-Patterson Air Force Base, Ohio 45433 *(Received July 20, 1970)*

Gouy diffractometry is one of the most precise methods for measuring isothermal diffusivities. As developed by Longsworth[1] and others,[2,3] this technique involves free diffusion from an initially sharp boundary, the diffusion zone being illuminated by a plane coherent beam of (effectively) infinite vertical width. It is also possible to conduct the same kind of experiment at finite beam width by using a masking slit centered on the diffusion boundary or to operate under conditions of restricted diffusion, in which case the beam width is necessarily limited by the vertical dimension of the cell. Previous treatments[4-6] of this class of problem have made use of the complete Airy integral and its derivatives, giving rise to somewhat elaborate formulations; here we show how the incomplete Airy integral, originally introduced[7,8] for thermal diffusion studies, affords a "natural" method of analysis that yields compact and useful results.

Consider the case of a binary system undergoing free diffusion. We assume a linear relation between composition and refractive index everywhere within the two interdiffusing solutions, the initial differences in refractive index being $\Delta\mu = \mu_2 - \mu_1$, where the subscripts 1 and 2 denote the lower and upper solutions, respectively. If light is passed through this medium and thence through a slit of width H centered on the diffusion boundary, a lens placed in the beam will form in its focal plane the Fourier transform $\Phi(H,\gamma)$ of the complex amplitude distribution in the slit[9]

$$\Phi(H,\gamma) = K\int_{-H/2}^{H/2} G(v)\exp(2\pi i\gamma v/\lambda)\,dv \qquad (1)$$

Here K is a constant, λ is the wavelength of the light, γ is the angular coordinate of the one-dimensional Fourier transform, measured from the optic axis (positive if upward), and v is the distance across the slit measured from its center line. $G(v)$ is the complex amplitude field within the slit; in the case of free diffusion, it is given by

$$G(v) = M\exp[-\pi ij\,\mathrm{erf}(z)] \qquad (2)$$

In this expression, $z = v/2(Dt)^{1/2}$ is the dimensionless diffusion coordinate, D being the diffusivity and t the time since the start. M is the (constant) complex amplitude of the illuminating wave; $j = L\Delta\mu/\lambda$, where L is the length of the diffusion cell, front to back.

At any instant, z has extreme values $B = \pm H/4(Dt)^{1/2}$ which are located at the edges of the slit; provided sufficient time has elapsed that $|B| \leq 1/2$, the error function can be expressed with negligible error—less than 1% at any z—by the truncated Taylor series

$$\mathrm{erf}(z) \approx 2\pi^{-1/2}(z - z^3/3) \qquad (3)$$

With this approximation, and introducing the abbreviation $\gamma^* = j\lambda/2(\pi Dt)^{1/2}$, eq 1 becomes

$$\Phi(B,\gamma) = 2MK(Dt)^{1/2} \times \int_{-B}^{B}\exp\left[2\pi^{1/2}ij\left\{\left(\frac{\gamma}{\gamma^*}-1\right)z + {}^1/_3z^3\right\}\right]dz = 4MK(Dt)^{1/2}\int_0^B \cos\left[2\pi^{1/2}j\left\{\left(\frac{\gamma}{\gamma^*}-1\right)z + {}^1/_3z^3\right\}\right]dz \qquad (4)$$

The angle γ^* is simply the deviation of the ray passing through $v = 0$, as predicted by geometric optics. Equation 4 cannot be integrated in closed form, but it can be rewritten as

$$\Phi(A,x) = (\pi HMK/A)Ai(A,x) \qquad (5)$$

in which the parameters are given by

$$A = (2j)^{1/3}\pi^{1/6}H/4(Dt)^{1/2} \qquad (6)$$

$$x = (2j)^{2/3}\pi^{1/3}\left(\frac{\gamma}{\gamma^*}-1\right) \qquad (7)$$

$$Ai(A,x) = \pi^{-1}\int_0^A \cos(xu + {}^1/_3u^3)\,du \qquad (8)$$

* To whom correspondence should be addressed.

(1) L. G. Longsworth, *J. Amer. Chem. Soc.*, **69**, 2510 (1947).
(2) G. Kegeles and L. J. Gosting, *ibid.*, **69**, 2516 (1947).
(3) L. J. Gosting and M. S. Morris, *ibid.*, **71**, 1998 (1949).
(4) L. J. Gosting and L. Onsager, *ibid.*, **74**, 6066 (1952).
(5) C. A. Coulson, J. T. Cox, A. G. Ogston, and J. Stl. Philpot, *Proc. Roy. Soc., Ser. A*, **192**, 382 (1948).
(6) H. Kim, B. S. Patel, and G. Kegeles, *J. Phys. Chem.*, **66**, 1960 (1962).
(7) J. A. Bierlein, *J. Chem. Phys.*, **36**, 2793 (1962).
(8) J. G. Becsey and J. A. Bierlein, *ibid.*, **41**, 1853 (1964).
(9) A. Papoulis, "Systems and Transforms with Applications in Optics," McGraw-Hill, New York, N. Y., 1968, pp 3, 5.

The function defined by eq 8 is the incomplete Airy integral; tables of its zeros and turning values are available,[7] corresponding, respectively, to the positions of dark and bright fringes in the diffraction pattern.

If the expressions 6 and 7 are multiplied together and solved for γ, the result is

$$\gamma_m = \gamma^* + (\lambda A/H\pi)x_m \qquad (9)$$

The subscript m identifies the experimentally observable feature to be found at the location γ_m for a prescribed value of A, and it is also the argument used to enter the published tables of the incomplete Airy integral. The principal maximum is coded by the fringe number $m = 0$, and the other bright fringes by even integers having the same algebraic sign as the corresponding x_m; the zeros are numbered serially by odd integers, using the same sign convention. The null diffractogram of the optical system (cell empty or containing an optically homogeneous medium) is simply the Fraunhofer image of the slit; the dark fringes (except for the central pair) then have a uniform angular spacing $\gamma_F = \lambda/H$. Normalizing eq 9 to this constant gives

$$R_m = P + C_m \qquad (10)$$

where

$$R_m = \gamma_m/\gamma_F,\ P = \gamma^*/\gamma_F,\ C_m = Ax_m/\pi$$

With the aid of eq 10, an estimate of A and P can be obtained for an experimental diffraction pattern taken at fixed t. Using measured values of γ_m from the Gouy diffractogram, together with γ_F as determined separately from the Fraunhofer pattern of the slit, a set of observed values of R_m is obtained. These observed values are compared with values calculated from the tables of the Airy integral until the best fit is secured, as judged from minimization of the least-squares residual function $\sum_{\text{all } m} [R_{m,\text{obsd}} - R_{m,\text{calcd}}]^2$. In practice, the tables do not necessarily contain an explicit set of $x_m(A)$ corresponding to the least sum of squares; usually it is necessary to interpolate between the round values of A for which the x_m are listed. In our work, we use a six-point Lagrangian interpolation; the interpolation and least-squares[10] calculations are performed on an IBM 7094 computer.

After A and P have been determined for each diffraction pattern, the optimum value of the product $k = PA(t + t_0)$ is computed, t_0 being the zero time correction which accounts for the unavoidable interdiffusion that occurs during the formation and sharpening of the initial boundary. Since

$$k \equiv (j/4)^{4/3}H^2/\pi^{1/3}D \qquad (11)$$

the diffusivity follows directly.

Figure 1 shows one typical Gouy pattern selected from a series obtained during the interdiffusion of pure water and an aqueous solution containing 7.5 g of sucrose/l.; also shown is one branch of the symmetrical Fraunhofer pattern taken with the diffusion cell empty to calibrate the optics. The measurements were taken in a flowing-junction cell about 8 cm high, $L = 7.948$ cm, $H = 0.3159$ cm; the light was produced with a low-power (1 mW) CW helium–neon laser, λ 632.8 nm, filtered through a pinhole of 10-μ diameter and collimated; $\Delta\mu$ at this wavelength was -0.00106, $j = 133.2$. The focal length of the camera lens was sufficiently large (about 94 cm) that distances measured on the diffractograms were proportional to angular displacement. Exposure time was $^1/_{20}$ sec on Kodak Super Panchro-Press plates. In this experiment, nine diffractograms were made at various times between 60 and 280 min. The average value of k was 23,438 min, the standard deviation being ± 194; t_0 was 3.9 min. Assuming negligible error in j and H, the value for D is $(5.192 \pm 0.043) \times 10^{-6}$ cm^2/sec; this is consistent with the mean (5.175×10^{-6}) of results reported by others.[3,11,12]

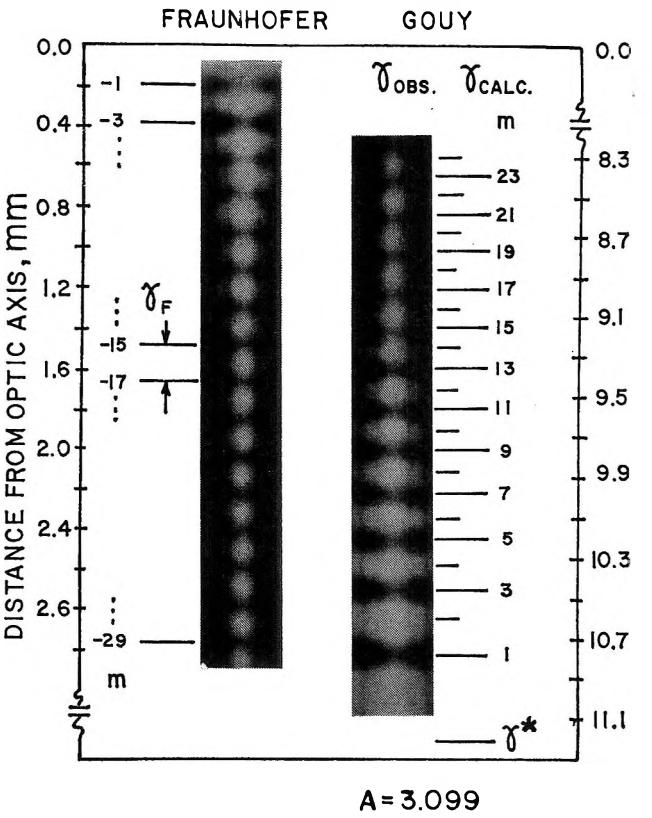

Figure 1. Typical diffractograms.

We now apply analogous methods to the problem of restricted diffusion. The general formula for diffusion

(10) A listing of the Fortran IV program in a subroutine form containing detailed tables of $C_m(A)$ is available on request. Input values are γ_F and a set of γ_{obsd}; the return values are A, P, and a set of γ_{calcd}.

(11) D. F. Akeley and L. J. Gosting, *J. Amer. Chem. Soc.*, **75**, 5685 (1953).

(12) J. F. Riley and P. A. Lyons, *ibid.*, **77**, 261 (1955).

from a boundary (located at the midplane of a cell of height a) is

$$\mu = {}^1/_2(\mu_2 + \mu_1) + \frac{2}{\pi}\Delta\mu \sum_{n=1,3,\ldots}^{\infty} \frac{1}{n} \times \exp(-n^2 t/\Theta) \sin \frac{n\pi v}{a} \quad (12)$$

where $\Theta = a^2/\pi^2 D$. The phenomenology for free diffusion, employed heretofore, is in fact the limiting case of this equation when t/Θ is sufficiently small. Eventually, however, appreciable changes in μ occur at the ends of the cell and restricted diffusion sets in; and if $t/\Theta > 0.6$, only the first term of the summation in eq 12 is important. Approximating sin $\pi v/a$ by a Taylor series terminating after the cubic term (valid provided that $H/a \leq 0.8$), it is a straightforward matter to show that the diffraction pattern is described by an incomplete Airy integral having the parameters

$$A = (H\pi/2a)[2j \exp(-t/\Theta)]^{1/3} \quad (13)$$

$$x = 2[2j \exp(-t/\Theta)]^{2/3}\left(\frac{\gamma}{\gamma^*} - 1\right) \quad (14)$$

where γ^* now has the value $(2j\lambda/a) \exp(-t/\Theta)$ which is appropriate to restricted diffusion. To find D, we note first that the experimental values of A and P, as estimated from the diffractograms, must satisfy the relation

$$k' \equiv PA \exp[{}^4/_3(t + t_0)/\Theta] = (2j)^{4/3}\pi H^2/2a^2 \quad (15)$$

the right-hand member of which is a known constant. The best values of t_0 and Θ are those for which the set of experimental values of k' have the prescribed average and the least standard deviation; this optimization is readily accomplished by a suitable computer program. Once Θ has been evaluated, the diffusivity is also known since $D = a^2/\pi^2\Theta$.

COMMUNICATIONS TO THE EDITOR

On Models of Dielectric Relaxation Due to Steady-State Chemical Processes

Sir: With the publication of the second paper by Dr. Gerhard Schwarz[1] in this journal (the first was in 1967[2]) on the dielectric relaxation of molecules in a steady-state chemical reaction, it may be appropriate to relate his derivations to earlier work. This will make it possible to show that two general equations, one a generalization of the solutions in ref 1 and 2, and the other derived in ref 3, describe the dispersion due to chemical processes in the two major classes of systems showing such effects.

Schwarz[2,3] has derived expressions for the fluctuation dielectric increment, $\Delta\epsilon_{ch}$, for each of several examples of chemical processes. With appropriate generalization of his nomenclature, these solutions can be generalized as

$$\Delta\epsilon_{ch}(\omega) = g\frac{N_A c_0}{3\epsilon_0 kT}\overline{\delta\mu^2}\left(\frac{1}{1 + i\omega\tau_2}\right) \quad (1)$$

where $\tau_2 = (\tau_r^{-1} + \tau_{ch}^{-1})^{-1}$, N_A is Avogadro's number, c_0 the molar concentration of the dipolar molecule, ϵ_0 the dielectric constant of free space, kT the thermal energy, $\overline{\delta\mu^2}$ the mean square fluctuation dipole moment, g the reaction field factor, τ_r the Debye relaxation time, τ_{ch} the rate constant of the chemical reaction, and ω the angular frequency of the impressed field.

The expression derived previously[3] for the general case of fluctuations resulting from the fixing and release of free ions on dipolar molecules, translated into this nomenclature and with the inclusion of the factor g is

$$\Delta\epsilon_{ch}(\omega) = g\frac{N_A c_0}{3\epsilon_0 kT}\overline{\delta\mu^2}\left(\frac{1}{1 + \tau_r/\tau_{ch}}\right)\left(\frac{1}{1 + i\omega\tau_2}\right) \quad (2)$$

which differs from (1) only by the factor $1/(1 + \tau_r/\tau_{ch})$. This difference turns out to be a consequence of a difference in assumptions. In deriving 2 it was explicitly assumed that the concentration of free ions does not reach equilibrium in the macroscopic potential gradient of the external field, but instead, as is usually assumed in conducting solutions, the free ion concentration is uniform. Hence, the chemical reaction equilibrium is independent of the direction in which the dipolar molecule happens to be turned in relation to the field.

On the other hand, the assumption made in Dr. Schwarz' calculations is that the equilibrium constant $\overline{K^*}$ of the chemical reaction depends on the field

(1) G. Schwarz, *J. Phys. Chem.*, **74**, 654 (1970).
(2) G. Schwarz, *ibid.*, **71**, 4021 (1967).
(3) W. Scheider, *Biophys. J.*, **5**, 617 (1965).

strength E, and on the instantaneous orientation of the molecule, as

$$\left(\frac{\partial \ln \overline{K^*}}{\partial E}\right)_{T,p} = \frac{\Delta M_E}{RT} \tag{3}$$

where ΔM_E is the component in the field direction, of the dipole vector increment created as a result of the chemical reaction.

The right side of (3) comes from the electrical term in the Gibbs free energy identity for thermal equilibrium. Equation 3 is hence equivalent to the assumption that dipoles are the only charge configurations involved in the chemical reaction.

It is also equivalent to the assumption that the system of dipolar particles is a closed thermodynamic system. Under a step function potential, it approaches thermodynamic equilibrium. Hence, any solutions obtained by use of the general theory of dielectric behavior of Glarum[4] and Cole[5] based on the statistical mechanical framework of Kubo[6] will have the same assumptions built into them as do Schwarz' solutions and eq 1. This is why the solutions of Williams[7] agree with those of Schwarz, and properly so because Williams has restricted himself to two cases where these assumptions are valid.

In a major class of chemical reactions, however, there is an exchange of charge between the dipolar particles and the solution, as for example in the case in which a dipole is formed by the binding of a free ion to the surface of a molecule with a central charge of opposite sign. Since in the chemical reaction neither charge is moved significantly, the total electrical energy of the two charges is unchanged during the reaction, even though a dipole of nonvanishing ΔM_E is created. The energy of ΔM_E is equal to that of the two charges from which it was formed.

As a consequence of the exchange of charge, the system of dipolar particles alone cannot be regarded as a closed thermodynamic system. A step function potential causes the system to approach a steady state which is not in thermodynamic equilibrium, because even under a constant field the elements of the system are driven in a cyclical, energy-consuming reaction, as described in ref 3. As a consequence, the system of dipoles does not conserve point density in phase space in the sense of the Liouville equation, and therefore the Kubo–Glarum–Cole approach will not give an appropriate result. For this reason a correlation function approach using superposition of response functions was used in ref 3 to obtain 2.

It is possible to view the distinction between systems obeying eq 1 and 2 by writing eq 3 to include free charges involved in the chemical reaction. This is done by inserting an additional term in the Gibbs free energy for the pairs of free charges Q_i which appear or are annihilated in the creation or annihilation of a dipole component. The resultant expression

$$\left(\frac{\partial \ln \overline{K^*}}{\partial E}\right)_{T,p} = \frac{\Delta M_E + \sum \Delta(Q_i x_{iE})}{RT} \tag{4}$$

can be used as a criterion to distinguish the principal classes of systems showing dielectric dispersion due to chemical reaction. x_{iE} is the coordinate, in the field direction, of Q_i. Since $\Sigma \Delta Q_i = 0$, the sum in eq 4 is invariant with choice of origin. When no free charge is involved in the chemical reaction, it is clear that (4) reduces to (3); in that case, and in such other special cases where the sum in (4) is zero, eq 1 holds. When the entire right side of (4) vanishes, as when dipole fluctuations are the result of the fixing of free charges, then eq 2 applies.

The examples of the Schwarz papers can now be examined in this light. The first[2] is the unimolecular reaction

$$A_1 \underset{K_{21}}{\overset{K_{12}}{\rightleftharpoons}} A_2 \tag{5}$$

where a charge rearrangement takes place within the molecule without interaction with free charges. The Schwarz result can be directly deduced from eq 1. Another example in this class is the jumping of hydrogen ions from one site on a protein molecule to another if no free hydrogen ion from the solution is involved. This process has been called "proton migration."

The reaction of a Zwitterion, Z, with free hydrogen ion or with hydrogen ion carrier, A^-, as in ref 1

$$HZH^+ + A^- \rightleftharpoons {}^-ZH^+ + HA \tag{6}$$

is in the other class of systems, as are macromolecule dipole fluctuations resulting from the steady state of "partially occupied" ion binding sites.[3] In all these cases, the right side of eq 4 vanishes. The fluctuation dielectric increment for the Zwitterion case should therefore be derived from (2), giving

$$\Delta\epsilon_2^0 = g \frac{N_A c_0}{3\epsilon_0 kT}\left(\frac{1}{1 + \tau_r/\tau_{ch}}\right) x_1 x_2 \mu_z^2 \tag{7}$$

where x_1, x_2, and μ_z are defined as in ref 1.

The other example in ref 2, the binding of small dipoles to the surface of macromolecules, is probably more complicated than is described. The example, to have measurable consequences, would require not only 0.5 M concentration of small dipole, but also 1 M binding sites, located on molecules so large that they, in effect, stand still for many times the characteristic time for the chemical reaction.

(4) S. H. Glarum, *J. Chem. Phys.*, **33**, 1371 (1960).

(5) R. H. Cole, *ibid.*, **42**, 637 (1965); and R. H. Cole, Theory of Electric Dipole Relaxation, "International Conference on Magnetic and Electrical Resonance and Relaxation," J. Smidt, Ed., Amsterdam, North-Holland Publishing Co., 1962, p 96.

(6) R. Kubo, *J. Phys. Soc. Jap.*, **12**, 570 (1957).

(7) G. Williams, *Advan. Mol. Relaxation Processes*, **1**, 409 (1970).

The advantage of the general formulations 1 and 2 is not only that they permit immediate solutions for the examples in ref 1 and 2, but also that they permit solution of cases of considerably greater complexity, in particular those in which the dipole vector fluctuations are not codirectional with the mean moment or with an axis of symmetry.[3]

Finally, the experimental data in ref 1 on ϵ-amino caproic acid supports the general results, but does not, in my opinion, afford quantitative differentiation between the predicted values from eq 1 and those from eq 2.

BIOPHYSICS RESEARCH DIVISION
INSTITUTE OF SCIENCE AND TECHNOLOGY
UNIVERSITY OF MICHIGAN
ANN ARBOR, MICHIGAN 48107

WALTER SCHEIDER

RECEIVED MAY 4, 1970

On the Nature of Bleached Color Centers in Irradiated Alkaline Ice

Sir: γ-Irradiation of alkaline ice[1-4] at 77°K leads to the formation of color centers (λ_{max} 585 nm) which can be bleached by visible light. This is another feature which emphasizes a similarity between trapped electrons in ice matrices and the F-centers in irradiated alkali halides. More recently bleached F-centers in alkali halides have been studied by Noble[5] and Markham who, however, did not reach any definite conclusions regarding the nature of these centers.

Ice matrices containing above 5 *M* alkali hydroxide are glassy and on γ irradiation at 77°K give esr spectra due to O^- ions and trapped electrons (e_t^-). At lower alkali concentrations one obtains polycrystalline specimens which show an additional resonance due to OH radicals, but annealing at 110°K leaves only the O^- and e_t^- spectra.[4]

The experiments reported below were carried out with 1 *M* alkaline ices (NaOH, KOH, and CsOH). Samples were prepared by the method described previously.[6] ^{60}Co γ radiation at a dose rate of 0.1 Mrad/hr was used with a total dose of 1.5–2.0 Mrads. Measurements were made on a "Microspin" esr spectrometer operating at 9.4 kMHz. Samples were annealed to the required temperature and then recooled to 77°K for taking spectra. Photobleaching was carried out with a 500-W tungsten lamp.

Esr studies on the bleached color centers in the 1 *M* alkaline ices showed that the spectra were different from that of the trapped electron before bleaching.

For these measurements the specimens were first annealed to 110°K to remove the OH radicals. After further annealing to 170°K (when the O^- resonance also disappears) a hyperfine structure reveals itself to some extent characteristic of the corresponding alkali metal nuclei. Similar experiments carried out in D_2O ices gave narrower lines, which shows that under these conditions the electron is also still interacting with the protons or deuterons in the ice matrix. Qualitatively similar results were also obtained after thermal bleaching alone. In the bleached centers, g values for the electron were found to be: NaOH ice, 2.0056 ± 0.0002; CsOH ice, 2.0048 ± 0.0002; and KOH ice, $g = 2.0060 \pm 0.0004$.

Further annealing to about 190°K gave in all cases a single broad line which would be compatible with a coagulation of the alkali atoms. The power saturation behavior of the bleached and of the coagulated centers is different from that of the trapped electron, which has the shape predicted by Portis[7] for the case of inhomogeneous broadening, whereas the bleached centers do not show power saturation under these conditions.

The hyperfine splitting of the spectra obtained after bleaching and annealing as described above could have an origin similar to that of impurity donor states in centain matrices,[8] and in this case could be due to the interaction of the electron with the nuclear moment of the corresponding (hydrated) alkali ion nucleus. The number of hyperfine lines corresponds roughly to the nuclear spin of the respective alkali nuclei (Na^{23}, $I = {}^3/_2$; Cs^{133}, $I = {}^7/_2$) so that one may conclude that in the bleached centers the electron is to some extent localized on the cation. However, the observed hyperfine spectra show unequal intensities and some asymmetry. This could be due to the superposition of a second spectrum, particularly that associated with the broad line which appears after further annealing, presumably due to coagulated alkali atom centers which may already be formed to a greater or lesser extent during the earlier stages of annealing.

Theoretically, the total hyperfine separation between the extreme lines of the multiplets should be proportional to the magnetic moment of the nucleus of the cation and the square of the (normalized) wave function of the electron at the alkali nucleus.[8] The observed total hyperfine separations in the ice matrices of 1 *M* alkali hydroxides were found to be: CsOH, 98.8 ± 1.0 G; NaOH, 44.6 ± 1.0 G; and KOH, 30.0 ± 1.0 G.

(1) D. Schulte-Frohlinde and K. Eiben, *Z. Naturforsch.*, *A*, **17**, 445 (1962).

(2) B. G. Ershov, A. K. Pikaev, P. Ya. Glazunov, and V. I. Spitsyn, *Dokl. Akad. Nauk SSSR*, **149**, 363 (1963).

(3) M. J. Blandamer, L. Shields, and M. C. R. Symons, *Nature*, **199**, 902 (1963).

(4) P. N. Moorthy and J. J. Weiss, *Phil. Mag.*, **10**, 659 (1964); *Adv. Chem. Ser.*, **50**, 180 (1965).

(5) G. A. Noble and J. J. Markham, *J. Chem. Phys.*, **36**, 1340 (1962).

(6) L. Kevan, P. N. Moorthy, and J. J. Weiss, *Nature*, **199**, 689 (1963); *J. Amer. Chem. Soc.*, **86**, 771 (1964).

(7) A. M. Portis, *Phys. Rev.*, **91**, 1071 (1953).

(8) J. M. Luttinger and W. Kohn, *ibid.*, **97**, 883 (1955).

In the absence of any independent knowledge of the wave function of the electron, it is not possible to test this theory.

In the photobleaching and annealing of irradiated alkaline ice it has previously been suggested, firstly by Moorthy and Weiss,[4] that the electron combines with the corresponding hole center (O^-) in the matrix according to: $O^-.H_2O + e^- \rightarrow 2OH^-$. Subsequently, the formation of dielectrons corresponding to the formation of F′ centers in alkali halides was also proposed.[9,10]

According to the observations reported above, there exists another possibility, *i.e.*, that the electron is trapped in an expanded orbit of a hydrated alkali cation.

Recently, Hart[11] reported some results from flash photolysis experiments of alkaline solutions which he could interpret on the assumption that the hydrated electron was trapped to some extent in an expanded orbit around a sodium ion. If this is confirmed, then this would represent a trapping mechanism in aqueous solution corresponding to that suggested here for ice matrices.

(9) J. Zimbrick and L. Kevan, *J. Amer. Chem. Soc.*, 89, 2483 (1967).

(10) A. S. Khodzhaev, B. G. Ershov, and A. K. Pikaev, *Izv. Akad. Nauk SSSR*, (8), 1882 (1969).

(11) E. J. Hart, paper presented at the 4th International Congress of Radiation Research, Evian-les-Baine, France, July 1970.

* To whom correspondence should be addressed.

LABORATORY OF RADIATION CHEMISTRY
THE UNIVERSITY
NEWCASTLE UPON TYNE, NE1 7RU, ENGLAND

N. B. NAZHAT
J. J. WEISS*

RECEIVED JULY 16, 1970

Remarkable Interstitial Hydrogen Contents Observed in Rhodium–Palladium Alloys at High Pressures

Sir: There has been considerable recent interest in the absorption of hydrogen by palladium alloys because these systems provide valuable tests for theories of hydrogen absorption. With the exception of the nickel–palladium system,[1] these investigations have been limited to palladium alloys in which the added metal is generally considered to absorb only insignificant amounts of hydrogen, *e.g.*, silver–palladium,[2-5] gold–palladium,[6,7] platinum–palladium,[8,9] rhodium–palladium,[10,11] copper–palladium,[12,13] tin–palladium.[14] In none of these studies have hydrogen-to-palladium atomic ratios in excess of 1 been reported; *i.e.*, there is no evidence that the added metal absorbs hydrogen when located within the palladium matrix.

In this research we wish to report for the first time hydrogen-to-palladium ratios well in excess of 1 (Table I) for an alloy system, rhodium–palladium, where the added metal is believed to be, itself, a nonabsorber of hydrogen. Evidence that pure, bulk rhodium absorbs appreciable amounts of hydrogen has never been presented.[15,16]

Table I: Hydrogen Contents Observed in Rhodium–Palladium Alloys after Removal from the High-Pressure Vessel

Alloy % Rh	Hydrogen-to-palladium	Hydrogen-to-metal	Max. H_2 pressure used, atm
5	0.90 ± 0.02	0.86 ± 0.02	2,300
5	0.86	0.82	5,100
5	0.95	0.91	23,200
10	0.99	0.89	2,300
10	1.02	0.92	21,300
15	1.07	0.91	21,300
20	1.15	0.91	2,300
20	1.26	1.01	5,100
20	1.22	0.97	23,200
30	1.34	0.93	2,300
30	1.44	1.00	5,100
30	1.46	1.01	23,200
40	1.52	0.90	2,300
40	1.61	0.96	5,100

The hydrogen was introduced into a high-pressure vessel (25°) described elsewhere.[17] The samples were in the form of thin foil. The pressure was applied to the samples in stages over a period of many hours. The final pressures (Table I) were applied for a period of at least 1 hr. The vessel was cooled (~−60°), the samples were removed and stored in liquid nitrogen prior to their examination with X-ray diffraction and

(1) F. A. Lewis, "The Palladium Hydrogen System," Academic Press, London and New York, N. Y. 1967.

(2) G. Rosenhall, *Ann. Phys. Leipzig*, 24, [5] 297 (1935).

(3) Z. L. Vert and I. P. Tverdovskii, *Zh. Fiz. Khim.*, 28, 317 (1954).

(4) E. Poeschel and H. Brodowsky, *Z. Phys. Chem. (Frankfurt am Main)*, 44, 143 (1965).

(5) A. Carson and F. A. Lewis, *Trans. Faraday Soc.*, 63, 1447, 1453 (1967).

(6) A. Maeland and T. B. Flanagan, *J. Phys. Chem.*, 69, 3575 (1965).

(7) K. Allard, A. Maeland, J. W. Simons, and T. B. Flanagan, *ibid.*, 72, 136 (1968).

(8) A. I. Stetsenko and I. P. Tverdovskii, *Zh. Fiz. Khim.*, 26, 647 (1952).

(9) A. Carson, T. B. Flanagan, and F. A. Lewis, *Trans. Faraday Soc.*, 56, 371, 1311 (1960).

(10) I. P. Tverdovskii and A. I. Stetsenko, *Dokl. Akad. Nauk SSSR*, 84, 997 (1952).

(11) J. C. Barton, J. A. Green, and F. A. Lewis, *Trans. Faraday Soc.*, 62, 960 (1966).

(12) R. A. Karpova and I. P. Tverdovskii, *Zh. Fiz. Khim.* 33, 1393 (1959).

(13) D. Chisdes and T. B. Flanagan, results to be published.

(14) H. Husemann, PhD Dissertation, Munster, 1968.

(15) E. Müller and K. Schwabe, *Z. Phys. Chem. Abt. A*, 154, 143 (1931).

(16) A. Sieverts and E. Jurisch, *Ber.*, 45, 228 (1912).

(17) B. Baranowski and W. Butjnowski, *Rocz. Chem.*, in press.

the analysis of their hydrogen contents mass spectrometrically.

The hydrogen-free alloys were fcc with lattice spacings corresponding quite well with those reported by Raub.[18] Upon absorption of hydrogen the alloys remained fcc with a single lattice spacing indicative of an increased lattice parameter. The observed parameters were consistent with the large hydrogen contents observed. For example, the 20% rhodium–palladium alloy's lattice parameter increased from 3.87 to 4.08 Å when the alloy's hydrogen content increased from 0 to hydrogen-to-metal = 1.01 ± 0.02. The consistency of this increase, 0.21 Å, with the observed hydrogen content can be more fully appreciated when compared to the increase of parameter of 0.151 Å for the palladium–hydrogen system when palladium absorbs hydrogen to form H-to-Pd = 0.7 at an equilibrium pressure of 1 atm (25°).[19]

At pressures between 2300 and 5100 atm stoichiometric 1:1 hydrides have been obtained for the 20 and 30% rhodium–palladium alloys. Concomitant measurements of the electrical resistance of the samples supports the view that these are limiting hydrogen contents, at least for the investigated pressure range, because significant resistance changes did not occur between 5100 and 23,200 atm, *i.e.*, changes which could not be attributed to purely hydrostatic effects. Such a limiting stoichiometry has not been obtained as yet even in the pure palladium–hydrogen system.[1,19] It can be noted from Table I that there is not always an increase of hydrogen content with pressure. This is because hydrogen may be lost from the sample upon cooling, reduction of the pressure, and removal from the vessel.

These results suggest that either rhodium itself can absorb hydrogen, but in a higher pressure range than palladium, or that rhodium can function as an absorber of hydrogen only when situated within the palladium matrix. So far we have not been successful in obtaining hydrogen absorption by pure, bulk rhodium but efforts are continuing in this attempt.

Acknowledgments. T. B. F. is grateful for his appointment as a participant in the exchange program between the National (U. S.) and Polish Academies of Sciences and for the hospitality of the Polish Academy of Sciences (Warsaw). The authors wish to thank Mr. M. Krukowski for valuable experimental aid. We are grateful to Professor E. Wicke for the 15% rhodium–palladium alloy.

(18) E. Raub, *Z. Metallk.*, **50**, 428 (1959).

(19) P. C. Abens and W. G. Burgers, *Trans. Faraday Soc.*, **58**, 1989 (1962).

* Chemistry Department, University of Vermont, Burlington, Vt. 05401.

THE INSTITUTE OF PHYSICAL CHEMISTRY
POLISH ACADEMY OF SCIENCE
WARSAW, POLAND

TED B. FLANAGAN*
B. BARANOWSKI
S. MAJCHRZAK

RECEIVED JULY 22, 1970